NIST-GCR-92-602

Solid Fuel Flame Spread and Mass Burning in Turbulent Flow

Liming Zhou

United States Department of Commerce
National Institute of Standards and Technology

NIST-GCR-92-602

Solid Fuel Flame Spread and Mass Burning in Turbulent Flow

Liming Zhou
University of California
Department of Mechanical Engineering
Berkeley, CA 94720

Issued March 1992
April 1991

Sponsored by:
U.S. Department of Commerce
Barbara Hackman Franklin, *Secretary*
Technology Administration
Robert **M.** White, ***Undersecretary*** of *Technology*
National Institute of Standards and Technology
John W. Lyons, ***Director***
Building and Fire Research Laboratory
Gaithersburg, MD 20899

Notice

This report was prepared for the Building and Fire Research Laboratory of the National Institute of Standards and Technology under grant number 60NANB7D737. The statements and conclusions contained in this report are those of the authors and do not necessarily reflect the views of the National Institute of Standards and Technology or the Building and Fire Research Laboratory.

Solid Fuel Flame Spread and Mass Burning in Turbulent Flow

By

Liming Zhou

B.S. (Qinghua University, Beijing) 1983
M.S. (Chinese Academy of Sciences, Beijing) 1986

DISSERTATION

Submitted in partial satisfaction of the requirements for the degree of

DOCTOR OF PHILOSOPHY

in

ENGINEEERING:
MECHANICAL ENGINEERING

in the

GRADUATE DIVISION

of the

UNIVERSITY OF CALIFORNIA at BERKELEY

Approved:

chair: ..... 4/23/91 .....
Date

..... 4/18/91 .....

..... 4/24/91 .....

* *

Acknowledgements

I would like to express my deepest gratitude to my research adviser, Professor Carlos Fernandez-Pello for his invaluable guidance, sincere help and special friendship over the years. I would also like to thank Professor Patrick J. Pagni for his constant encouragement and sound advice since the very beginning of my study at the Mechanical Engineering Department. I am obliged to Professor R. Brady Williamson for his helpful comments on my dissertation.

The friendship and advice of Dr. Robert Cheng have been most propitious. Special thanks go to Professor Antoni K. Oppenheim for providing constant inspiration. I gratefully thank all my Hesse Hall fellow students, especially Jose Torero, Betsy and Corey Dunsky, Javier Trelles, Aruna Joshi, Frank Schipperijn, Ofodike Ezekoye, Andrew Maxson and David Faris. The never failing help of Ken Horn, Dick Jensen and the Hesse Hall technical staff has been essential to this work.

I greatly appreciate the K. C. Wang Education Foundation for providing me the opportunity to study abroad. The financial support of the National Institute of Standards and Technology is also sincerely acknowledged.

My very special thanks go to my faithful friend Anthony Wu and his family whose genuine friendship and continuous help have made my stay in Berkeley a wonderful experience.

I am forever indebted to my parents who have provided me with bounteous trust, support and encouragement. This work would not have been possible without their endless love.

Table of Contents

Dedication	ii
Acknowledgements	iii
Table of Contents	iv
Nomenclature	viii
Chapter 1. Introduction	1
1.1 General Statements	1
1.2 The Specific Objectives of the *Study*	7
Chapter 2. Experimental Apparatus	9
2.1 Introduction	9
2.2 Wind Tunnel and Test Section	9
2.2.1 Wind Tunnel and Flow System	9
2.2.2 Turbulence Generating Section and Perforated Plates	14
2.2.3 Test Section and Ignitor	17
2.2.3.1 Test Section	17
2.2.3.2 Ignition Arrangement	17
2.2.4 Exhaust Section	19
2.2.5 Test Tables	19
2.3 Fuel Arrangement	21

2.3.1 Thermally Thick Fuel 21

2.3.2 Thermally Thin Fuel 23

2.4 Laser Doppler Velocimeter 23

2.4.1 Operation Description 23

2.4.2 Laser and Optical System 30

2.4.3 Signal Processor 32

2.4.4 LDV Seeding 33

2.5 Interferometer 37

2.6 Schlieren Photography 37

2.7 Flame Spread Rate and Mass Burning Rate Measurements 39

2.8 Gas Concentration Analysis 43

2.9 Data-acquisition and Test-control Software 45

2.10 Flow Fields 48

2.10.1 Axial Distribution 50

2.10.2 Cross-section Distribution 55

2.11 Error Analysis 58

2.11.1 Flame Spread Rate and Surface Regression Rate 58

2.11.2 Flow Velocity and Turbulence Intensity 60

2.11.3 Gas Concentrations 62

Chapter 3. Opposed Turbulent Flow Flame Spread 66

3.1 Introduction 66

3.2 Literature Review 67

3.3 Experimental Arrangement 73

3.4 Experimental Results and Discussion 74

3.4.1 Thick PMMA Sheets 74

3.4.2 Thin Paper Sheets 85

3.4.3 Turbulence Effect on Thin Paper Flame Extinction 89

3.5 Conclusion 91

Chapter 4. Concurrent Turbulent Flow Flame Spread 93

4.1 Introduction 93

4.2 Literature Review 94

4.3 Experimental Arrangement 104

4.4 Experimental Results 104

4.5 Discussion 108

4.6 Conclusion 123

Chapter 5. Mass Burning of a Solid Fuel Surface 126

5.1 Introduction 126

5.2 Literature Review 128

5.3 Experimental Arrangement 139

5.4 Experimental Results 140

5.5 Discussion and Data Correlation 148

5.6 Conclusion 156

Chapter 6. Ceiling Flame Spread and Mass Burning 158

6.1 Introduction 158

6.2 Literature Review 160

6.3 Experimental Arrangement 165

6.4 Flame Spread Rate 167

6.4.1 Velocity and Turbulence Effect 167

6.4.2 Buoyancy Effect 169

6.5 Mass Burning Rate 186

6.5.1 Velocity and Turbulence Effect 186

6.5.2 Buoyancy Effect 192

6.6 Conclusion 198

Chapter 7. Conclusions and Future Work 200

7.1 Summary of Results 200

7.2 Future Work 203

References 204

Appendix: Data-acquisition and Test-control Software 218

Nomenclature

c	Speed of light
c_p	Specific heat
f	Doppler frequency (Dual beam LDV)
h	Enthalpy
k	Thermal conductivity
l	Length of surface exposed to heat flux
l_f	Flame length
l_p	Pyrolysis length
L	Latent heat
$\dot{m}''$	Mass burning rate
N	Sample number
$\dot{q}''$	Heat flux
Re	Reynolds number
t	time
T	Temperature
u	Flow velocity in the x direction
u'	Fluctuating velocity
U	Free flow velocity in the x direction
v	Flow velocity in the y direction
V_f	Flame spread rate

V_r Surface regression rate

x Coordinate parallel to the fuel surface

Y Coordinate perpendicular to the fuel surface

Z Mixture fraction

Greek

a Diffusivity

δ Thickness of pyrolysis layer

ϵ Eddy kinematic viscosity

η Local similarity variable

λ Gas thermal conductivity

μ Viscosity

ρ Density

Subscripts

f Flame

g Gas phase

i Initial state

P Pyrolysis region

r Surface regression

s Solid phase

∞ Infinity

Superscripts

"	**Per unit area**
.	**Per unit time**

SOLID FUEL FLAME SPREAD AND MASS BURNING IN TURBULENT FLOW

by

Liming Zhou

ABSTRACT

An experimental study has been carried out to investigate the controlling mechanisms of solid fuel flame spread and mass burning in turbulent flows. The effects of flow velocity, turbulence intensity and buoyancy on concurrent and opposed flame spread rate and surface regression rate have been examined in both floor and ceiling configurations. It is found that for opposed flows, the flame spread rate of thermally thick PMMA sheet increases initially with the flow velocity, reaches a peak value and then decreases as the flow velocity increases further. The flow turbulence effect is to increase the flame spread rate initially and then decreases it at higher turbulence intensity. The flame spread rate of thermally thin paper sheet in an opposed flow decreases monotonically with the flow velocity and turbulence intensity. The flow turbulence also has a significant effect on the flame extinction conditions, resulting in a smaller extinction velocity for larger flow turbulence intensity.

For concurrent flow flame spread, it is found that the flow turbulence decreases the flame spread rate for both floor and ceiling geometries, mainly as a result of the flame length shortening at high turbulence intensity. It is also found that flow velocity intensifies the spread of the flame. The experimental data of flame

spread rate, flame length and surface heat flux agree well with the formula obtained from a simplified thermal model, indicating that the heat transfer from flame to solid surface is the dominant controlling mechanism in the turbulent concurrent flame spread and, that the gas phase chemical reaction is of secondary importance.

For solid fuel mass burning, it is found that the solid fuel surface regression rate decreases with the downstream distance and the flow velocity in both floor and ceiling configurations. The flow turbulence increases the surface regression by enhancing the mixing and bringing the flame closer to the solid surface. Empirical correlations between the non-dimensional surface regression rate and the non-dimensional flow parameter are obtained, which indicates the possibility of incorporating the flow turbulence intensity explicitly in a non-dimensional analysis or a numerical simulation of the problem.

The results from floor and ceiling geometries are compared to determine the effect of buoyancy on flame spread and mass burning. It is shown that for ceiling configuration, buoyancy enhances the heat transfer from the flame to the solid surface by pushing the flame closer to the wall. However, it also causes the gas phase chemical reactions to proceed less completely through insufficient gas mixing and surface quenching.

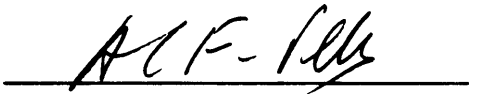

A. C. Fernandez-Pello

Chairman, Dissertation Committee

Chapter 1 Introduction

1.1 General Statements

The problem of a flame spreading over a solid combustible surface has been receiving much attention for the last two decades and extensive studies have been conducted to better understand the phenomenon [1] [2]. There are two main motivations for the persistent effort on this subject. First, the study of solid fuel flame spread can improve our fundamental understanding of the physical and chemical mechanisms that govern the process [3]. The results from these studies can provide us insights to the interaction of various controlling mechanism of other reacting flow problem and broaden our knowledge about combustion in general. The more important reason that has motivated the large quantity of work in this field is the practical significance of flame spread studies on fire prevention and control in real life situations. Hazardous fires caused by nature or human error can be found almost anywhere and at any time, which bring very large amount of material damage and tragic human loss. Many of those fires fall into the category of solid surface burning, such as the fires in buildings, vehicles, and forests. A thorough understanding of the mechanisms controlling the fire propagation process is essential to conduct more reliable material flammability tests, to design structures that are less prone to hazardous fires, and to extinguish fires faster and safer [4].

Many real fires involve diffusion flames spreading over the solid combustible surfaces such as the walls and ceilings of a building [5]. The spread of a flame is the

result of complex interactions among heat and mass transport processes and chemical reactions taking place in the gas and solid phases. Flames are usually initiated at small areas of the fuel surface by external heat sources such as a radiation heat panel or a strong electric spark. For the resulting flame to be self-sustained and subsequently to propagate over the surface of the solid combustible, sufficient fuel vapor has to be produced to join the reacting flame zone, which requires that a certain amount of heat be transferred from the flame to the unburned fuel surface. This incoming heat flux raises the fuel surface temperature to the pyrolysis point and provides the necessary energy for the subsequent pyrolysis. The fresh fuel vapor is diffused and convected to the flame region where it mixes with the oxidizer from gas flow, and exothermal reactions then take place in the reaction zone. In order to maintain the flame spread process, certain conditions have to be met in two operations: the heat transfer from the flame to the unburnt fuel and the gas phase chemical reaction. These two mechanisms are considered as the primary controlling factors governing most flame spread processes [6]. The effects on the flame spread process of various parameters such as gas flow velocity and turbulence intensity, atmospheric oxygen concentration, external radiation source, fuel type and size are often expressed in terms of their individual contributions to the two main controlling mechanisms.

Different types of flame spread processes *can* be grouped into two main categories based on the relative direction of the propagating flame to the gas oxidizer flow: flame spread in gas flows moving in the opposite direction of the flame

propagation, and flame spread in the gas flows moving in the same direction as thatof the flame. In the first case, as shown in Fig. 1.1, the flame front is usually distinctive and well-behaved and the flame propagates rather slowly because the heat transfer from the flame to the unburned fuel is hindered by the opposing gas flow. In the second case, as shown in Fig. 1.2, the gas flow drives the diffusion flame ahead of the pyrolysis region of the solid surface and largely enhances the heat transfer from the flame to the fuel. Therefore, the concurrent flame propagates much more rapidly than other cases and is known as the most dangerous type of flame spread.

Extensive studies have been conducted both analytically and experimentally in order to study opposed and concurrent flame spread processes [6] [7]. One frequently used approache is to isolate the effects of individual parameters and concentrate on the influence of one parameter at a time for the sake of simplicity. Among most frequently studied is the effect of gas flow velocity, external radiation, oxygen concentration, buoyancy and fuel sample dimension. A relation to determine the flame spread rate can be obtained from a simple energy balance at the fuel surface [5] [8]:

$$\rho V_f \, Ah \, \delta = \dot{q}'' \, l \qquad (1.1)$$

where ρ is the fuel density, V_f is the flame spread rate, δ is the thickness of the pyrolysis layer, l is the length of the surface region exposed to heat flux, q is the energy per unit area per unit time transferred across the surface, and Ah is the critical enthalpy increase per unit mass of fuel needed for ignition to occur. The critical enthalpy can be determined by employing a critical temperature such as the

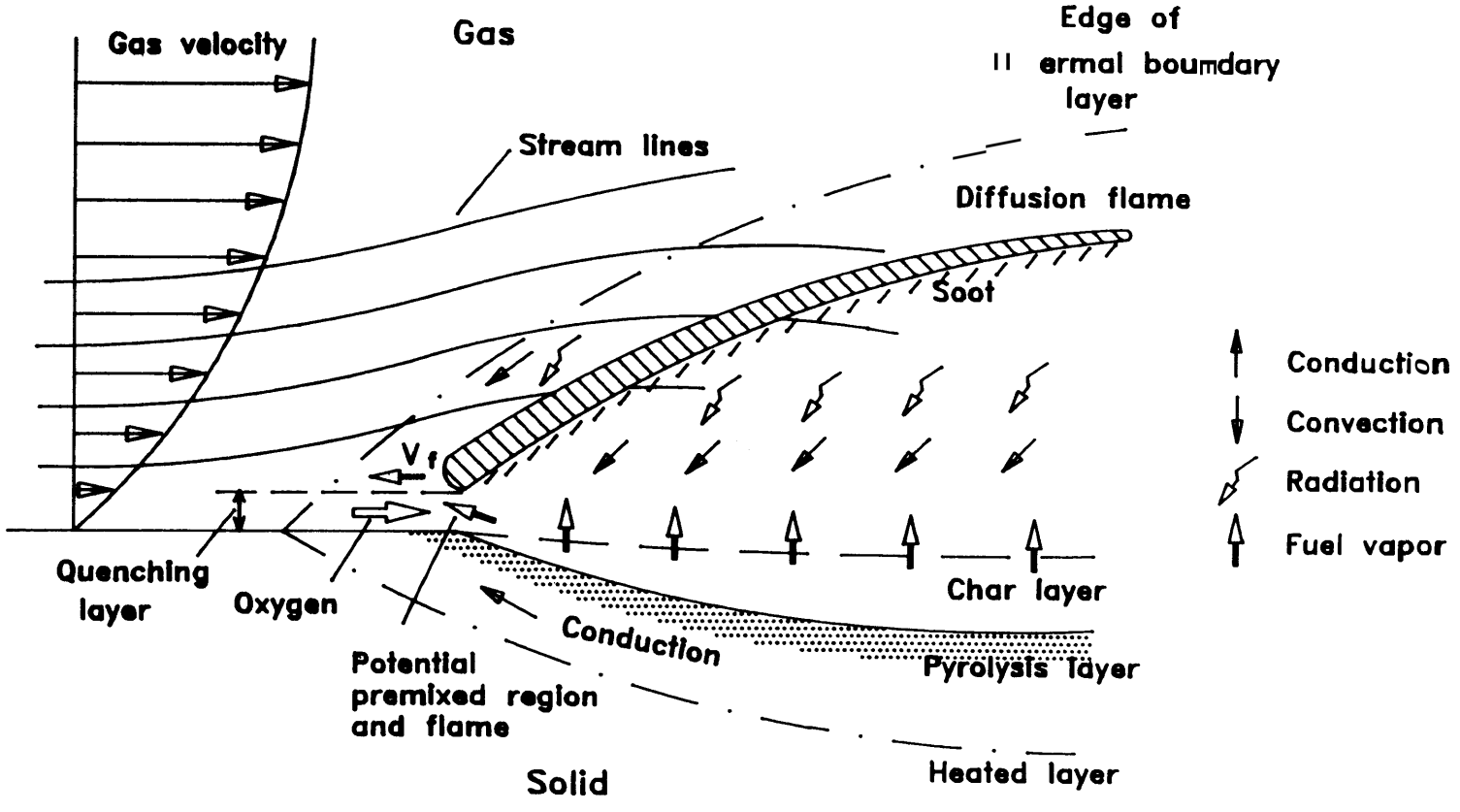

Fig. 1.1 Schematic of opposed flow flame spread process.

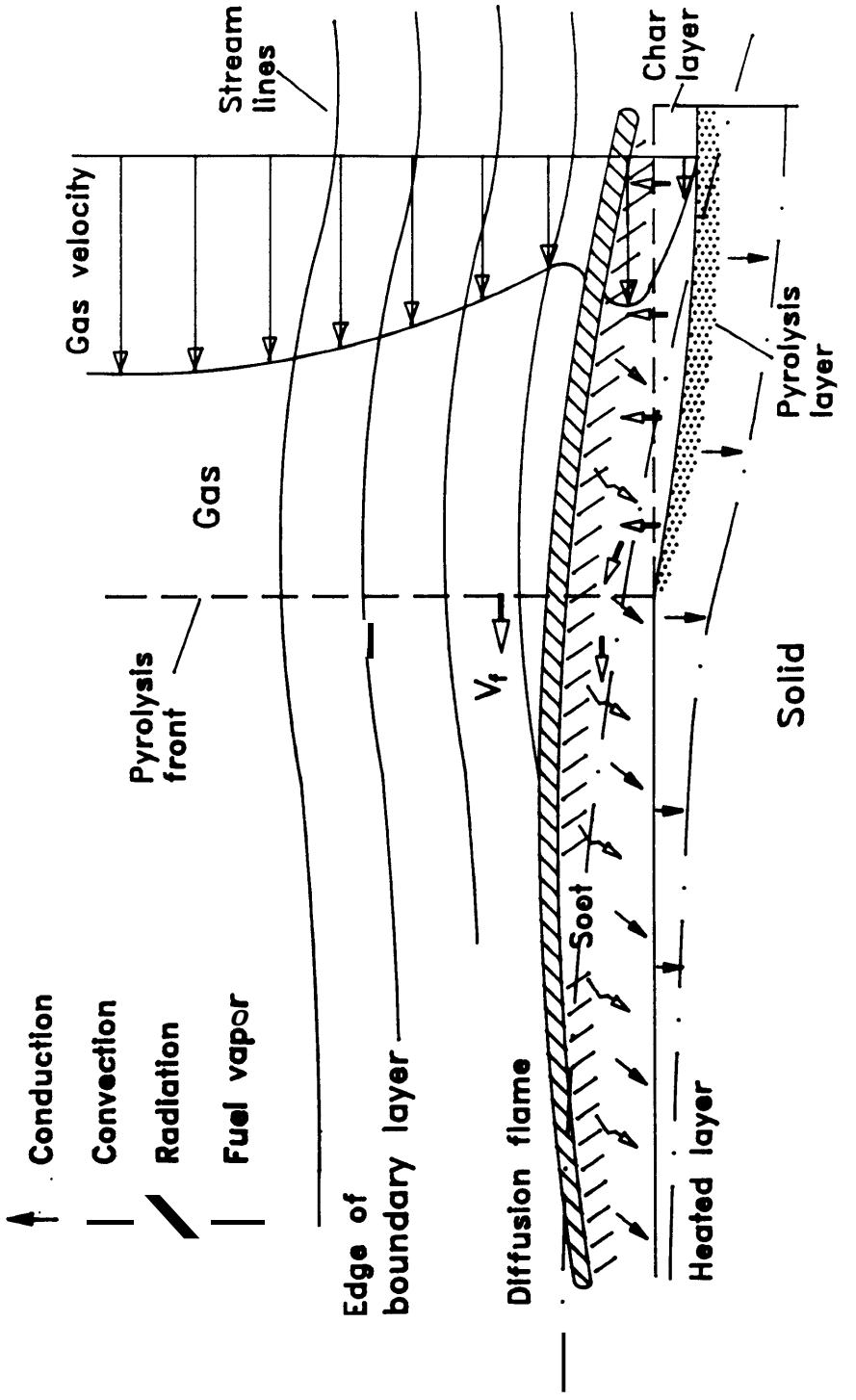

Fig. 1.2 Schematic of concurrent flow flame spread process.

pyrolysis temperature of materials:

$$\Delta h = \int_{T_0}^{T_c} c_p \, dT \qquad (1.2)$$

where T_0 is the initial temperature of the fuel and c_p is its specific heat. If approximations for ρ, c_p and T_c are available, then the problem of obtaining V_f is reduced to one of studying the heat transfer mechanisms that determine q. More complete literature reviews are presented in the later chapters on the different topics discussed there. Excellent review papers [1 - 3] [6] [7] have been published on the progress of the studies of flame spread problems.

Once the flame front has spread over the solid fuel surface, mass burning process takes place subsequently. In this phase of a developing fire, the heat continues to be transferred from the flame to the solid surface and the fuel pyrolysis continues on. As the result of the continuous pyrolysis of the solid combustible, the fuel surface recedes inward. The study of mass burning includes determining the basic information such as surface regression rate, flame stand-off distance, heat release rate and flow structure, etc. It also provides the non-dimensional parameters that properly Scale and describe the physical systems. Emmons [8] established the foundation for the modern study of the mass burning process by solving the problem of a burning liquid fuel surface in a forced oxidizer flow. Since then many more studies have contributed to the further understanding of the mass burning process and its application in fire research.

1.2 The Specific Objectives of the Study

Most of the existing studies on solid fuel flame spread and mass burning have been carried out under laminar flow conditions. Less attention has been paid to the turbulent flame spread and subsequent mass burning process due to the complication introduced by flow turbulence. However, most conventional fires take place in turbulent flows caused by external forces such as wind and indoor ventilation, or by strong natural convection induced by the large temperature gradient existing in the combustion zone. The lesser understanding of the turbulent problem and relatively scarce information on this subject have provided the incentives for conducting the current work the solid fuel flame spread and mass burning in turbulent flows.

The main objective of this work is to investigate experimentally a diffusion flame established over a solid fuel surface in a turbulent environment, focusing on its propagation and subsequent mass burning process. The present study will be conducted in the order that follows.

(1) An experimental study of flame spread over thermally thick PMMA and thermally thin paper sheets in an opposed turbulent air flow is conducted to examine the effect of flow velocity and turbulence intensity on the flame propagation rate and the flame extinction conditions.

(2) An experimental study is conducted to determine the flow velocity and turbulence effect on the flame spread rate of PMMA sheets placed in floor configuration in a concurrent air flow. The measured flame spread rates are summarized with a simplified analytical model.

(3) Experiments are carried out to study the mass burning process of PMMA in floor configuration in a turbulent air flow. The surface regression rate is measured as a function of the flow velocity and turbulence intensity. Empirical correlations between the mass burning rate and flow parameters are derived from the experimental data with a phenomenological analysis.

(4) Experiments are carried out to study the flame spread and mass burning of PMMA sheets in ceiling geometry, focusing on the effect of buoyancy. The ceiling flame spread rate and surface regression rate of PMMA sheets are measured as functions of the flow parameters. The ceiling and floor results are compared to determine the buoyancy effect.

Chapter 2 Experimental Apparatus

2.1 Introduction

The experimental facility is designed to provide a versatile and easily controlled test means with various diagnostic capabilities for the purpose of investigating flame spread and mass burning process of a solid combustible. In accordance with the main objectives of the study, the test installation should be able to produce air flows with adjustable flow velocity and turbulence intensity and to facilitate accurate measurements of flow parameters and solid surface temperature histories that are essential for further investigation.

An overview of the experimental setup for opposed flow experiments can be seen in Fig. 2.1. Similar setups used in other experimental conditions will be shown in later chapters.

2.2 Wind Tunnel and Test Section

2.2.1 Wind Tunnel and Flow System

The wind tunnel provides a steady air flow with low turbulence. It consists of five parts as shown in Fig. 2.2 :

(1) A premixing section made of a circular tube of 4 inch in diameter and a mixing chamber with a dimension of 7 inch x 12 inch x 8 inch. The round tube has two sections of 6 inch and 12 inch in length, respectively. The 6 inch section of the tube is connected to the wind tunnel and filled with honeycomb material of 1/4 inch

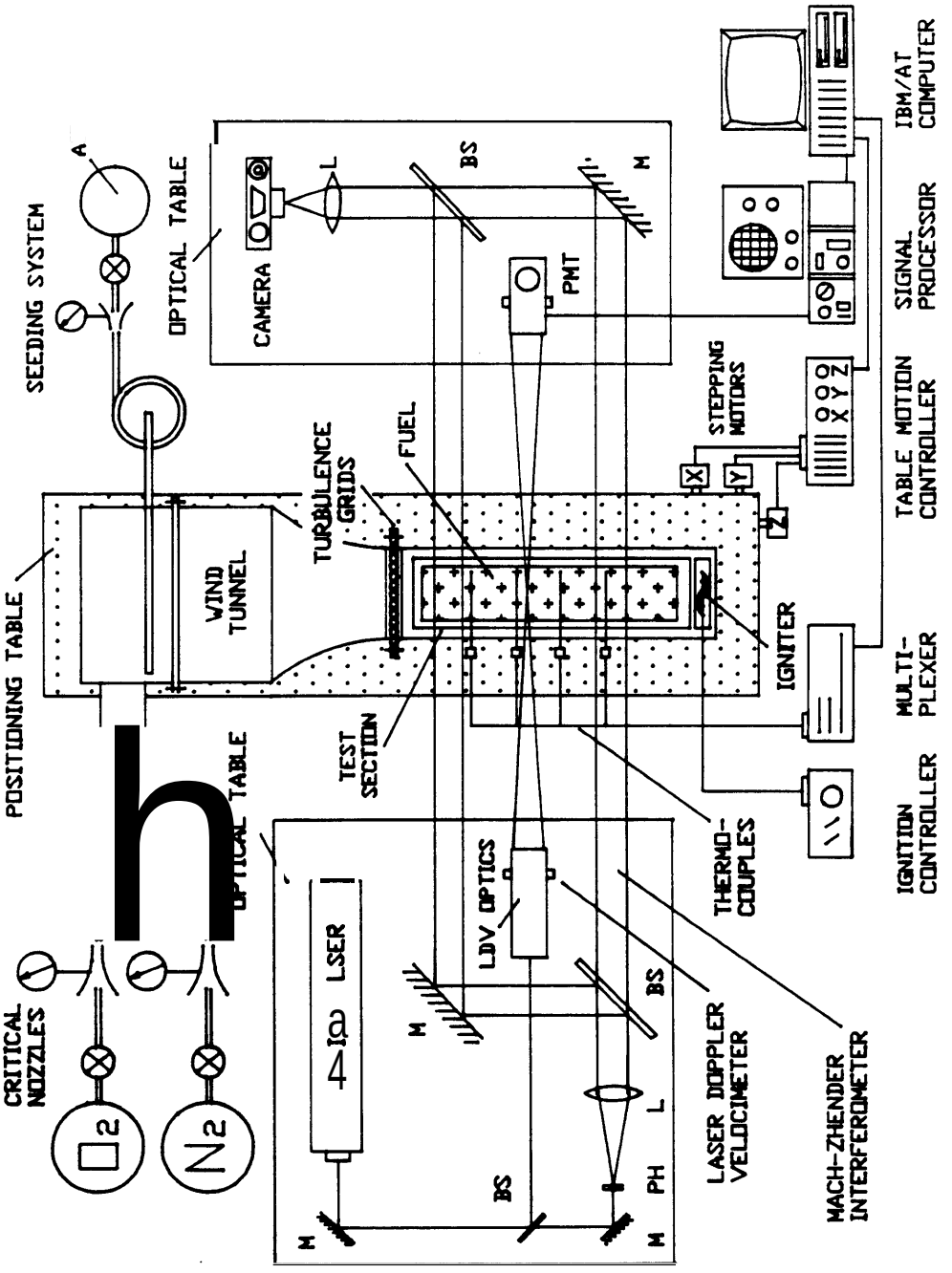

Fig. 2.1 Schematic of experimental facility for opposed flow flame spread study.

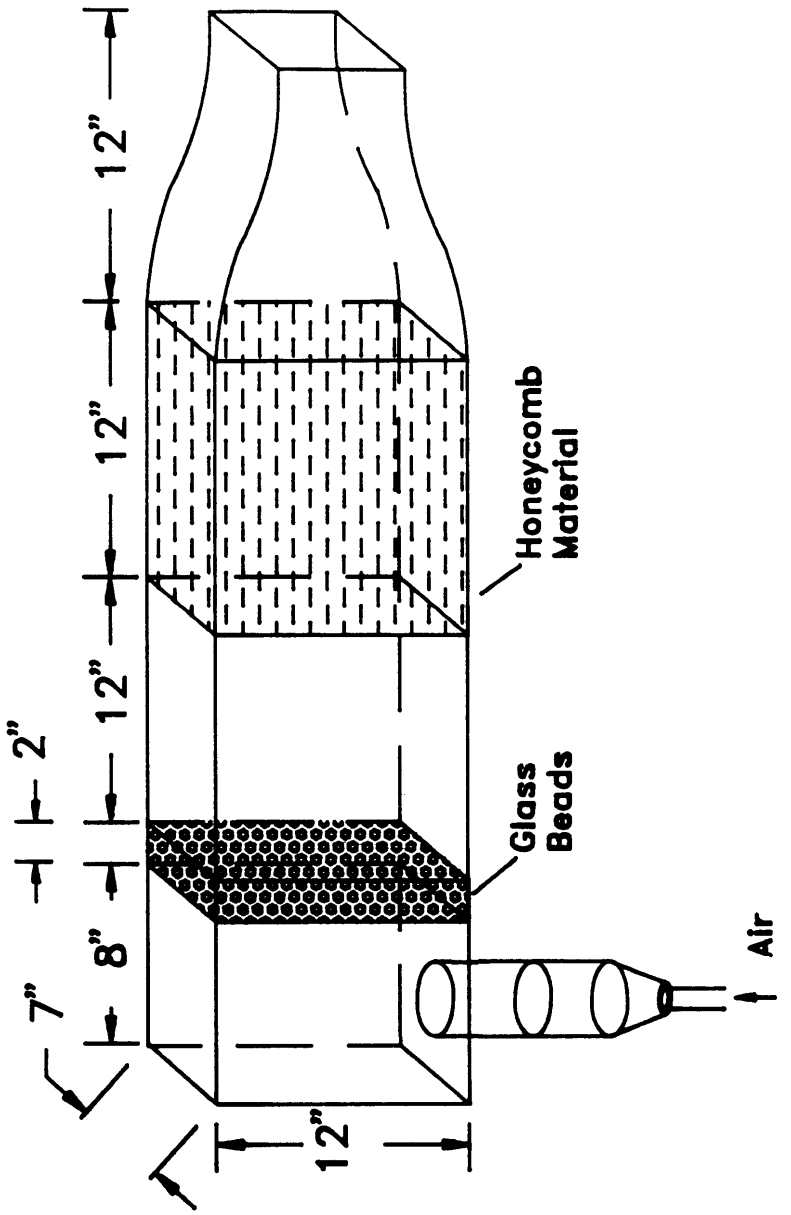

Fig. 2.2 Schematic of wind tunnel.

in side length. The premixing chamber laminates the incoming air flow and reduces the flow turbulence.

(2) A section with a dimension of 7 inch x 12 inch x 2 inch filled with glass beads of 5 mm in diameter. Mesh screens are placed at the two ends of the section. This section is used to reduce the local Reynolds Number and homogenize the flow.

(3) A section 12 inch long for laser Doppler velocimeter seeding. It provides the space for small alumina particles to *mix* thoroughly with the main flow.

(4) Another section 12 inch long filled with honeycomb material with a dimension of 1/4 inch in side length. This section further reduces the flow turbulence.

(5) And a converge section as shown in Fig. 2.3. The cross sections of the inlet and the outlet are 7 inch x 12 inch and 3 inch x 5 inch, respectively. This last section of the wind tunnel serves to decrease the flow turbulence to a minimum value.

Air supplied by an centralized air compressor is used as the oxidizer for all the tests of this work. Two pressure regulators and an oil filter are utilized to stabilize and clean the air flow, and pressure gages are used to monitor the flow conditions. Flow rate *can* be controlled with a main valve and a fine-adjustment valve manually. The air compressor also supplies the driving air flow needed for LDV seeding. A cylinder of compressed nitrogen is connected to the flow system and the nitrogen is used to extinguish the flame in the test section when an experiment has finished.

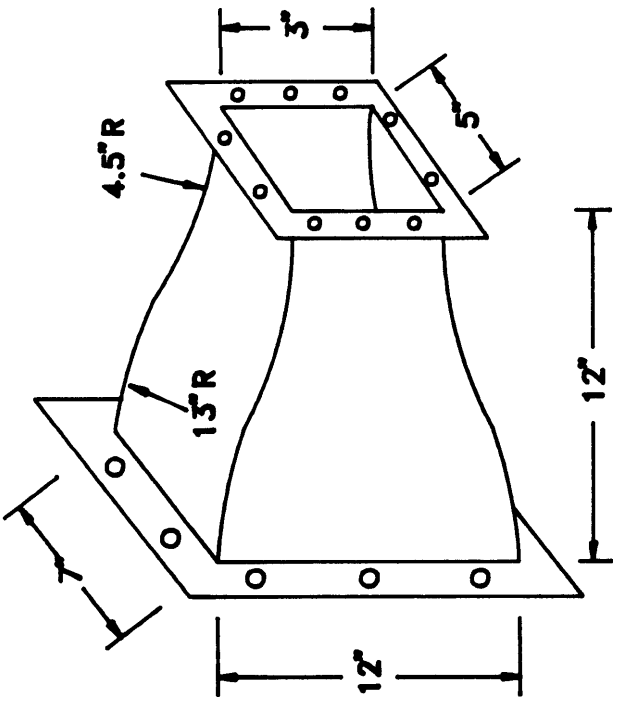

Fig. 2.3 Schematic of convergent section of wind tunnel.

The flow system described above can provide air flows with mean velocity ranging from 0.2 to 5 m/sec.

2.2.2 Turbulence Generating Section and Perforated Plates

This section is 6 inch long and has a cross section of 3 inch x 5 inch as shown in Fig. 2.4. It is made of plastic glass 1/4 inch thick and is placed between the wind tunnel exit and the test section. The main function of the section is to house perforated plates which are used to introduce turbulence to the passing air flow. The frame holding the perforated plates is firmly placed inside the section to reduce possible vibration of the plate caused by the flow pressure, which could result in irregularities in the downstream flow field.

Various perforated plates with different hole size and spacing distance are tested to generate desired turbulence intensities in the flow. The plates used for the experiments are made of 1/16 inch thick aluminum sheet and have a dimension of 3 inch by 5 inch. A typical perforated plate with dimensions is shown in Fig. 2.4. The horizontal and vertical distances between holes are d_H = 6 mm and d_V = 7 mm, respectively. The turbulence intensity depends on the flow velocity, the geometry and the position of the perforated plate. The hole sizes and their correspondent turbulence intensities at various flow velocities are presented in Table 2.1. The turbulence intensity, u'/U, is calculated as the ratio of the fluctuating flow velocity and the mean flow velocity. The distributions of flow velocity and turbulence intensity are discussed later.

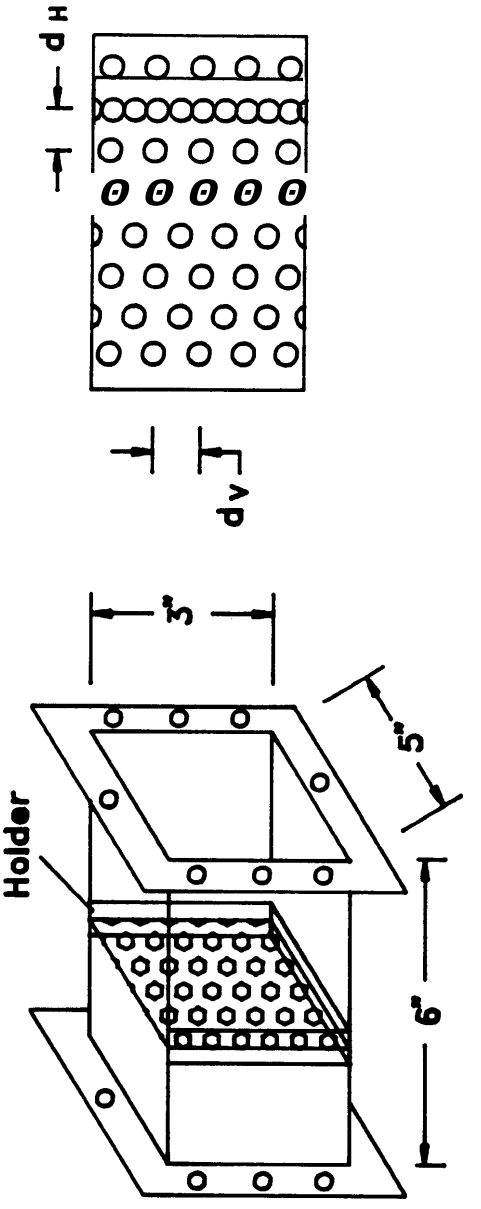

Fig. 2.4 Schematic of turbulence generating section and perforated plate.

Table 2.1 Hole size and correspondent turbulence intensity (%).

Hole *Size* r_0 (mm)	2.5	2.2	1.8	1.5	1.1
U = 0.25 m/s	4.5	9.6	13.9		
0.50 m/s	4.8	9.2	14.2		
0.75 m/s	5.1	9.5	15.3		
1.0 m/s	5.6	9.8	14.4	20.8	24.1
2.0 m/s	5.5	9.5	14.2	19.1	26.8
3.0 m/s	5.4	10.5	14.6	19.5	26.7
4.0 m/s	6.0	10.4	15.7	21.1	
4.5 m/s	6.2	11.1	16.3	22.2	

2.2.3 Test Section and Ignition System

2.2.3.1 Test Section

The test section shown in Fig. 2.5 is 24 inch long and has a rectangular cross section of 3 inch by 5 inch. The side walls are made of 1/4 inch thick, high temperature resistant Pyrex glass to provide access for visual observation and optical diagnostic path. The floor and ceiling of the test section are made of 1 inch thick Marinite slab and 1/4 inch thick aluminum plate, respectively. For thermally thick fuel experiments, a steel holder is used to embed fuel sheets flush in the Marinite floor. For thermally thin fuel experiments, the fuel sheet is fixed on another holder which is placed in the middle of the air flow.

The test section can be turned upside down, therefore, both floor and ceiling burning experiments can be conducted.

2.2.3.2 Ignition Arrangement

The ignitor for thermally thick fuel experiments is placed flush with the fuel surface in the metal holder with one side in firm contact with the front edge of the fuel sheet, as shown in Fig. 2.5. A ceramic tube of a nearly rectangular cross section is used as the ignitor body, which is wrapped with Nichrom wire of 0.02 inches in diameter. The total electric resistance of the wire is 10 ohms. The Nichrom wire is connected to a Variac and the output voltage is set at 30 to 40 V which generates a power output of 90 to 160 watts. To start an experiment, the output voltage from the Variac is increased gradually from zero to the full scale in about 5 to 10 seconds, and

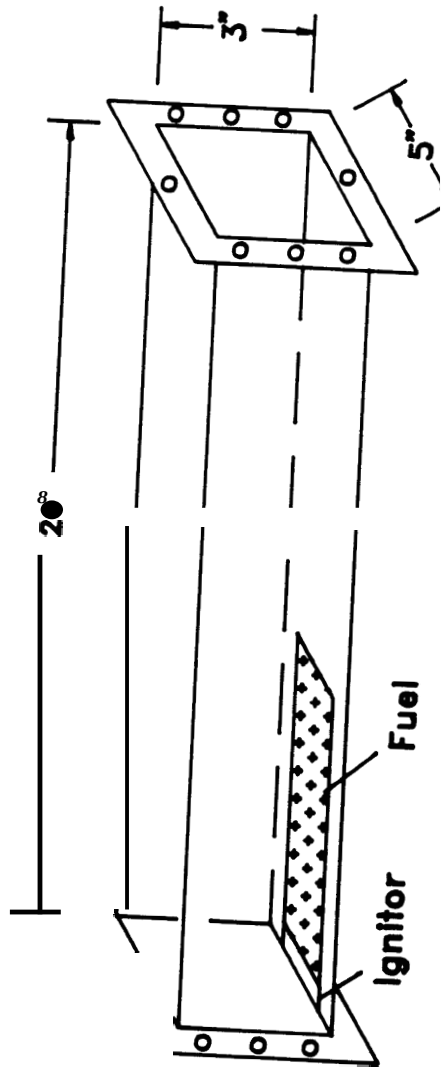

Fig. 2.5 Schematic of test section and ignitor.

then is kept at that level until the front edge of the fuel sheet is ignited. The ignitor first heats the fuel and brings the fuel temperature to the pyrolysis point, and then the hot Nichrom wire surface ignites the fuel vapor in the air. Depending on the test conditions, the entire ignition process takes approximately 40 seconds. The ignitor is turned off as soon as the flame is started on the fuel surface.

The ignition in thermally thin experiments is achieved by a single Nichrom wire placed on the fuel surface.

2.2.4 Exhaust Section

This section is designed to homogenize the species concentration distributions in the exhaust gas flow which makes it possible an accurate measurement of the gas concentrations. The exhaust section is made of a 1/8 inch thick steel pipe 48 inch long with a rectangular cross section of 3 inch x 5 inch. To ensure a complete mixing of the gas flow, four mixing plates of different geometric shapes are placed inside the section as shown in Fig. 2.6. These plates disturb the exhaust flow and generate sufficient turbulence in the flow by changing the flow path, therefore, a uniform gas concentration distribution *can* be achieved.

2.2.5 Test Tables

Two optical tables made by *NRC* are used to provide stable surfaces to hold optical diagnostic components. A three-dimensionally movable platform made from a milling machine is placed between the fixed optical tables. The wind tunnel and

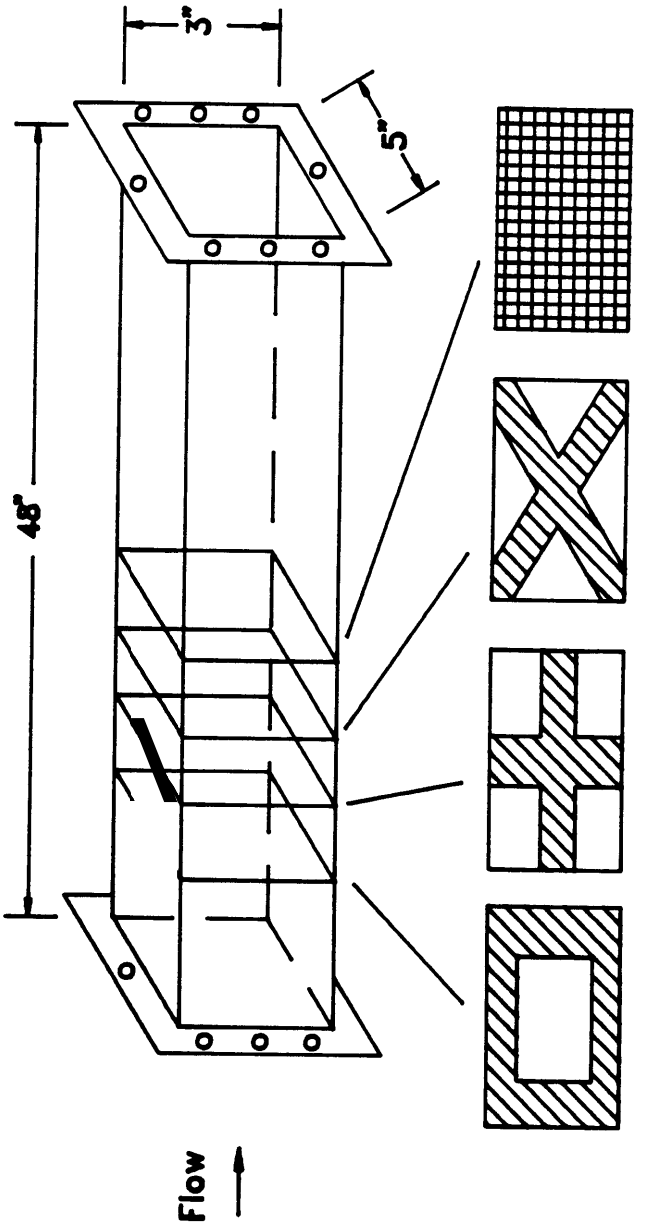

Fig. 2.6 Schematic of exhaust section and mixing plates.

the test section are mounted horizontally on the movable table. The movement of the 3-D table is driven by three stepping motors which can be controlled either manually with a control box or automatically with a computer.

2.3 Fuel Arrangement

Two kinds of solid materials are used to represent thermally thick and thermally thin fuels in the experiments.

23.1 Thermally Thick Fuel

Thermally thick fuel samples are made of PMMA (polymethylmethacrylate) sheets manufactured by Rohm-Hass (Plexiglas G) with a dimension of 3 inch x 12 inch x 1/2 inch. Fig. 25 shows the position of the fuel sample in the test section. The PMMA sheet is clamped to a steel bed which has holes on its back to allow thermocouple wires to pass through, as shown in Fig. 2.7. The tight clamping is to prevent the PMMA sheet from buckling in the process of burning. An accurate experiment of solid surface combustion requires that the material retain its physical integrity and do not soften or melt noticeably during combustion. Solid combustible that possesses these characteristics are few, among the conventional polymeric materials, only PMMA satisfies these requirements. PMMA has rather uniform and well-documented properties [9] [10], and in addition, it produces little char during burning. Many previous studies on this subject have used PMMA as the thermally thick fuel. Based on the above knowledge, PMMA is chosen to represent thermally

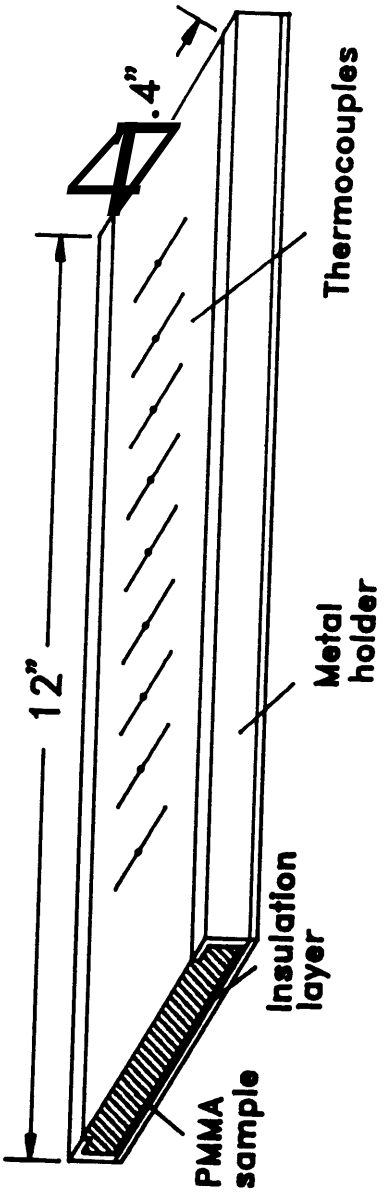

Fig. 2.7 Thermally thick fuel (PMMA) arrangement.

thick fuel in this study.

2.3.2 Thermally Thin Fuel

The fuel used for thermally thin fuel tests is 0.33 mm thick Whatman filter paper with a dimension of 3.5 inch x 12 inch. The paper sheet is mounted on a metal frame with 24 spikes placed 1/2 inch apart on each side, as shown in Fig. 2.8. The paper sheet is pushed onto the spikes which hold the paper in slight tension to provide a flat surface which favors a uniform ignition and burning. The holder positions the paper sheet in the middle of the flow in the test section. The paper sheets are dried and kept in an oven for about forty-eight hours prior to the measurements.

2.4 Laser Doppler Velocimeter

Instantaneous measurements of the gas flow velocity are made possible with a one-dimensional Laser Doppler Velocimeter operating in the dual-beam (differential configuration) and forward scattering mode. The LDV system mainly consists of an argon-ion laser, transmitting optics, receiving optics, a photo-multiplier and a counter type data processor.

2.4.1 Operation Description

The LDV system uses the Doppler phenomenon, namely, the change or apparent change in the frequency of wave motion (electromagnetic or any other type)

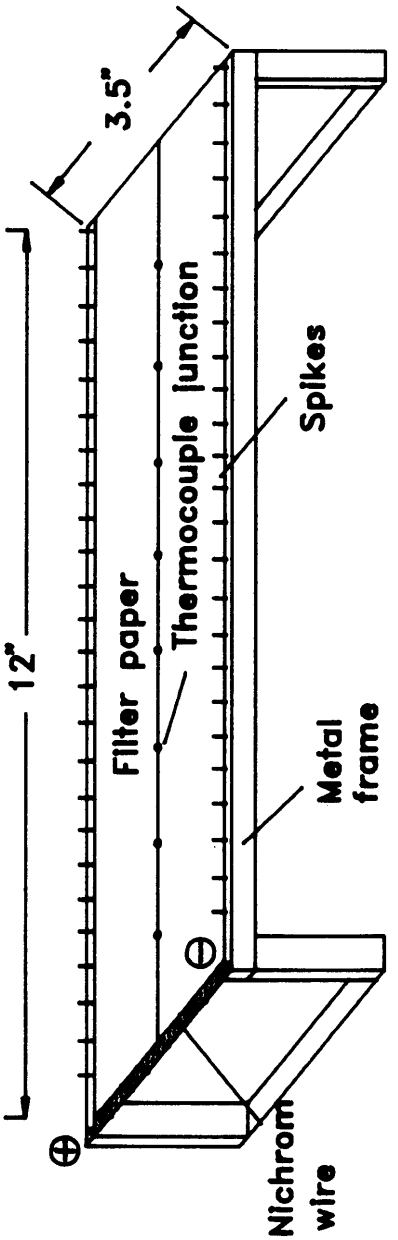

Fig. 2.8 Thermally thin fuel (PMMA) arrangemω

due to the relative motion of the source and receiver. The same principle can be conveniently extended to the case where the frequency shift is produced by the movement of an intermediate inert object through which wave motion is transferred from a source to a receiver. This is the usual situation in laser Doppler measurements of flow velocity.

The Doppler shift derivation can be seen from Fig. 2.9(a). To perform this calculation rigorously, it is necessary to use the relativistic transformation formulae of space and time coordinates from one observer to another moving with constant relative velocity. From [11] it is shown that the frequency detected by the receiver moving at a velocity v relative to the source is

$$\nu' = \frac{\nu}{\sqrt{1 - v^2/c^2}} \left(1 + \frac{v}{c} \cos\theta\right) \tag{2.1}$$

where c is the light speed and θ is the angle of the relative velocity.

And the difference of the frequencies is

$$\Delta\nu = \nu' - \nu = \nu \left(\frac{1 + (v/c)\cos\theta}{\sqrt{1 - v^2/c^2}} - 1\right) \tag{2.2}$$

which can be approximated to

$$\Delta\nu = \nu' - \nu = \nu \frac{v}{c} \cos\theta \tag{2.3}$$

for non-relativistic case ($v << c$).

In laser Doppler velocity measurements, the mainly concerned is the

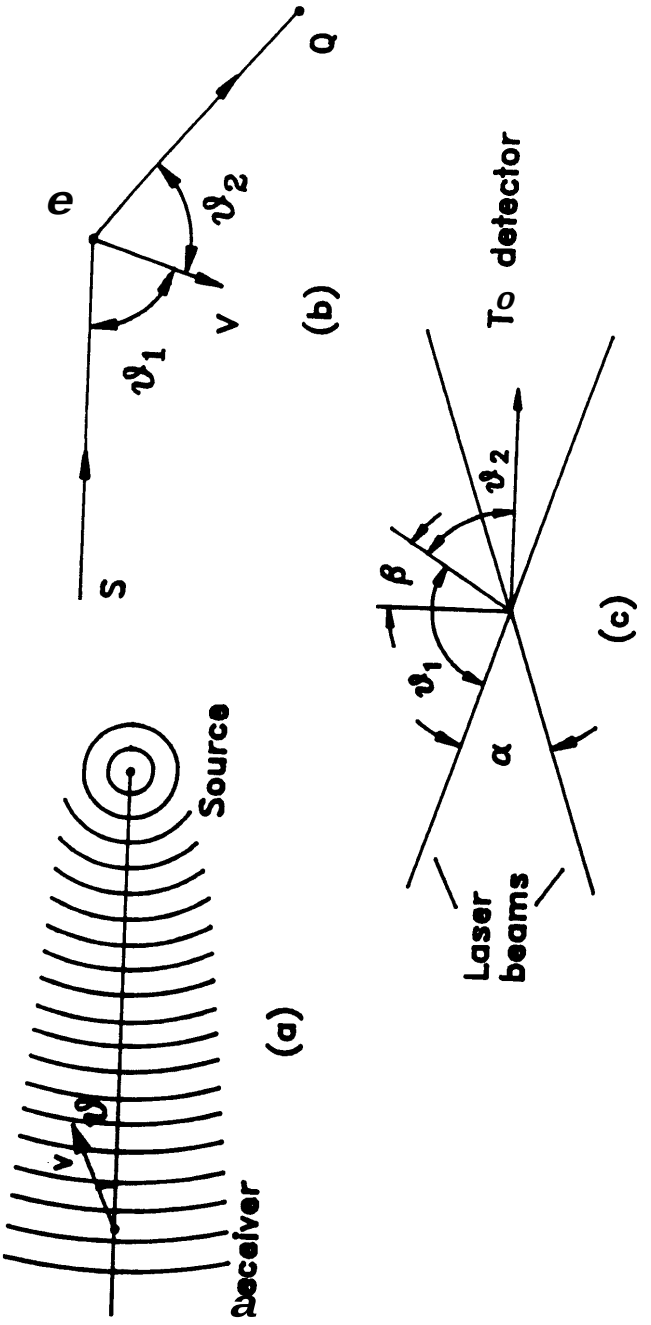

Fig. 2.9 Schematic of Doppler principles.

frequency shift of light scattered from a moving object while the source and the observer being relatively stationary to each other. This may be considered as a double Doppler shift [12], from the source to the moving object and then from the object to the observer. In Fig. 2.9(b) a light wave comes from a source S and is scattered by a moving object P, and the scattered light then is observed at Q. From Eq. (2.1), the frequency observed by P is

$$\nu' = \frac{\nu}{\sqrt{1 - v^2/c^2}} \left(1 + \frac{v}{c} \cos\theta_1\right) \tag{2.4}$$

Light of this frequency is re-emitted by P and received at Q as

$$\nu'' = \frac{\nu \sqrt{1 - v^2/c^2}}{1 - (v/c) \cos\theta_2} \tag{2.5}$$

Thus,

$$\frac{\nu''}{\nu} = \frac{1 + (v/c) \cos\theta_1}{1 - (v/c) \cos\theta_2} \tag{2.6}$$

If the moving velocity of P is small compared to the light speed and α and β are defined as $\pi - (\theta_1 + \theta_2)$ and $(\theta_1 - \theta_2)$, respectively, we have

$$\begin{aligned} \Delta\nu = \nu'' - \nu &= \frac{v\nu}{c}(\cos\theta_1 + \cos\theta_2) \\ &= \frac{2v\nu}{c}(\cos\theta_1 + \cos\theta_2) \\ &= \frac{2v\nu}{c} \cos\beta \sin\frac{\alpha}{2} \end{aligned} \tag{2.7}$$

It is shown that the Doppler shift depends on the sine of the half the angle of scattering and on $v\cos\beta$ which is the component of the moving velocity in the direction of the scattering vector. This formula is usually written in terms of wavelength:

$$\Delta v = \frac{2v}{\lambda} \cos\beta \, Sin\frac{a}{2} \qquad (2.8)$$

If the Doppler shift is large enough it is possible to detect and measure the shift frequency directly with a conventional spectrometer of high resolution. However, in most LDV applications, the Doppler shift frequencies are usually in the range of 10 kHz to 10 Mhz which are beyond the resolution of conventional optical spectrometer and not suited for direct measurements [13]. Therefore, most laser Doppler measurements have to make use of the technique called optical beating or interference in one form or another. Heterodying or time-dependent interference of two optical beams describe the phenomena in which two signals with close frequencies f_1 and f_2 are added to give the resulting signal which has a wave front amplitude modulated at $(f_1 - f_2)$ due to the alternating constructive and destructive interference of the two signals. This new wave front has much smaller frequency which can be easily detected by conventional electronic devices.

The differential doppler or duel beam technique is employed in this study, which means that the optical beating takes place between two beams scattered at different directions. The beat signal has a frequency equal to the difference between the two Doppler shifts generated by two beams scattered at different angles. As

shown in Fig. 2.9(c), the scattering volume is illuminated simultaneously by two focused beams of similar intensity and inclined at an angle a. The scattered light is observed in a third direction. The Doppler shifts on scattering to the detector from the two beams are given by:

$$\Delta \nu = \frac{v \nu}{c} (\cos\theta_1 + \cos\theta_2) \tag{2.9}$$

and

$$\Delta \nu' = \frac{v \nu}{c} (\cos\theta_1' + \cos\theta_2) \tag{2.10}$$

Thus, the difference frequency f, observed by the detector is

$$\begin{aligned} f = A\nu - \Delta\nu' &= \frac{v \nu}{c}(\cos\theta_1 - \cos\theta_1') \\ &= \frac{v}{\lambda} \sin\frac{\alpha}{2} \cos\beta \end{aligned} \tag{2.11}$$

where $\alpha = (\theta_1' \cdot \theta_2)$, the angle between the illuminating beams and $\beta = (\theta_1 + \theta_2 - \pi)/2$, the angle the direction of motion makes with the normal to the bisector of the beams. For the measurements in this study β is set at 90 degrees. Eq. (2.11) demonstrates that the dual beam Doppler frequency is linearly proportional to the particle velocity and the sine of the half angle. It is important to note that the interference frequency is independent of the direction of reception, which makes it possible to use a large aperture without reducing resolution. This LDV mode is particularly suitable for the measurements in gas flows where low particle concentrations are usually expected.

2.4.2 Laser and Optical System

The LDV optical arrangement can be seen in Fig. 2.10. An argon-ion laser is used to provide the coherent light source for the LDV system. The laser made by Spectra-Physics (Model 165) has a maximum power output of 1 watt and the main wavelengths are 448.0 and 514.5 nm. For the experiments in this work the laser is operated at the power output of 0.2 watts and the wavelength of 488.0 nm.

The transmitting optics can be divided into two main parts:

(1) A prism type beamsplitter with equal optical path-lengths for each beam. It splits the incoming laser beam into two parallel beams each of which is 25 mm from the entering beam and has equal intensity.

(2) A cemented doublet achromats with dielectric, multi-layered and anti-reflective coatings. It brings two out-going beams from the beamsplitter to its focal point. The focus length of the transmitting lens is 600 mm and the half angle of the two crossing beams is 2.45 degrees. The resulting probe volume is also shown in Fig. 2.10 and has 64 fringes with 6.27 μm in spacing. The length and diameter of the measuring volume are 1.96 mm and 0.39 mm, respectively.

The beamsplitter and the transmitting lens are supported with two rotating mounts which enable the whole assembly to rotate 360 degrees continuously.

The optical collecting system also consists of two parts:

(1) A transmitting lens with a focal length of 250 mm which collects the optical signals and brings them to the receiving assembly.

(2) A receiving assembly made of a series of lens which focuses the collimated

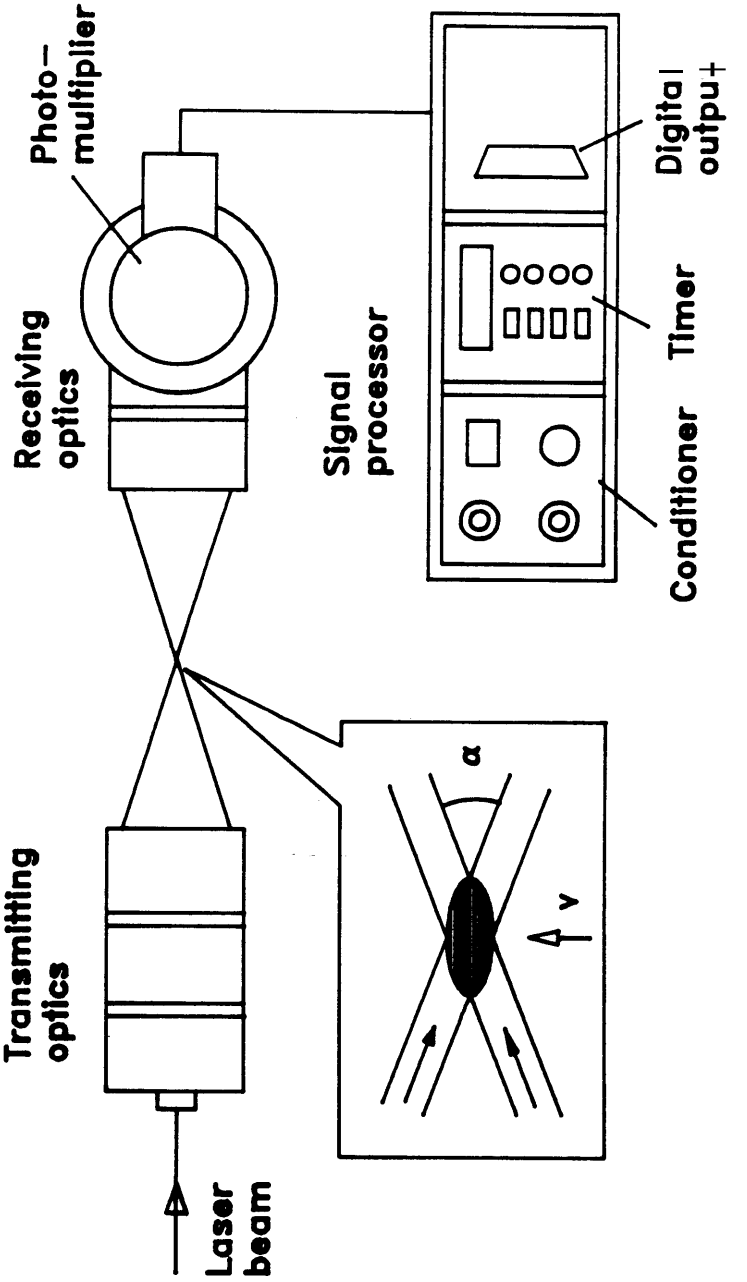

Fig. 2.10 Schematic of LDV system and probing volume.

light from the collecting lens onto the photodetector aperture which is mounted directly in the optics assembly for on-axis back-scattering. The adjustable focal length of the assembly provides a relatively easy means for adjusting and aligning the LDV system. The quality of alignment can be examined through an eyepiece (a x7 magnifier) by viewing the focused scattered light through the receiving unit.

A photomultipiler is firmly attached to the receiving assembly. The photodetector system has high quantum efficiency, and the side window configuration of the device makes the alignment convenient.

The entire optical system is carefully aligned and rigidly mounted on the optical tables. All the supporting optical components used in the experiments are made by TSI.

2.43 Signal Processor

The raw voltage signals from the photomultiplier are transmitted to the data processor where they can be read and processed. Due to the very intermittent nature of LDV signals in applications to gas flows, counter type data processor is selected in this study to measure individual burst of LDV signal on a particle-by-particle basis over a relatively large range of particle concentrations and flow conditions. The basic principle governing the counting technique is for the processor to measure the time for either a fixed number or for a complete burst (variable number of doppler cycles) from which the particle velocity (i.e. the flow velocity) can be deduced with the additional information of the cycle number and the fringe spacing. The diagram

in Fig. 2.11 shows the simplified version of this process [14]. A raw LDV signal is filtered to eliminate the low frequency pedestal and a symmetrical signal is generated. Then the filtered signal enters a Schmitt trigger which converts the input frequency signal above a certain amplitude into a square wave. The resulting square wave is timed against a high speed clock and the time duration for a certain number of squares to pass is measured. The frequency, therefore, can be calculated simply as

$$f = \frac{N}{\Delta t} \qquad (2.12)$$

where f is the Doppler frequency, N is the cycle number and At is the time duration measured.

The data processor used is made by TSI (Model 1980) which operates with a timer of 1 nanosecond resolution. The manual 8 cycle counter mode of the data processor is applied for most experiments.

The LDV signals and the sampling data rates are also continuously monitored on a Hitachi V-352 oscilloscope and a Fluke 1910A multicounter during the experiments.

2.4.4 LDV Seeding

The LDV technique relies on the presence of suitable particles in the flow which produce the necessary amount of scattered light for frequency measurements. The basic requirements for choosing scattering particles are that they

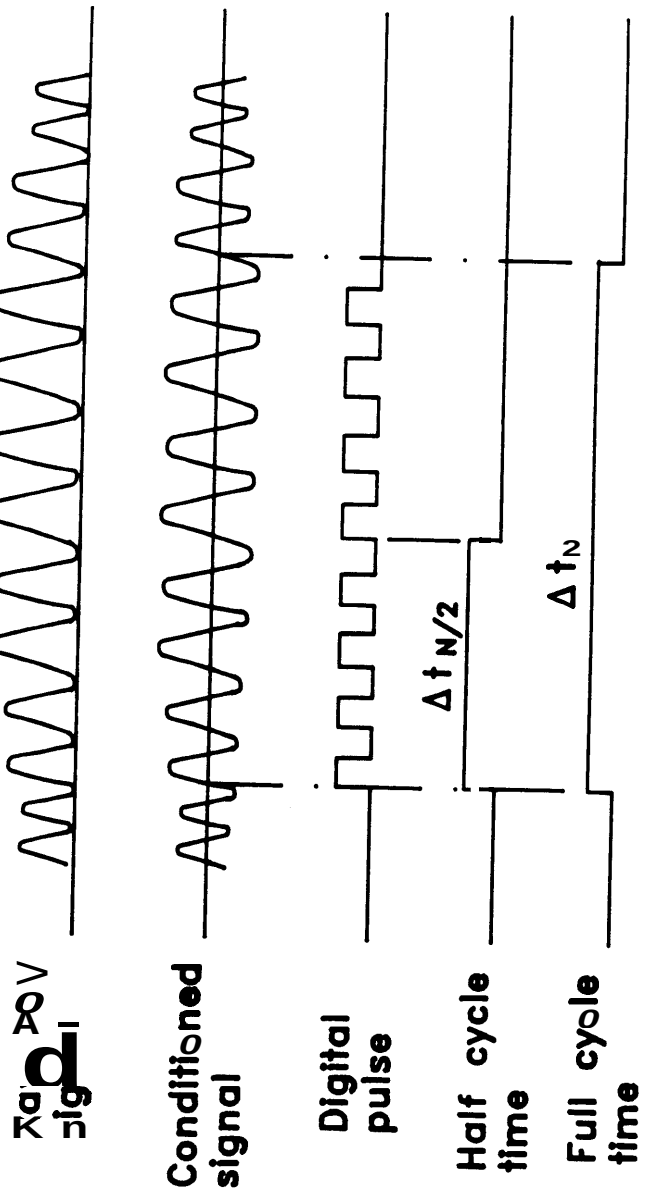

Fig. 2.11 Schematic of LDV signal processing.

(1) follow the flow sufficiently close and make least disturbance to the flow.

(2) scatter enough light to give an acceptable signal to noise ratio from the detector under the conditions of the experiments.

Other factors such as the type of fluid problem being studied, the velocity fluctuations expected and the data collecting technique used also affect the selection of the particle type [13]. Based on these criteria, aluminum oxide power manufactured by Union Carbide is used as the flow marker. The powder particles are 0.3μm in diameter.

The seeding system can be seen in Fig. 2.12. Filtered air flow from the centralized compressor is used to drive the alumina powder stored in a cylindrical container. The air flow is introduced to the particle container through a nozzle connected to its side wall and a swirling flow is generated inside the container. The bottom half of the container is filled with the fine alumina powder and the small particles are forced by the circular flow to gush through an opening on the top cover of the seeding chamber. The air flow carrying small particles then passes through the particle distributer inserted to the mixing chamber of the wind tunnel. The particle distributor is made of a circular brass tube 7 inch long and 1/2 inch in diameter with 12 holes (1/12 inch in diameter) evenly spaced on its side. The holes on the distributor are positioned to face the main air flow in the wind tunnel in order to create a better mixing of the particles and the main flow in the mixing chamber. The air flow used to carry the particles accounts for less than 10% of the total flow in most cases.

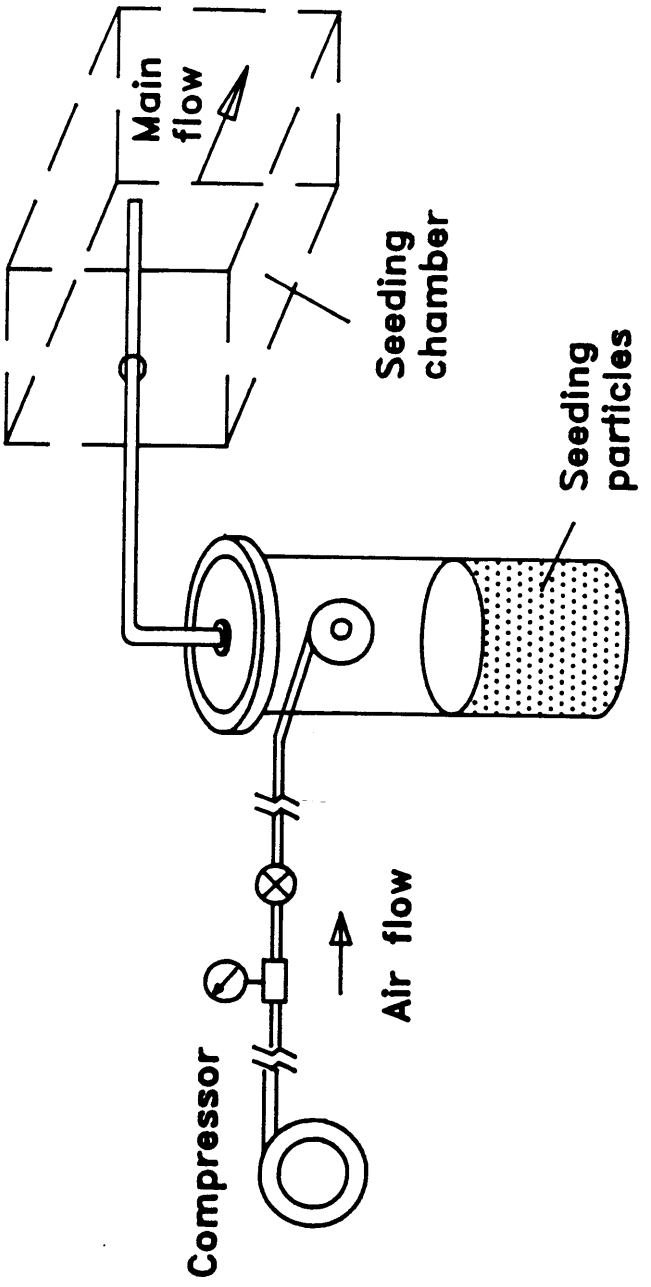

Fig. 2.12 Schematic of LDV seeding system.

2.5 Interferometer

A Mach-Zehnder interferometer is set up for the opposed flow flame spread experiments. The schematic diagram in Fig. 2.13 illustrates the optical layout. The argon-ion laser for the LDV system is also used here to provide a coherent light beam at wavelength 488 nm for the interferometer. An optical splitter plate S_1 permits half of the light to be transmitted to mirror M_2 while reflecting the other half toward the mirror M_1. Two beams are expanded and collimated with a set of lenses The test beam passes through the test section while the reference beam travels an alternative path of approximately equal length. The two beams are brought together again by means of another splitter plate S_2 and eventually focused on a camera. The optical length difference of the two beams is proportional to the difference of the refractive index of the test and the reference path. The relationship between the optical length and the gas density can be proved as following [15]:

$$\Delta L = C \Delta T \tag{2.13}$$

where L is the optical length, T is gas temperature and C is a constant. Therefore, the resulting interferograms should indicate the temperature variations in the test region. The collimated beam going through the test zone has a circular shape of 2 inch in diameter. The lenses L_1, L_2 and L_3 have focal lengths of -200 mm, 600 mm and 300 mm, respectively.

2.6 Schlieren Photography

A schematic of Schlieren system used in concurrent experiments is shown in

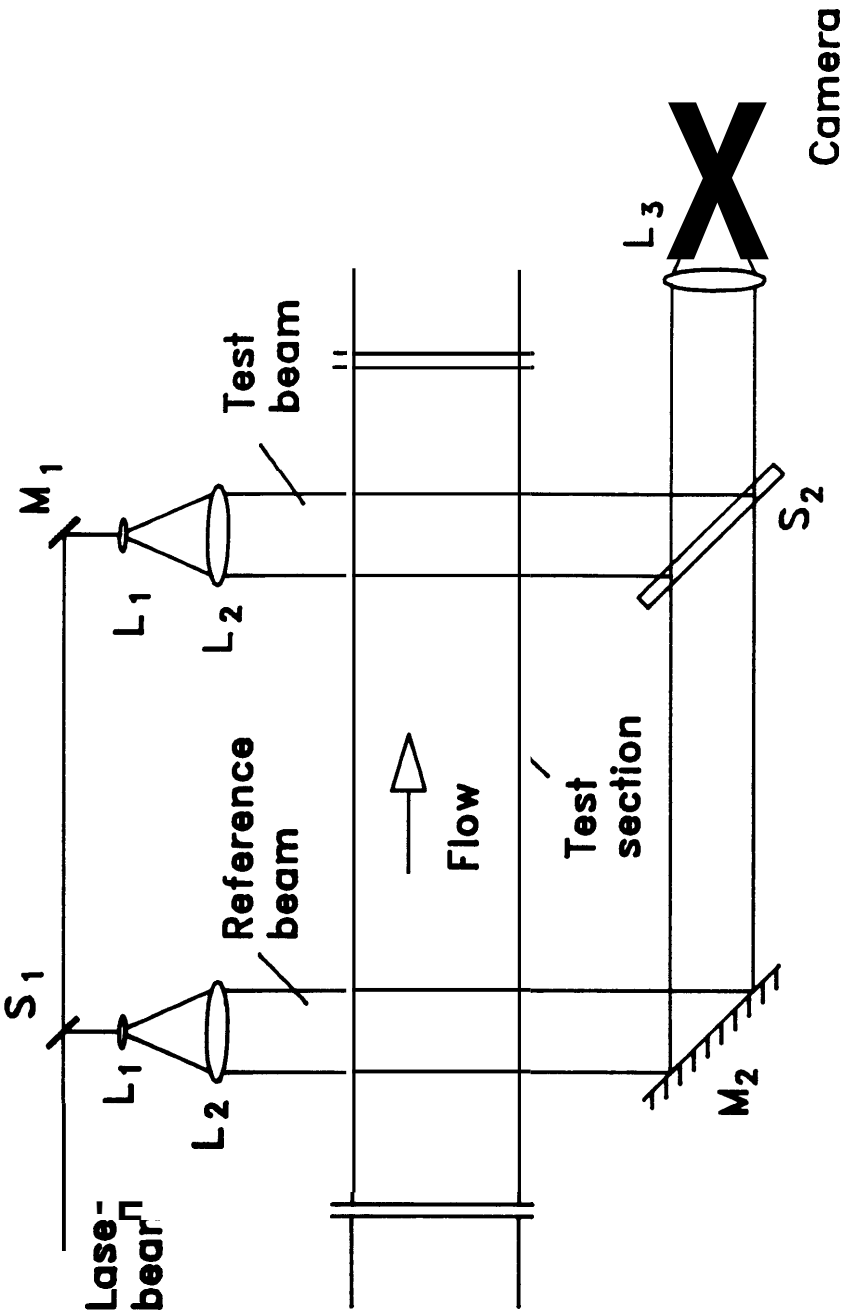

Fig. 2.13 Schematic of interferometer.

Fig. 2.14. A tungsten lamp is used to provide the uniform white light source through a slit opening. A condenser lens with a focal length of 40 mm is placed in front of the light source to focus the light onto the focal plane of the first spherical mirror SM_1. Mirrors M_1 and M_2 are used to reduce the space the Schlieren system occupies. Both spherical mirrors are 0.508 m in diameter and have focal lengths of 3.96 m. The angles of tilt of both mirrors are about 10 degrees. The first mirror is placed 4.12 m from the center plane of the diffusion flame while the second one is 4.17 m away. The collimated light beam has a circular shape with a diameter of 0.45 m.

A knife edge is placed on the focal plane of the second spherical mirror. Both rectangular and circular knife edges are tested for the experiments. The rectangular knife edge is made of a razor blade and the circular one is an adjustable iris diaphragm. It is found that the rectangular knife edge results in higher resolution than the circular one mainly due to the horizontal configuration of the experiments.

A 35 mm SLR camera (Nikon FM) is used to record the still Schlieren images and interferograms, and both black and white films (Kodak Tri-x 400) and color slide films (Kodak Ektachrome 160) are used. Various shutter speeds are tested to obtain the sharpest resolution possible and it is found that 1/500 second gives the best result. Also used is a Sony f99 video camcorder which records continuous Schlieren images of reacting flows.

2.7 Flame Spread Rate and Mass Burning Rate Measurements

Flame spread rates can be calculated from the solid fuel surface temperature

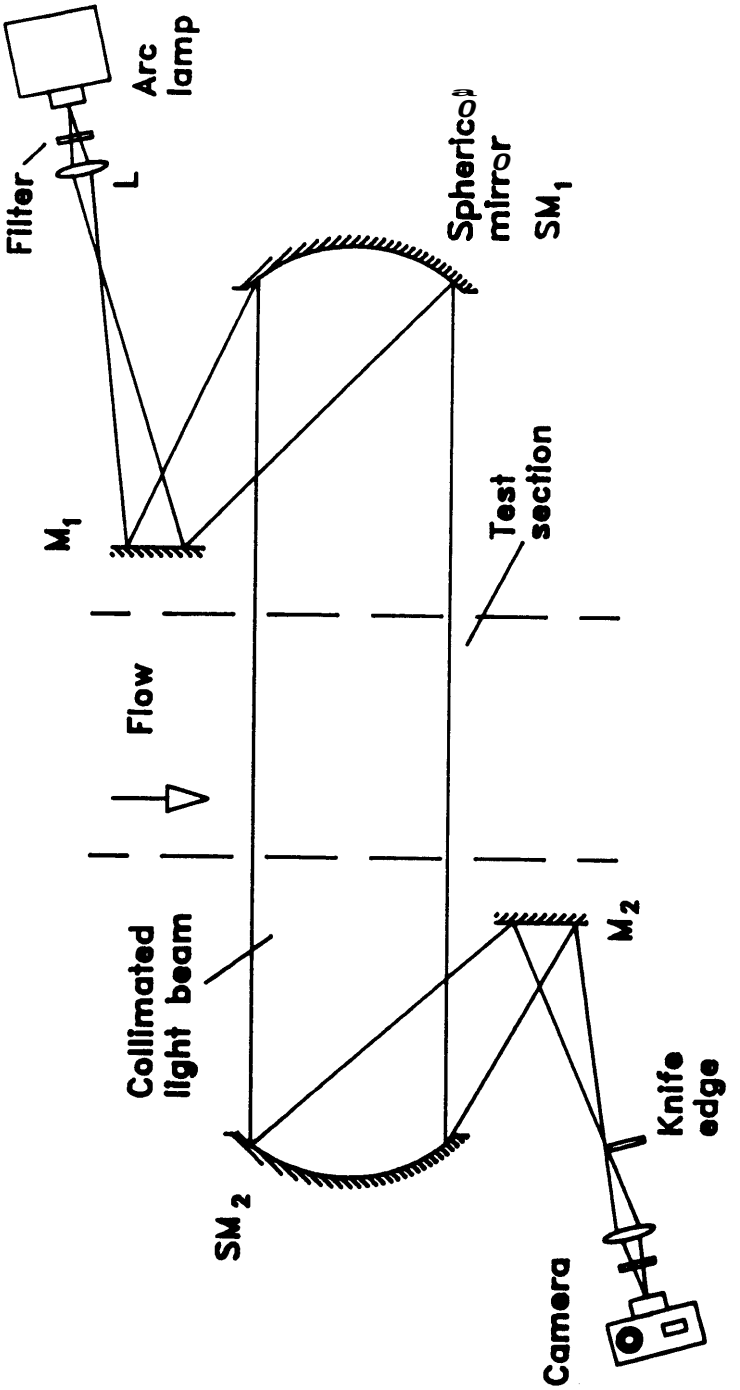

Fig. 2.14 Schematic of Schlieren setup.

histories measured at eight locations on the fuel surface, as shown in Fig. 2.15. K-type thermocouples made of 0.03 inch diameter columel and alumel wires are used with their junction beads carefully soldered flush on the fuel sheet surface, as shown in Fig. 2.4. The distance between two neighboring thermocouples is 31.5 mm. It is assumed that the time when the surface temperature is raised to the pyrolysis temperature corresponds the arrival of the flame front. The time duration for two consecutive thermocouples to reach the pyrosis temperature can be deduced from the surface temperature history. The flame spread rate can then be calculated from the time duration and the known distance between the two locations. The voltage output of the thermocouples is amplified with a universal analog input sub-multiplixer (Model EXP-16) made by Metrabyte with an automatic cold-junction compensation. The gain of multiplixer is set at 100 for all the tests. The amplified analog signals are then sent to a high speed A/D converter and timer counter interface (Model DASH-8) and converted to digital signals which can be processed further by the IBM-PC AT computer. The maximum data processing rate of DASH-8 is 4000 sample/sec. For slow flame spread process as observed in most opposed flow cases, the flame spread rate can also be determined by visual observation of the pyrolysis front and recording the time of flame front arrival manually with a stop watch.

For the mass burning experiments, the combustion is kept for an extra amount of time after the flame has spread over the fuel surface. After a burning test has finished, the burnt sample is cut into half along the longitudinal line and its surface is slightly smoothed for a uniform thickness measurement. Then the solid fuel

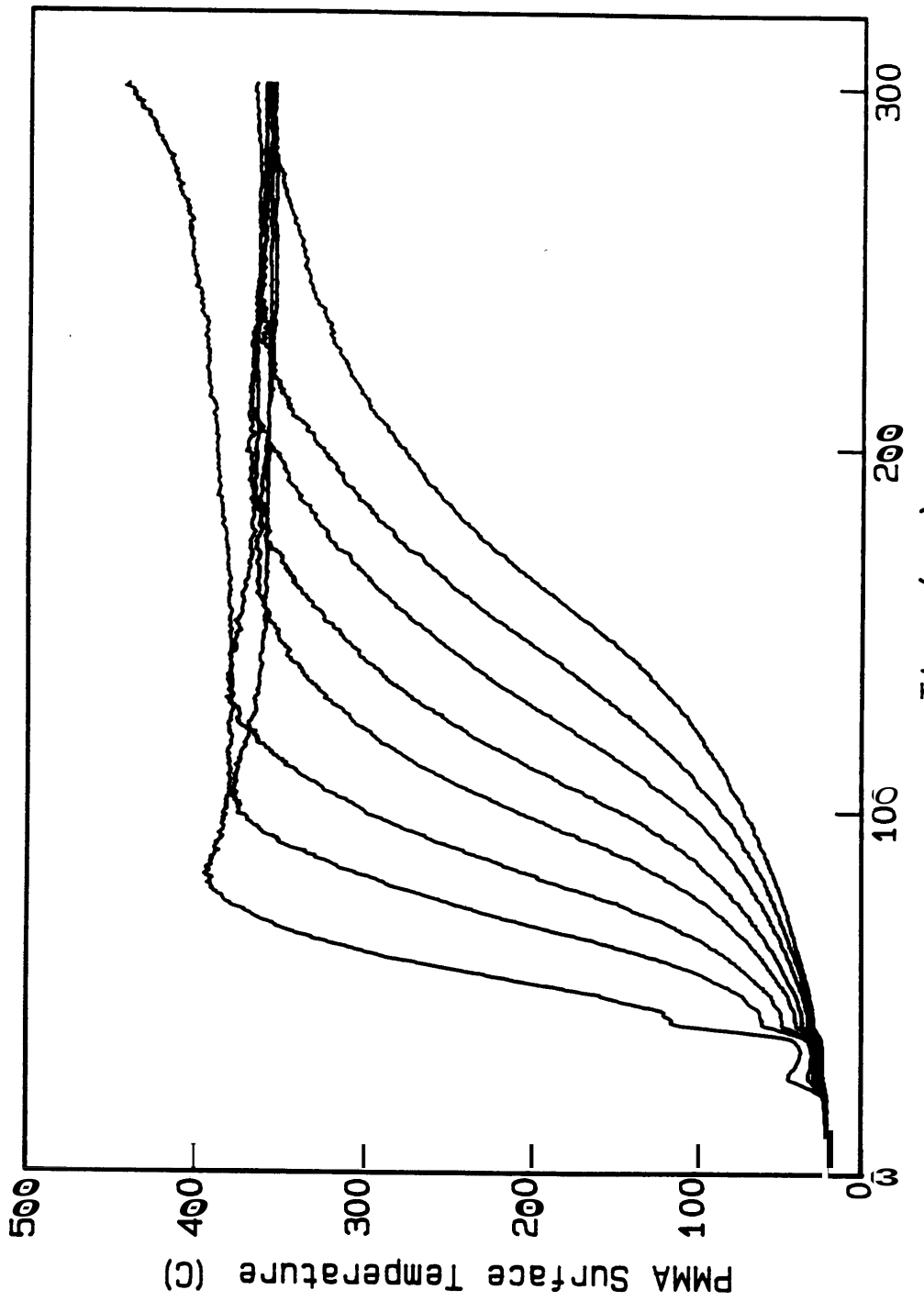

Fig. 2.15 Thermocouple measurements of PMMA surface temperature histories.

thickness is measured at the positions along the center line. The fuel surface regression rate is calculated by dividing the sample sheet thickness difference before and after the burning by the effective burning time that can be obtained from the surface temperature histones by subtracting the time of pyrolysis front arrival from the total burning time.

2.8 Gas Concentration Analysis

The exhaust gas collecting and analyzing system includes an oxygen analyzer, four infrared gas analyzers for CO, CO_2, NO and unburnt hydrocarbons, a sampling probe and necessary plumbing as shown in Fig. 2.17.

The oxygen content is measured with a Beckman OM-11 Oxygen Analyzer which consists of a pickup head containing a polarographic oxygen sensor and a console with the major portion of the controls and electronics. The oxygen sensor is made of a gold cathode 0.04 inch in diameter and a silver anode. These two electrodes are mounted behind a permeable membrane which permeates diffusion of oxygen for the measurement. In operation, a polarizing voltage is applied between the two electrodes and the resultant current flow is directly proportional to the oxygen partial pressure to which the sensor is exposed.

Other major species, CO, CO_2, NO and unburnt hydrocarbons, in the exhaust gas are measured with non-dispersive infrared gas analyzers made by Horiba (Model AIA-21). Based on the principle of infrared absorption, the instrument *can* continuously measure the concentrations of the components in a sample stream. A

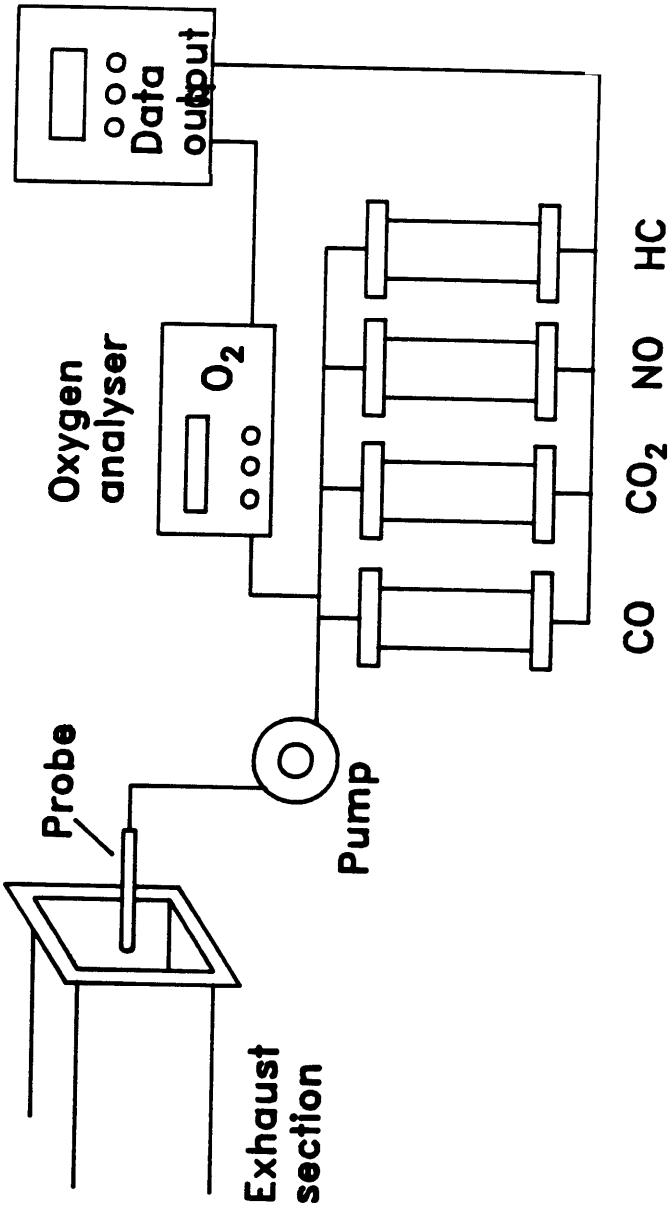

Fig. 2.16 Schematic of gas analysis arrangement.

sample cell and a reference cell filled with non-absorptive gas are arranged in parallel and two infrared beams from dual collimated light sources pass through the cells. The portion of the infrared radiation absorbed is proportional to the concentration of the species being tested in the sample cell [16]. The intensity difference between the sample beam and the reference beam after passing gas cells are measured and then converted to the concentration data.

A sampling probe made of 1/4 inch diameter aluminum tube is inserted to the exhaust section and a pump are used to supply the continuous exhaust gas flow to the analyzers. A series of tests are performed to determine the optimum shapes and positions of the mixing plates in the exhaust section in order to produce a uniform spatial distribution of the gas concentrations.

2 3 Data-acquisition and Test-control Software

A data-acquisition and test-control software has been developed in C especially for this study to accommodate the need of instantaneous velocity and temperature measurements and flow field mapping. The programs are written in menu-driven style for IBM-PC AT computer and most features are self-explaining. The main programs are listed in Appendix and their principle functions are described below as to:

(1) Convert digital signals of the Doppler shift frequency from the LDV counter processor to instantaneous velocity values, and then compute flow mean velocity and turbulence intensity. The digital signals from the data processor are

transferred through a regular 36-pin parallel interface which includes 12 bits for Mantissa, 4 bits for exponent, 1 bit for data ready signal and other bits for cycles and burst information. For N-cycle processor mode, the Doppler frequency can be calculated according to

$$f = \frac{N_c \times 10^9}{D_m \times 2^{n-2}} \tag{2.14}$$

where f = Doppler shift frequency

N_c = number of cycles measured

D_m = mantissa of digital word

n = exponent of digital word

And the flow velocity can be calculated as

$$U = \frac{f \lambda}{2 \sin(\alpha/2)} \tag{2.15}$$

where U = flow velocity

λ = laser beam wavelength

α = angle of laser beam intersection (dual beam system)

A large number of velocity samples (usually at about 5000) are measured in order to obtain the mean flow velocity and the corresponding turbulence intensity at one point which are calculated according to the statistical formula listed below:

$$\bar{U} = \frac{\sum_{i=1}^{N} U_i}{N} \tag{2.16}$$

and

$$u' = \left(\sum_{i=1}^{N} \frac{U_i^2 - \bar{U}^2}{N} \right)^{\frac{1}{2}} \qquad (2.17)$$

where N is the total sample number.

The sampling rate of flow velocity depends on many parameters such as flow conditions, particle density in the measuring volume, probing position, etc., which make the data rate vary from time to time. The average velocity sampling rate is around 4 kHz and it usually takes approximately 5 seconds to finish the entire process of taking data and performing necessary calculations.

(2) Scan thermocouples at a variable rate and convert analog voltage signals to temperature data. An input signal from a thermocouple is received through DASH-8 interface board and compared with a temperature conversion table residing inside the program, and then the correspondent temperature is calculated taking account of the cold junction temperature. The same procedure is repeated for the next thermocouple until all the temperatures have been measured. In most experiments, eight thermocouples are read in each scan and the scan rate is usually set at 1 Hz even though it could be made as high as 250 Hz by using the time counters on DASH-8 board.

The temperature measurements can be coupled with the flow velocity measurements. In this case the mean flow velocity and flow turbulence are determined first, and then a scan of thermocouples is performed. The Same procedure is repeated throughout the entire experiment. Since the measurement of

flow parameters usually takes longer time than that of temperatures the sampling rate of the whole process mainly depends on the flow measurement speed.

(3) Control the stepping motors installed in the moving table in order to move the wind tunnel and the test section precisely in all three directions. The communication between the motors and the computer is conducted through a regular 24 bit parallel digital 1/0 interface (Metrabyte Model PIO 12). A sequence of high and low voltage signals are sent from the computer to the motor control unit at a suitable speed and transferred to the step-by-step motion of the stepping motors. The tolerance of the test section movement in all three directions is less than 0.2 mm. The moving speed of the test section can be changed and is usually kept at 1 mm/sec. This feature of the software is mostly used to combine with LDV measuring capability to map the flow fields.

The program also provides other functions such as monitoring test results on the computer screen, saving data files, plotting and listing the data and performing PDF analysis for velocity data, etc. Extensive use has been made of the C graphics library for a convenient operation of the program.

2.10 Flow Fields

The control of the flow velocity in the test section is a relatively easy task, compared to the maintenance of a reasonably stable flow turbulence level. A common way to create a turbulent flow is to increase the flow velocity, and therefore, generate turbulence in the flow with strong shear stress. Most turbulence studies in

fluid mechanics have been conducted under such conditions. Following the development in fluid mechanics, much effort has been made to study shear-generated turbulent combustion as well.

An alternative way to generate a turbulent flow is by means of placing obstacles such as grids or perforated plates in the flow and introduce strong disturbance to the flow [17] [18]. Some studies [19] [20] have utilized this method to study turbulent combustion. The grid-generated turbulence has nearly homogeneous and isotropic distribution in the flow [21] - [23], which makes it much easier to control and categorize the flow turbulence. Relatively large turbulence level can be obtained in slow speed flows as well. The homogeneous and isotropic characteristics of this type of turbulence can also provide experimental data that are easy to be compared with the results from computational models.

Based on the merits of the grid-generated turbulence and the practical limitations of the test facility used in the present study, the grid method is chosen to provide an adjustable turbulent flow environment for the flame spread and mass burning tests. Extensive measurements have been made to map the flow velocity and turbulence intensity distributions in the test section for the determination of flow characteristics and the selection of the suitable flow conditions for the experiments. The major effort has been focused on the measurements in the non-reacting flow since it is more convenient to characterize the flow fields of cold flows. In this section the flow velocity and turbulence intensity profiles at U = 2 m/sec are discussed to present the flow field characteristics.

2.10.1 Axial Distribution

2.10.1.2 Velocity

Fig. 2.17, 2.18 and 2.19 show the axial flow velocity and local turbulence intensity for U = 2 m/sec with turbulence levels of u'/U = 1.1%, 5.5% and 19.8%. The measurements are made along the longitudinal centerline of the test section with an interval of 10 mm. For flows with low turbulence intensities, the mean velocity distribution displays quite stable features and maintains almost a constant along the distance downstream, which can be seen in the cases of Fig. 2.17 and 2.18. For flows with higher turbulence levels such as the one shown in Fig. 2.19, the mean flow velocity exhibits some fluctuating characteristics along the centerline, which is apparently caused by the more chaotic flow motion in high turbulence case.

2.10.2.2 Turbulence Intensity

Due to the nature of flows with low velocity such as ones used in this study, the weak shear stress in the flow does not generate much turbulence, and therefore, the artificially introduced turbulence by perforated plates can not be sustained at a constant level. The turbulence intensity decays inevitably as the flow moves downstream as the result of energy dissipation [21] - [23]. A decaying turbulence intensity distribution could make it rather difficult to characterize the whole turbulence field with simple parameters. However, the decaying rate of the flow turbulence intensity is observed to be reasonably small over the length of fuel sheets used in the present study, and therefore, the practice of using a single parameter to

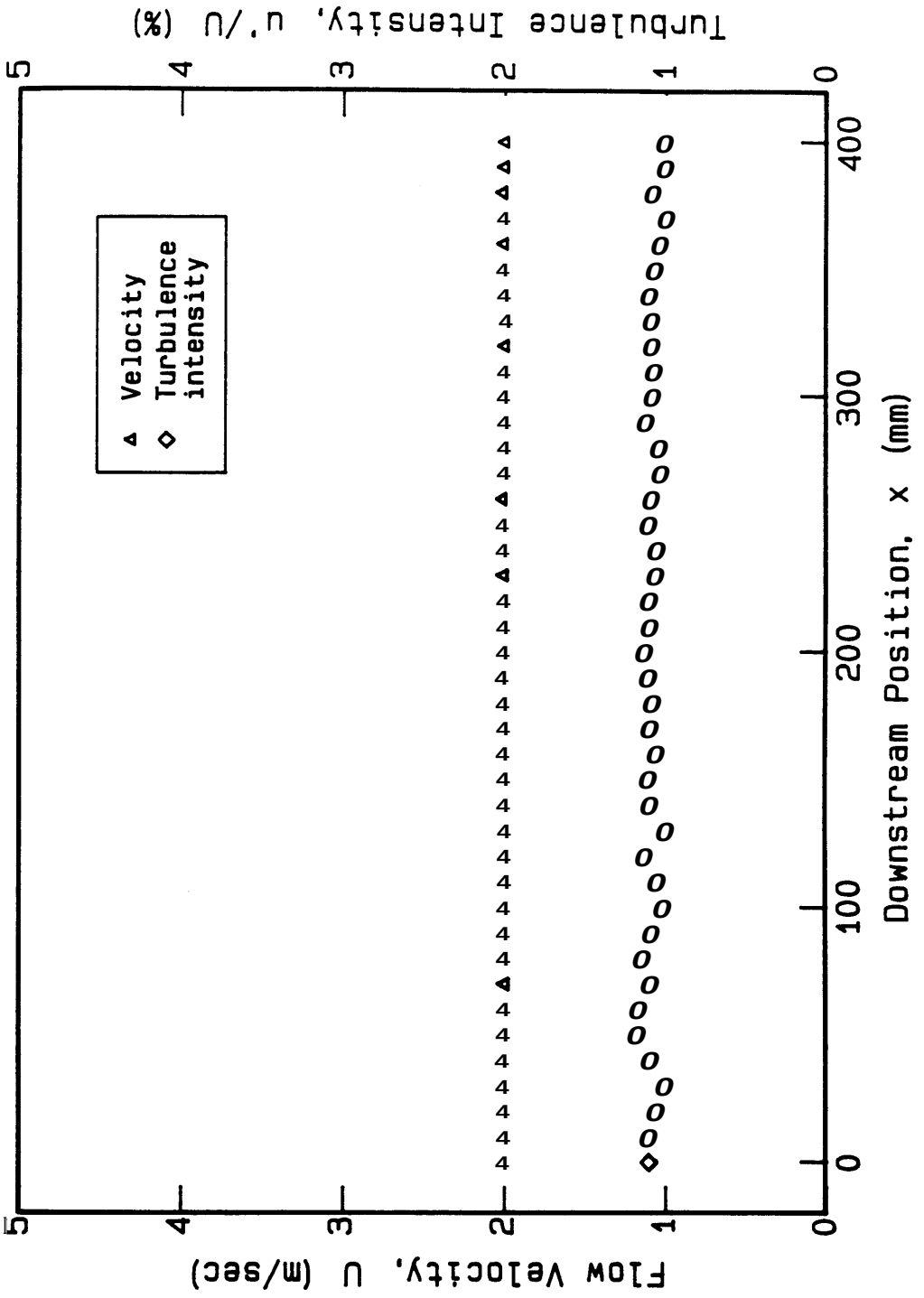

Fig. 2.17 Axial distribution of flow velocity and local turbulence intensity.

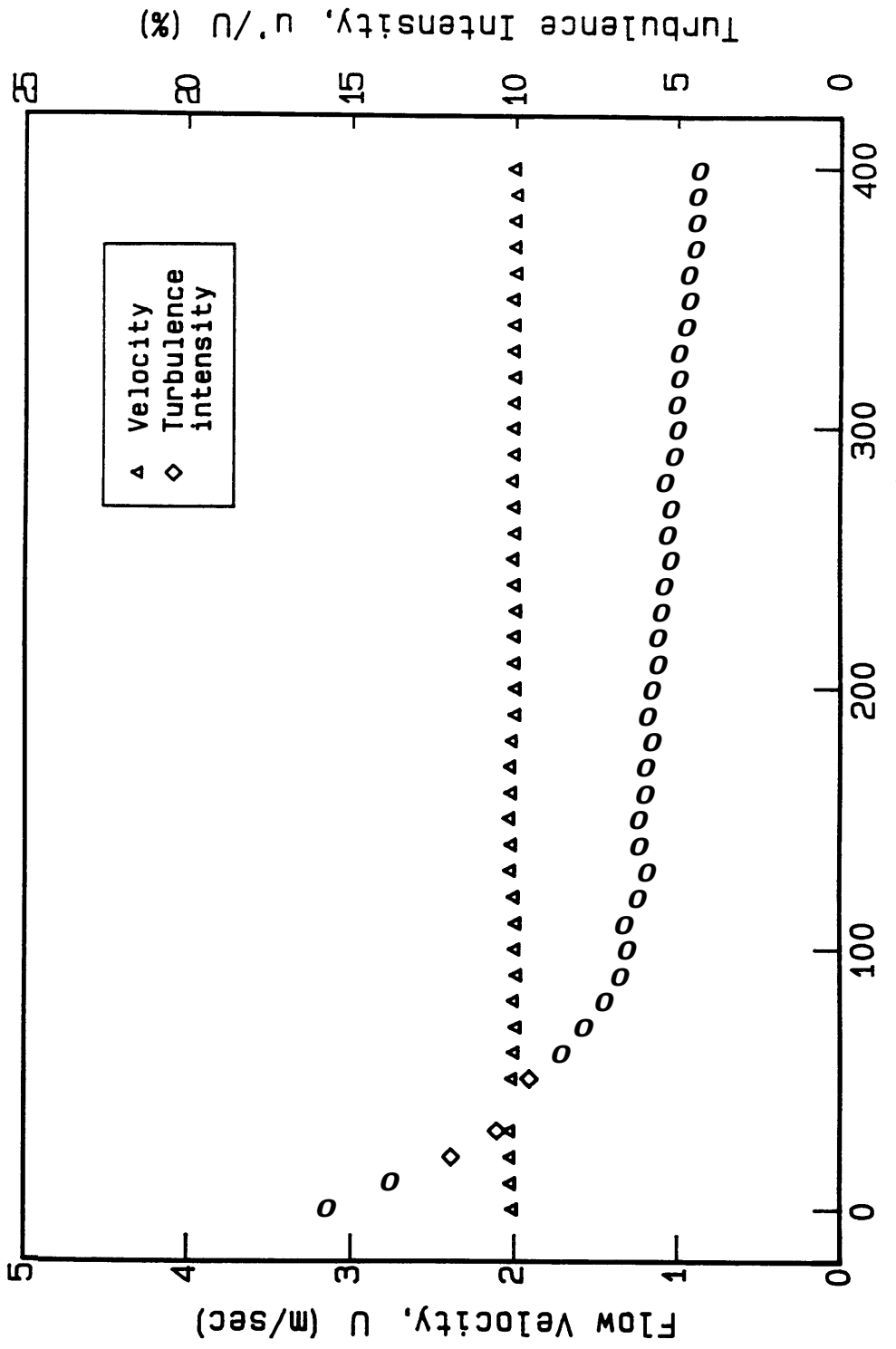

Fig. 2.18 Axial distribution of flow velocity and local turbulence intensity.

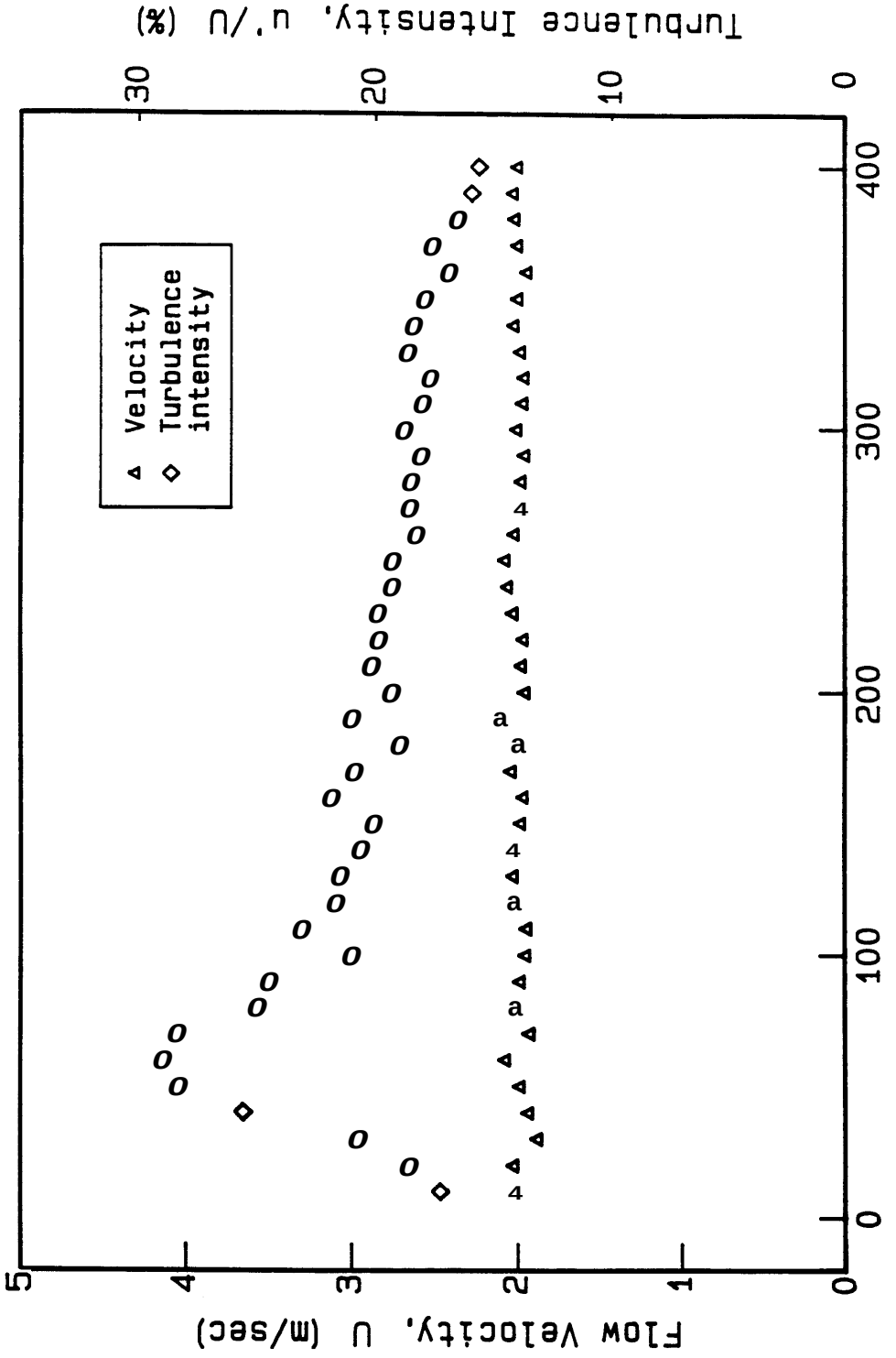

Fig. 2.19 Axial distribution of flow velocity and local turbulence intensity.

describe the turbulence intensity level is adopted for the current work.

As shown typically in Fig. 2.18, the longitudinal turbulence profile possesses a large value in the initial region where strong vortexes are created by the flow separation and subsequent mixing process taking place after the perforated plates. The flow turbulence level then experiences a rapidly decrease in a region about 100 mm long, and the actual length varies from case to case. The decaying rate levels off after the initial fast decreasing period and then becomes less prominent, as displayed in the figure, which results in a region where a relatively constant turbulence intensity can be observed. An average value of the turbulence intensity is calculated over this relatively stable region of approximately 250 mm in length.

In flows with high turbulence intensities, an interesting phenomenon as displayed in Fig. 2.19 is observed. The turbulence intensity increases first, and then reaches a peak as the downstream distance increases, unlike in the low turbulence cases where the turbulence intensity always decreases downstream. The turbulence peak value can be twice as large as that at the vicinity of the perforated plate. This phenomenon may be explained as the result of a more intensive mixing between the jet-like flows coming out of the holes of the perforated plate at a distance from the plate than at the proximity of the plate. Plates with higher blockage ratios are used to generate stronger disturbances, and therefore, the distances among exiting small "jets" are wider compared to that in the lower turbulence cases. It takes a certain distance for these small "jet" flows to meet and start mixing, and for the turbulent eddies to completely develop. After the peak region the turbulence profiles of high

turbulence flows show the similar decaying pattern as observed in the low turbulence flows: a sharply decreasing region followed by a relatively slow changing region.

For the flows with the lowest turbulence level of about 1%, the turbulence intensity maintains a quite uniform level throughout the whole test section, as shown in Fig. 2.17. This case can be considered as a laminar flow and the nearly constant turbulence intensity level through the test section is the combined result of dissipation, production of the flow and the possible disturbance caused by the walls of the test section.

2.10.2 Cross-section Distribution

Two typical profiles of horizontal mean flow velocity and turbulence intensity in the vertical direction are presented in Fig. 2.20 and 2.21 for U = 2 m/sec and the turbulence levels of 1.1% and 5.5%. The cross-section where the measurements are made is 150 mm downstream from the entrance of the test section. All the profiles exhibit similar characteristics which consist of a central plateau where a relatively constant value is observed, and boundary layer regions where sharper changes take place. The wall effect can be readily seen from these profiles as the flow velocity decrease rapidly to zero at the walls subjected to the "non-slip" condition. The local turbulence intensity is observed to increase as the profiles approach the walls. At the vicinity of a wall, the flow velocity approaches zero very fast and the turbulence velocity, u, decays at a slower pace, which causes the observed increase of the local turbulent intensity at the wall. It is seen that the flow velocity profile keeps a

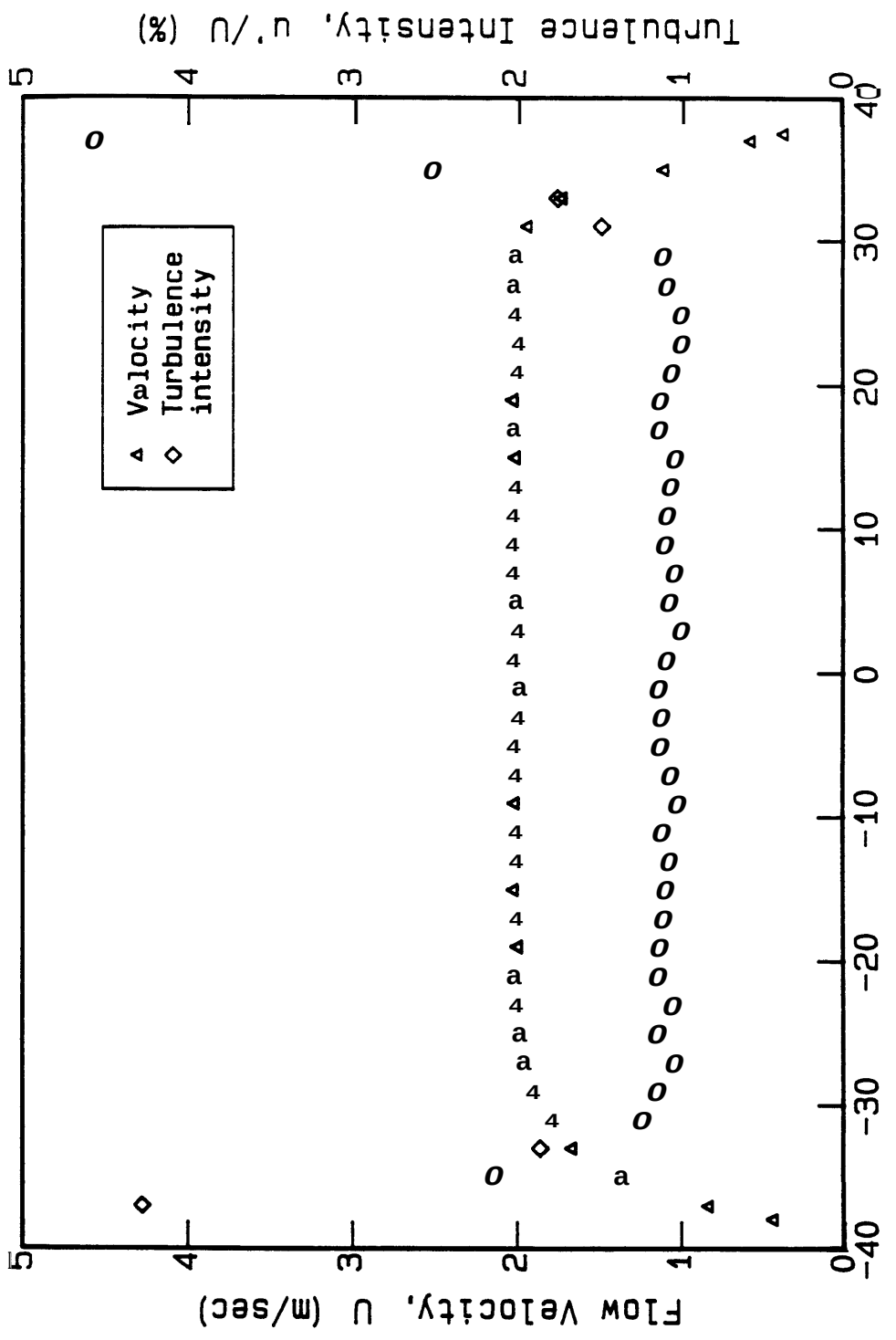

Fig. 2.20 Cross-section distribution of flow velocity and local turbulence intensity.

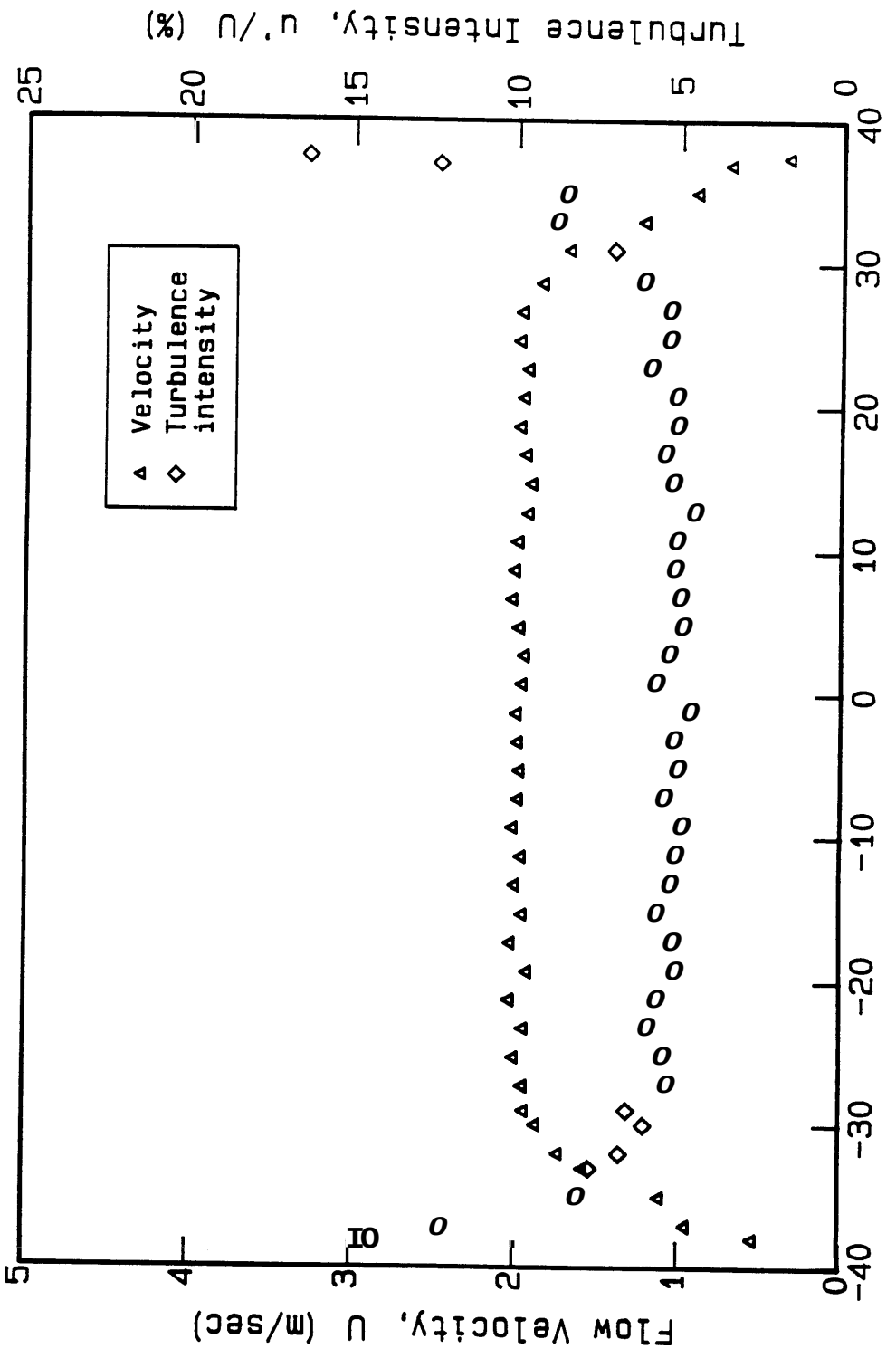

Fig. 2.21 Cross-section distribution of flow velocity and local turbulence intensity.

relatively smooth curve at low flow turbulence intensity and becomes less stable as the turbulence intensity increases. It is also found that the profiles have reasonably good symmetry about the center line which reduces the possible three-dimensional effect on the experiments.

The flow velocity and turbulence intensity profiles at U = 2 m/sec and u'/U = 1% in the azimuthal direction is displayed in Fig. 2.22. Similar characteristics are observed as in the vertical direction discussed above.

2.11 Error Analysis

2.11.1 Flame Spread Rate and Surface Regression Rate

Several factors can affect the accuracy of the flame spread rate measurements. Since the flame spread rates are deduced from the surface temperature histories, the error caused by the thermocouple measuring technique should be taken into account. K-type thermocouples are produce an errors less than 0.5% in the temperature range (0 to 500 C) in which the tests are conducted [24]. Therefore, the absolute error is about 2.5 degrees which is small enough to be neglected in the study. In most tests the flame front propagates quite evenly on the fuel surface, however, two-dimensional characteristics are observed in some cases. In those tests, the flame fronts are tilted to one side, which is possibly caused by uneven ignition or strong irregularities encountered in the flows with high turbulence intensity. The treatment of such a case is to discard its results and perform a substitute test under the same flow conditions.

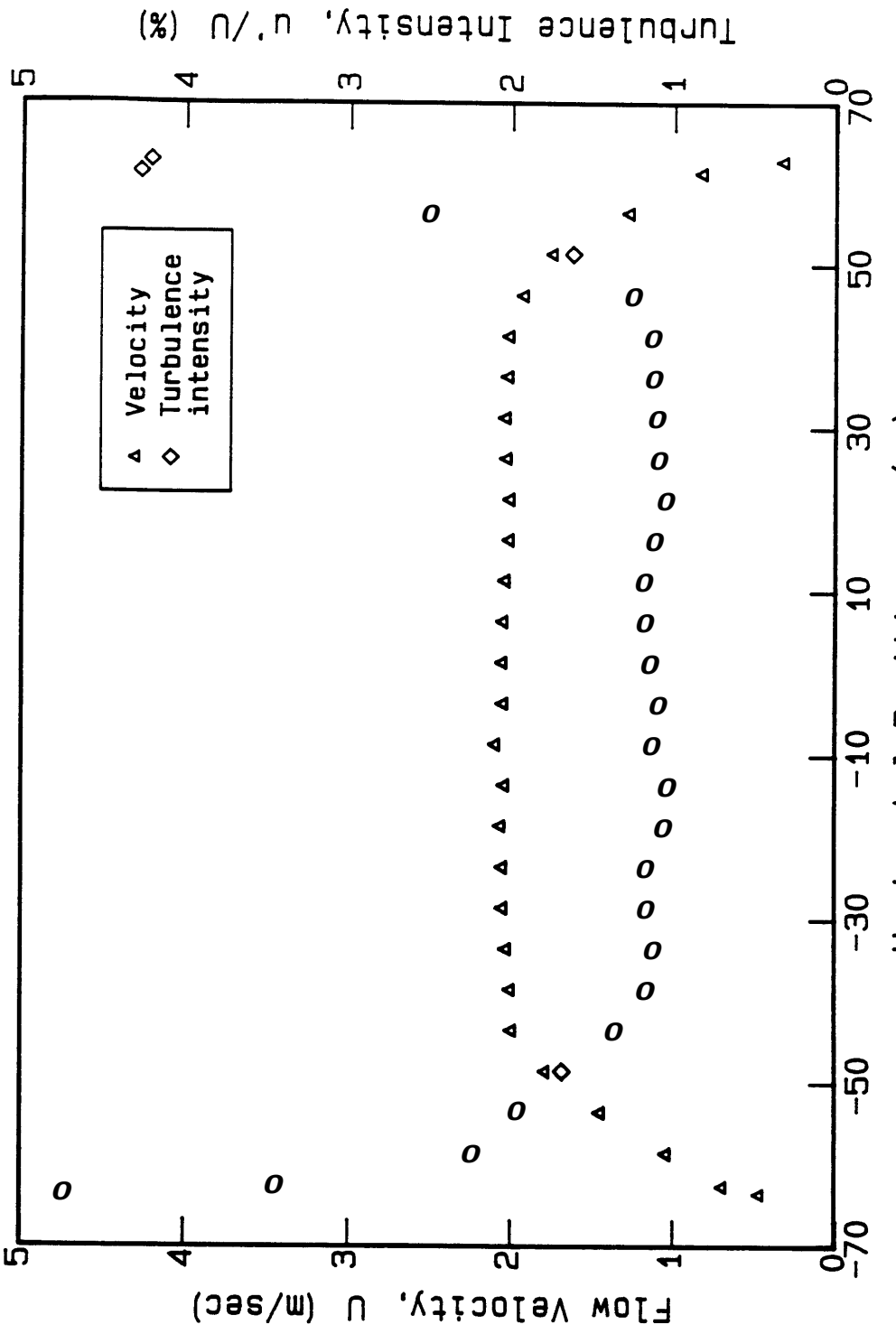

Fig. 2.22 Azimuthal distribution of flow velocity and local turbulence intensity

In the PMMA mass burning experiments a thin char layer usually forms on the solid fuel surface with an uneven thickness which prevents an accurate fuel sheet thickness measurement. A polishing procedure is applied to smooth out the fuel surface, which can introduce an error of about 5% to the surface regression rate measurement.

In most cases three tests are performed for each data point and the standard deviation is less than 10% for flame spread rate experiments and 15% for the mass burning rate ones. Additional tests are conducted to reach the final result if the experimental data show large discrepancy.

2.11.2 Flow Velocity and Turbulence Intensity

The linear relation between the Doppler shift frequency and the flow velocity produces very little error in the velocity data-acquisition process. The total error in the LDV system caused by A/D conversion, electronic circuit irregularities, round-off errors and other factors is less than 0.5% [12].

Some errors *can* arise if the Doppler signals are generated from the particles that do not pass through the fringe system, if there are not sufficient cycles left in a burst after passing the threshold, if a second particle enters the volume during the timing period of the first particle, or if a timing interval starts in one burst and ends in another. All these irregularities *can* be checked and prevented by making two measurements of the period of the same Doppler signal using different numbers of cycles. This process is shown in Fig. 2.11. If the two measurements of the Doppler

period agree to a specified degree of precision they are validated and accepted for output and further processing. If not, the result is discard and a new measurement has to be conducted. In this study cycle numbers of 8 and 4 are used for comparison and the comparison coefficient is set at 1 percent.

Since the velocities measured by an LDV system are that of particles in the flow instead of that of flow itself it is necessary to investigate how closely the particles follow the gas flow. From fluid dynamics it is known that the viscous drag due to the relative motion of a particle and its surrounding fluid drives the particle. The magnitude of this force in relation to the inertia of the particle determines the response of the particle to the fluctuations of the flow velocity. Because of the small size of the particles, the Stokes' law for low Reynolds flow can be used for the analysis. Assume that the particle has a spherical shape and the force on the particle is [25]:

$$F_p = m_p \frac{dv_p}{dt} = 6\pi\mu r_0 (U - v_p) \tag{2.18}$$

where U and v_p are the velocities of the fluid and particle, respectively, μ is the Viscosity of the fluid, and m_p and r_0 are the mass and radius of the particle.

For constant flow velocity the solution of the particle motion can be obtained as:

$$v_p(t) = U + (v_p(0) - U)\, e^{-t/\tau_p} \tag{2.19}$$

where $v_p(t)$ is the velocity of the particle at time t.

This equation shows that the particle responds a change in the flow velocity

with a time constant defined by:

$$\tau_p = \frac{m_p}{6\pi\mu r_0} = \frac{2\rho_p r_0^2}{9\mu} \qquad (2.20)$$

where ρ_p is the density of the particle. For aluminum oxide particles of 0.3 μm in diameter in air flow ($\mu = 1.8 \times 10^{-5}$ kg/ms) as in this study, the respond time is less than 1 psec which is short enough for the measurement of this study, and therefore, the lag of the particle behind the flow fluctuation can be neglected and particles of this size are well suited for the flow velocity measurement.

The accuracy of mean flow velocity and turbulence intensity measurements also depends on the number of samples taken in one measurement. Fig. 2.23 and 2.24 shows the dependence of uncertainties of the mean flow velocity and turbulence intensity on the total number of sampling data points. U_{max} and $(u'/U)_{max}$ are calculated with N = 8,000. It is seen that the larger the sample number, the smaller the deviation from the real velocity. However, larger number samples take longer time to finish than smaller ones. The experimental results show that the measurements taken with sample number larger than 2,000 give satisfactory data. Therefore, for most experiments in this study, 2,000 to 4,000 samples are usually applied to obtain one statistical value.

2.113 Gas Concentrations

The non-uniformity of the exiting flow in the exhaust section produces an error less than 5% to the exhaust gas concentration measurements, which is

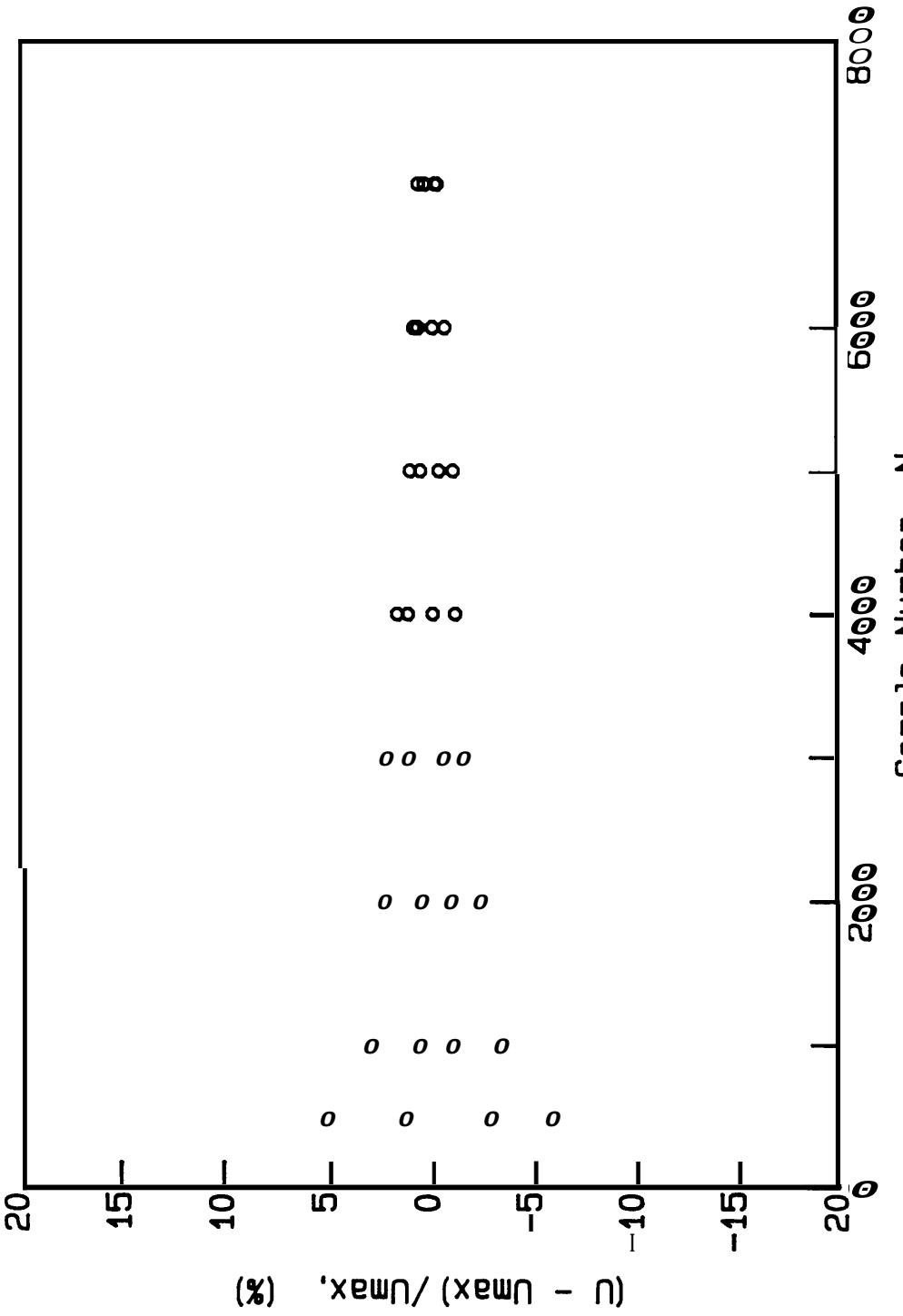

Fig. 2.23 Dependence of uncertainty of mean flow velocity on sampling data point.

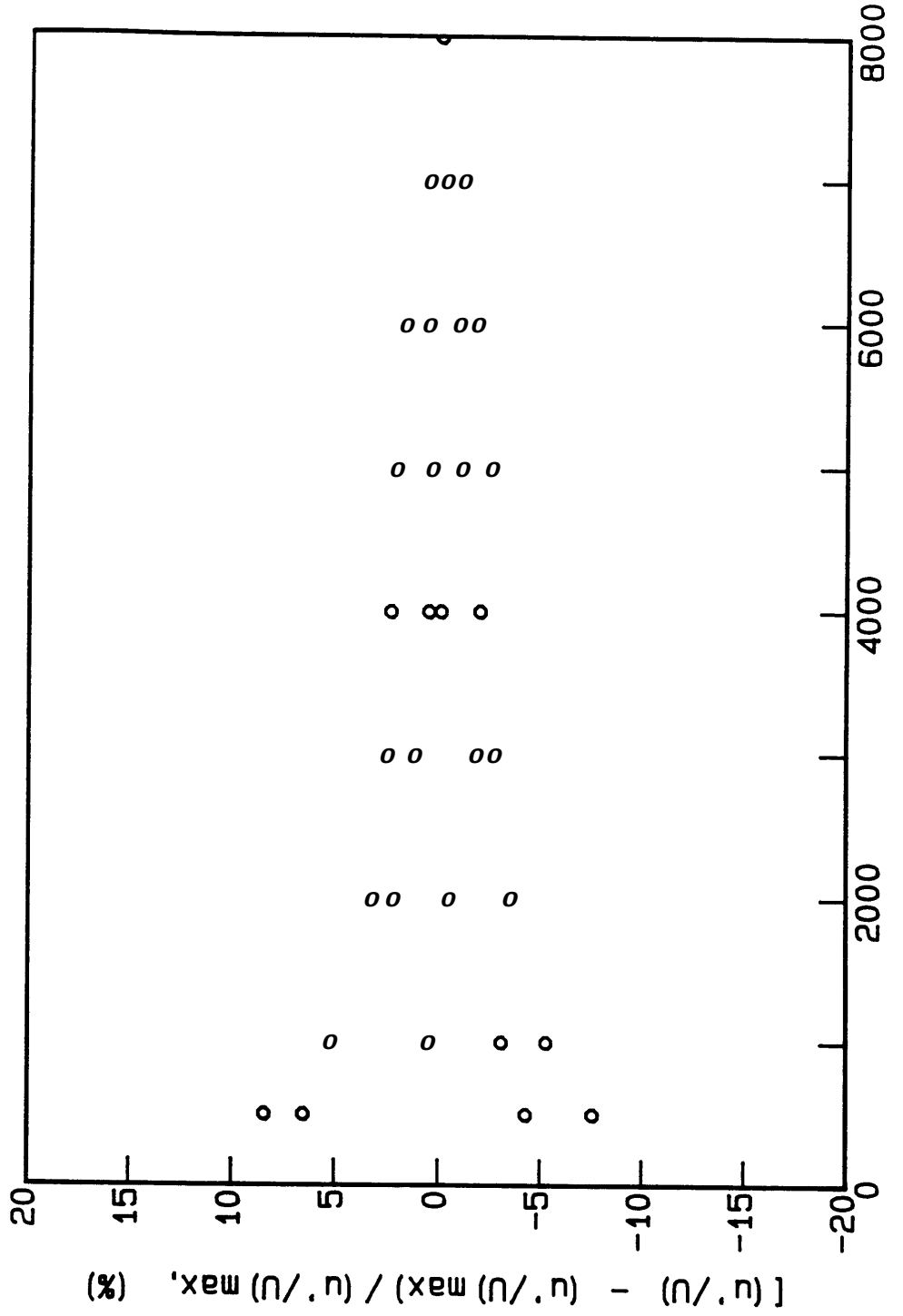

Fig. 2.24 Dependence of uncertainty of turbulence intensity on sampling data point

calculated from the measurements at different locations of the exhaust section. The systematic errors of analyzers are 0.5% for O_2 [26], and 1% for *CO*, 2% for CO_2, 1% for hydrocarbons and 2% for NO [27].

Chapter 3 . Opposed Turbulent Flow Flame Spread

3.1 Introduction

The opposed flow flame spread is often observed in the development of a fire. It is characterized by a diffusion flame spreading over a solid combustible in an oxidizing gas flow moving in the direction against that of the flame, as shown schematically in Fig. 1.1. The opposed gas flows are usually generated by natural convection induced by buoyancy force, or external sources such as wind or ventilation.

For the flame front to travel over the solid combustible surface against the gas flow, sufficient amount of heat has to be transferred to the unburnt fuel from the already pyrolyzed region or external heat sources. The flame established over the fuel surface usually serves as the main heat source and provides the energy necessary to raise the temperature of the unburned fuel surface from an initial temperature to the pyrolysis point and to sustain the subsequent pyrolysis process. The resulting fuel vapor moves away from the surface through transport processes and then mixes with the incoming oxidizer flow in the burning zone where the exothermal reactions take place. The flame spread over the solid surface is the result of complex interactions of heat transfer from the flame to the unburned fuel, fuel pyrolysis, mixing of fuel vapor and oxidizer ahead of the flame, ignition of the combustible gas mixture by the flame, and gas phase chemical reactions. These factors intertwine in the opposed flow flame spread process and *can* be important at the same time, which makes this

problem particularly difficult to study [6] [7].

3.2 Literature Review

Various studies on the opposed flow flame spread have showed that all the controlling effects can be summarized with two major mechanisms: the heat transfer from the flame to the virgin fuel and the gas phase chemical reaction. A common practice in experimental data analysis [28] - [30] is to correlate the experimental results in terms of a Damkohler number describing the gas phase kinetic effect and a non-dimensional flame spread rate describing the process of heat transfer. The Damkohler number is defined as the ratio of the residence time (time required for a fuel particle to travel the gas preheated region) to the chemical time (time required for a fuel particle to react with the oxidizer) [31]. The non-dimensional flame spread rate is defined as the ratio of enthalpy flow in the solid ahead of the flame to the heat transferred from the flame to the fuel based on the analysis in [32] which assumes infinite fast chemical reactions in the gas phase and results in a non-dimensional parameter that only represents the heat transfer process.

The heat transfer from the flame to the solid surface can be achieved by conduction, convection and radiation. Conduction takes place in both gas and solid phase while convection is only through the gas phase. And radiation heat transfer takes effect in both direct and indirect path. All three heat transfer mechanisms are always involved in the flame spread process simultaneously, therefore, it is essential to determine the dominant mode of the heat transfer in order to develop a relative

simple and yet complete analysis of the process. Some studies including [33] [34] have been conducted to determine the relative importance of each heat transfer modes in the flame spread process. In these investigations the temperature distributions in the gas and solid phase are measured for various flow conditions and the heat fluxes by each mechanism are calculated by performing energy balance in the solid and gas phase. The results have shown that the thickness of fuel sample sheet determines the dominant heat transfer mode. For fuel sheets less than 2 mm thick the heat conduction through the gas phase is the dominant mode, whereas for fuel sheets thicker than 20 mm the heat conduction through the solid phase plays the more important role. The radiation heat transfer always contributes to the total heat flux. However, for small scale fires, the direct radiation from the flame to the virgin fuel is insignificant due to the small view factor between the flame and the virgin fuel. The leading edge of the flame in opposed flow situation is considered to be in a near-extinction condition because of low temperature and low fuel concentration in the region caused by the unfavorable convection effect of the opposing gas flow [35] - [39]. Under such conditions, the chemical reactions are extremely sensitive to the external parameters, which leads to the conclusion that the flame leading edge region is controlled both by the chemical kinetics and heat transfer. The flame leading zone *can* be considered as a premixed flame anchoring the bulk diffusion flame that follows behind, which provides the heat for conduction to the unburned fuel and for the mass burning of the solid material behind the pyrolysis line. The pyrolysis front propagates over the solid fuel surface at a rate almost equal to the

moving speed of the leading flame. The fuel vapor generated in the downstream region can diffuse ahead of the pyrolysis front through the quenching layer very close to the fuel surface, as the result of large fuel concentration gradient and low flow velocities enforced by the non-slip condition in the vicinity of the fuel surface [40]. However, the exact controlling mechanisms in the leading flame region are still not fully understood due to the complexity caused by the participation of chemical kinetics under near-extinction conditions.

The intricacy of the problem and the relatively easy experiment requirements due to low flame spread rate and uniform flame front have attracted many experimental investigations. Among them are the studies on flames spreading downward over thin paper sheets [41], over thick PMMA sheets and rods [36], and on flames spreading horizontally over thin paper sheets [42] and on liquid fuels [43]. Air is used as the opposing gas flow in all the above cases. The results from these studies show that the flame spread rate decreases as the opposing gas flow velocity increases, once the gas flow is the dominant influence in the flame spread process. Other experimental work has been performed with high oxygen concentration gas flow for flames spreading horizontally over PMMA sheets [44] [45], which show that the flame spread rate increases as the opposed gas velocity increases, opposite to that from the first group of studies. Further work on this subject demonstrates that these seemingly contradictory results *can* be explained as the result of the interaction of the two main controlling mechanisms, heat transfer and gas phase kinetics, under different flow conditions [31]. The variation of the oxygen concentration of the gas

flow changes the relative importance of the above two effects, and as a result, changes the dependence of the flame spread rate on the flow velocity. The results indicate that for thermally thick fuel the solid phase conduction is the dominant heat transfer mode, a flow with higher velocity forces the flame to move closer to the solid surface and increases the heat transfer, resulting in an increase in the flame spread rate before the following decline caused by the convective cooling and low fuel concentration in the leading edge of the flame. This increasing effect is usually observed for high oxygen concentration flows. For thermally thin fuels, however, the main heat transfer mode is the conduction through the gas phase and an increased flow velocity only reduces the heat transfer and results in a decrease of the flame spread rate for all flow oxygen concentrations.

Other aspects often studied of the opposed flame spread include the effect of external radiation flux, fuel initial temperature, ambient pressure and buoyancy force. Much work has been done on the effect of the external heat source [42] [46] - [48]. The external radiation heat flux increases the fuel surface temperature and reduces the energy needed for the fuel surface to pyrolyze, and therefore, enhances the flame spread process. The initial temperature of the fuel has the similar effect on the flame spread rate as that of the external radiation heat sources [3] [49]. A higher initial temperature of the solid fuel results in a faster flame spread. The influences of buoyancy and pressure have been studied [28] [29] on the downward flame spread rate over thick PMMA and thin paper sheets. It is found that the buoyancy assists the flame spread when the solid surface is inclined an angle to the horizontal

position and the ambient pressure has the similar influence on the flame spread as the gravity since the pressure affects the buoyancy through the gas density.

Many theoretical studies have also been performed on the opposed flow flame spread and a good understanding of the major controlling mechanisms is achieved [7]. However, the predictions from these analysis are only moderately successful due to the complexity of the problem. Some analytical solutions are able to predict the flame spread rate under certain limiting cases and provide physical insights to the process, while numerical analysis *can* solve more realistic problems without neglecting the complicate processes such as phase change, finite chemical reactions and radiation. The modelling of the opposed flame spread problem has experienced several stages. Many of the early analysis [SO] - [56] solve only the solid phase equations with some prescribed boundary conditions at the solid and gas interface which are obtained through various empirical methods. The gas phase is not treated in those models and its effect on the process has to be coupled into the solution by utilizing the experimental data in the boundary conditions.

The gas phase governing equations are included and solved with the coupled solid equations by De Ris [32] and later by Wichman and Williams [57] to solve the flame spread problem for thick PMMA sheets and thin paper sheets. Fast chemical reaction rate (flame sheet assumption) is used along with some other simplifications such as uniform flow velocity distribution (Oseen approximation). The inclusion of the gas phase in the governing equations ensures the solution to be self-contained and makes it possible to predict the flame spread rate without using empirical data.

It is concluded in these studies that the flame spread rate is determined by an energy balance between the heat generation in the flame and the heat removal to the downstream region by convection. The analytical flame spread results agree well with the experimental data for flows with low velocity and high oxygen concentration, where the infinite chemical reaction assumption is a close representative of the real situation. The flame spread rate increases with the flow velocity according to these studies at least for thick fuels.

Since the flame leading edge is under near-extinction condition an accurate opposed flame spread model must consider the chemical kinetic effect (finite chemical reaction rate). Many attempts have been made in this direction both analytically and numerically [37] [39]. The results from these studies indicate that the flame spread rate decreases with the flow velocity. The numerical models usually involves two media with phase change at the interface. Steady-state, two-dimensional energy equations in both media are solved with the proper interface conditions and boundary conditions. The effect of many parameters such as gas phase flow velocity, Lewis number, oxygen concentration, external radiation have been investigated.

In most real situations, fire propagation takes place under turbulent flow conditions; thus it is of practical interest to study the effect of flow turbulence on the spread of flames over the surface of a combustible material. However, due to the difficulties brought upon by turbulent flows, only a few studies have treated the turbulent flame spread process while most of the effort has been devoted to the better behaved laminar problems. They include [58] for upward turbulent flame

spread over large PMMA sheets, and [59] [60] for thick PMMA sheets and wood plates. In these studies, the gas flows are naturally induced and the turbulence is also buoyancy-generated depending on the sample size. The dependence of the flame spread on the sample size [59] and the external thermal radiant flux [59] [60] has been studied. The studies above serve well as models for wall fire without external flows. However, no systematic study has been performed so far on opposed flame spread in a forced turbulent flow.

The purpose of this work is to provide a parametric study of opposed flame spread in an forced, turbulent air flow with the main interest on the effect of flow turbulence on the flame spread rate. Also studied is the turbulent effect on the flame extinction conditions. Due to the complexity of the flame spread process, an accurate determination of the turbulence effect on the spread of the flame is extremely difficult. The scope of this work is limited to the measurement of the flame spread rate as a function of the velocity and turbulence intensity. These direct measurements, in conjunction with complementary experimental observations and previous information about the flame spread controlling mechanisms, are used to describe the effect produced by the flow turbulence and the interactions among different mechanisms.

3 3 Experimental Arrangement

The experimental setup can be seen in Fig. 2.1. The flow velocity and turbulence intensity profiles are determined prior to the flame spread. The

instantaneous velocity of the flow is monitored with LDV during the course of the experiments. Since the flame propagates very slowly in opposed flows the flame spread rate is measured by timing visually the pass of the pyrolysis front over previously made marks on the fuel surface. The surface temperature histones at various locations are also measured to deduce the effect of turbulence on the leading edge of the flame. A Mach-Zehnder interferometer is used to get qualitative information of the temperature field of reacting flow. Both PMMA sheets and paper sheets are used in the experiment to represent thermally thick and thermally thin fuels, respectively.

3.4 Experimental Results and Discussion

3.4.1 Thick PMMA Sheets

The measurements of the flame spread rate over PMMA sheets as a function of the opposed air flow velocity and turbulence intensity are presented in Fig. 3.1 and 3.2. The flow velocity ranges from 0.35 to 2.3 m/sec and the turbulence intensity from 1% to 25%. Because of the difficulty of producing high turbulence intensity at low flow velocities, no flame spread measurements are made under such conditions. The flame spread rate is measured in the test section region where an approximately constant turbulence intensity profile is observed.

Fig. 3.1 shows the dependence of the flame spread rate on the flow velocity for several levels of flow turbulence intensity. It is seen that for low turbulence intensity the spread rate first increases sharply and then decreases as the flow

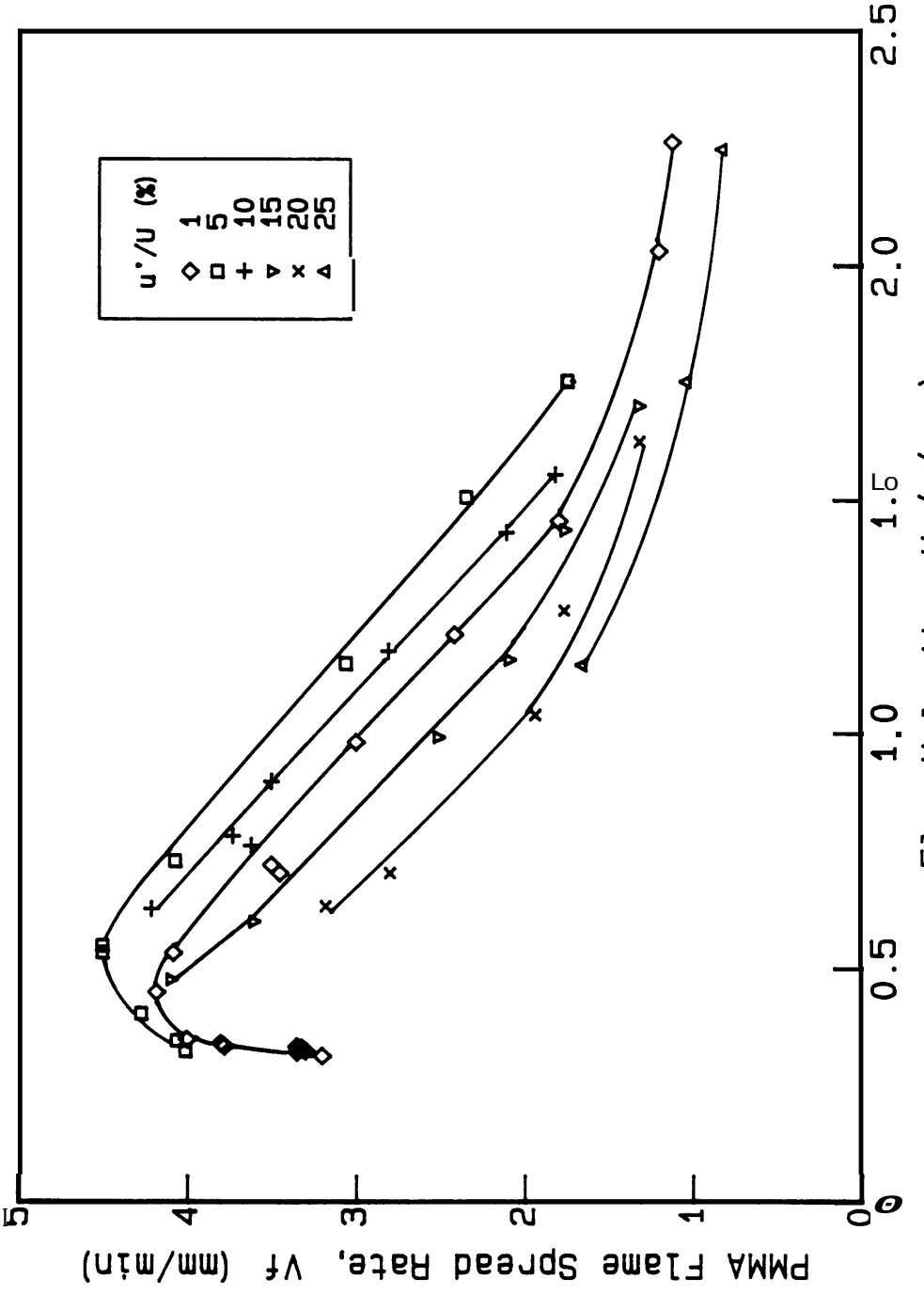

Fig. 3.1 Flame spread rate over thick PMMA sheets as a function of the opposed air flow velocity.

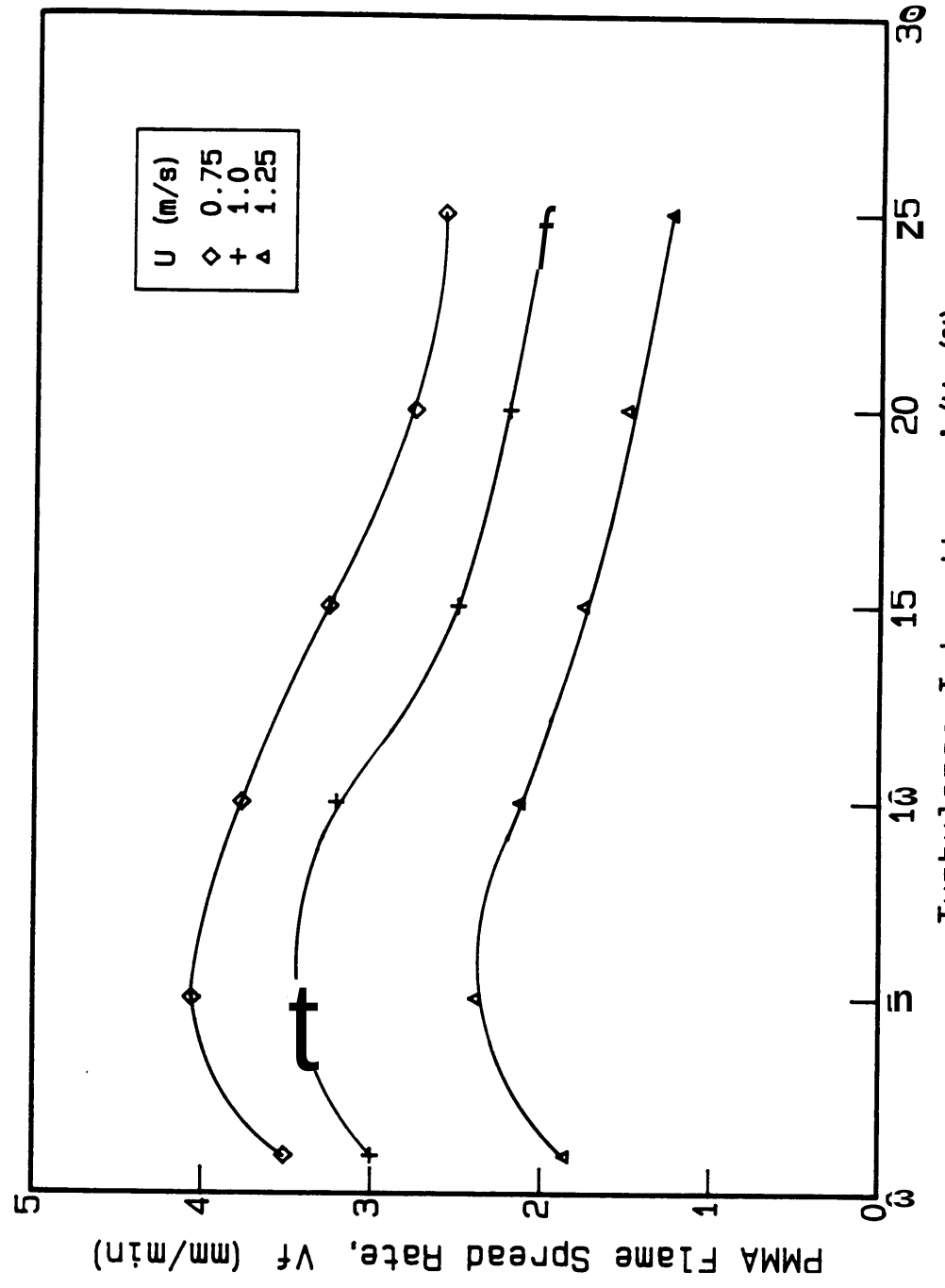

Fig. 3.2 Variation of the flame spread rate over thick PMMA sheets with the flow turbulence intensity.

velocity is further increased. The initial rapid increase appears to be caused by the under-ventilated conditions that the flame encounters at very low velocities. The chemical reaction is not proceeded completely due to the insufficient oxygen supply in the incoming flow. Increasing the flow speed brings more oxygen to the reacting region, and therefore, more heat is generated by more complete chemical reactions, which results in an increase of flame spread with the flow velocity at the low flow velocity region.

The initial increase of the flame spread is also caused by the enhanced heat transfer through the solid phase by the increasing flow velocity. As mentioned before, the heat transfer to the flame leading edge for thermally thick fuel is mainly controlled by the conduction through solid phase. As the flow velocity increases the gas flow tends to push the flame closer to the fuel surface and results in a steeper temperature gradient from the flame to the fuel surface which causes more heat transfer to the solid. As a result, the flame spread rate increases. This mechanism can be seen from Fig. 3.3 which shows two interferograms taken of the reacting flows with velocity of 0.2 and 0.5 m/sec and turbulence intensity of 1%. The thermal layer is apparently thinner in the flow with higher velocity. Buoyancy effect is also important in low velocity flows, which always lifts the flame away from the solid surface and reduces the heat transfer.

As the flow velocity increases further, the stronger convection caused by the mixed flow (buoyant and forced) conditions brings the transition to the flame spread process, which induces the flame spread rate to decrease with the gas flow velocity.

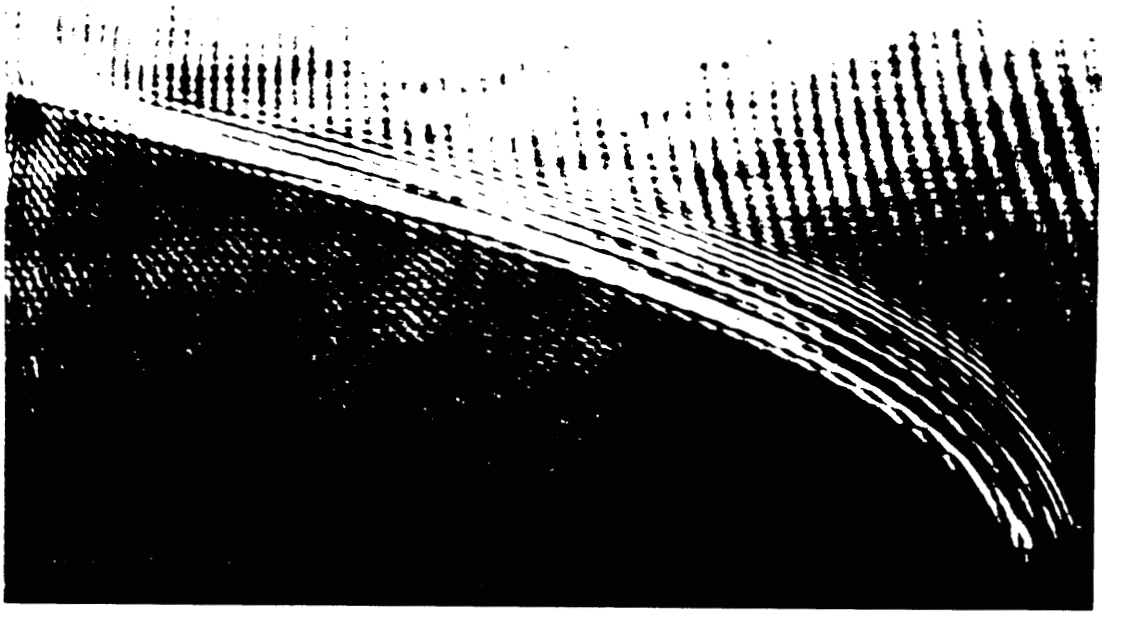

(a) **U = 0.2 m/sec,** **laminar**

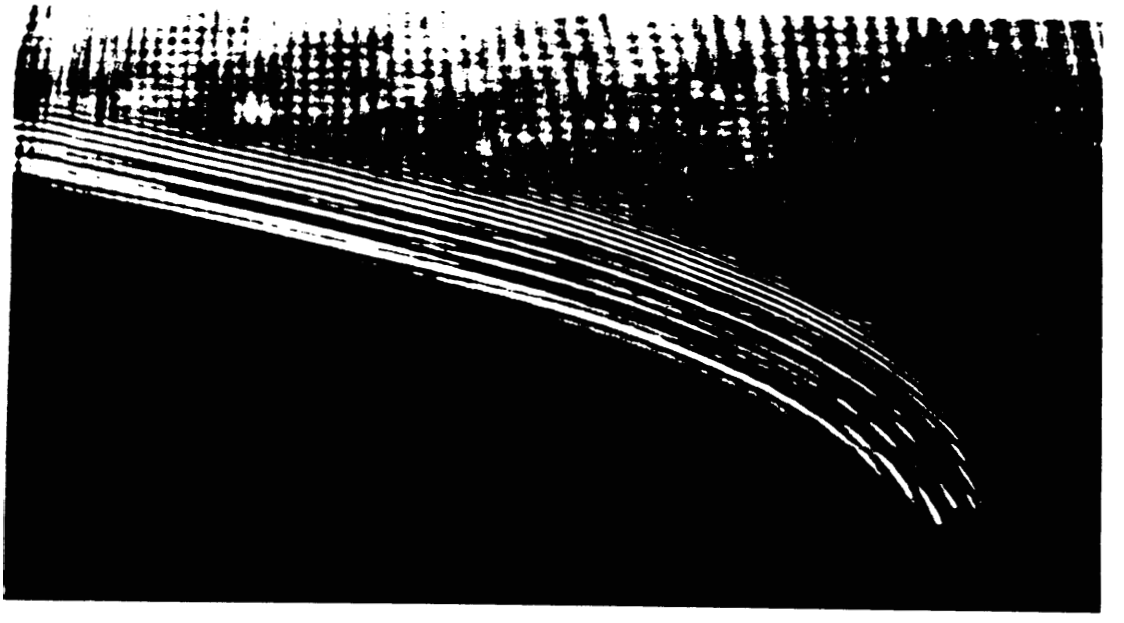

(b) U = **0.5 m/sec,** **laminar**

Fig. 3.3 **Interferometric photographs of flames spreading horizontally along** PMMA **sheets in opposed air flows** of **(a) 0.2 and** (b) *0.5* m/sec

The decrease trend of the flame spread rate with the opposed flow velocity at higher air velocities is in agreement with the result of previous work [31] [61] which have studied the ambient oxygen concentration effect on the flame spread in an opposed forced flow. The enhancing effect by the flow velocity on the flame spread process still exists as discussed in the low flow velocity cases and an increase of the flow velocity results in a higher heat transfer rate to the unburned solid fuel. However, the flow velocity has an opposite effect on the flame spread process as well, which is to affect the gas phase chemical kinetics in the leading region as indicated in [31] [61]. As the opposed flow velocity increases the residence time of the fuel vapor-air mixture ahead of the flame decreases, i.e., the Damkohler number decreases if assuming the chemical time remain constant. The combustible gas mixture does not have sufficient time to react completely in the leading edge that sustains the propagation of the flame. Therefore, less heat is generated in the flame leading edge and the flame spread rate is reduced as a result. In this study, the decreasing effect of the flow velocity is observed to occur at all turbulence intensity levels. For flows with velocities larger than 2 m/sec, the flame propagates at very small rates due to the strong cooling effect and the fuel surface recedes rapidly compared to the speed of flame spread process, producing a stagnation region behind the flame front that acts as a flame holder. As a consequence, at air flow velocities larger than 2 m/sec the flame propagation becomes a surface burning rather than a flame spread process, and therefore, is not investigated here.

The flow turbulence effect on the flame spread process can be seen in Fig. 3.2

which shows the flame spread rate as a function of the turbulence intensity for three velocities. The flow turbulence intensity can alter both controlling mechanisms, namely, the heat transfer to the unburned fuel and the gas phase chemical kinetics, and ultimately affect the flame spread process and change the flame spread rate. The turbulence could produce an increased convective cooling of the unburned fuel surface and gas region ahead of the flame, which would results in a decrease of the flame spread rate. On the other hand, the higher turbulence intensity in the flow could cause an increased conductive heating through the solid ahead of the flame by bringing the reaction region closer to the fuel surface, which would increases the flame spread. The chemical reaction in the gas phase would be subjected the similar effects from the flow turbulence. The flow turbulence could enhance the chemical kinetics by favoring the mixing of fuel vapor and oxidizer and thus enhancing combustion reaction, which raises the flame spread rate. But at the same time the flow with stronger turbulence could dilute the combustible gas mixture by larger and stronger eddies, which could weaken the reaction. Therefore, the flame spread could be hampered by this effect. It is necessary to consider the role of each of the above mechanisms in the flame spread process in order to resolve a complete picture of the flow turbulence effect on the flame spread.

From Fig. 32 it is seen that the flame spread rate increases initially and then decreases as the turbulence intensity increases for the flow velocity range from 0.7 to 2 m/sec. The maximum value of the flame spread rate is achieved in the flow with turbulence intensity of approximately 6%. The results reflect the characteristic

change in the flame-generated thermal boundary layer and its effect on the controlling mechanisms, as the result of the increasing turbulence in the flow. A sequence of interferograms of the flame leading edge are utilized to assist the interpretation of the results. Fig. 3.4 provides a graphic indication on how turbulence affects the flame and the thermal boundary layer generated by the flame. The Shilieren photographs are taken of the flame leading edge in flows with velocity of 1m/sec and three turbulence levels of 1%,10% and 25%. It is observed that as the turbulence intensity increases, more eddies are introduced to the flow which cause the flow to become more fluctuating, and more cold air is entrained to the leading edge of the reacting zone. It is also seen that the thermal layer thickness decreases in more turbulent flow as the flame moves closer to the fuel surface. A flame closer to the fuel surface results in an enhancement of the heat conduction to the solid ahead of the flame, particularly if solid phase heat conduction is a dominant mode of heat transfer, as is the case with PMMA. On the other hand, more turbulent entrainment of cold air results in stronger convective cooling of the fuel surface and of the gas ahead of the flame. The relative magnitude of these two counteracting effects determines the behavior of the heat transfer ahead of the flame front, and consequently of the rate of flame spread.

From the flame spread rate data it can be inferred that the enhancing effect of flow turbulence on flame spread plays the dominant role for flows with turbulence intensity less than 6%, and thereafter, the cooling effect becomes more prominent. This conclusion is also confirmed by the surface temperature profiles of the unburned

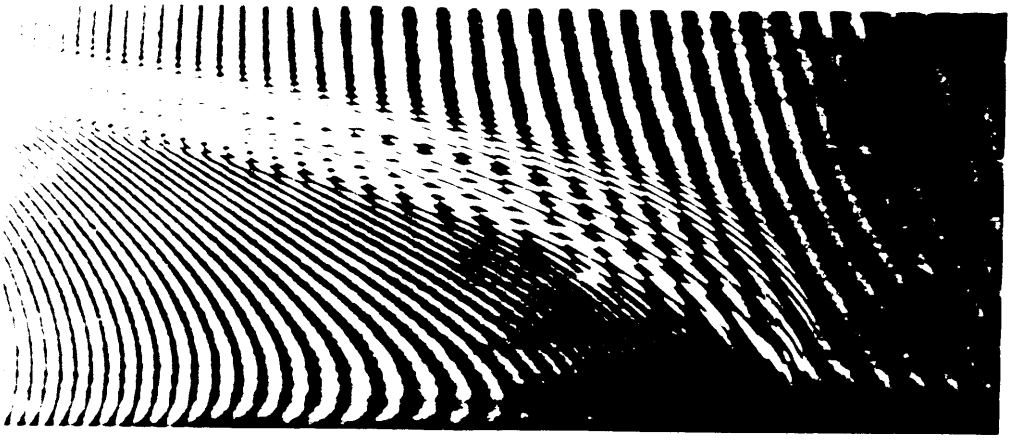

(a) U = 1 m/sec, u'/U = 1%

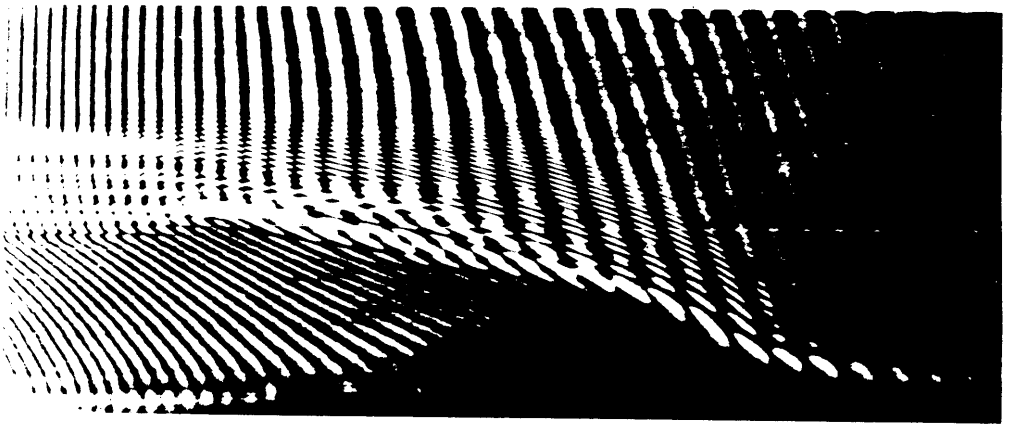

(b) U = 1 m/sec, u'/U = 10%

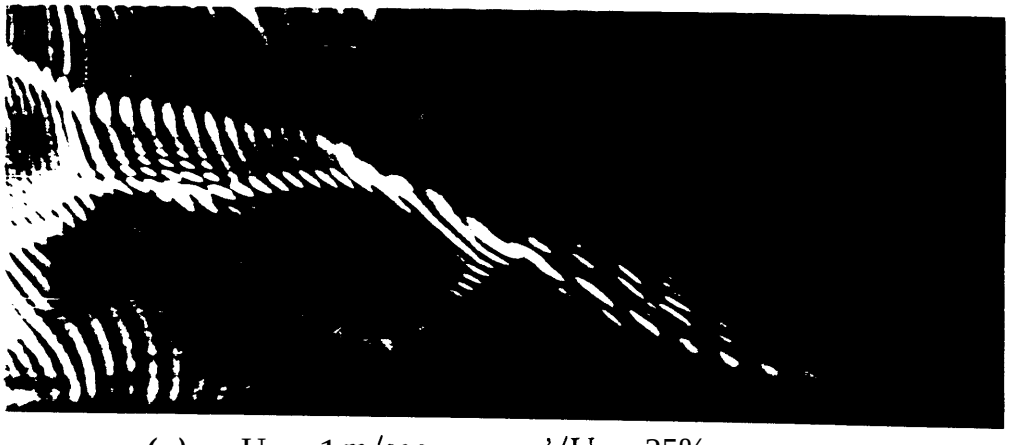

(c) U = 1 m/sec, u'/U = 25%

Fig. **3.4** Interferometric photographs of flames spreading horizontally along PMMA sheets in opposed air flows of 1 m/sec and varied turbulence intensities.

fuel surface ahead of the flame, as shown in Fig. 3.5. This figure presents the surface temperature in front of the propagating flame as a function of the upstream distance from the flame for flows with velocity of 1 m/sec and several turbulence intensity levels. The surface temperature rises as the flame front is approaching. The growth slope increases from turbulence of 1.1% to 5.6%, and then drops as the turbulence increases further. This observation suggests that as the turbulence increases, the preheating zone also increases and then reaches a maximum value at about 6% and then decreases with further increase of the turbulence, which is in agreement of the above argument of the turbulence effect on the flame spread.

Other possible mechanisms that should be considered are the effects of turbulence on radiation heat transfer and gas phase chemistry. As the thermal layer becomes thinner there is a potential reduction of radiation from the flame to the fuel ahead of the flame due to the smaller view factor that results from the flame being pushed closer to the surface. However, this mechanism is secondary given the already small view factor that the flame projects in opposed forced flow flame spread. With regard to gas phase chemistry effects, there exists the possibility of an enhancement of the gas phase reaction due to increased mixing of the fuel vapor and air ahead of the flame as discussed before, which would result in an increase of the spread rate. However, it is considered that the dominant mechanism is the convective cooling of the gas and consequently weakening of the reaction ahead of the flame, which together with the cooling of the fuel surface results in the observed decrease of the spread rate with the turbulence intensity, for large flow velocity.

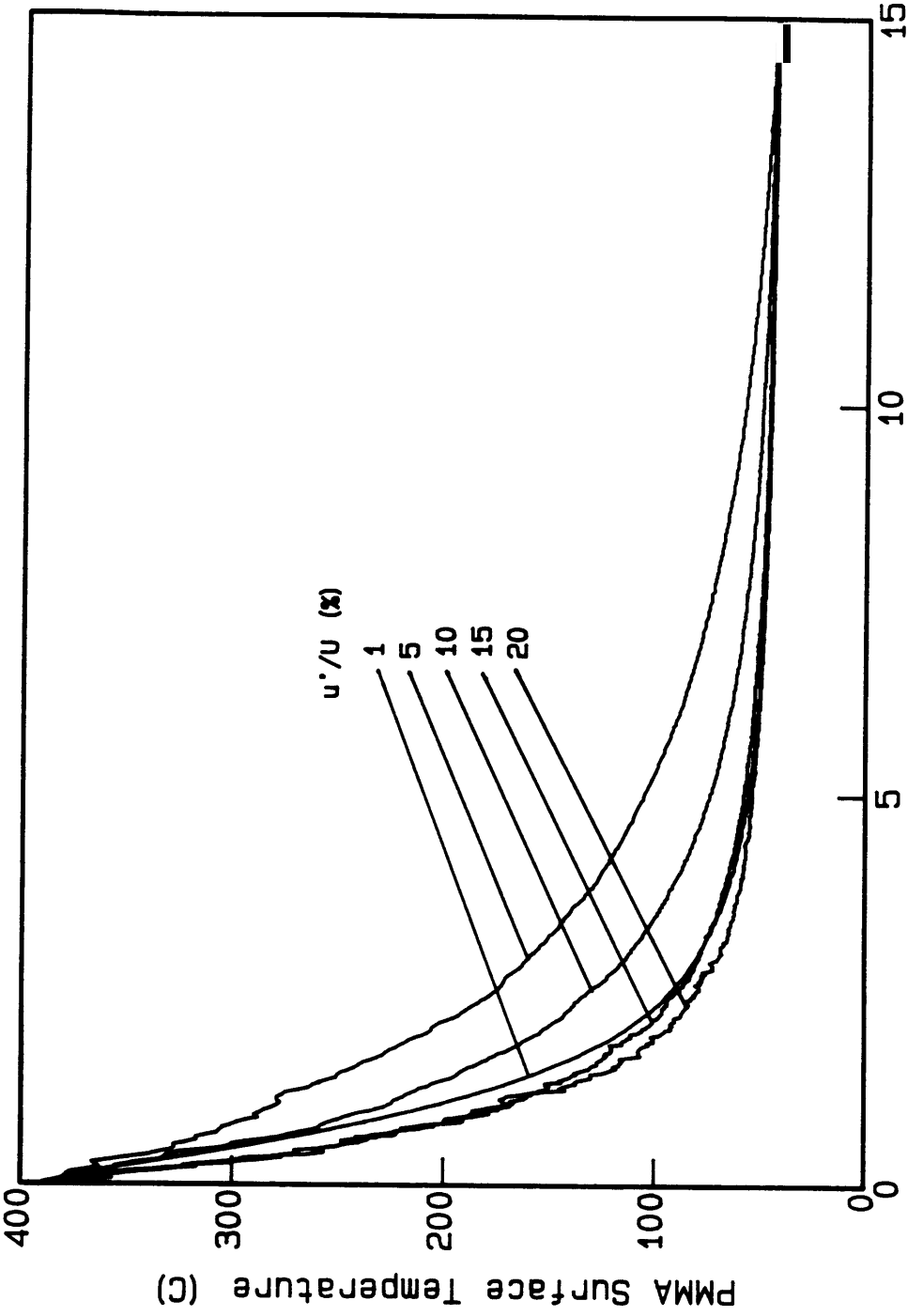

Fig. 3.5 Variation with the turbulence intensity of the surface temperature ahead of the flame front for flame spreading over thick PMMA sheets.

3.4.2 Thin Paper Sheets

The measurements of the flame spread rate as a function of the air flow velocity and turbulence intensity are also performed with paper sheets as the representative case of thermally thin fuels. The results are presented in Fig. 3.6. and 3.7. Due to the large heat loss in the gas phase and little heat transfer through the solid phase, the flames are unable to propagate over the paper sheets in gas flows with velocities larger than 1.5 m/sec, at least for the tests conducted in this work. The low flow velocities at which the tests are performed limit the maximum range of turbulence intensities attainable to approximately 15%. The flame spreads over both sides of the paper sheets, unlike in the PMMA case where flame only propagates on one side.

It is seen from Fig. 3.6 that for all turbulence intensities tested, the flame spread rate decreases as the opposed gas velocity increases. The extent of the decrease in the low velocity region, however, is smaller than that in the high velocity region. This appears to be caused by the buoyancy effect on the flame spread process at low flow velocities. The buoyancy force lifts up the flame away from the paper sheet at low velocities and the heat transferred through radiation from the flame to the unburned fuel becomes important because of the larger view factor. The flame spread process is determined mainly by this mode of heat transfer and the flame spread rate only weakly depends on the flow velocity for the low flow velocity region. As the flow velocity increases further the flow velocity drives the flame to lay more parallel to the fuel surface and the heat conduction through the gas phase

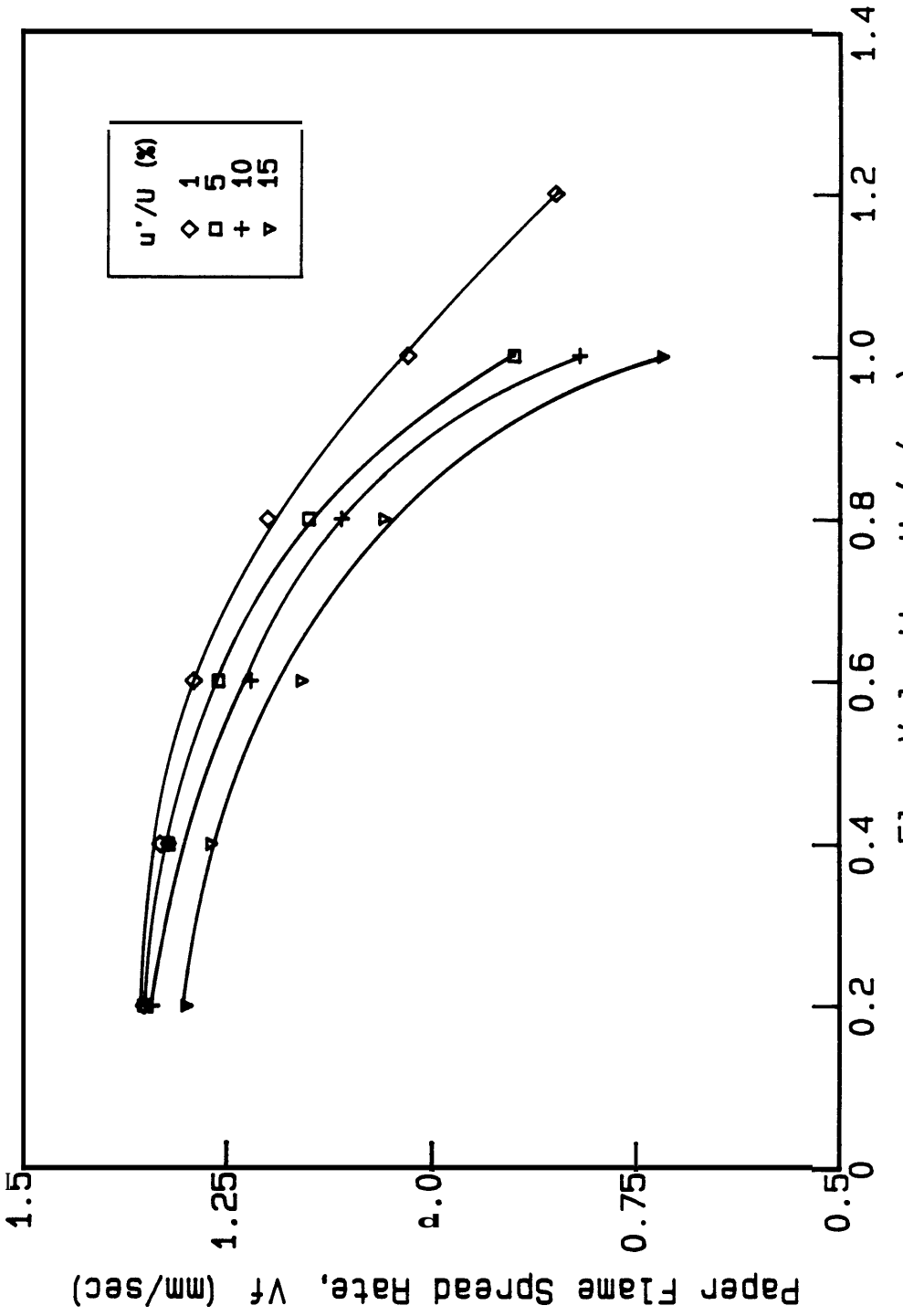

Fig. 3.6 Flame spread rate over thin paper sheets as a function of the opposed air flow velocity.

replaces the radiation as the main mechanism of heat transfer.

The strong decrease of the flame spread rate with the flow velocity observed for larger air velocities can be explained in the same way as for the thermally thick fuel case. The results are in agreement with that obtained by [6], which studied the effect of ambient oxygen concentration on the flame spread rate. The principle effect by flow velocity appears to be the combined result of convective cooling and weakening of the chemical reaction caused by smaller residence time.

The influence of the turbulence intensity on the flame spread rate for paper sheets can be seen from Fig. 3.7. It is found that the flame spread rate weakly depends on the turbulence intensity for low velocities. This can be explained the same way as for its dependence on velocity discussed above. Since the heat transfer is mainly accomplished by radiation for low velocities the flow turbulence casts minor influence on the flame spread process. For thin paper sheets the flame spread rate always decreases with the increasing flow turbulence intensity, with no apparent transition region from lower to higher values of the turbulent intensity as observed in PMMA tests. The different mechanisms of heat transfer that control the spread of the flame in each case can elucidate this observation. For thin paper sheets, heat conduction through the gas phase ahead of the flame is the dominant mechanism of heat transfer during the flame spread. Thus, the enhanced heat transfer through the solid caused by the thinning of the boundary layer as inferred in the PMMA tests should have little effect. The flow turbulence enhances the convective cooling at the flame front region, which controls the flame spread process for most flow conditions

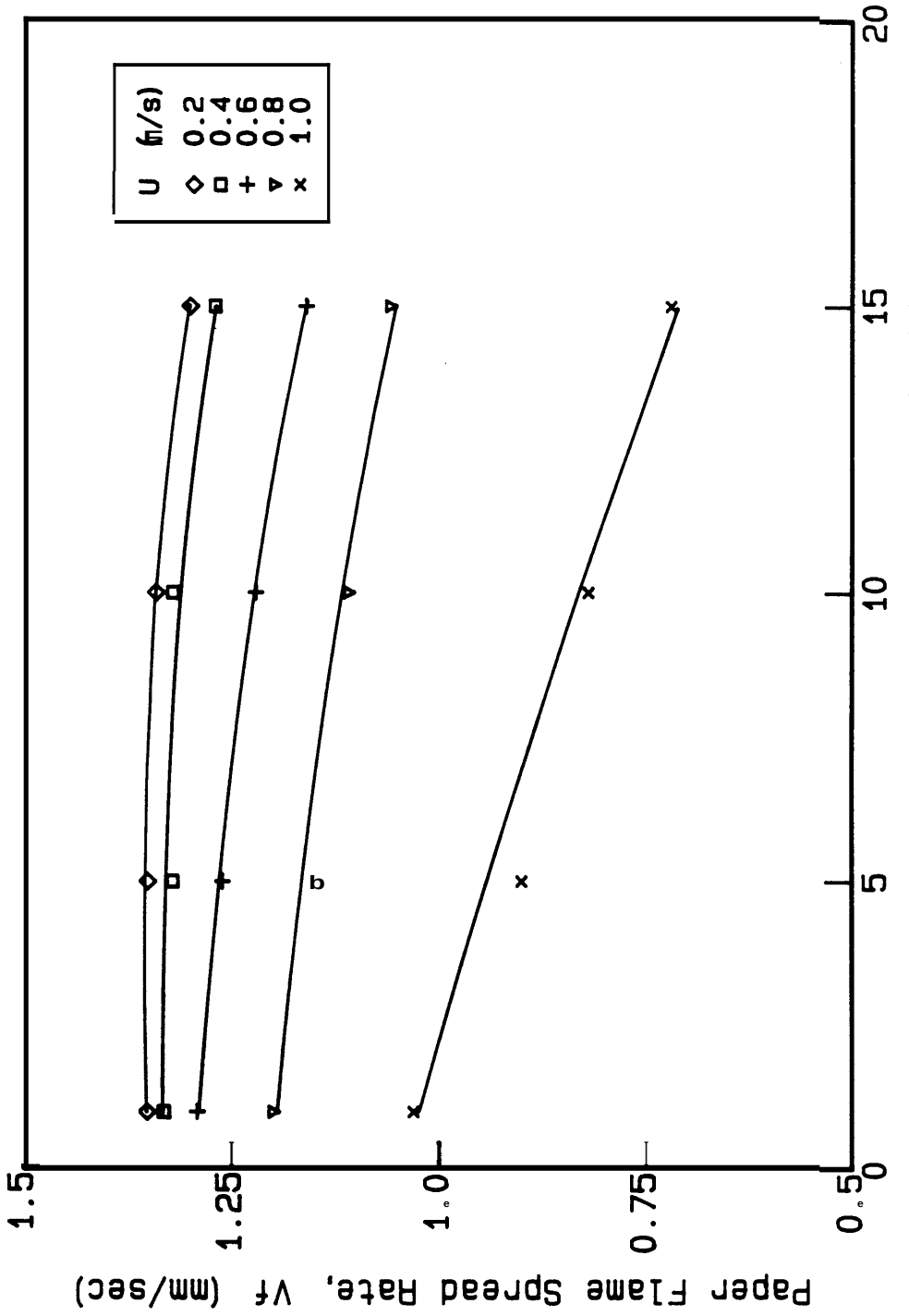

Fig. 3.7 Variation of the flame spread rate over thin paper sheets with the flow turbulence intensity.

tested except at very low velocities flows. Therefore, it is understandable that flame spread rate displays the monotonically decreasing character as the flow turbulence intensity increases.

3.43 Turbulence Effect on Thin Paper Flame Extinction

As the opposed flow velocity increases, the flame propagates at a decreasing speed, and is eventually extinguished. The flame extinction usually takes place as the result of the inability of the chemical reactions to keep in pace with the depletion process of the thermal energy from the reaction zone. An increased flow velocity reduces the residence time of the combustible mixture and decreases the gas phase temperature by convection, and blows out the flame as the final step.

An interesting phenomenon observed in the experiments is the effect of flow turbulence intensity on the flame extinction conditions. The results are shown in Fig. 3.8, where the gas velocity at which flame extinction occurs is presented as a function of the flow turbulence intensity. It is found that the flame extinction happens at a lower flow velocity for a larger turbulence intensity level, which is in general agreement with the flame spread rate results in this test. This result is somewhat unexpected because turbulence is often viewed as a means to enhance fuel combustion processes, and therefore should assist the flame against unfavorable conditions. However, the fact that in this study the flow turbulence tends to accelerate the flame extinction indicates that the convective cooling of the reaction zone by the turbulent flow, in conjunction with possible reduction of radiation from

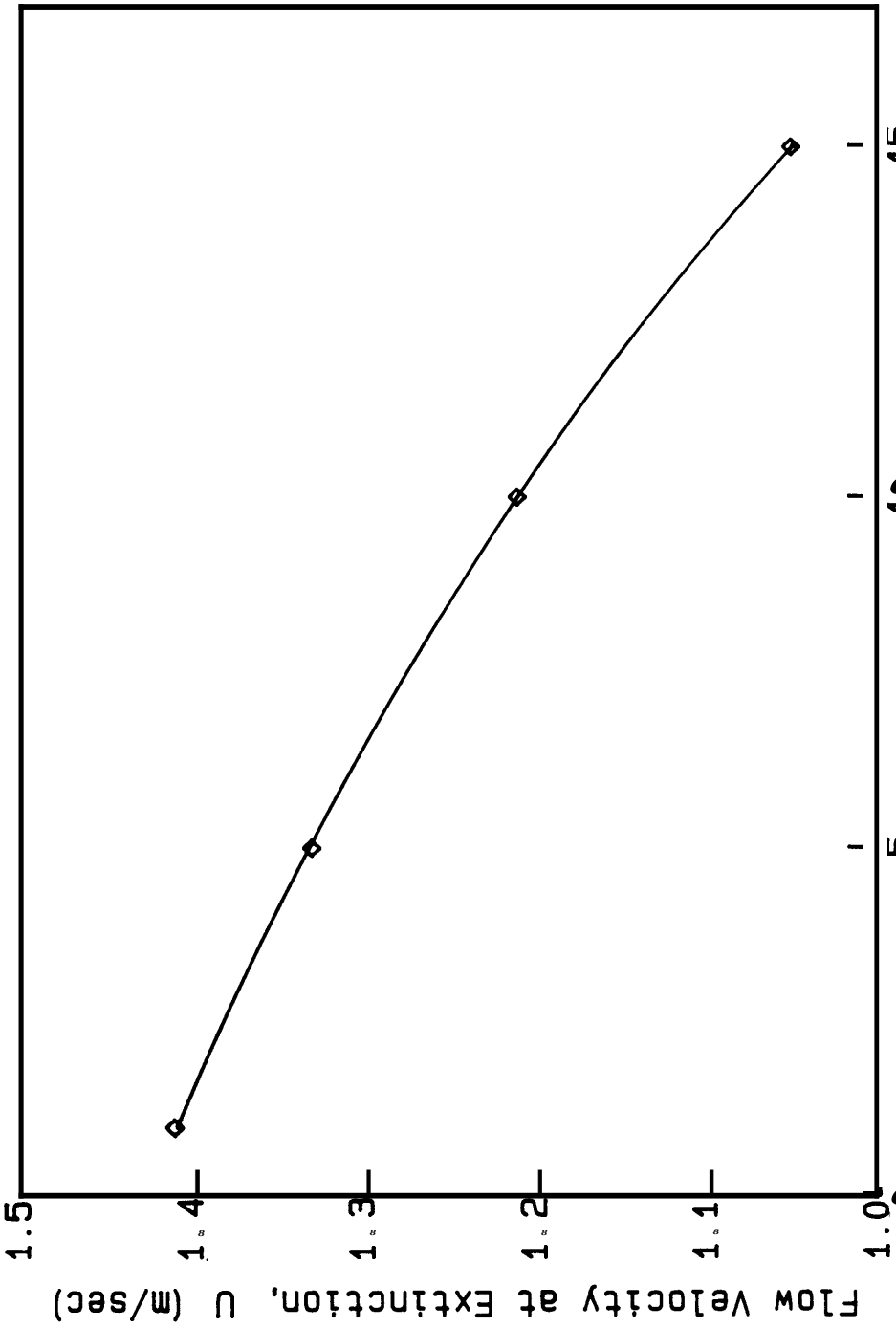

Fig. 3.8 Dependence on the turbulence intensity of the opposed air flow velocity at which extinction of flame spreading over thin paper sheets is observed.

flame to fuel, increased re-radiation from the fuel surface, and flame-stretching effects, is the dominant mechanism in the flame extinction process. The enhancement of the fuel-air mixing by the turbulence appears to only have a secondary influence on the gas phase reaction, at least for the present experimental conditions.

3.5 Conclusion

The parametric study conducted in the present work of the spread of flames in an opposed turbulent forced flow has shown that flow turbulence intensity has a significant effect on the rate at which the flame propagates, and on the conditions leading to its extinction. The study has introduced a new aspect of the flame spread problem that is of special interest given the fact most practical fires take place under turbulent flow conditions. The nature of the results indicates that the flow turbulence may affect both the heat transfer and the chemical kinetic mechanisms that control the spread of flame. Although throughout this work phenomenological arguments are given in an attempt to explain the different experimental observations, more detailed experiments are needed to provide sufficient data in order to prove the certainty of these arguments.

To *fully* understand the effect of turbulence on the flame spread process it appears that it may be necessary to *study* its influence individually in each one of the flame spread controlling mechanisms. This could be done by conducting experiments under conditions where the flame spread process is controlled only by heat transfer

effects (high oxygen and low gas velocity) or only by gas phase chemical kinetic effects (low oxygen concentration and/or high flow velocity) [31]. The characteristics of the flow turbulence may also change the quantitative influence of the flow turbulence on the flame spread process. Thus, it would be interesting to perform experiments to seek other parameters of a turbulence flow other than the intensity, such as the turbulent scales of the mean flow, the turbulence intensity in other directions, or the turbulence field generated by tripping the boundaxy layer. In addition, it would be important to identify the non-dimensional parameters that determine the turbulent flow flame spread process, and to correlate the experimental results in terms of these parameters.

Also interesting is the observation that an increase in the flow turbulence causes an earlier extinction of the spreading flame, at least in the case with air as oxidizer. The fact that this result is somewhat contraxy to the more common observation that turbulence enhances the combustion reaction by better mixing of the fuel and oxidizer suggests that different controlling mechanisms may influencing the flame extinction. It is possible that under other experimental conditions, such as a higher oxygen concentration, or an enhancement of the fuel evaporation by external radiation or preheating, the influence of turbulence on the flame extinction may be different than what observed here. The elucidation of this aspect of the flame spread phenomenon deserves further attention.

Chapter 4 Concurrent Turbulent Flow Flame Spread

4.1 Introduction

In the concurrent mode of flame spread, the gas oxidizer gas flow moves in the same direction as that of the propagating flame, thus assisting the further spread of the flame. The oxidizer flow can be induced naturally by hot reacting gas mixture as in upward wall fires, or by externally applied pressure gradients as in wind-aided forrest fires. Among the different modes of flame spread, the concurrent flow flame spread is the fastest and most hazardous one because the gas flow carries the high temperature diffusion flame over the unburnt fuel surface, which greatly enhances the heat transfer from the flame to the unburnt material and consequently increases the flame spread rate. Concurrent flow flame spread is often encountered in practical cases, especially in open space fires where external flows are easily attainable. The danger brought by such a fire provides the main incentive for the studies in this area of fire research.

The concurrent, or flow assisted, flame spread is characterized by the following mechanisms, as shown in the schematic of Fig. 1.2. Upstream from the pyrolysis front, heat is transferred from the diffusion flame to the solid surface. The solid fuel is pyrolyzed into vapor and an approximately constant temperature is maintained at the surface through an energy balance between the net heat flux and fuel vaporization. The pyrolysis temperature is usually regarded as one of material properties for many solid fuels. The vaporized fuel is diffused and convected

outward and forward, reacting with the incoming ambient oxidizer and sustaining the diffusion flame over the solid combustible. The fuel vapor which is not consumed in the upstream reaction is carried downstream by the external flow from the pyrolysis region. The excess fuel vapor keeps reacting with the oxidizer and extends the diffusion flame further downstream. Heat transfer from the flame to the fuel downstream from the pyrolysis front causes the unburnt solid surface temperature to increase until it reaches the pyrolysis point. The downstream diffusion flame is generally independent of the flame spread process, except that the flame length is a function of the length of the pyrolysis region. The onset of fuel pyrolysis determines the progress of the pyrolysis front and consequently the flame spread speed. As in other flame spread processes, the concurrent flame spread is controlled by both the heat transfer from the flame to the solid fuel and the physico-chemical mechanisms that govern the combustion region in the gas flow.

4.2 Literature Review

Because of the potential hazardous nature of the concurrent flow flame spread encountered in conventional fires, much effort has been devoted to the study of the controlling mechanisms from both experimental and analytical point of view. Experimental study of the concurrent flame spread proves to be more difficult to pursue than that of the opposed flow flame spread due to the faster propagation and more complicated control needed in the former case. These technical difficulties have caused the relatively scarce experimental information about the concurrent

flame spread process in the early years. However, this situation has been greatly improved by the later effort.

A large number of the early studies have focused on the upward wall fire problem, which involves a diffusionflame spreading over a vertically placed solid fuel surface in a naturally generated flow. The geometry of the test sample and the scale of the fire play very important roles in this mode of flame spread. The studies conducted on small scale fires [62] - [65] have observed typical laminar reacting flow characteristics and the experimental results agree each other quite successfully. The general results are that the upward laminar flame spread rates decrease with the quarter power of the height, and are affected by the mass control number with a correction for the radiant heat losses from the vaporizing surface. The flame and pyrolysis height increase with the square of time. These laminar flame spread studies apply to flame heights less than 100 mm where transition to turbulent flows typically occurs. The heat transfer by convection through the gas phase is found to be the main controlling factor and the radiation from the flame is neglected in all these studies due to the small size of the test samples.

Large scale experiments of flame spread in upward wall configuration have been performed in [58] with thick PMMA sheets and in [66] with cotton fabrics, observing different characteristics of flame spread from that of the laminar case. The heat transfer from the flame to the solid is still found to be the dominant mechanism controlling the flame process. The naturally generated flow develops to a turbulent region from an initial laminar period as the flame dimension increases with time.

Thermal radiation is observed to be the dominant form of the heat transfer from the flame to the solid surface in the turbulent region, whereas the convection transports most energy in the laminar region. For the cotton textile, a power law of the flame spread rate has been deduced from the experimental data and phenomenological arguments, in the form of $V_p = \beta\, l_p^n$, where V_p is the pyrolysis rate, l_p is the pyrolysis length, β and n are constants with $n < 1.0$. The correlation indicates that the flame spread accelerates over the course of the test, even though an asymptotic constant flame spread rate is expected. For PMMA sheets it is also found that the fire spread rates increase exponentially with time. The flame length and the flame spread rate data is correlated with the pyrolysis length in the form of $l_f = 0.345\, l_p^{0.781}$ and $V_p = 0.0041\, l_p^{0.964}$. Other experimental studies [67] [68] also indicate the similar accelerative nature of the flame spread in the vertical configuration. The experimental data in [67] is used to obtain the power law correlations for the flame spread rate and pyrolysis length, $V_p = dl_p/dt = t^{0.7}$. The flame length data can be expressed as a function of the pyrolysis length, $l_f = l_p^{0.71}$. Similar relations are also observed for upward flame spread tests conducted in [68]. The measurements of spread rate have also been made in [59] of a upward spread of diffusion flame with both PMMA and Douglas-fir particle board, representing non-charring and charring fuels, respectively. Power law relations are also deduced between the flame spread rate and the fuel pyrolysis length. For the charring Douglas-fir wood surface, the flame spreads at a lower rate due to the inhibition effect on the heat transfer by the char layer.

The experimental observation of the power laws for the flame spread rate and time or for the flame length and pyrolysis length is significant because similar results can be obtained from most analytical work on the upward flame spread process. These analytical solutions are based on heat transfer model with the assumption of infinite chemical kinetics. The agreement between the experimental data and analytical predictions seems to indicate that the heat transfer from the flame to the solid surface is the dominant mechanism in this mode of flame spread and the gas phase chemical kinetics has a secondary importance.

Many studies have been conducted on other effect such as external heat source [60] [67] [68] on the vertical wall flame spread. An external heat source affects the flame spread rate mainly by raising the fuel surface temperature and increasing the convective heat transfer at the solid surface, as already observed in opposed flame spread studies. Since the fuel surface temperature has been elevated by the external heat source prior to the arrival of the flame less heat is needed from the flame for the pyrolysis of the solid fuel. Therefore, the flame spread rate is increased as the overall result of the imposing external heat source. The experimental data indicates that the flame spread rate has a power law dependence on the difference between the material pyrolysis temperature and the surface temperature prior to the flame tip arrival. Similar results are also obtained by [41] on the mixed flow flame spread. The flame spread rates are obtained as a function of the initial surface temperature which increases with the radiant heat flux. The external radiant heat flux on the upward flame spread over thermally thick, charring

wood surface has been studied in [60]. It is found that the upward flame spread is accelerative with time, and an application of modest level of external radiant energy flux can sustain the upward flame spread. In general, the external radiation seem to have duel effects, preheating the fuel prior to pilot activation and augmenting the energy flux to the surface adjacent to the flames, therefore, resulting a increasing flame spread rate.

The ambient pressure effect on the vertical wall flame spread has also been studied in [69] for a variety of airplane interior materials. It is found that the pressure effect can be modeled by properly accounting for thermal radiation. The pressure modeling demonstrates greatest accuracy when the tests are performed at high ambient pressures, apparently due to thermal radiation effects. Since the pressure modelling approach basically preserves the non-dimensional parameters controlling the convective flow field, the results reassure that heat transfer from the flame to the fuel surface is the controlling mechanisms in the concurrent mode of flame spread.

The studies above are mainly concerned with the concurrent flame spread in buoyancy generated flows, whereas many real cases are accompanied with external forced flow. The effect of forced flow velocity has been investigated in [70] with thermally thick PMMA sheets in a small scale, horizontally placed wind tunnel with air as oxidizer. The flame spread rate is measured as a function of the laminar mean flow velocity. One of the important results is that the flame propagates at a constant speed over the solid surface in the concurrent flow. As the flame spreads over the

fuel surface, the flame length increases with the aid of the external flow and the heat flux from the flame to the solid surface decreases due to the thermal layer growth over the distance from the fuel leading edge. These two effects, lengthening of the heated region and decreasing of heat transfer, counterbalance each other, resulting in a time-independent flame spread rate. It is also found that the flame spread rate is a linear function of the outer flow velocity, which is in good agreement with the analytical solution given in the same work. The controlling mechanisms of the concurrent flow flame spread process has been further studied for thermally thick fuel [71], and thermally thin fuel [72]. In [71] a forced gaseous flow with various oxygen concentration is used to create adjustable chemical kinetic conditions for the flame spread. It is shown that rate of spread of the pyrolysis front is time independent and displays a linear dependence on the flow velocity for all the oxygen concentration range from 0.2 to 1, confirming the results of [70]. The dependence of the flame spread rate on the gas oxygen concentration can be expressed with a square power law relation. The experimental data of the spread rate correlates very well in terms of parameters deduced from heat transfer models of the concurrent flame spread process, indicating again that heat transfer from the flame to the condensed fuel is the primary mechanism controlling the spread of flame. Finite rate chemical kinetic effect has apparently small influence on the flame spread process. It is also pointed out that the extinction processes are limited primarily to the upstream leading edge of the flame and to the flame tip. In the study of [72], filter paper sheets are used as solid fuel to study the flow velocity and oxygen

concentration effects on the flame spread over thermally thin fuels. The variation with time of the pyrolysis region and burn-out distances are measured to reach the conclusion that after an initial accelerating stage, the flame spread rate becomes constant as the flame progresses over the fuel surface. The initial acceleration period becomes shorter as the oxygen concentration is increased. The flame spread rate is weakly dependent on the gas velocity for low gas velocities due to the possible buoyancy influence, but becomes independent of the flow velocity for forced flow conditions. The flame spread rate is almost linearly dependent on the oxygen concentration of the flow over the range tested in that work. The experimental data of flame spread rate are also correlated in terms of the parameters deduced from the heat transfer models for the flame spread process over thermally thin fuels.

Large scale experiments of wind-aided flame spread over solid combustible (PMMA) surface have been performed with air as the oxidizer [73]. The wind tunnel in that study has a cross section of 2.4 m x 5.4 m and produces flow velocity from 1 to 2.1 m/sec. Because of the large dimension of the test sample, which is made of 2.4 m long, 0.65 m wide and 6 mm thick PMMA sheet, the buoyancy and radiation pose significant importance to the flame spread process, unlike in the small scale studies. It is found that the flame propagation takes place in two successive modes. In the first mode, the flame is confined within a boundary layer and the flame spread rate increases almost linearly with time and weakly depends on the wind velocity. The second stage is characterized with a pool-fire like flame plume caused by the upward force of buoyancy. The transition from the first to the second stage occurs

sooner for lower flow velocity. The flame is lifted away as the buoyancy force and pyrolysis flux dominates over the horizontal forced flow and the heat is transferred from the flame to the surface mainly through radiation. The heat flux from the flame and the fuel vapor flux increase rapidly in the second stage. The flame spread rate increases with the wind velocity, reaches a peak value and then decreases with the further increase of the flow rate. The flame length is found to have a simple relation with the pyrolysis length, $l = 1.25 l_p$. In the second stage, a correlation between the flame length and the energy release is also obtained. The experimental data are compared with the theoretical predication from heat transfer model and a reasonably good agreement is achieved.

Along with the development made by the experimental studies of knowledge of concurrent flow flame spread process, much effort has also been contributed to solve the problem analytically. A complete mathematical description of this mode of flame spread should include coupled governing equations for both solid and gas phase, which are usually too complicated to resolve theoretically. However, as seen in the experimental studies, the heat transfer is identified as the dominant mechanism in the propagation process. Therefore, it is possible to decouple the original problem into two separate parts for the gas phase and the solid phase with simple interface conditions connecting the two regions. The solid phase equations can then be simplified further into a one-dimensional, transient heat conduction problem because the variation of the temperature in the longitudinal direction is much smaller than that in the normal direction. And the flame spread rate can be

deduced from the solid phase solution.

The accuracy of the solid phase solution depends on the heat flux at the interface to a great extent which can be obtained by either solving the gas phase equations or by using empirical information obtained from experiments. Because of the strong mixing in the gas phase by the concurrent flow, the assumption of infinite chemical reaction is widely used in the treatment of the gas phase with good accuracy. Most of the theoretical analysis so far assume that the concurrent flow is under laminar condition and the radiation heat transfer is negligible, which makes the results from those analysis unsuitable for turbulent and large scale cases. The analytical results from the heat transfer models are usually in good agreement with the experimental data. For flame spread on vertical wall a power law in the form of $V_p \sim L_p^n \sim t^m$ is predicted for the dependence of flame spread rate on the pyrolysis length [7], which correspond the experimental observations. For flame spread in a forced flow the linear dependence of the flame spread rate on the gas flow velocity is also correctly predicted.

A typical example of the analytical procedures used to solve the problem is presented in [74] of flame spread over a tilted wall. The analysis has assumed a boundary layer reacting flow with a one-step gas phase chemical reaction and an infinite fast chemical reaction rate, and therefore, the source terms in the energy and species equations can be eliminated by using Shvab-Zeldovich formulation. The solution is sought in the upstream and downstream region separately. In the upstream the interface temperature is assumed to be constant and equal to the

pyrolysis temperature of the material and the gas phase and the solid phase equations become uncoupled, and a similarity solution is found to exist for the boundary layer equations. In the downstream region the interface is assumed to hold the isothermal wall condition which greatly simplifies the governing equations. The uncoupled equations also produce a similarity solution for the gas phase, which can be utilized to solve the one-dimensional solid phase conduction problem. The flame spread rate and the pyrolysis length are found as follows

$$V_p = A(2Ant)^{(1-2n)/2n}$$

and

$$1_p = (2Ant)^{1/2n}$$

where t is time, A and n are constants.

Among more recent analytical studies on this subject is [75], which seeks the parametric dependence of the rate of wind-aided flame spread across a thick horizontal fuel slab by approximate analysis. Similar assumptions as in [74] are used and similarity solutions are obtained from the simplified equations. The flame spread rates are expressed explicitly in terms of boundary layer non-dimensional parameters and the ratio of streamwise distance and time.

Most of the work mentioned above only deals with laminar flows except for the large scale vertical wall flame spread work on PMMA sheets [58] [59] and on wood sheets [60]. The flows in these studies are buoyancy induced and the turbulence in the flow is also naturally generated depending on the sample scale. Most effort in these work has been focused on the dependence of the flame spread

rate on the sample scale [58] or on the magnitude of an imposed radiant heat flux [59]. No systematic experimental study has been performed to date on the effect of flow turbulence intensity on the rate at which flames spread over the surface of a solid fuel. The present work is to carry out an parametric study on the spread of flames in a concurrent turbulent forced flow with the main objective of determining the effect of external flow velocity and turbulence intensity on the flame spread rate, and inferring from the experimental measurements the influence of flow turbulence on the different mechanisms controlling the spread of the flame.

4 3 Experimental Arrangement

The schematic of the experimental installation for concurrent flame spread tests is shown in Fig. 4.1. The flow velocity and turbulence intensity are measured and monitored with the LDV system. The fuel surface temperature histories are measured with thermocouples at eight equal-spaced locations along the centerline of the PMMA sample, from which the propagation rate of the pyrolysis front is determined. A Schlieren imaging system of large light beam size is used to replace the interferometer used in the opposed flame spread experiments because the whole reacting region is of interest in this case. Thermally thick PMMA sheets are tested in the experiments.

4.4 Experimental Results

The measurements of the flame spread rate over PMMA sheets as a function

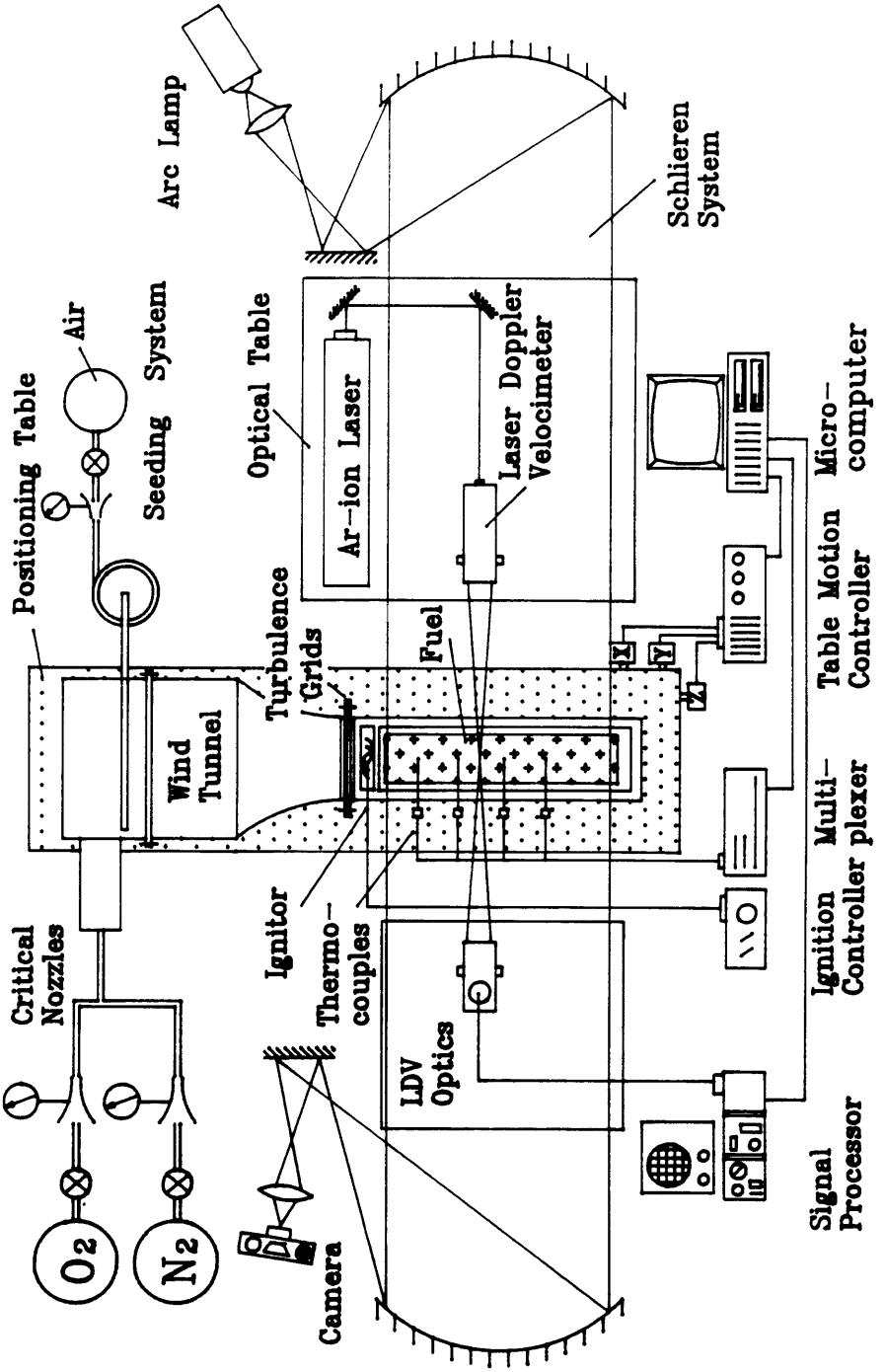

Fig. 4.1 Schematic of experimental facility for concurrent flow flame spread study.

of concurrent air flow free stream velocity are shown in Fig. 4.2 for several values of flow turbulence intensity. The spread rate is calculated as an average of the values deduced from the consecutive thermocouple throughout the specimen length and from different tests. Neither apparent increasing nor decreasing trend is observed from the local measurement and consequently, the spread rate is considered as time-independent over the test sample, which is in agreement with the results of [70] [76]. The forced flow velocity tested ranges from 1 to 4 m/sec. Measurements for flow velocities smaller than 1m/sec are not made because buoyancy casts strong influence on the flame spread process at low flow velocities. For velocities larger than 4 m/sec, extinction signs start to appear at the upstream leading edge, especially for large turbulence cases, which makes accurate measurements difficult.

It is seen from Fig. 4.2 that the concurrent flame spread rate increases with the flow velocity monotonically for all turbulence intensity levels tested. At low turbulence flows, the flame spread rate has an almost linear dependence on the flow velocity, which agrees with the results for laminar flow flame spread [76]. The monotonic increase of the flame spread rate with the flow velocity is predicted by most models of concurrent flame spread [7] and is consistent with heat transfer processes in forced flow flat plate boundary layer [77]. As the flow velocity increases, the thickness of the boundary layer, and consequently the flame stand-off distance, decreases. As a result, the heat flux from the flame to the solid fuel surface is enhanced and the flame spread rate is increased.

The dependence of the concurrent flame spread rate on the turbulence

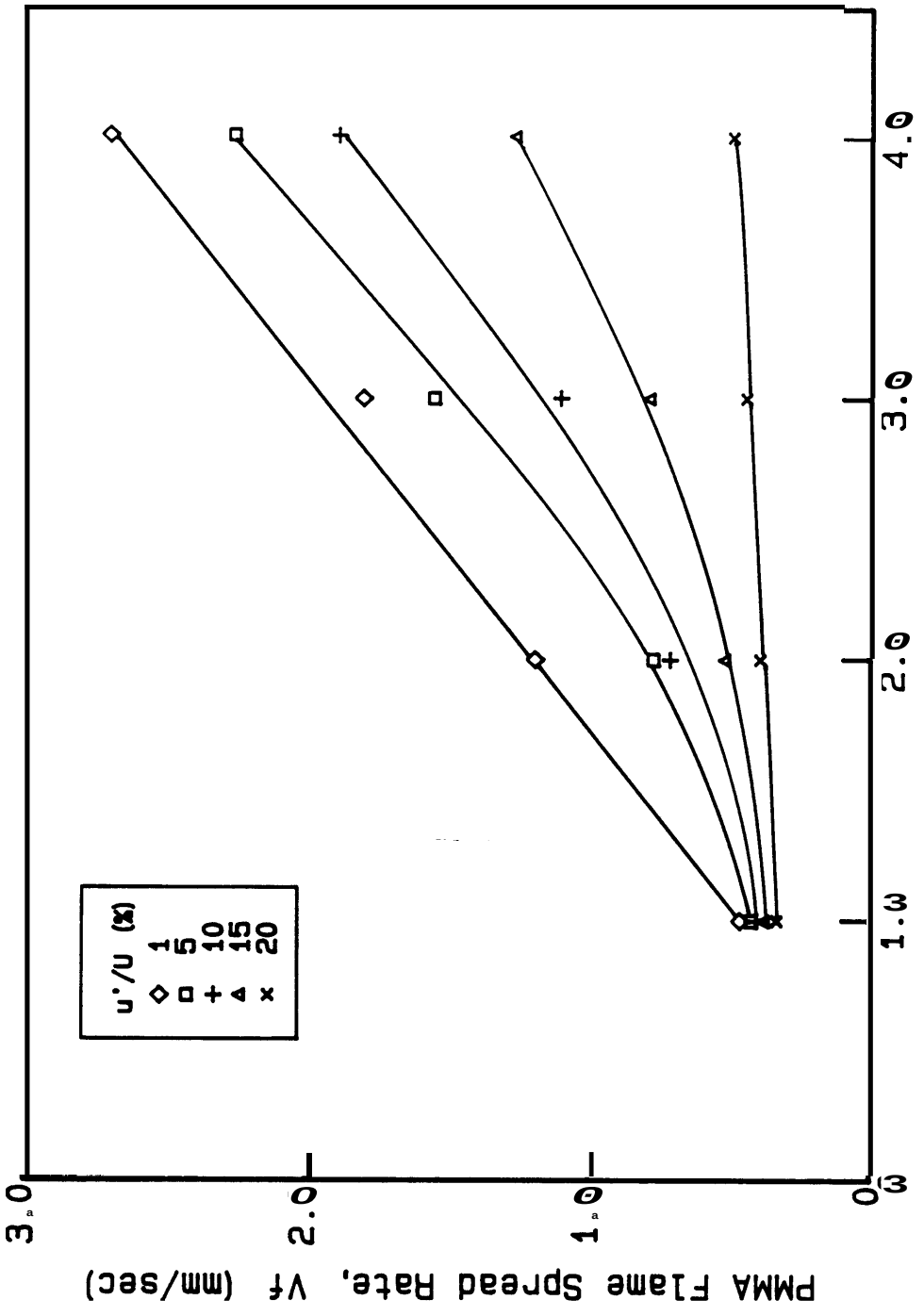

Fig. 4.2 Flame spread rate over thick PMMA sheets as a function of the concurrent air flow velocity.

intensity is presented in Fig. 4.3. It is found that the spread rate decreases as the turbulence intensity increases, and that the effect is more pronounced for larger flow velocities. The dependence of the flame spread rate on the turbulence intensity is almost linear for the velocities tested. These results are very interesting and somewhat surprising since this mode of flame spread is controlled by heat transfer from the flame to the fuel, and it is well known that turbulent boundary layer heat transfer is stronger than the laminar flow one. The results are important not only because they introduce new aspects about the flame spread process not previously predicted, but also because it may have significant influence in the application of flame spread formulas in models of real fire development.

4.5 Discussion

In order to understand the characteristics of the experimental results, it is helpful to examine the mechanisms determining the spread of the flame. As previous experimental and theoretical studies have indicated, the heat transfer from the flame to the solid fuel is the dominant controlling mechanism. A simple energy analysis applied to a control volume in the unburned solid fuel downstream from the pyrolysis front yields an expression for the flame spread rate [48] that seems to describe well the process under investigation.

The solid phase can be assumed as a semi-infinite medium, which can be justified by comparing the heat conduction time and the time for the flame to spread over the entire length of the fuel sample. The conduction time is calculated as:

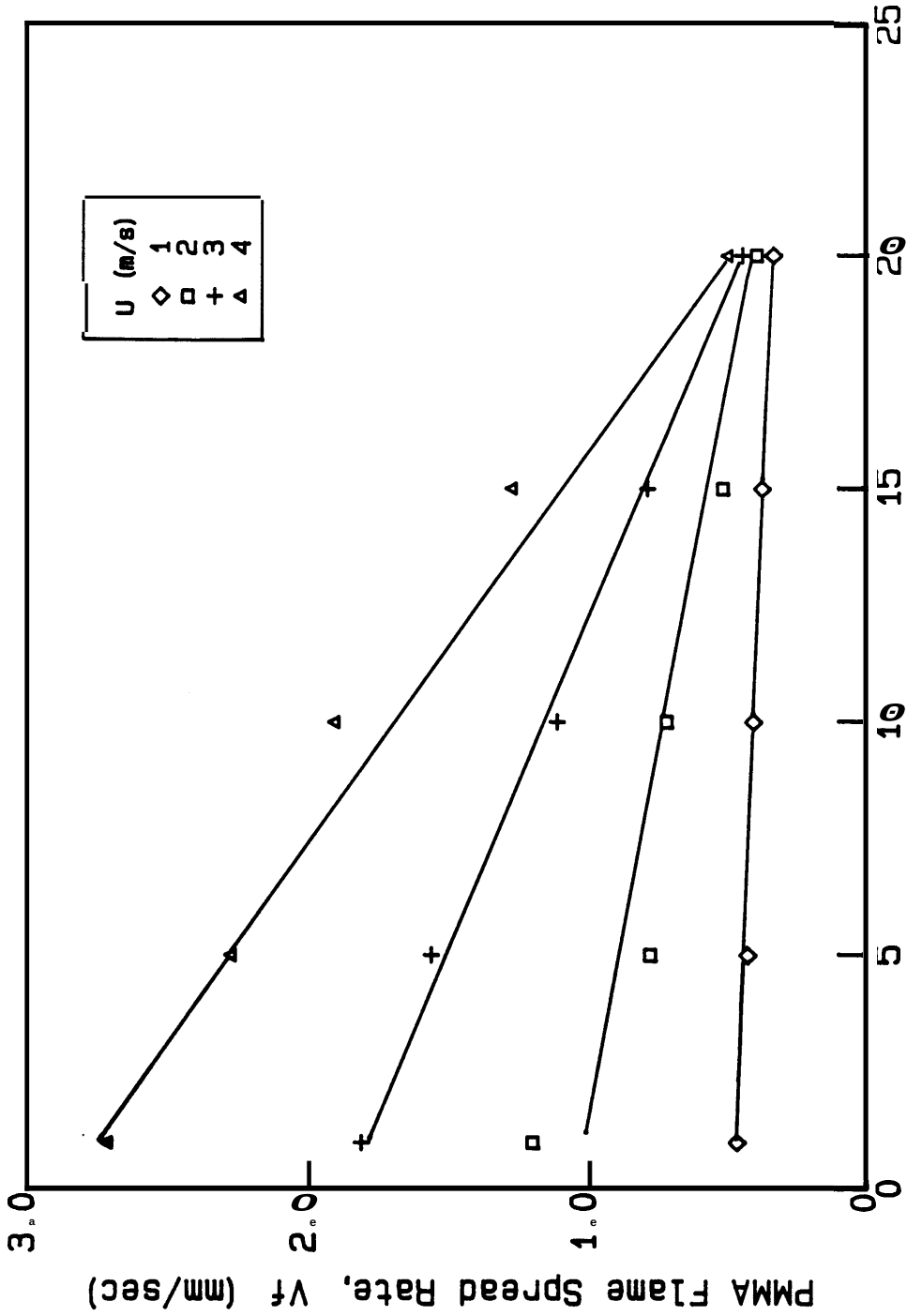

Fig. 4.3 Variation of the flame spread rate over thick PMMA sheets with the concurrent flow turbulence intensity.

$$t_{conduction} = d/4\alpha_p \sim 4000 \text{ sec}$$

where d and α_p are the thickness and thermal diffusivity of PMMA fuel sample. And the flame propagation time is in the order of

$$t_{propagation} = L/V_p \sim 200 \text{ sec}$$

The propagation time is one order smaller than the conduction time, therefore, the semi-infinite approximation is valid in this case. Since the temperature gradient in the longitudinal direction is much less than that in the normal direction, further assumption of one dimensional conduction is made for this problem. Therefore, the solid phase problem is considered to be governed by a transient, semi-infinite, one-dimensional heat conduction equation as follows:

$$\frac{\partial T}{\partial t} = \alpha \frac{\partial^2 T}{\partial x^2} \tag{4.1}$$

with the initial and boundary conditions:

$$T(x, t=0) = T_i$$

$$T(x=\infty, t) = T_i$$

$$-k\left[\frac{\partial T}{\partial x}\right]_{x=0} = q_f$$

where T_i is the initial temperature and q_f is the heat flux at the solid surface. The solution for the surface temperature ($x = 0$) is [78]:

$$T_{surface} - T_i = \frac{2q_f\sqrt{\alpha t/\pi}}{k}$$

Let the surface temperature be the pyrolysis temperature T_p and assume that the relation between the flame length and flame spread rate is simply as

$$l_f = V_f \times t$$

then an expression for the flame spread rate can be obtained as

$$V_f = \frac{4q_f^2 l_f}{\pi k\rho c(T_p - T_i)^2} \qquad (4.2)$$

where $k\rho c$ are the thermal properties of the solid. This equation indicates clearly that the flame spread rate is dependent on the flame length and heat flux from the flame at the fuel surface.

The flow velocity and the turbulence intensity can affect the flame spread rate through the heat flux and the flame length primarily, although other mechanisms are also possible. Therefore, it is important to determine how each property changes under different flow conditions. The flame length and the heat flux have not been measured directly in this study. However, an approximate estimation of their values can be deduced from the fuel surface temperature histories. The flame length can be obtained by determining the position of the flame tip under which the surface temperature starts rising. It should be noted that the resulting length is not necessarily the actual visible flame length, but the length of the elevated temperature region ahead of the pyrolysis front. For simplicity, this length is called flame length

here. Using this method, the variation of the flame length to the pyrolysis length ratio with the flow velocity and turbulence intensity are determined, and presented in Fig. 4.4 and 4.5, respectively. The ratio of the flame length and the pyrolysis length is found to be approximately constant along the PMMA surface, and the value presented in the figures corresponds to an average of all the calculated ratios from eight locations. From Fig. 4.4 it is seen that the flame length to pyrolysis length ratio increases approximately linearly with the flow velocity although the rate of increase is smaller for high turbulence intensity. Fig. 4.5 shows that for all flow velocity tested, the flame length to pyrolysis length ratio decreases as the turbulence intensity increases.

Schlieren images taken during the flame spread tests are used to confirm the effect of flow turbulence on the flame length and the thermal boundary layer. A typical sequence of Schlieren pictures are presented in Fig. 4.6 for the flow of velocity of 2 m/sec and turbulence of 1%, 5%, 15%. The images show that the thermal layer has the characteristics of a flat plate forced flow boundary layer with its thickness increasing with the distance from the upstream leading edge. It is also seen that the strong inducement of cold air into the flame zone by the flow turbulence, which reduces the reaction zone temperature.

The flame shortening can be the result of either quenching or enhancement of the combustion reaction. In the former case, the strong inducement of cold air into the reaction zone, and the interaction of the cold solid wall with the flame, could quench the reaction downstream where the fuel is less abundant and consequently,

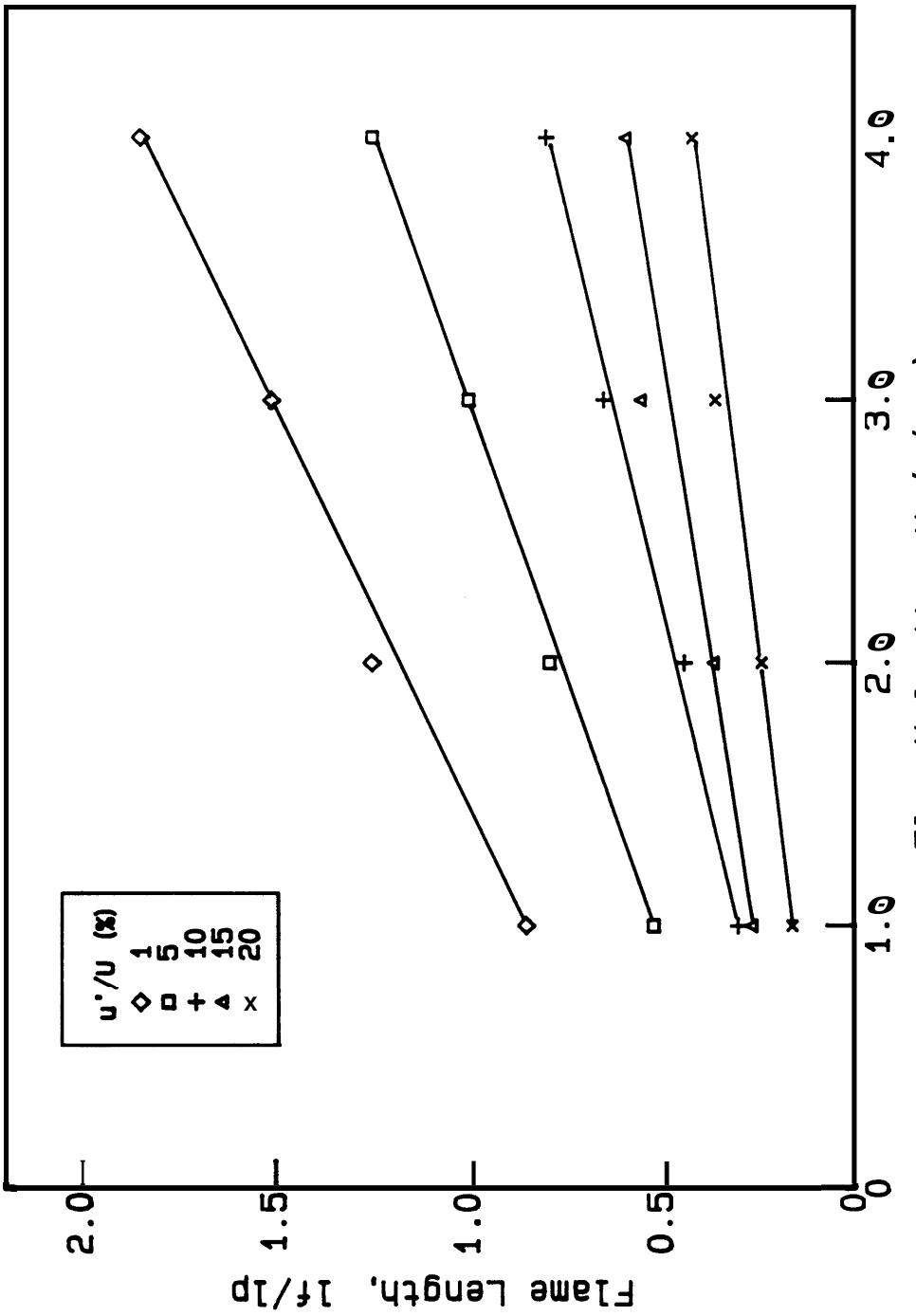

Fig. 4.4 **Dependence of the downstream flame length to pyrolysis length ratio on the flow velocity.**

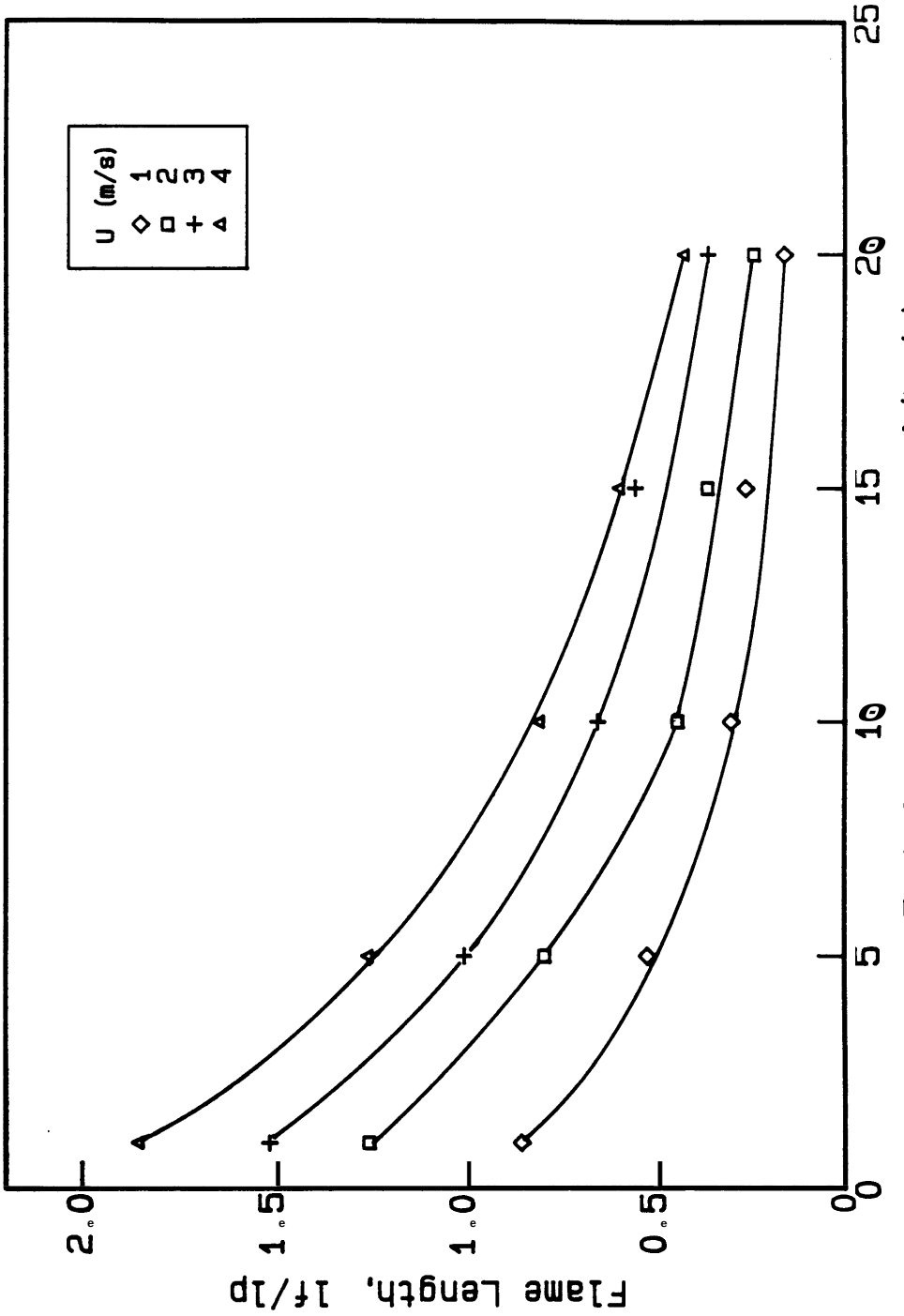

Fig. 4.5 Dependence of the downstream flame length to pyrolysis length ratio on the flow turbulence intensity.

(a) U = 2 m/sec, u'/U = 1%

(b) U = 2 m/sec, u'/U = 5%

(c) U = 2 m/sec, u'/U = 15%

Fig. **4.6** Schlieren images describing the flame characteristics in concurrent air **flows** of 2 m/sec and varied turbulence intensities.

shorten the flame. In the latter case, the possibly increased mixing of the fuel vapor and oxidizer could enhance the reaction, consumes the fuel faster and ends the flame sooner [79]. Visual observation during the experiments suggests that the former factor may be more dominant, which is later confirmed by the exhaust gas concentration measurements. The major species O_2, CO_2, CO and unburned hydrocarbons in the combustion exhaust flow are measured to determine how thorough the chemical reaction proceeds. A good indication of the completeness of the gas phase chemical reactions is the CO concentration in the exhaust flow, which is presented in Fig. 4.7 and 4.8 for two flow velocities of 1 and 4 m/sec under laminar and turbulent conditions. The horizontal coordinate is chosen as the flame front position from the leading edge for easier comparison between two cases. It is seen that at the same velocity, more carbon monoxide is generated in the high turbulence flow than in the lower turbulence one. Similar trend has also been observed at other flow conditions with different flow velocities. This observation seems to suggest that the chemical reactions are less complete for flows with larger turbulence intensity. Therefore, it can be inferred in the cases studied that the strong turbulence quenches the flame, and as a result, the flame length is shortened and the flame spread rate decreased.

Another important parameter in the problem is the surface heat flux of the unburnt solid downstream from the pyrolysis front. The heat flux has been calculated from the surface temperature histories by assuming that the fuel behaves as a semi-infinite solid exposed to a constant surface heat flux. It is found that the product

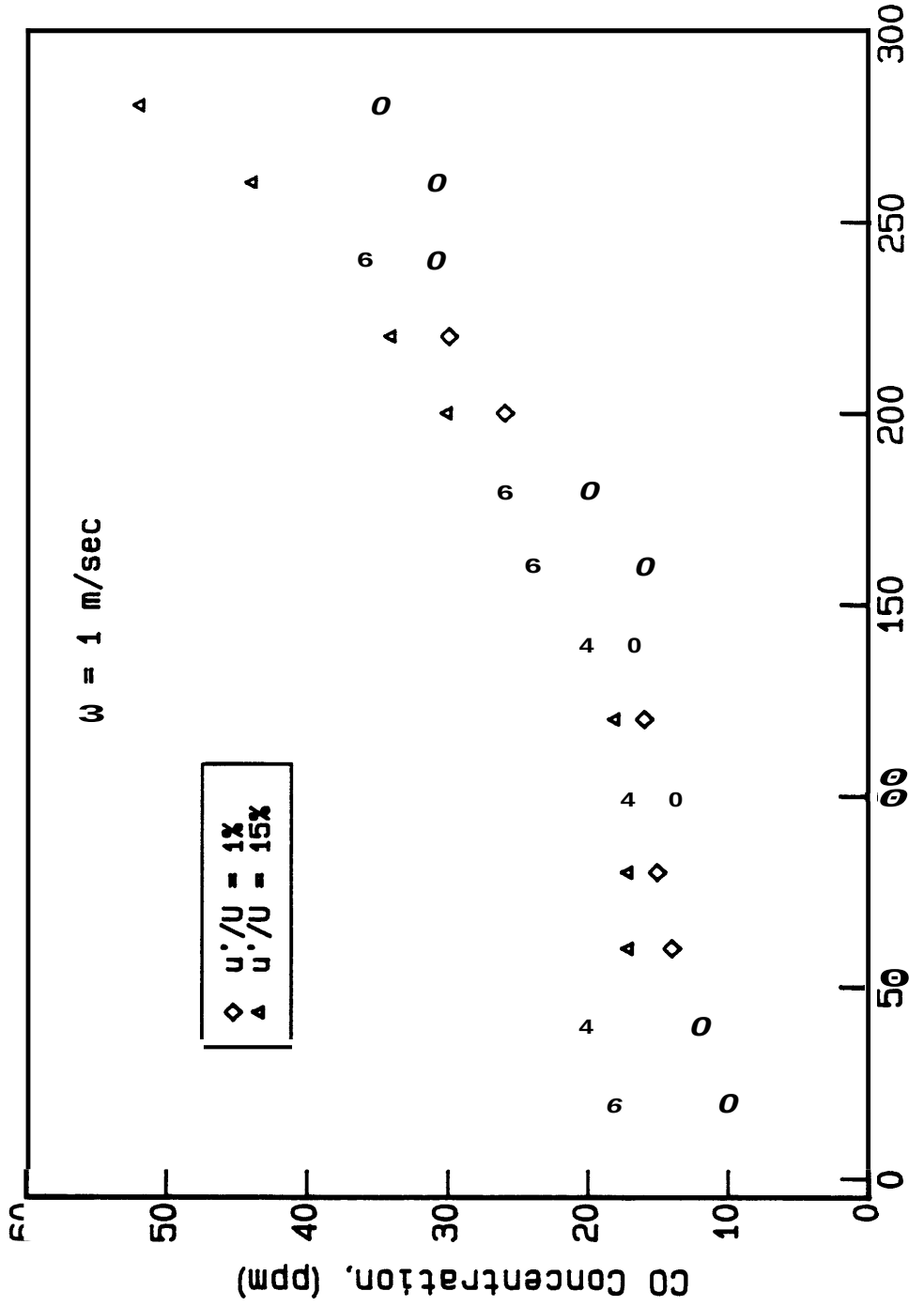

Fig. 4.7 CO concentrations in the exhaust gas flow for two turbulence intensities at U = 1 m/sec.

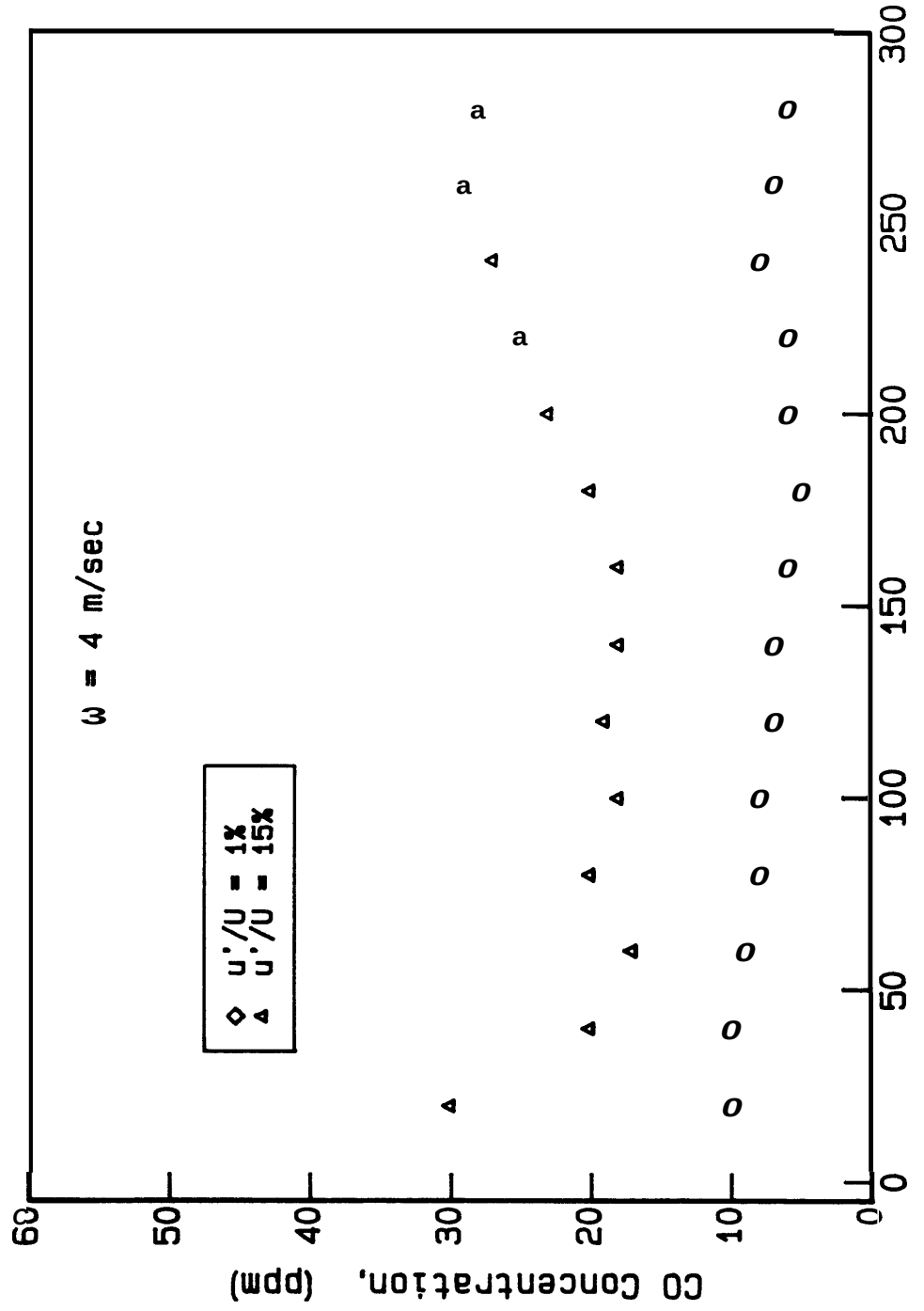

Fig. 4.8 CO concentrations in the exhaust gas flow for two turbulence intensities at U = 4 m/sec.

$q_f l_p^{1/2}$ keeps an approximately constant value through the entire surface, in qualitative agreement with the forced flow boundary layer heat transfer predictions [80]. The calculated variation of the heat flux with the flow velocity and turbulence intensity is shown in Fig. 4.9 and 4.10. The heat flux data is an average value of those obtained over the fuel surface and corresponds to that received by a surface element that is midway between the flame tip and the pyrolysis front. The results show that the product of the surface heat flux and the pyrolysis length increases monotonically with the flow velocity although the increase is less prominent for higher turbulent intensities. For a fixed flow velocity the product increases with the turbulence intensity.

In order to verify the predicting capability of Eq. (4.2), a new expression of that equation is used as :

$$V_f = \frac{4(q_f l_p^{1/2})^2 (l_f/l_p)}{\pi k \rho c (T_p - T_i)^2} \qquad (4.3)$$

where l_p is the pyrolysis length.

All the data presented in Fig. 4.2, 4.5 and 4.10 have been combined to produce the overall result shown in Fig. 4.11, where the non-dimensional flame spread rate deduced from Eq. (4.2) is plotted versus the turbulence intensity for all the flow velocity tested. It is Seen that the correlation of the measurements is remarkably good considering the simplifications made in the derivation of Eq. (4.2) and the diversity of the measurements. The deviation from unity in the non-dimensional flame spread rate and the scatter on the correlation are attributed to the

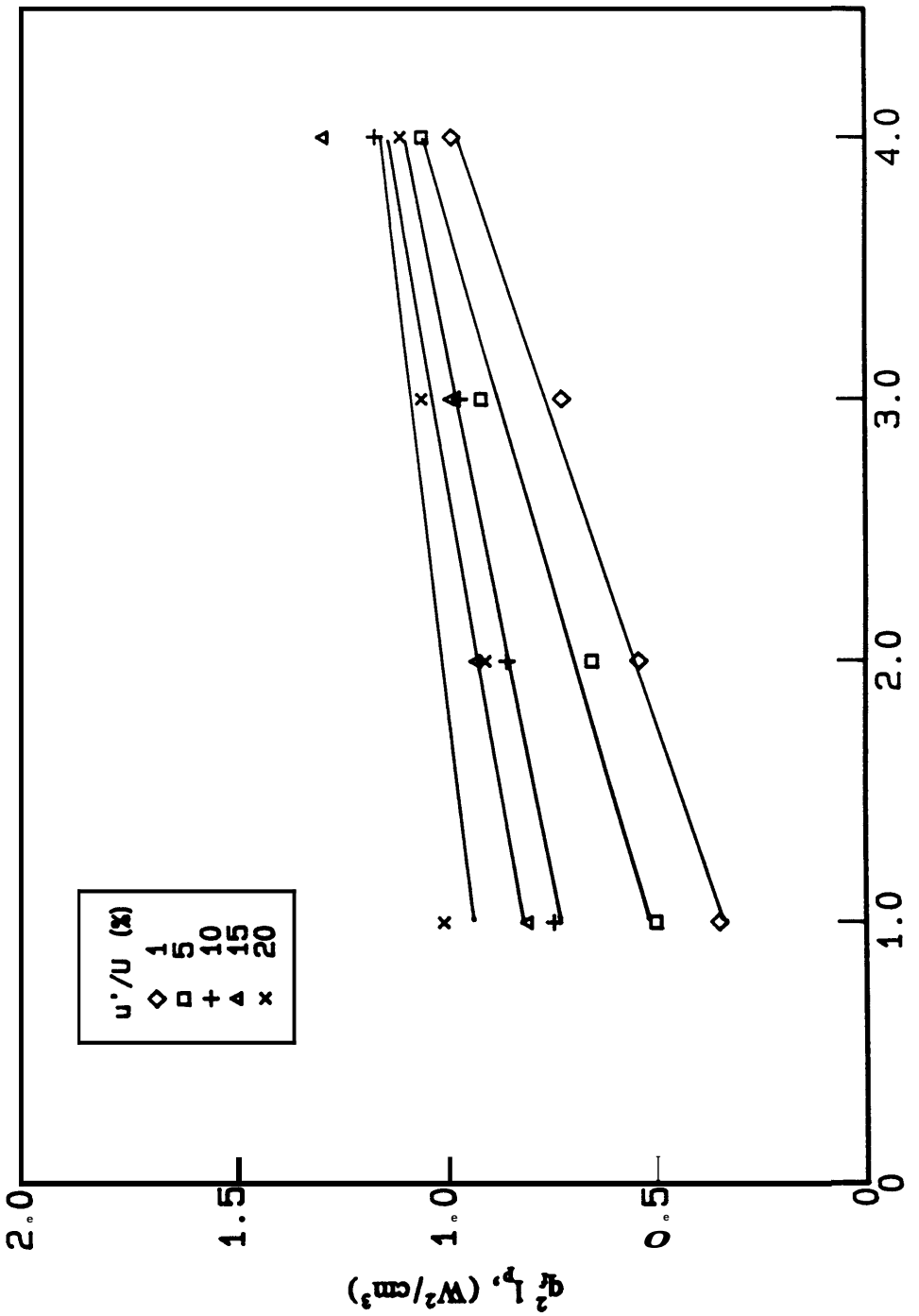

Fig. 4.9 Variation of surface heat flux with the concurrent air flow velocity.

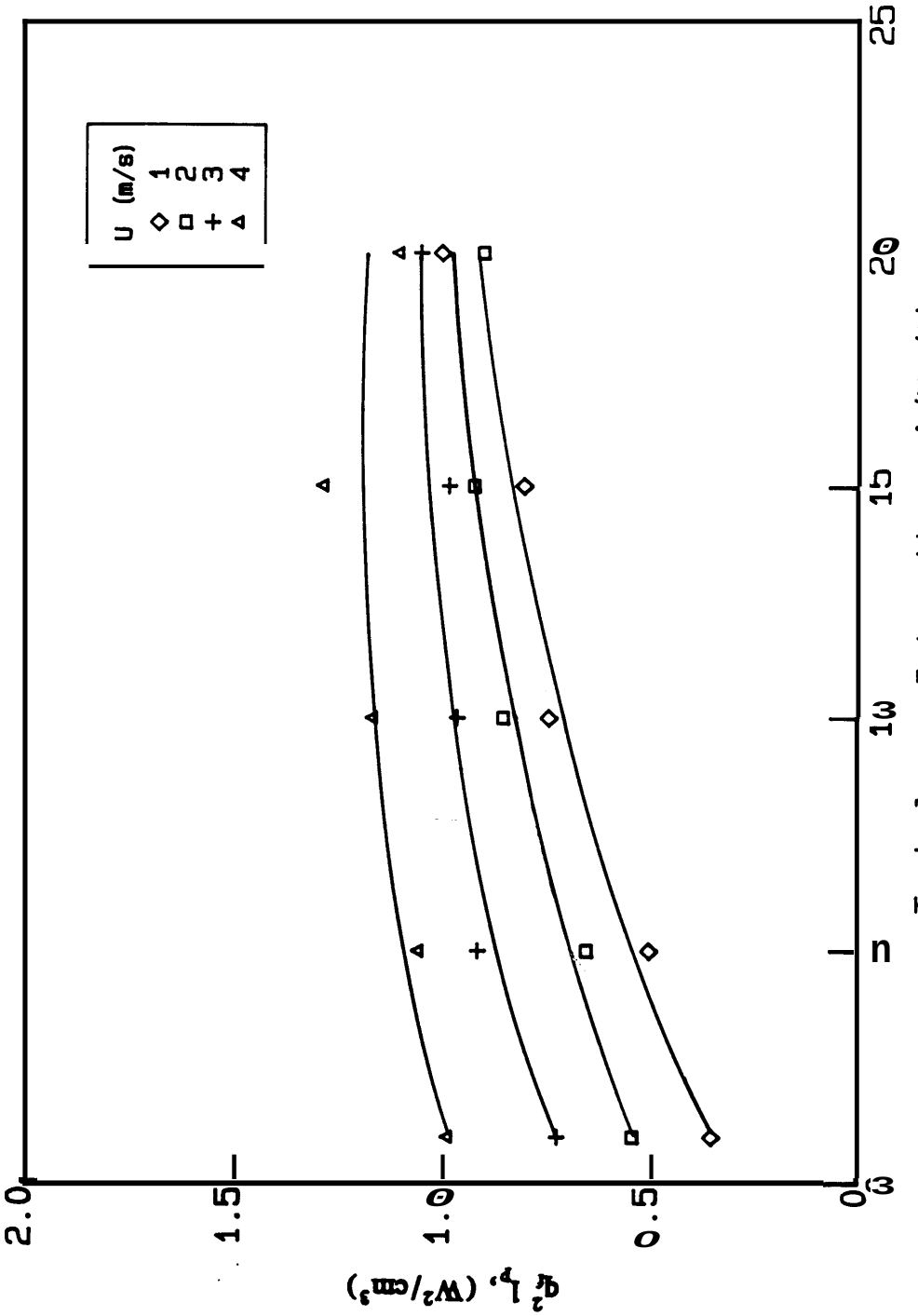

Fig. 4.10 Variation of surface heat flux with the flow turbulence intensity.

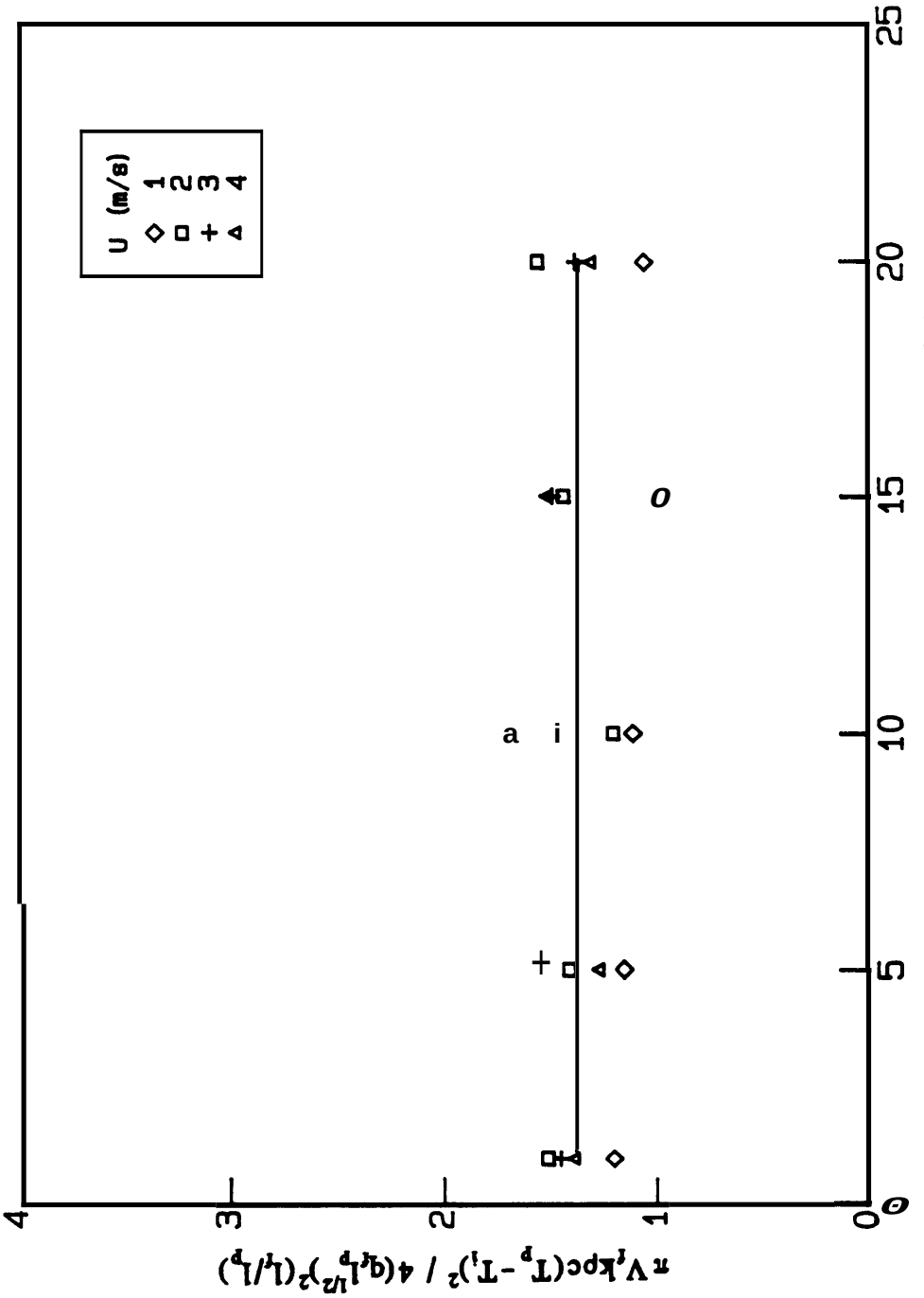

Fig. 4.11 Correlation of the flame spread data in terms of a non-dimensional flame spread rate deduced from Eq. (4.3).

indirect determination of the flame length and surface heat flux, and the uncertainty of the pyrolysis temperature. The results of Fig. 4.11 in conjunction with the results from other figures corroborate the above arguments that the shortening of the flame length with the turbulence through quenching is the primary reason for the observed reduction of the flame spread rate as the turbulence intensity increases. The good agreement between the measured and predicted flame spread rate confirms that the heat transfer from the flame to the solid surface is the dominant controlling mechanism in the concurrent flame spread process in forced turbulent flows.

4.6 Conclusion

The results of this study show that flow turbulence has a strong influence on the flame spread process in the concurrent flow. The turbulence reduces the flame spread at the flow velocities tested, mainly through the shortening of the flame length by quenching. Both the observed shortening of the flame length and decrease of the flame spread rate as the turbulent intensity increases are significant new observations that may have an important impact in fire modeling since the prediction of flame lengths and flame spread rates as functions of the environmental conditions is the foremost concern in the development of room fire studies and the establishment of material flammability tests.

The limitations of this experimental work such as specimen size, indirect data for heat transfer and flame length, etc., have not allowed the extraction of more accurate information about the problem. For example, a convection based heat

transfer analysis applied to Eq. (4.2) predicts

$$V_f = C\frac{(T_f - T_v)^2}{(T_v - T_i)^2}\frac{l_f}{l_p}\frac{U^{2a}}{l_p^{1-2a}} \qquad (4.3)$$

where the surface heat flux has been taken as $q_f = CRe^a Pr^{1/3}(T_f - T_v)/l_p$ according to boundary layer theory. Thus, if l_f/l_p remains constant along the fuel surface, Eq. (4.3) predicts a constant spread rate that increases linearly with the flow velocity for laminar flow, and one that accelerates as it spreads over the solid surface and has a power law dependence on the flow velocity for turbulent flow. The present data does not show an accelerating trend in turbulent flow perhaps because the data is not detailed enough for such an analysis, due to the above indicated experimental limitations. However, it should be noted that in this work the free stream is relative small and that turbulence is generated by introducing vorticity in the downstream free stream flow. Thus, the classical heat transfer approach may not be totally appropriate unless an eddy related Scale is introduced in the problem. More detailed work is needed to determine the actual process through which the flow turbulence affects the flame process.

Given the potential impact of the present results on the theoretical prediction of the spread of flames, it is important to extend the work to the study of other aspects of the process. For example, it is important to know how turbulence affects the flame spread process in a vitiated environment, or how the characteristics of the flow turbulence (free flow or boundary layer turbulence) may quantitatively affect the rate of spread for a given turbulence intensity. Also important is to know if and

how turbulence affects the rate of mass burning in the pyrolyzing region, the rate of soot production and the radiative properties of the flames.

Chapter 5 Mass Burning of a Solid Fuel Surface

5.1 Introduction

Solid fuel mass burning is defined as the combustion process taking place behind a pyrolysis front, which causes the fuel surface to recede into itself. A simplified schematic of mass burning is illustrated in Fig. 5.1 for the pyrolyzing region of a solid combustible surface in a external flow. Heat is transported from the diffusion flame to the condensed fuel surface through convection and radiation to maintain the pyrolysis of the fuel. The resulting fuel vapor mixes and reacts with the oxidizer from the gas flow in the combustion region. The mass burning process sustains itself by the energy released in the reacting zone, and assists the further spreading of the accompanying flame. As a typical non-premixed combustion process, the solid fuel mass burning has been considered [5] to be controlled dominantly by heat and mass transfer, even though other mechanisms can be important in some special cases.

The surface regression of a solid combustible burning in a convective oxidizing gas flow is an important subject in problems related to the development of fires, materials processing and rocket propulsion. Parameters in a mass burning process that are of particularly importance and often studied in fire research include surface regression rate, flame height or length depending on the configuration of the problem. Especially important is the burning rate that often determines the heat release rate, and smoke and CO emission, among others, which in turn determine the

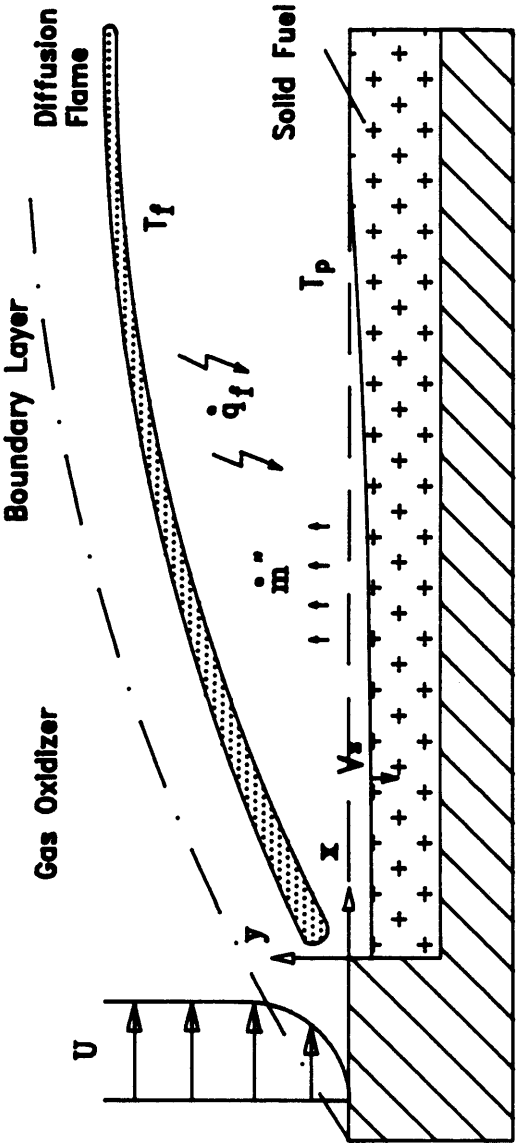

Fig. 5.1 Schematic of solid fuel mass burning process.

growth rate of the fire and its potential hazard. The distinction between the regression rate and the flame spread rate studied in the previous chapters must be made to clarify the two different processes which often intertwine in real cases. The velocity at which the fuel surface recedes perpendicular to itself along the portion bathed by flame is the normal surface regression rate or surface burning rate, and the velocity at which the boundary of the burning area moves along the fuel surface is the flame spread rate.

5.2 Literature Review

A large number of theoretical and experimental studies have been conducted of laminar and turbulent burning of a flat surface. The analytical solution of the problem is mostly obtained by using coupling functions in gas phase energy and species equations as often practiced in many other diffusion flame problems. By introducing coupling function and applying proper interface conditions, the governing equations *can* be greatly simplified and often solved with similarity solutions.

The first attempt using the coupling function concept was made by Burke and Schumann [81] on the problem of flame locations in concentric duct burners. More detailed analyses were made by Shvab [82] and Zeldovich [83] of the temperature and velocity distributions of gas burners. Spalding [84] [85] used similar methods to solve the problem of fuel pyrolysis caused by combustion released energy transport. However, it was the work by Emmons [8] on the liquid fuel surface burning that established the foundations for the modem theoretical modelling of the mass burning

process of condensed fuels. Emmons' work addressed the problem of a flat plate consisting of evaporating fuel burning in a laminar flow. The fuel vapor convects along the surface and diffuses away from it until it is mixed with oxygen and is sufficiently heated to bum. Infinite fast reaction rates are considered, and therefore, the combustion zone can be simplified as a thin sheet. Boundary layer flow is also assumed due to the configuration of the problem. The assumptions also include Lewis number and Prantle number being unity, among others. The governing equations are uncoupled by the use of Shvab-Zeldovich variables and similarity solutions are obtained for the distributions of temperature, flow velocity and species concentrations in the flow. The regression rate of the fuel surface can be readily deduced from the boundary condition,

$$\frac{\rho_s V_r}{\rho U} = C\, Re_x^{1/2}$$

where V_r is the surface regression rate and U is the flow velocity and ρ_s and ρ are the densities of the gas and the solid fuel, respectively. The equation above indicates that the non-dimensional regression rate is proportional to the square root of the flow Reynolds number for laminar flows. The dependence of the regression rate on the flow oxygen concentration and fuel thermal properties, namely the dependence on the mass transfer B number of the problem has also been determined, which displays a monotonically increasing trend. More advanced work on condensed fuel burning has been following the similar methodology used in this work with some alterations for the specific problem.

In fire related mass burning problems, the most frequently studied is the burning of a thick wall in vertical configuration under natural convection flow conditions. The solutions usually consider the transport characteristics and flame structures of two regions: the pyrolysis zone, where the wall material decomposes to provide gaseous fuel for the fire; and the wall plume region above the pyrolysis zone, where combustion is further completed and the fire generated plume decays by mixing with the ambient gas and heat loss to the wall. Initial effort in [63] [64] is aimed at the laminar flow problem by using the similar methodology as in [8]. A similarity theory for the natural convection boundary layer adjacent to a vertical flat plate is developed in [64] for large temperature variations, of wall mass transfer and of boundary layer combustion. The theory is used to calculate the flame stand-off distance and proved to be in good agreement with the experimental results for alpha-cellulose cylinder burning, and therefore confirms the validity of the analysis. A more generalized theoretical treatment is developed in [63] for the free-convective laminar burning of vertical, inclined and horizontal cylindrical surfaces, with the assumptions of one-step chemical reaction, no radiation and unity Lewis number. The solution shows that the laminar burning rates are governed by both fluid mechanical and chemical effects. The fluid effects (or geometric effects) are described by the Grashof number, and the chemical effects are described by the mass driving force B, the stoichiometry coefficient and the surface temperature. The burning rates are computed over a wide range of situations and the results show that the mass-transfer driving force B is the most dominant chemical parameter. The

theoretical predictions from this analysis agree well with experimental data except for the higher molecular weight fuels. The related laminar flame plume region problem is analyzed in [86] [87].

The gas phase chemical reaction rates in the analysis above are generally assumed as infinite fast, resulting in flame sheet approximation in the reaction zone. The radiation heat transfer is usually not considered in those analysis either. Since such a model does not contain any mechanisms which can cause extinction the solutions are unable to predict the flammability limits even though the results may be sufficient to predict the mass burning rate. The first step is taken in [88] to predict the extinction limit for vertical surface burning by considering the effect of radiation on wall fires while retaining the flame sheet approximation. It is found that even in the limit of an infinite chemical reaction rate, extinction is obtained when sufficient surface radiation is included. However, when the results are applied to PMMA burning in O_2/N_2 mixtures, the predicted extinction limit ($Y_{o,\infty} = 0.12$) is significantly lower than the measured value of 0.18, which indicates additional factors are presumed to affect the extinction. In [89] the finite rate chemical reaction is used for gas phase and the effect of chemical reaction is determined on the mass burning rate and flame extinction limit. As indicated by more complete work on this subject [90], the predicted mass burning rate with finite rate is essentially independent of the assumed chemical reaction rate except for small difference when the flame is close to extinction. Thus, simpler flame models are sufficient to provide accurate results when only burning rates are concerned. It is also found that for solid

fuels with high surface temperature while burning, the predicted burning rate has a strong dependence on the heat loss from the surface due to thermal radiation. The extinction limits are sensitive to a combination of the assumed chemical reaction rate and the radiative heat loss from the fuel surface. This leads to extinction occurring at different flame temperature for different combinations of fuel size and ambient oxygen concentration. This analysis can also be used to predict a minimum oxygen concentration which will sustain burning.

The turbulent mass burning in wall fires has also been intensively investigated. Ahmed and Faeth [91] have used an integral model developed in [92] to provide an expression for mass burning rate. Radiation heat transfer is not considered in this analysis. Relatively low turbulence intensity is assumed in the mode, which implies that products of fluctuating quantities are small in comparison to products of mean quantities, when integrated across the flow. Empirical information is required to represent friction and heat and mass transfer at the wall for the theoretical model. Assuming completely turbulent flow from the lower edge of the wall, the average burning rate for a smooth wall is obtained. Also found is the average burning rate for laminar flow from the integral model. Therefore, a united correlation of laminar and turbulent mass burning rate is obtained, which is compared with various experimental data with satisfactory result. The integral models also provide good estimations for flame length, which indicate that flame lengths for laminar wall fires axe 2 to 3 times longer than those for turbulent flows. For the flame plume region, a mixing length model is used to simulate the turbulent flow and an expression for

wall heat flux is obtained. The integral model is also used in [93] [94] to predict the wall pyrolysis rate, the mass flow rate and the maximum velocity and the maximum mean gas temperature for turbulent wall fires. A simple algebraic model is developed in [95] to discuss the difficulties for employing integral models for turbulent diffusion fires, and to further understand the possible simplifications for more involved models.

Numerical solutions of turbulent mass burning are provided in many studies including [89] [90] and [95] - [97]. The main differences among these studies lie in the treatment of the turbulent flow involved. In [96], a k-e-g model is utilized for the turbulent flow in a wall injection problem, which simulates mas burning processes. The turbulence energy k and its dissipation rate ϵ are calculated by means of transport equations which are solved simultaneously with the conservation equations for the mean flow. A probablistic combustion model is developed for the reacting species, which introduces the influence of species mass fraction fluctuation. The burning rate obtained is related to the turbulent characteristic and the mass burning rate. Further effort in this direction [97] has incorporated radiation effect on the wall fires together with turbulent flow. A modified version of the k-e-g model of turbulence is used to calculate the rate of burning of large-scale vertical walls where radiation heat transfer is significant. The standard k-e-g procedure is generalized by the introduction of algebraic formulas for the stresses and the mass/energy turbulent fluxes, and by the use of wall correction factors. Two models for predicting flame radiation are employed: the "constant-X" approach, according

to which the *radiationpower is a constant fraction of the energy liberated per unit time by chemical reaction, and the "soot-band concept, which postulates that radiation is emitted by a thin, constant-temperature layer of particles at flame fronts. Calculation of a radiation-controlled paper wall fires has been used to evaluate the performance of two models for the radiation emitted by the luminous flames. It is found that better agreement with experiment can be obtained with the soot-band model than with the constant-X model of radiation. Turbulent reacting wall plumes are also studied in [98] which considers a diffusion flame fueled by a source at the base of a wall by using a k-e-g model, in [99] with a integral model and in [100] with a mixing length model. In spite of the large amount of work on the turbulent wall fires, more accurate models are still in demand due to the complication introduced by the turbulent flow.

Much experimental work has also been conducted on the vertical wall burning problem. The laminar flow tests have been carried out in [63] - [65]. In [63], vertical oriented cylinders of alpha-cellulose and birch-wood are used as fuels with air as oxidizer. Experimental measurements of the flame standoff distance are reported and support the similarity hypothesis used in the analysis of the same work with good agreement with the theoretical predictions. Experimental measurements of mass burning rates are correlated with the measured flame-plume heights for both materials by use of the Froude number. The test scales in the experimental studies above are usually quite small. To simulate real fires realistically, larger scale tests have been performed [58] [91] [101] [102], where the naturally-induced flows are

turbulent and the radiation from the flame is the dominant heat transfer mechanism. PMMA sheets of 3.56 m high have been tested in [58] [102]. The mass burning rates and heat fluxes at the surface are measured as functions of the vertical position. It is found that the burning rates increase nearly linearly with the height along the fuel slab. Radiative heat transfer is found to account for 75 to 87 percent of the total heat flux to the burning surface. The gray flame assumption of the analysis is confirmed by the agreement between theoretical predictions and experimental measurements of radiative fluxes from the flame to the surface. Turbulent natural convection fires are also simulated in [63] by 51-305 mm high wicks with methanol, ethanol and propanol. Measurements are made of burning rates in the pyrolysis zone, radiative and convective heat fluxes to the wall and profiles of mean flow velocity, temperature and concentrations in the flow. It is found that the non-dimensional mass burning rate increases with the free convection Rayleigh number and the increase slope is more pronounced in turbulent flows than in laminar ones. The surface heat flux decreases with the distance from the surface leading edge as the result of the flame moving away from the surface. It is also found that radiation comprises only 10 to 20 percent of the heat flux to the surface in the tests probably due to low soot content in the flames. The role of buoyancy direction is investigated in [101] on steady turbulent fires over a wide range of mass transfer driving forces, B. It is found that three principal burning modes exist based on the inclination angle: turbulent pool fires, upward turbulent burning and cellular ceiling fires. Steady burning rates decrease rapidly with inclination within the pool regime,

followed by a more gradual decrease with inclination angle within upward turbulent burning region. This trend is ascribed to the decreasing direct gravitational generation of turbulent kinetic energy, causing a reduction in the turbulent flame thickness with their reduced radiant fluxes. Radiation is found to exceed convective heat transfer to the fuel surface for B number larger than one. At large B numbers the burning is increasingly radiation-dominated as convection decreases due to heat blockage.

All studies presented above have concerned the mass burning process of fires in natural convection flows. Relatively less work has been reported on the forced flow fires, among which are [103] - [105]. In [103] [104], a one-dimensional Couette flow is assumed and the turbulent flow is treated with the concept of effective viscosity of Van Driest's formulation [106]. The influence of coupled convective, conductive and radiation heat transfer has been taken into account in the theoretical model. Regression rate of the solid surface is measured as a function of the oxygen and air flow rate. The mass burning rate increases with the forced flow rate and strongly depends on the oxygen concentration or more generally, on the mass transfer B number. In [105] an analysis is developed for mixed, forced, and free combustion on a flat fuel surface of arbitrary inclination that makes use of the laminar boundary layer approximation to describe the gas flow and of the flame-sheet approximation to describe the gas-phase reactions. A mixed-convection parameter $(Re^n Gr^m)^{1/2n}$ that properly scales the dependent and independent variable fields and a mixed convection ratio $(Gr^m/Re^n)^{1/2}$ that plays the role of the downstream local similarity

coordinate are introduced in the non-dimensionalization of the equations. It is shown that these two parameters, rather than the standard Reynolds number and Grashof number are the optimum choice of governing non-dimensional groups for this problem. The problem with a horizontal surface is solved in the analysis by selecting m = 2 and n = 5, and therefore obtaining a similarity solution of the governing equations. The mass burning rates, velocity and temperature profiles and other flow parameters *can* then be readily solved. More rigorous integral solutions is possible with this formulation while both the boundary layer and flame sheet approximations are disregarded.

Another area related to the present work is the study of hybrid rocket fuel combustion. Unlike normal erosive burning in solid propellent rocket motors where the premixed combustion is usually assumed in the gas phase, the hybrid rocket combustion has similar characteristics to those in wall burning problems, even though the later is more concerned with the fire related properties. The configuration of a hybrid rocket engine is basically similar to that of a regular solid rocket, where a fuel surface is exposed to the hot, reacting gas flow, except that the mixed fuel and oxidizer solid propellent of the latter is replaced by a pure solid fuel. A vaporized oxidizer streams axially through the core of the solid fuel, and after ignition the gas phase combustion of the oxidizer and fuel provides the heat necessary to vaporize the fuel. Combustion is then self-sustaining, and the combustion products are raised to a high temperature. Among many studies published to date on turbulent flow hybrid fuel rocket burning problem are those of Marxman and others [107] - [109]. In [107],

boundary layer flow and flame sheet approximations are used for the formulation of the problem with the surface regression rate as a boundary condition. Empirical friction coefficient is used to derive an explicit expression for the regression rate, which depends on flow velocity and the characteristics of the fuel and oxidizing flow. More general formulation is considered in [108] and the surface burning rate is found to depend on B number substantially. The formula for the regression rate is improved in a more recent work [110] with a new theory and the resulting equation agrees well with experimental data. It should be noted that the studies on hybrid rocket engines are more concerned with conditions of very high temperature, pressure and oxygen concentration that are not frequently encountered in conventional fires.

As mentioned before, relatively fewer studies have been conducted on the forced turbulent flow mass burning in the field of fire research and insufficient experimental data are available of the qualitative dependence of the mass burning rate on the flow velocity and turbulence intensity in a forced flow. Since many practical fires develop in wind-aided, turbulent environment, it is of great interest to investigate this problem and obtain necessary information for accurate material flammability test.

The turbulence in some studies mentioned above are either buoyantly-generated as in vertical wall fires or shear-generated as in rocket engine, and the flow structures are usually very complex since turbulence generation and dissipation occur simultaneously. Another alternative to study flow turbulent effects

is to introduce the turbulence artificially into the flow by means of a grid or perforated plate placed perpendicular to the flow direction. In grid-generated turbulent flow, the mean velocity gradient is small so that the flow structure can be considered as isotropic and homogeneous, and therefore, also relatively easier to characterize and to model theoretically. It is helpful to use simple turbulence flow such as grid flow to determine the relations between the flow and the flame [111].

This work presents a systematic study of the mass burning process of a solid fuel in a forced grid-generated turbulent air flow with the goal of experimentally determining the effects of the external flow velocity and turbulence intensity on the mass burning process. The experiments focus on the measurements of the surface regression rates and further effort is made to obtain the proper correlations between the regression rate and the flow parameters.

5.3 Experimental Arrangement

The experimental facility in this work is very similar to that described in Chapter 4 and the schematic of the setup can be seen in Fig. 4.1. The flow velocity and turbulence intensity are measured and monitored with a one-dimensional LDV and the surface temperatures are measured at eight locations. The experiments focus on the burning of PMMA sheets after the diffusion flame has spread over the fuel surface. The surface regression rates at a series of locations on the fuel center line are obtained from the thickness difference of the fuel slab before and after the burning and the effective burning time. Schlieren system is used to obtain qualitative

information of the reacting gas flow.

5.4 Experimental Results

The measured surface regression rates of PMMA sheets are shown in Fig. 5.2 to 5.5 for four different flow velocities of 1, 2, 3, 4 m/sec. The regression rates are presented as functions of downstream distance from the flame leading edge for several turbulence levels. It is found that the functional dependencies of the regression rates on the downstream distance are similar for all the flow conditions. The regression rate decreases with the distance from the upstream edge of the PMMA sample, which is in qualitative agreement with the theoretical predications for flat plate boundary layer mass burning. In a mass burning process, heat transfer from the flame to the solid determines the rate of solid pyrolysis, and consequently of the mass burning rate, as the result of fast chemical reaction assumption for the combustion region. Since the flow boundary layer grows thicker downstream the flame moves away from the surface, the heat transfer by convection to the solid is reduced downstream. Therefore, the surface regression rate decreases as the distance from the PMMA sheet leading edge increases, which is confirmed by the experimental data. It is also found that the decreasing slopes of the measured regression rate curves with the distance become more pronounced as the flow turbulence increases.

The results of Fig. 5.2 to Fig 5.5 also show that the flow turbulence affects the surface regression rate substantially, and that the regression rate value can increase

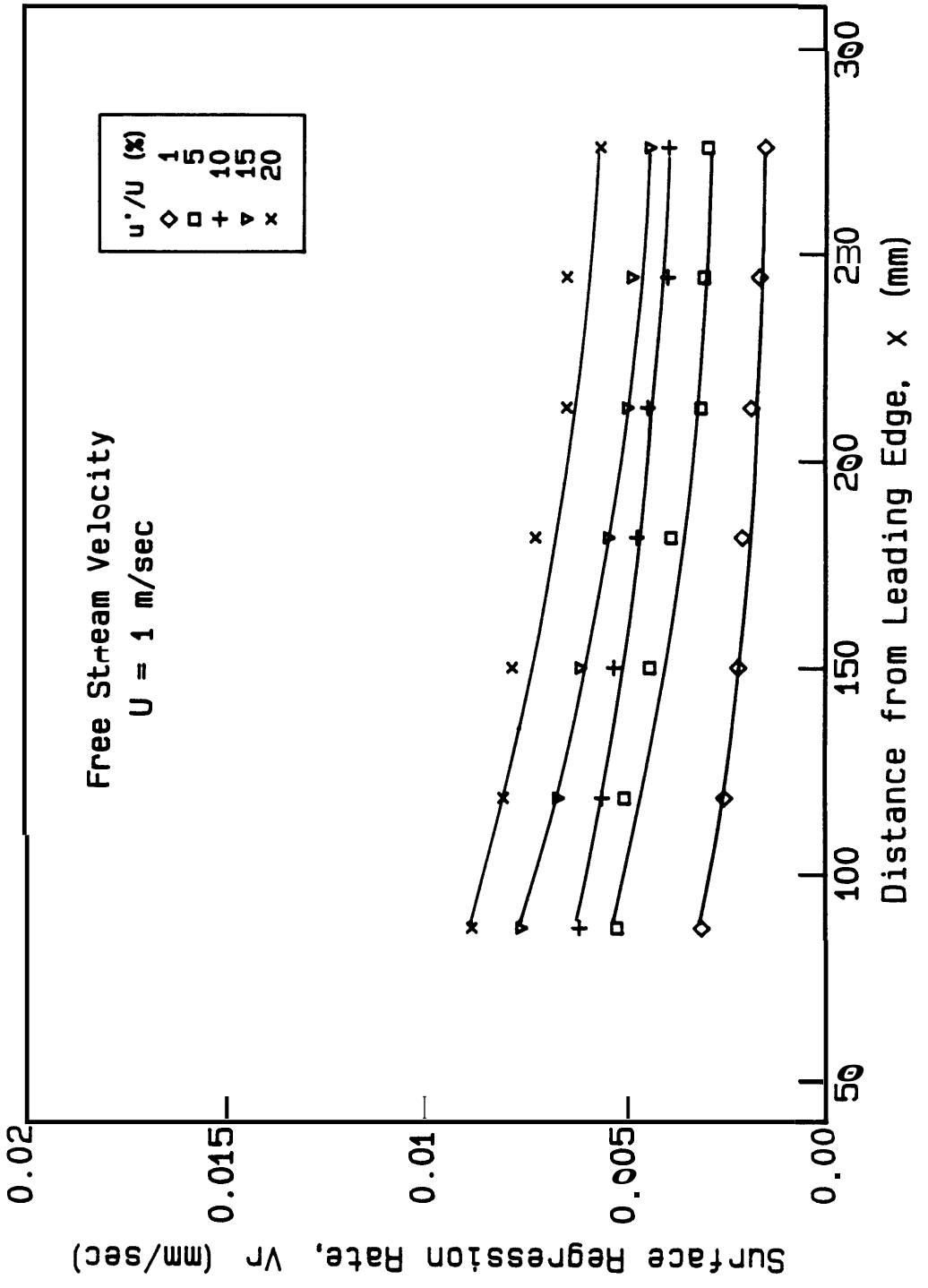

Fig. 5.2 Surface regression rate along the PMMA sheet for a flow velocity of 1 m/sec.

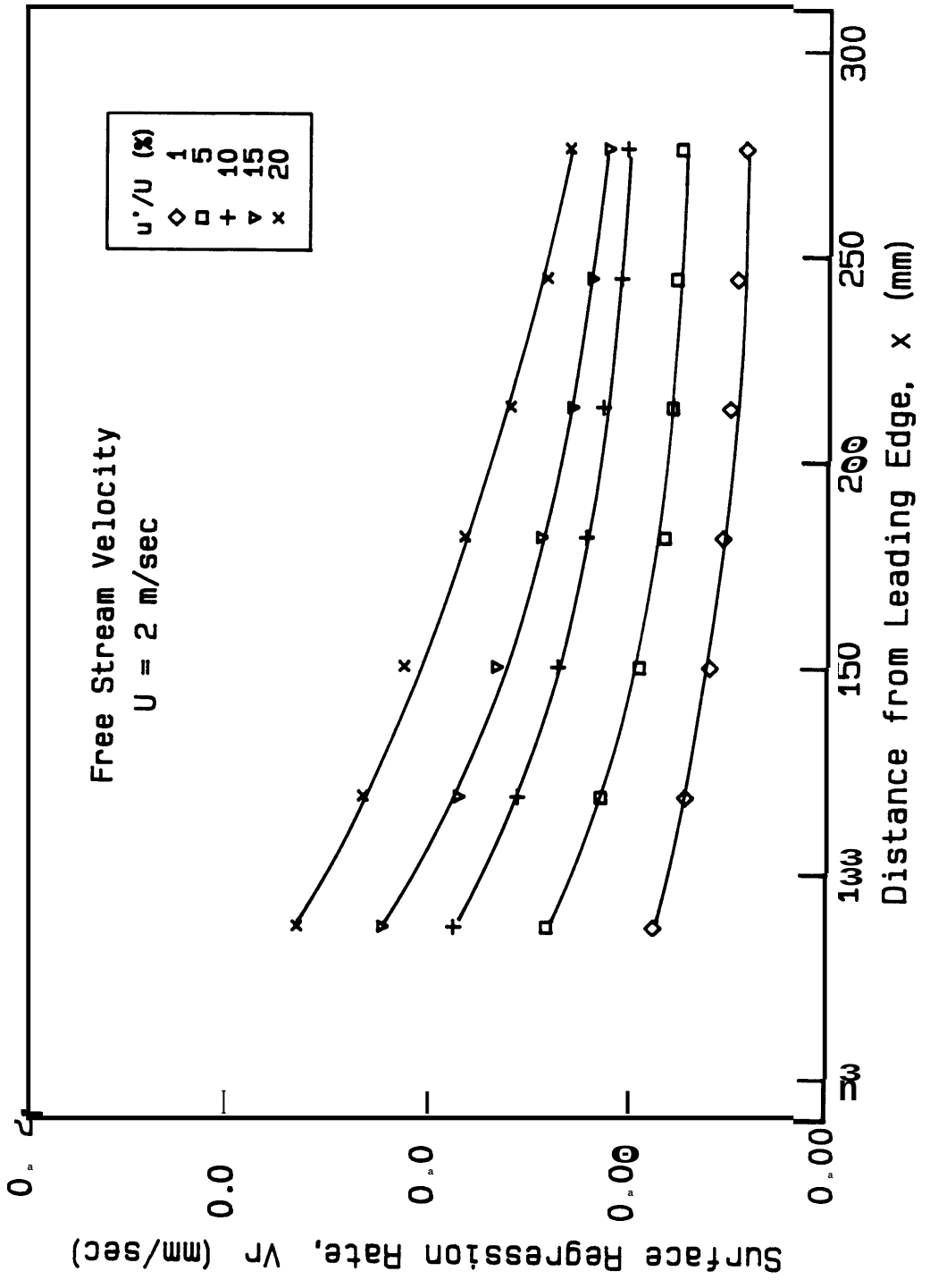

Fig. 5.3 Surface regression rate along the PMMA sheet for a flow velocity of 2 m/sec.

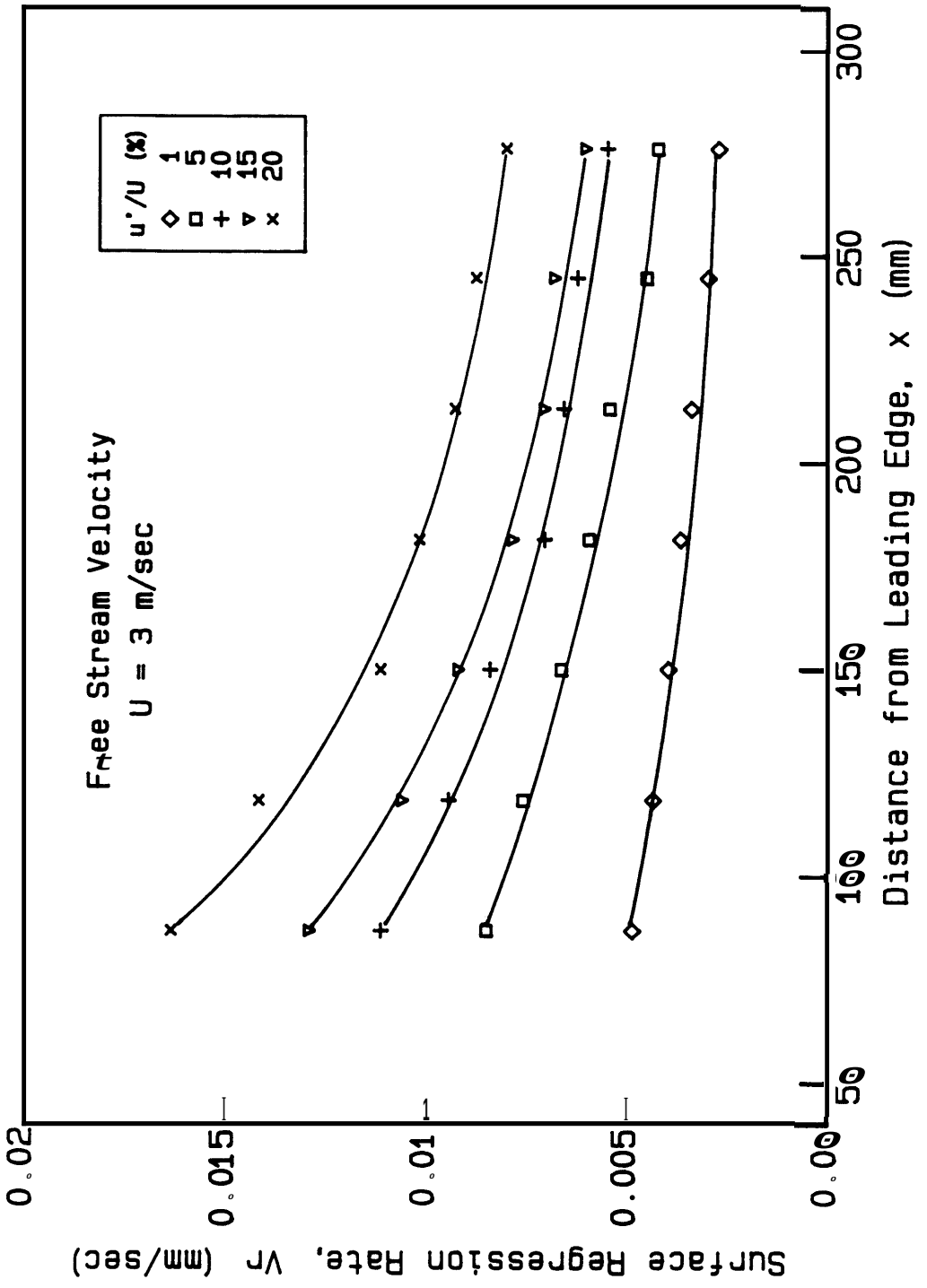

Fig. 5.4 Surface regression rate along the PMMA sheet for a velocity of 3 m/sec.

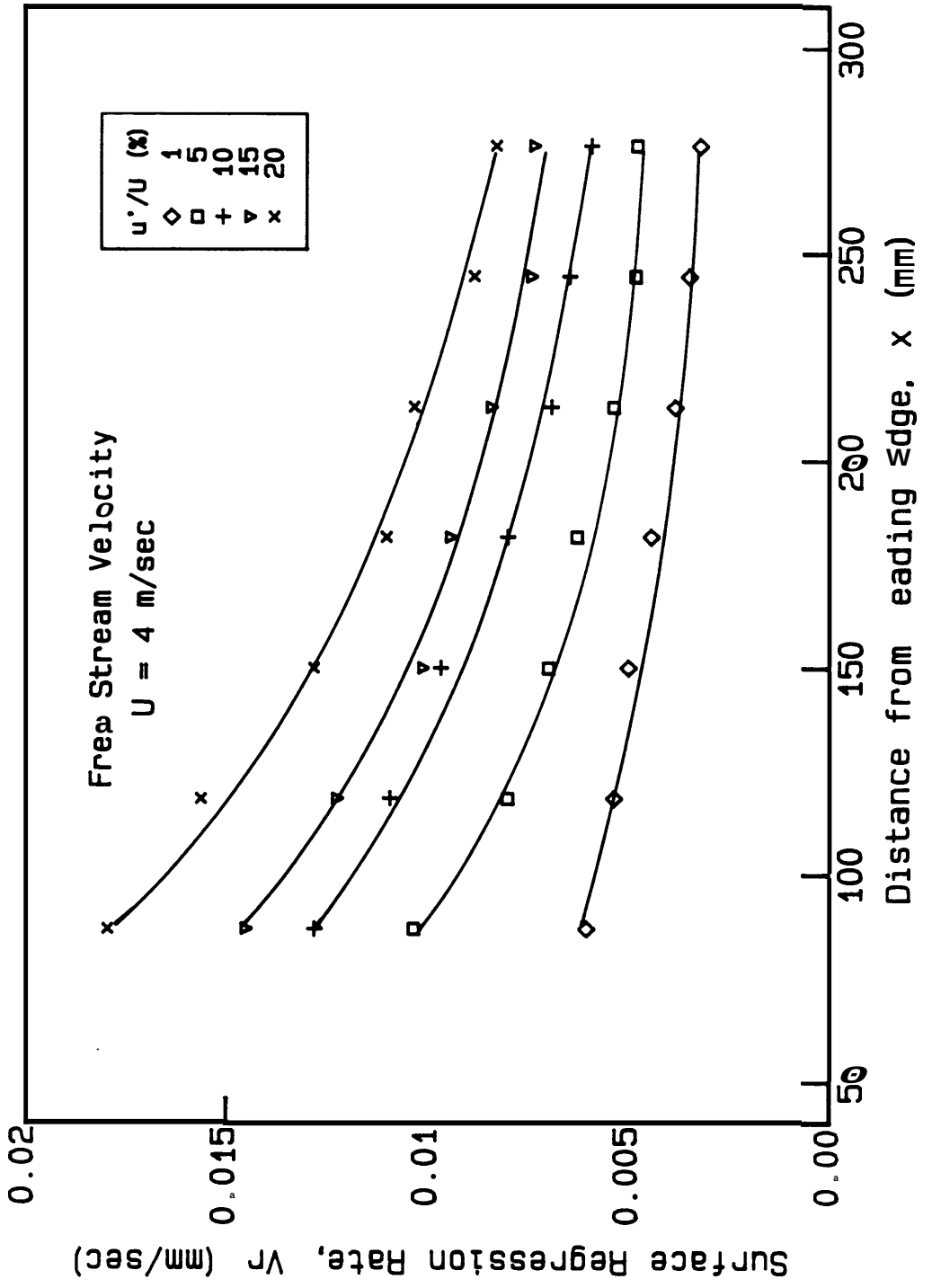

Fig. 5.5 Surface regression rate along the PMMA sheet for a velocity of 4 m/sec.

more than two times when the turbulence intensity is increased from the lowest to the highest level. The turbulence usually affects the mass burning process by enhancing the mixing processes. Some qualitative information about the turbulence effect can be obtained from Schlieren images of the reacting zone and thermal boundary layer. Two Schlieren images are shown in Fig. 5.6 to illustrate the characteristic difference between a laminar flow and a turbulent one. In the laminar flow, it is observed that the flame is relatively smooth and stable. As the flow turbulence is increased, the flame becomes much more unstable and stronger turbulent vortexes curl the flame and bring the flame closer to the fuel surface. From the photographs, it can be inferred that the mixing becomes more thorough and more heat is transferred to the fuel surface at higher turbulence intensities because of the proximity of the reaction zone to the fuel surface, and that this is the primary reason for the observed regression rate increase with the turbulent intensity.

The air flow velocity effect on the regression rate along the PMMA sheet is presented for one turbulence intensity of 10% in Fig. 5.7. It is seen that the surface regression rate is an increasing function of the flow velocity. Similar results are also obtained at other flow turbulence intensity levels. The characteristics of the regression rate dependence on the flow velocity is in qualitative agreement with the predictions from boundary layer mass burning analysis [8] [112]. As the flow velocity increases, the boundary layer becomes thinner and the flame moves closer to the fuel surface. The result is an enhancement of the convective heat transfer from the flame to the fuel, and therefore, is an increase of the regression rate.

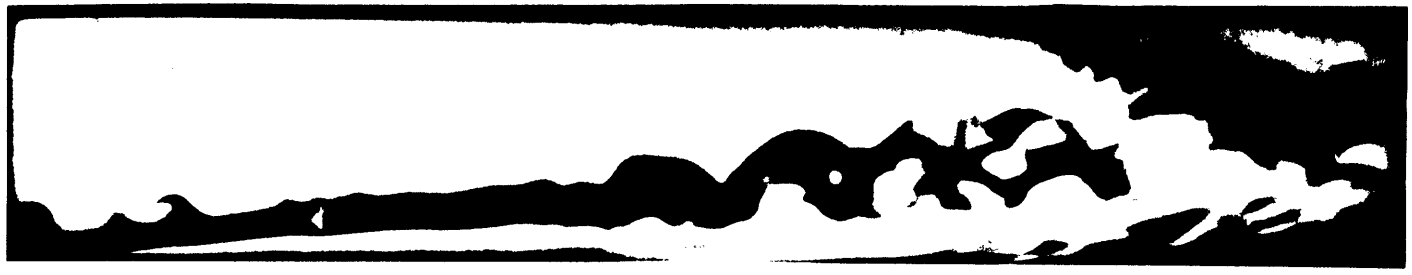

(a) U = 1 m/sec, u'/U = 1%

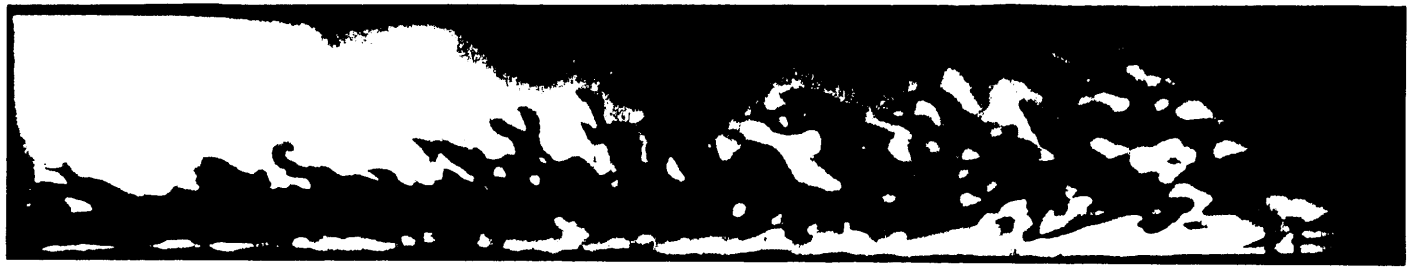

(b) U = 1 m/sec, u'/U = 15%

Fig. 5.6 Schlieren images of the reacting flow for a flow velocity of 1 m/sec and turbulence intensity of (a) 1% and (b) 15%.

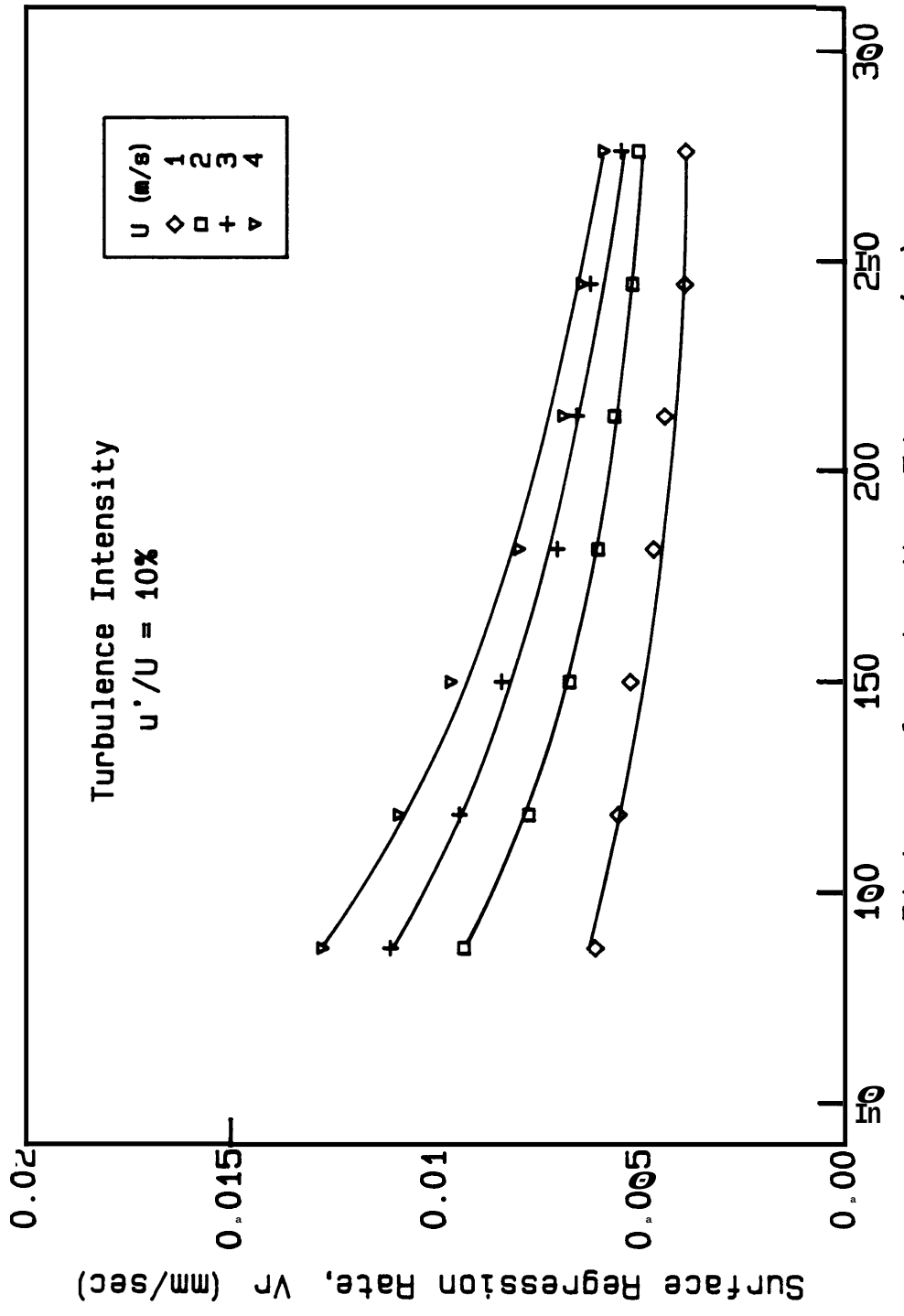

Fig. 5.7 Surface regression rate along the PMMA sheet for a turbulence intensity of 10% and several flow velocities.

5.5 Discussion and Data Correlation

The qualitative agreement between the regression rate measurements and the predictions of the boundary layer analyses suggests the existence of a correlation of the experimental data in terms of non-dimensional variables that can be extracted from these analyses. In Fig. *5.8,* the surface regression rate data is presented in terms of the non-dimensional burning rate $\rho V_r/\rho U$ and the Reynolds number, as proposed by Emmons [8] for laminar flow mass burning process. The gas flow rate is used to non-dimensionalize the surface mass burning rate. The data correlated are for all the flow velocities tested and the turbulence of 1, 10 and 20%. It is found that the non-dimensional regression rate $\rho V_r/\rho U$ decreases with the flow Reynolds number and increases with the turbulence intensity. From Fig. 5.8 it *can* be observed that for a given turbulence intensity level, the regression rate data correlate well with the selected non-dimensional parameters not only for laminar flow with low turbulence intensity, but also in flows with higher turbulence. This observation indicates that the turbulence intensity should be included in one of the non-dimensional parameters in the correlation.

In this regard, the analysis of [113] for the convective heat transfer in a turbulent stagnation point flow, provides a potential method to incorporate the measured flow turbulence intensity in an analyses of the present mass burning problem, and to deduce the proper non-dimensional parameters in order to correlate the experimental data. Following the analysis in [113], an eddy kinematic viscosity is defined in the form of

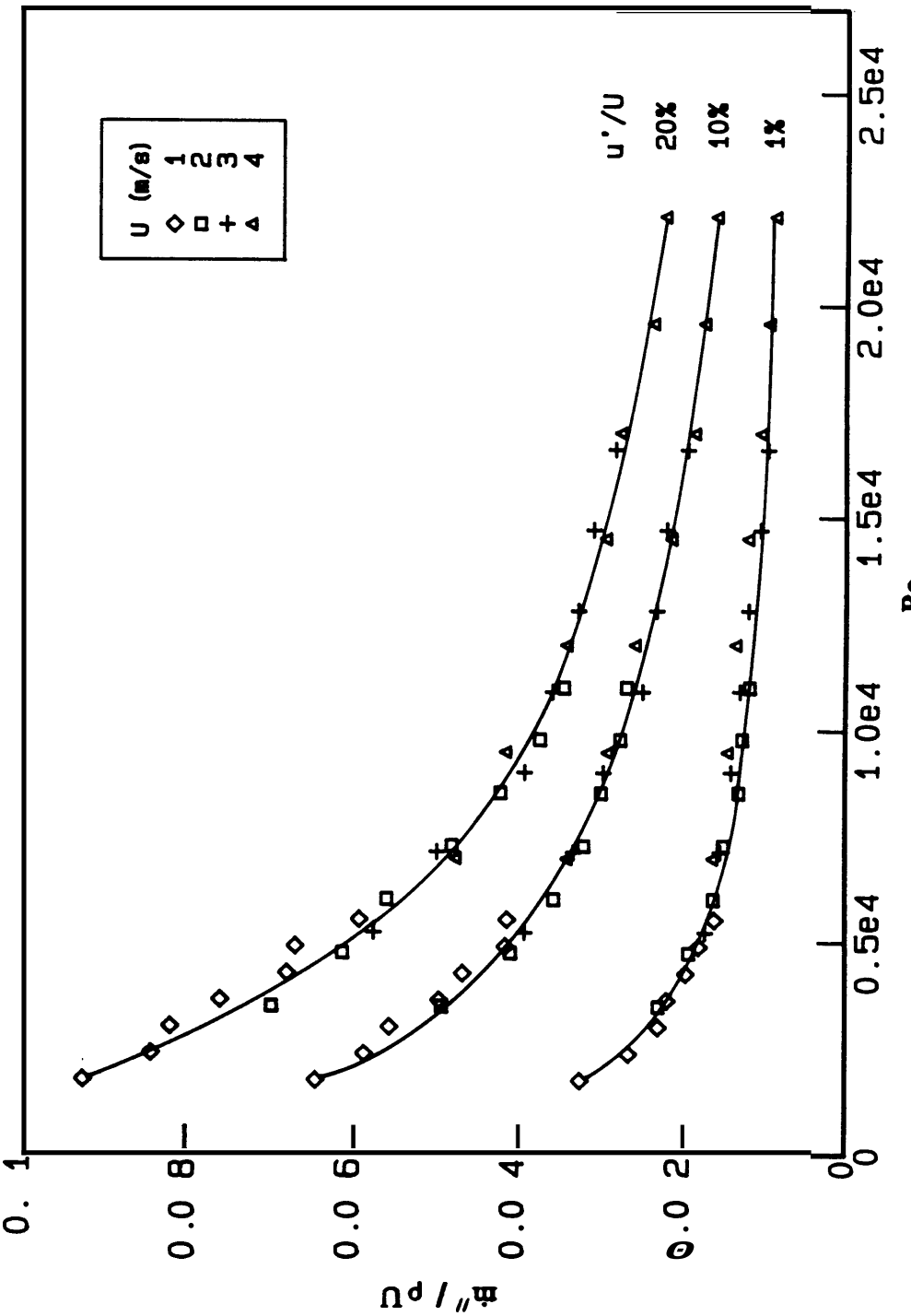

Fig. 5.8 Non-dimensional regression rate versus Reynolds number for turbulence intensities of 1%, 10%, 20%

$$e = a\left(\frac{u'}{U}\right)Uy \tag{5.1}$$

where a is a constant and y is the distance from the surface. The formulation assumes that the eddy viscosity is proportional to the turbulence in the free stream and to the distance from the wall. The assumption of unity turbulent Prantle and Lewis numbers is also made, and therefore the thermal diffusivity and species diffusivity have the same form as the viscosity in Eq. (5.1). The shear stresses, and heat and mass fluxes are then expressed in terms of the laminar quantities with addition of the turbulent eddy contribution. With the coordinate origin at the upstream fuel sheet edge, the flat plat boundary layer conservation equations that describe the gas phase problem can be written in the form

$$\frac{\partial(\rho u)}{\partial x} + \frac{\partial(\rho v)}{\partial y} = 0 \tag{5.2}$$

$$\rho u\frac{\partial u}{\partial x} + \rho v\frac{\partial u}{\partial y} = \frac{\partial}{\partial y}\left[\rho(\mu + e)\frac{\partial u}{\partial y}\right] \tag{5.3}$$

$$\rho u\frac{\partial Z}{\partial x} + \rho v\frac{\partial Z}{\partial y} = \frac{\partial}{\partial y}\left[\rho(\alpha + e)\frac{\partial Z}{\partial y}\right] \tag{5.4}$$

where Z is the mixture fraction [5] formulated in terms of the Shvab-Zeldovich temperature and species coupling functions. The infinite chemistry is assumed for the gas phase reactions. The boundary conditions for the above governing equations are that at $x = 0$, $y = \infty$; $u = U$, $v = 0$, and $Z = 0$, and that at $y = 0$; $u = 0$, and $Z = 1$. The mass burning rate is given by

$$\dot{m}'' = \rho_s V_r = (\dot{q}_c'' + \dot{q}_r'')/L$$

where the convective surface heat flux is given by

$$\dot{q}_c'' = -\lambda(\beta_{T_p} - \beta_{T_\infty})\left(\frac{\partial Z}{\partial y}\right)_{y=0}$$

Introducing the similarity variable

$$\eta = y\sqrt{\frac{U}{\nu x}}$$

and assuming that there is a local similarity solution of the problem such that the stream function can be expressed as

$$\Psi = \sqrt{\nu U x}\, f(\eta)$$

and the mixture fraction as

$$Z = Z(\eta)$$

Eqs. (5.2) to (5.4) are reduced to the similarity form

$$\left[1 + a\left(\frac{u'}{U}\right)Re_x^{1/2}\eta\right] f''' + a\left(\frac{u'}{U}\right)Re_x^{1/2} f'' + \frac{1}{2} f f'' = 0 \qquad (5.5)$$

$$\left[1 + a\left(\frac{u'}{U}\right)Re_x^{1/2}\eta\right] Z'' + \left[\frac{1}{2} f + a\left(\frac{u'}{U}\right)Re_x^{1/2}\right] Z' = 0 \qquad (5.6)$$

with boundary conditions

$$f(0) = f'(0) = 0 \qquad f'(\infty) = 1$$

and

$$Z(0) = 1 \qquad Z(\infty) = 0 \tag{5.7}$$

The non-dimensional mass burning rate is then given by

$$\frac{\dot{m}''_f x}{\lambda (T_f - T_p)} = Re_x^{1/2} \frac{\partial Z}{\partial \eta}\Big|_{\eta=0} \tag{5.8}$$

From Eqs. (5.5) to (5.8), it is seen that the solution of the problem has as parameter the product $(u'/U)Re_x^{1/2}$ and therefore that the value of $(\partial Z/\partial \eta)_{\eta=0}$ and consequently of the mass burning rate, will be a function of this flow parameter. Thus, it can be inferred that $(u'/U)Re_x^{1/2}$ should be the proper parameter to correlate the experimental data of forced turbulent mass burning process since it describes the flow characteristics through the turbulence intensity and Reynolds number, and appears as a parameter in the solution of the governing equations of the problem.

Correlation of the laminar flow surface regression rate data in terms of the non-dimensional mass burning rate (Eq. (5.8)) and the square root of the number is presented in Fig. 5.9. The laminar solutions of a flat plate boundary layer mass burning can be found in [5] [8] [112]. It is seen that there is a linear dependence between the two non-dimensional parameters as predicted by the theoretical models of the problem. From the experimental data, the following expression is deduced forthe mass burning rate

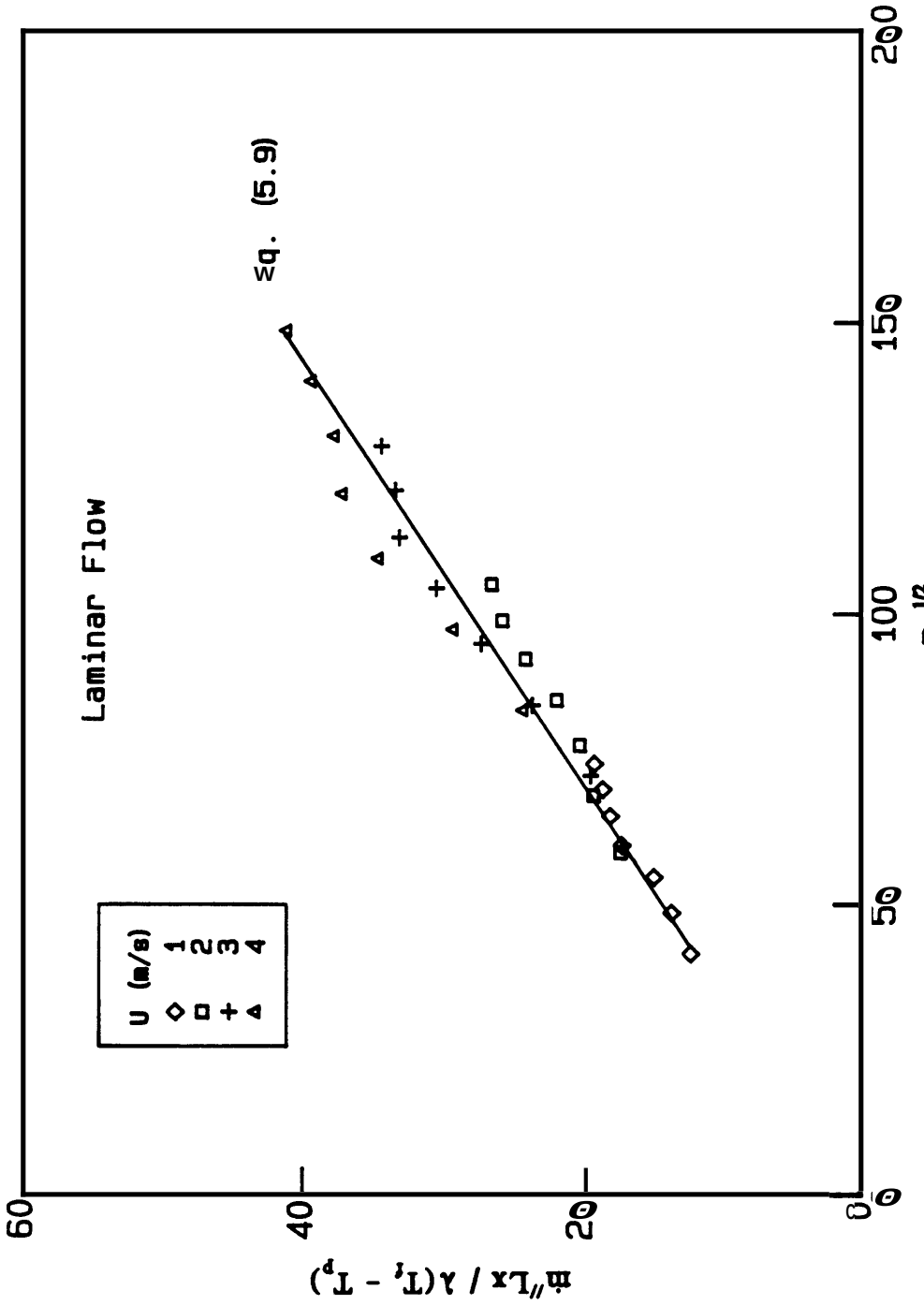

Fig. 5 Non-dimensional mass burning rate for laminar flow versus the square root of the Reynolds number.

$$\frac{\dot{m}''Lx}{\lambda(T_f - T_p)} = 0.28\ Re_x^{1/2} \qquad (5.9)$$

which is very similar to relation between the Nusslt number and Reynolds number obtained in non-reactive laminar flows for the surface Nusslt number [80].

Correlation of the turbulent flow surface regression rate data according to the predictions of Eq. (5.8), gives an approximately linear dependence between the non-dimensional mass burning rate and the square root of the turbulent flow parameter, i.e., $(u'/U\ Re_x^{0.5})^{0.5}$, although the data is somewhat scattered. The scatter of the data is reduced if a 0.8 power is used in the Reynolds number, rather than the 0.5 power as predicted in the analysis. The better correlation brought by 0.8 power seems reasonable since in non-reacting turbulent flows, it is also found that the Nusslt number correlates with the 0.8 power of the Reynolds number [80]. The results of the correlation of the turbulent flow regression rate measurements in terms of the non-dimensional mass burning rate (Eq. (5.8)) and the new turbulent flow parameter $((u'/U)Re_x^{0.8})^{0.5}$ is presented in Fig. 5.10 for all tests conducted. It is seen that all the experimental data correlates well with these non-dimensional parameters and apparently there is a linear relationship between them. From Fig. 5.10, the following explicit expression is deduced for the mass burning rate in turbulent flows

$$\frac{\dot{m}''Lx}{\lambda(T_f - T_p)} = 4.5\left[Re_x^{0.8}\left(\frac{u'}{U}\right)\right]^{0.5} \qquad (5.10)$$

This empirical formula provides the relationship between the mass burning rate and

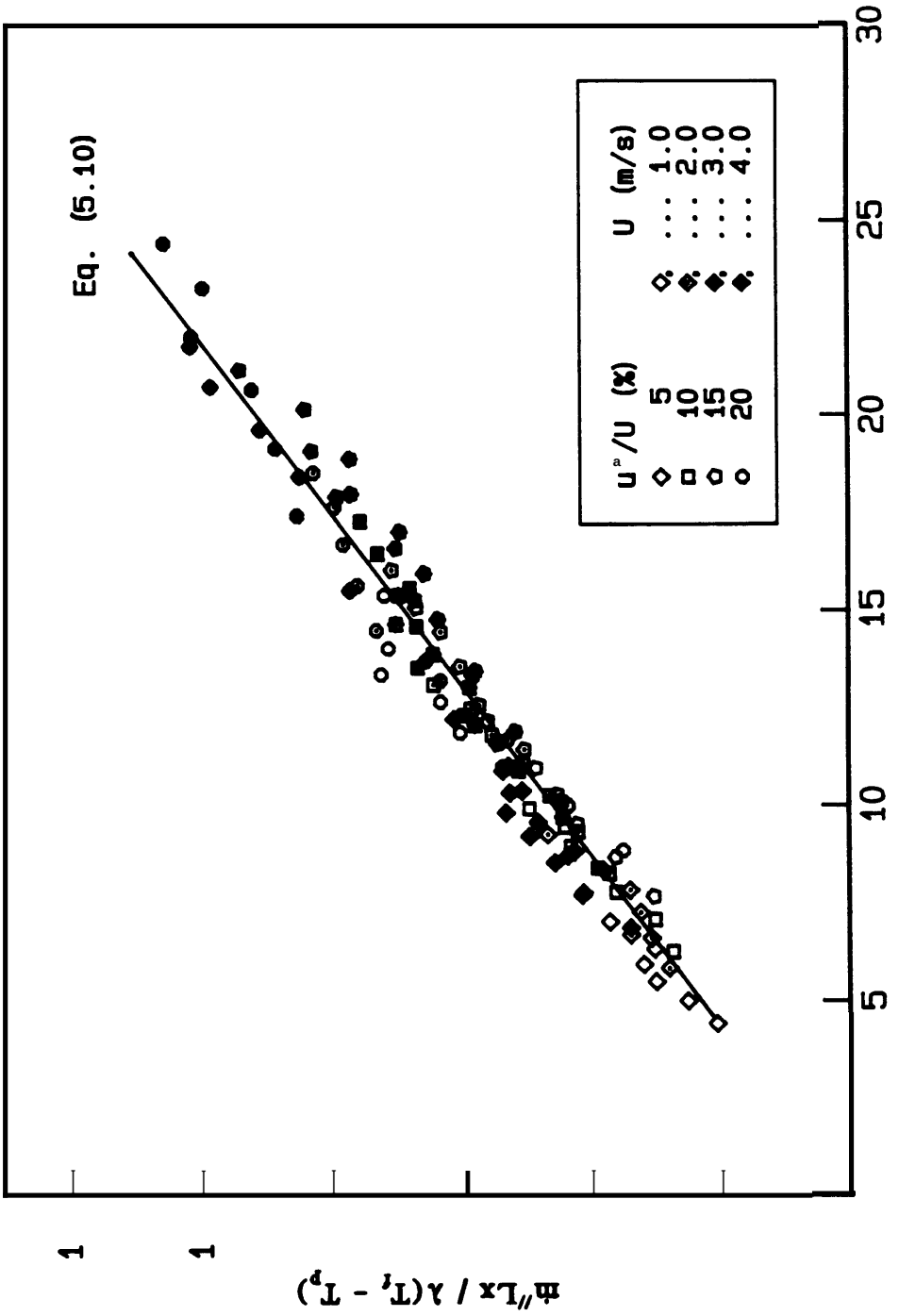

Fig. 5.10 Non-dimensional mass burning rate for turbulent flow versus the non-dimensional flow parameter.

the fuel and oxidizing flow properties, and corroborates the potential predictive capabilities of the theoretical model introduced above.

The correlation of the data in terms of convective heat transfer parameters in this work indicates that for these particular experiments, radiation heat transfer from the flame to the solid only has a secondary role. It should be noted, however, that the scale of these experiments is small. As the size of the fuel sheet is increased, the radiation heat transfer from the flame will become increasingly important. The model introduced above could be extended to include flame radiation effects approximately by adopting the approach utilized in [%] of the analysis of the burning of large vertical walls in turbulent, natural convection flows.

5.6 Conclusion

Conducting mass burning rate experiments with non-charring, homogeneously burning solid fuel in a forced flow with artificially induced turbulence, has made it possible to determine the effect of the flow parameters on the mass burning rate, and to obtain information useful in the development of theoretical models of solid fuel burning in turbulent flows. The results of the experiments show that flow turbulence can have a strong effect on the mass burning rate and that this effect is due primarily to the enhancement of the convective heat transfer at the fuel surface caused by the flame fluctuations. Correlation of the data shows that this effect can be expressed in terms of a flow turbulent parameter that includes both the Reynolds number and the turbulence intensity. It also shows that the boundary layer model that considers

infinite chemistry and incorporates the flow turbulence through an eddy viscosity and diffusivity may be used to predict burning rates, at least in turbulent flows with a turbulent structure similar to that generated with grids.

Chapter 6 Ceiling Flame Spread and Mass Burning

6.1 Introduction

Solid fuel flame spread and mass burning in a ceiling configuration are most frequently encountered in fires occurring inside buildings. The spread of fire and subsequent mass burning of a solid combustible in ceiling geometry, as shown in Fig. 6.1, have many similarities to those of the more frequently studied floor problems discussed in previous chapters. The major differences between the ceiling and floor case are caused by gravity. The buoyancy effects are different in these two cases because of the opposite acting direction of the gravity. The extent of buoyancy effect depends on the geometrical configuration, physical size of the fire, and the external flow conditions of the particular problem involved. Buoyancy *can* affect both heat and mass transport processes and gas phase chemical reactions, hence changing the characteristics of the flame spread and mass burning process. For a diffusion flame in the horizontal direction, the up-lifting force of buoyancy drives the flame upward, which alters the flame position relative to the fuel surface and the heat transfer to the solid, and also introduces the conditions which may cause the flame more prone to extinguish. Buoyancy *can* also influence the flow pattern by changing the velocity and turbulence distributions. In general, buoyancy *can* play an important role in flame spread and mass burning processes, as in many other combustion phenomena with relatively low flow velocities.

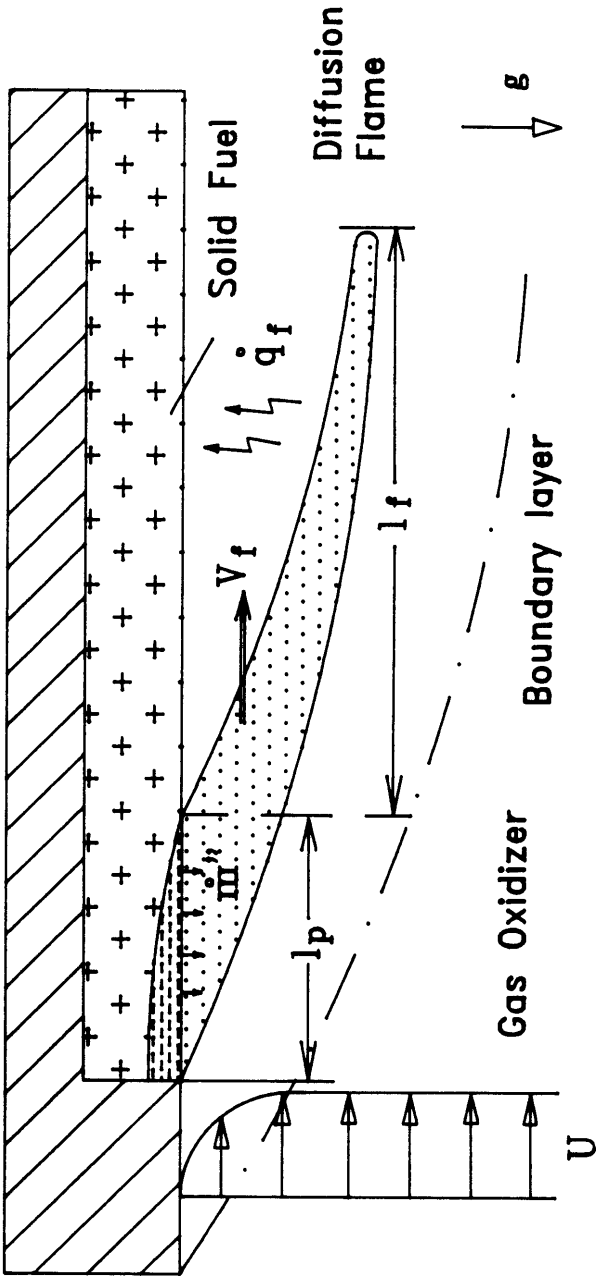

Fig. 6.1 Schematic of solid fuel flame spread and mass burning process in ceiling configuration.

6.2 Literature Review

Burning characteristics of solid materials, particularly polymeric materials under real fire conditions are important for fire safety research. In many occasions, polymeric materials are used in buildings as upholstery fillings and various interior furnishings including floors, walls and ceilings. A large number of studies have been conducted on the problem with floor or vertical wall configuration, as reviewed in previous chapters. However, only a few studies have concentrated on the other surface orientations such as a ceiling.

One of the initial studies on ceiling burning was carried out by Blackshear and Murty [114]. The combustion rate of variations of methyl alcohol burning is investigated on ceramic wicks of various shapes, sizes and orientations. Orloff and De Ris [115] [116] have studied ceiling combustion using a porous burner to simulate the pyrolysis gas ejection from the solid and liquid surfaces. Their experimental device allows the reproduction of a wide variety of heat and mass transfer modes. In [115], heat and mass transfer is scaled with the ceiling size and the fuel B number. It is shown that the non-dimensional mass burning rate can be correlated for significant variation in diameter and fuel-inert composition with B number and the 1/5 power of the Grashof number, which is also used to describe the natural convective flow. The non-dimensional flame standoff distance is obtained for various conditions and found to increase with the B number. It is also found that ceiling fire in quiescent air generates a cellular instability of Rayleigh type with internal flow of fuel vapor. Further study [116] deals with large scale ceiling fires which are

characterized by cellular and turbulent flames. It is shown that the non-dimensional burning rate is essentially controlled by the B number, which characterizes the chemical properties of the combustion process. The burning rate per unit area appears to be independent of both the surface area of the ceiling and the depth of the flame zone. The studies above provide helpful information of the phenomenology for this type of combustion. However, none of these experiments uses real solid fuel and takes into account of the occurrence of softening, fusion, evaporation and pyrolysis, all processes which are closely related to the burning characteristics of solid materials.

The major work dealing with ceiling combustion of polymeric materials in natural convection conditions is carried out by Ohtani *et al.* [117] - [119]. These studies have treated ceiling burning of various kinds of PMMA pieces: square pieces with flat bottom surfaces [117], pieces of circular and rectangular sections burning in transverse direction [118]. In [117], it is found that the surface regression rate is almost constant during the combustion period. For either of the sample pieces, the regression rate decreases as the characteristic length of the test samples (the diameter or width of the pieces of the test sample section) increases and that the relation between them *can* be approximately expressed as:

$$V_r = aL^{-0.25} + b$$

where a and b are constants; b is estimated to be finite and negative . However, as the sample dimension increases to a limiting length, the steady ceiling surface burning *can* not sustain, as inferred from the equation. The characteristics of ceiling

burning have been compared with those of floor burning. It is found that the surface regression rate of the former is only one third of the latter. From the temperature-time diagram in ceiling burning, a distinct sub-layer, which can not detected in floor burning, is found to exist between the solid and the gas phases. The properties of this sub-layer can be considered different from those of the solid or gas phase. A phenomenological argument has been developed to elucidate the difference. It is also shown that as the test sample dimension increases, the distance from the material surface to the flame front increases and that a limiting dimension is inferred when the convective heat flux to the surface becomes comparable to the radiative heat flux from the surface.

Experimental work on ceiling burning has also been conducted in [120] with PMMA disks burning freely in air. The mass loss of the samples is measured as a function of time. As in previous studies, convection is found to be the dominant mode of heat transfer. It is observed that the combustion rate and the flame stand-off distance increases as the sample dimension increases, which show the importance of the heat convection. The influence of imposed external radiative flux in addition to the flame radiation has also been considered in the experiments. It is found that the burning rate increases with the imposed radiative fluxes. However, for a given sample dimension, the increase in the rate vanishes as the imposed radiative flux increases. It is due to the increased heat-blocking effect on the convective flux by the enhancement of the blowing of the gases leaving the surface. The measurements of concentration and temperature profiles have also been performed to reveal that

the flame position shifts toward the surface as samples size decreases, which is consistent with the results from the previous experimental work and theoretical predictions.

An analytical solution is sought in [115] for laminar ceiling fires to predict the mass burning rate and flame stand-off distance, and a non-dimensional formulation of the governing equations and boundary conditions are obtained. The results show that the laminar problem scales as the 1/5 power of Grashof number, which arises as a result of gravity acting normal to the horizontal ceiling. Similarity solution is not found for the equations, instead, a Polhausen technique is used to solve the general equations. The mass burning rate is found as:

$$\dot{m}'' = C\frac{Gr^{1/5}B}{PrL}$$

where L is the dimension of the sample and C is a constant. The analytical solution is found to be in good agreement with the experimental results. In [120], a numerical analysis has been carried out on the bottom stagnation region combustion of cylindrical and spherical **PMMA** pieces under natural convection. The gas temperature, gas velocity, and species profiles across a flame established at the bottom stagnation region and the surface regression rate are examined for each case. The analysis has studied the effect on the surface mass burning rate of the difference of the diffusion coefficient of the pyrolysis gas from that of other species and the radiative heat exchange at the material surface. The numerical results are compared with the experimental data for cylindrical PMMA burning, yielding good agreement.

The radiative heat exchange is also estimated in this study using a simple formulation. The equations are developed by making the assumption that only the gasifying surface and not any of the gases between the radiative source and the surface absorbs radiation; the radiation term appears only in the boundary conditions to the problem. More detailed radiative properties are calculated in [121] for a fully developed laminar diffusion flame over the ceiling of disks of PMMA. The results show that for combustion driven by natural convection, the contribution of radiative heat transfer to the burning rate is a "negative" contribution: the solid surface emits much more heat by radiation than it receives from the gas phase. This effect of surface re-radiation allows one to interpret the previously observed linear correlation between combustion rate and characteristic dimension of the samples. In the case where additional radiative flux is imposed, the contribution to the burning rate by radiation becomes "positive" and this contribution increases logically with the increase of the additional flux. An enhancement of the heat blocking effect of the heat blocking effect of the convective flux can be observed simultaneously.

Also related work includes the studies of mixed convective burning of a fuel surface in arbitrary inclination [105] [122] and buoyancy effect on downward flame spread in high oxygen concentration [123].

All the work above has considered the problem of ceiling burning in natural convection condition. A recent work [124] by Mekki *et al.* has experimentally studied the laminar forced flow flame spread over wood and PMMA in the ceiling configuration. It is found that the flame front changes nearly linearly with the free

stream velocity as predicted by the theoretical models for laminar flow. It is also observed that the pyrolysis mass flux decreases with the downstream distance near the leading edge and then becomes almost constant for both wood and PMMA, which is used to argue that the steady state mass burning is not achieved in the far downstream region. However, it is considered that the flame spread rate is well predicted by the models that use Emmons' solution in the burning zone.

Scarce fundamental information on this subject and the potential effect that buoyancy has on the ceiling burning have provided the motivation for this work. The objective of the present work is to carry out a systematic study of ceiling flame spread and mass burning in a forced turbulent flow, and to determine the controlling mechanisms of the flame spreading and burning process in ceiling configuration by comparison of the ceiling results with those obtained from previous work on the related floor problem.

6.3 Experimental Arrangement

The schematic of the experimental setup is shown in Fig. 6.2. As in previous chapters, the LDV system is used to determine the flow patterns and the thermocouples are used for the solid surface temperature histories. The Schlieren system is utilized to provide qualitative information of the reacting flow. A major addition in the ceiling study is the employment of the oxygen detector and the infrared gas analyzers which measure the species concentrations in the gas exhaust flow. The concentration results can be used to determine the completeness of the

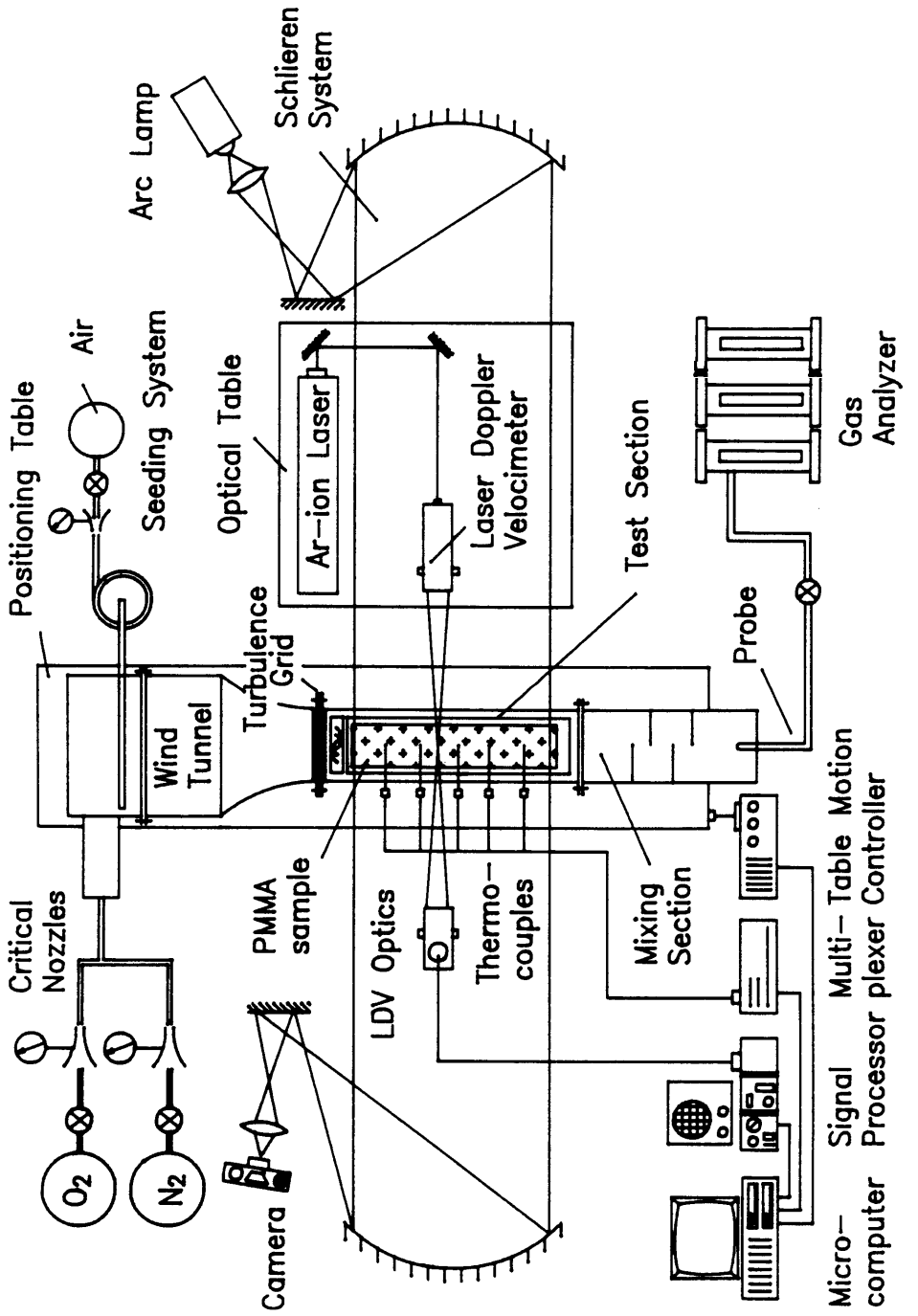

Fig. 6.2 Schematic of experimental facility for ceiling flame spread and mass burning study.

gas phase chemical reactions and to infer the buoyancy effect on the chemical kinetics.

The ceiling configuration is achieved by turning the test section upside down from the initial position for the floor experiments. The flame spread rate and mass burning rate are measured as functions of flow parameters. Some additional experiments are also performed to supplement data for the floor configuration.

6.4 Flame Spread Rate

6.4.1 Velocity and Turbulence Effect

Measured flame spread rates over PMMA sheet surface in the ceiling configuration are shown in Fig. 6.3 versus the free stream flow velocity and in Fig. 6.4 versus the flow turbulence intensity. The flow velocity used in the experiments ranges from 0.25 to 4.5 m/sec. Small flow velocities (< 1 m/sec) are applied in this study because the buoyancy effect is expected to be more significant at flows with small convection force. The turbulence intensity ranges from 1% to 15%. No higher turbulence level is applied due to the difficulty in generating high turbulence at low flow velocities.

From Fig. 6.3, it can be seen that the ceiling flame spread rate increases with the flow velocity for all turbulence intensities tested, which agrees with the boundary layer theory and the results from the floor experiments. As the flow velocity increases, the main flow tends to push the boundary layer and the flame as well to move closer to the fuel surface, and therefore, the heat transfer from the flame to

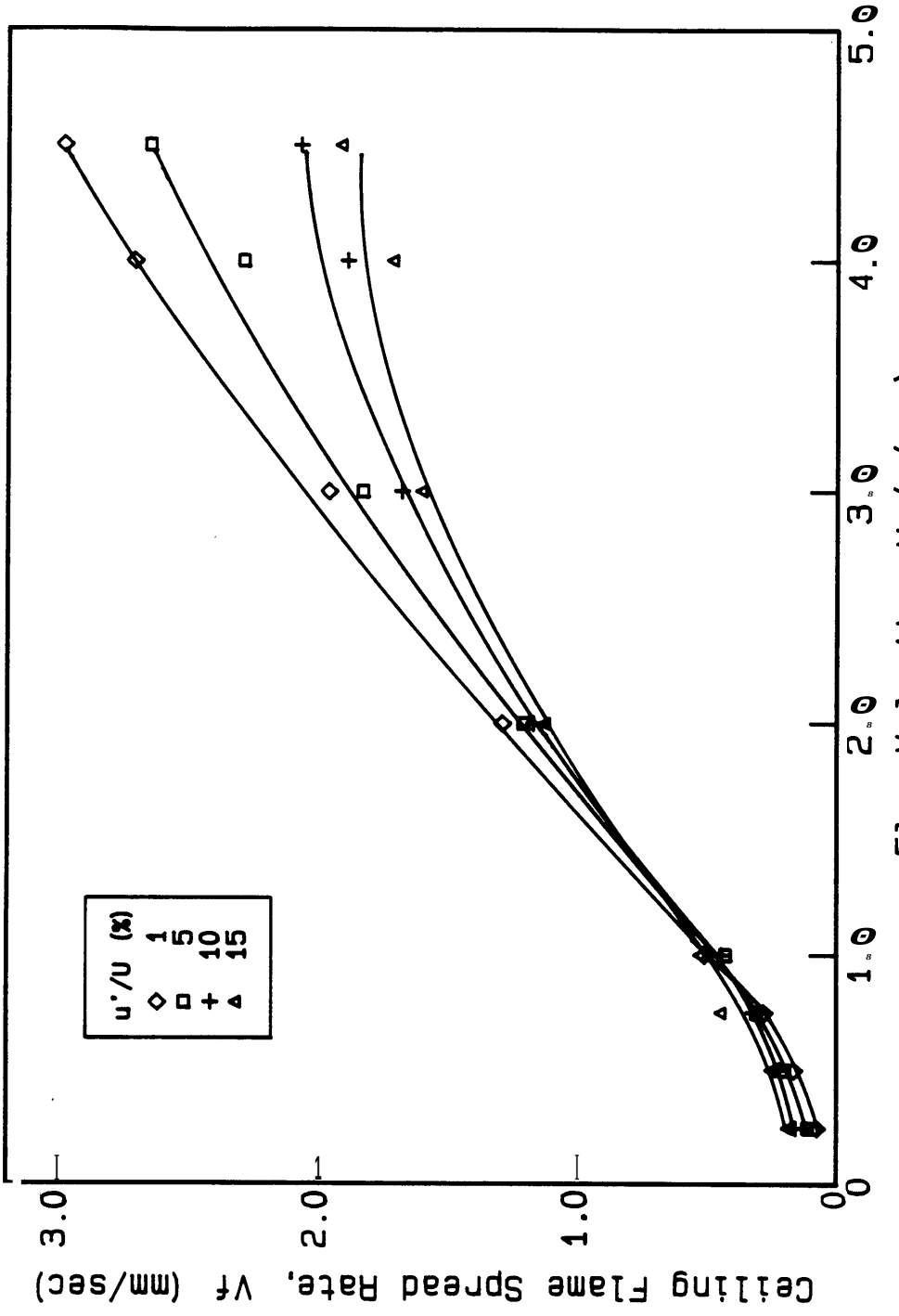

Fig. 2 Ceiling Flame spread rate over thick PMMA sheets as a function of the concurrent air flow velocity.

PMMA sheet is enhanced, which intensifies the pyrolysis process and increases the flame spread rate. It is also observed from Fig. 6.3 that the increasing slope of the flame spread rate is larger for flows with lower turbulence intensities.

The flow turbulence affects the ceiling flame spread rate quite significantly. From Fig. 6.4, it is seen that the flow turbulence causes the ceiling flame spread rate to decrease for flow velocities larger than about 1 m/sec, which is consistent with the previous observations of the floor flame spread rate. The decreasing effect of the turbulence can be explained primarily as the result of a shortened flame length by higher turbulence intensities as discussed in Chapter 4. However, for flows with velocities less than 1 m/s, the flow turbulence intensity seems to have an opposite effect on the ceiling flame spread process, which is to increase the flame spread rate slightly. This increasing effect is not observed in the floor tests. At low flow velocities, the flame length itself is very small and the shortening effect of turbulence diminishes. As turbulence intensity is increased, larger and stronger eddies generated by the high turbulence may bring the flame closer to the fuel surface and increase the heat transfer to the solid, and subsequently the flame spread rate.

6.4.2 Buoyancy Effect

The concurrent flame spread process over solid combustible is mainly controlled by the heat transfer from the flame to the solid surface as demonstrated in many studies on the floor problem. The buoyancy effect on the flame spread process can be studied by investigating its influence on each of the controlling

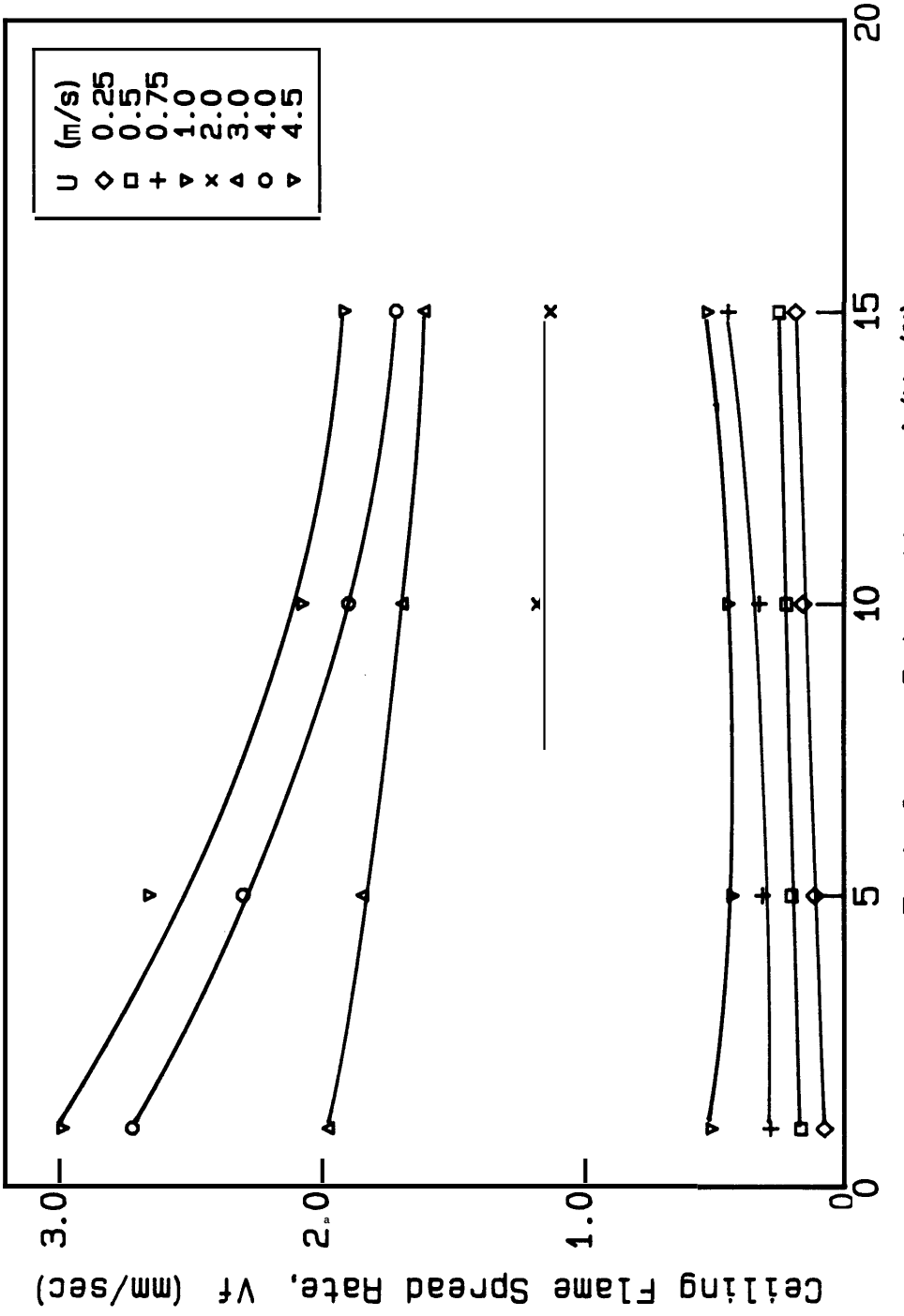

Fig. 6.4 **Variation of the ceiling flame spread rate over thick PMMA sheets with the concurrent flow turbulence intensity.**

mechanism that affects the heat transfer process. Always lifting flames upward, the buoyancy pushes the flame closer to the top surface in the ceiling flame spread and moves the flame away from the bottom surface in the floor case. Therefore, the buoyancy could affect the flame spread rate in following ways. It could change the magnitude of the heat transfer from the flame to the solid surface by changing the distance between the flame and the solid surface, which would result in an increased heat flux in ceiling and a decreased one in floor. Consequently, the flame spread rate should be enhanced in the former case and hindered in the latter. The effect of pushing the flame too close to the solid surface could quench the flame in the ceiling burning by large heat loss to the cold wall. The mass transport process could be altered by the buoyancy due to the different uplifting force in each configuration on the hot surface fuel vapor and the air of lower temperature, which could change the characteristics of the flow field, especially the flow turbulence intensity. The overall buoyancy effect on the flame spread process should be the combined influence of all the above factors. Whether the buoyancy enhances or inhibits the flame spread process depends on which effect is the most dominant in a particular test condition.

In Fig. 6.5, the flame spread rates from typical case of the floor and the ceiling experiments are presented together for comparison. Two turbulence levels of 1% and 15% are used to represent low and high turbulence cases, respectively. It is seen that for flows with velocities larger than 1 m/sec, the flame propagates faster in the ceiling configuration than in the floor case, which is more noticeable for

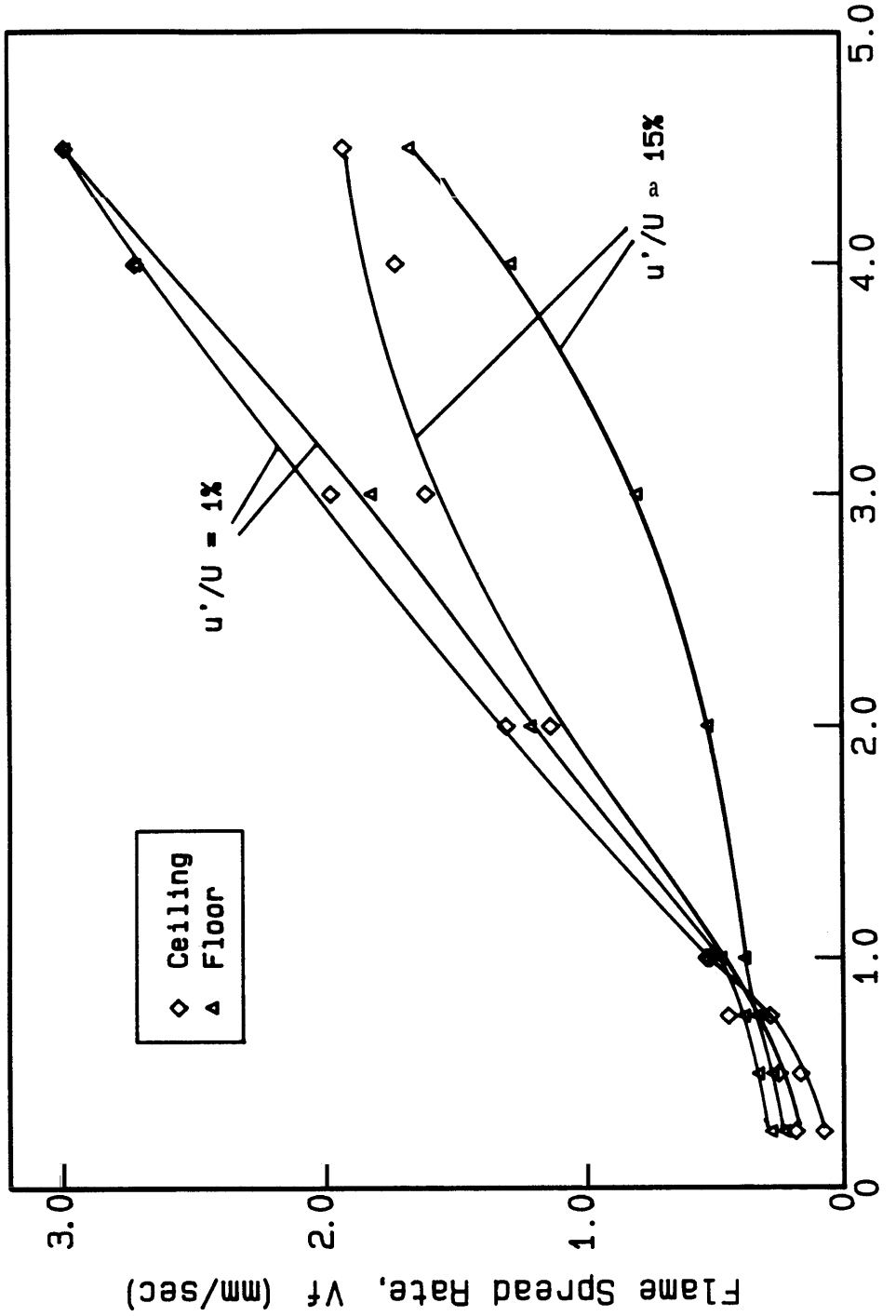

Fig. 6.5 Comparison of ceiling and floor flame spread rate for turbulence intensities of 1% and 15%.

high turbulence intensities. This result seems to be caused by enhanced heat transfer from flame to solid fuel in the ceiling case. The flame in the ceiling configuration is visually observed to be closer to the fuel surface than that in floor case, as shown by Schlieren images of Fig. 6.6. The flow conditions for these two images are U = 2 m/sec and u'/U = 1.1%. In the ceiling case, the thermal boundary layer is seen to be thinner than the floor one and the flame to be closer to the fuel surface. As the flow velocity increases, the natural convection effect is expected to become less significant compared with the forced convection force. The measurements show that for all turbulence levels, the spread rate difference between the two cases becomes smaller as the flow velocity increases.

For the flows slower than 1 m/s, however, an opposite trend is observed. The flame propagates at a slower rate in the ceiling than in the floor, which indicates that mechanisms other than heat transfer may become more important under low flow velocity conditions under low flow velocity conditions. During the experiments, it is observed visually that in the low flow velocity range, flames in the ceiling spread are very weak and display a distinct blue color, unlike in the floor case where yellow color flames are always observed. Since in combustion reaction the blue color is mainly emitted by the CO spectrum at low temperature and the yellow flames are caused by soot at relatively high temperature, this observation suggests that the flame in the ceiling configuration may be near extinction due to heat loss to the wall. The complex-molecule chains of PMMA break down under the heat from the flame and produces single molecules which go on to react with the oxidizer. Under favorable

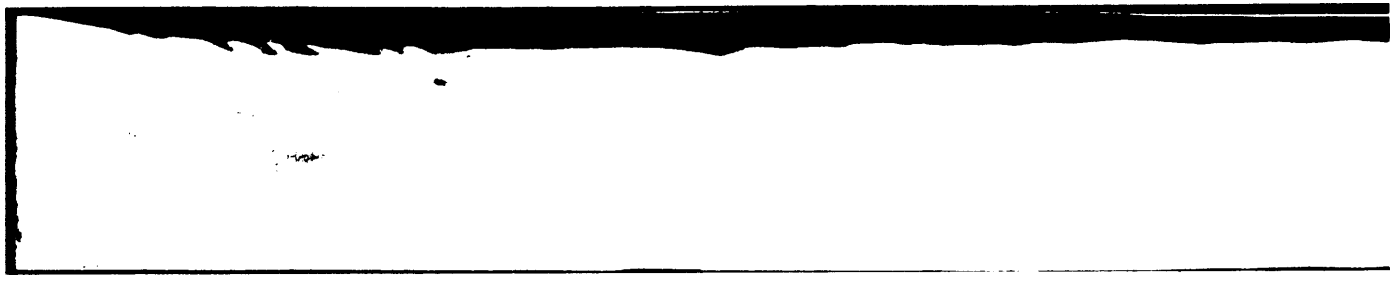

(a) Ceiling flame spread.

(b) Floor flame spread.

Fig. 6.6 Schlieren images of spreading flames (a) and (b) floor configurations with laminar flows of U = 2 m/sec.

conditions, the complete overall chemical reaction should be

$$C_3H_8O_2 + 5(O_2 + 3.76N_2) \rightarrow 3CO_2 + 4H_2O + 5\times3.76N_2 \qquad (6.1)$$

If the reaction takes place under unfavorable conditions such as large heat loss or insufficient oxygen, the reaction becomes incomplete and CO starts to occur:

$$C_3H_8O_2 + 3.5(O_2 + 3.76N_2) \rightarrow 3CO + 4H_2O + 3.5\times3.76N_2 \qquad (6.2)$$

which releases much less energy than Eq. (6.1). In order to investigate the combustion completeness in each case, the exhaust gas concentrations are measured under various flow conditions. Some typical results are shown in Fig. 6.7 to Fig. 6.14., which present the major species concentrations as functions of the pyrolysis front position. The pyrolysis front position is chosen here as the horizontal coordinate for simplifying the comparison among different cases. It is determined by multiplying the measured flame spread rate with the test running time. The major species O_2, CO, CO_2, NO and unburned hydrocarbons in the gas flows are measured. The concentration of NO is not presented in the figures because of its small value of less than 5 ppm. Fig. 6.7 and 6.8 show the concentration results in the ceiling and floor tests for laminar flow of U = 0.5 m/sec. It is found that in the ceiling flame spread, much more carbon monoxide and unburnt hydrocarbons are detected than in the floor case as shown in Fig. 6.7, while less oxygen is consumed and less carbon dioxide is generated in the ceiling flame spread than in the floor case as shown in Fig. 6.8. These trends of the exhaust gas concentrations have also been observed under other conditions of flow velocity and turbulence intensity as shown in Fig. 6.9

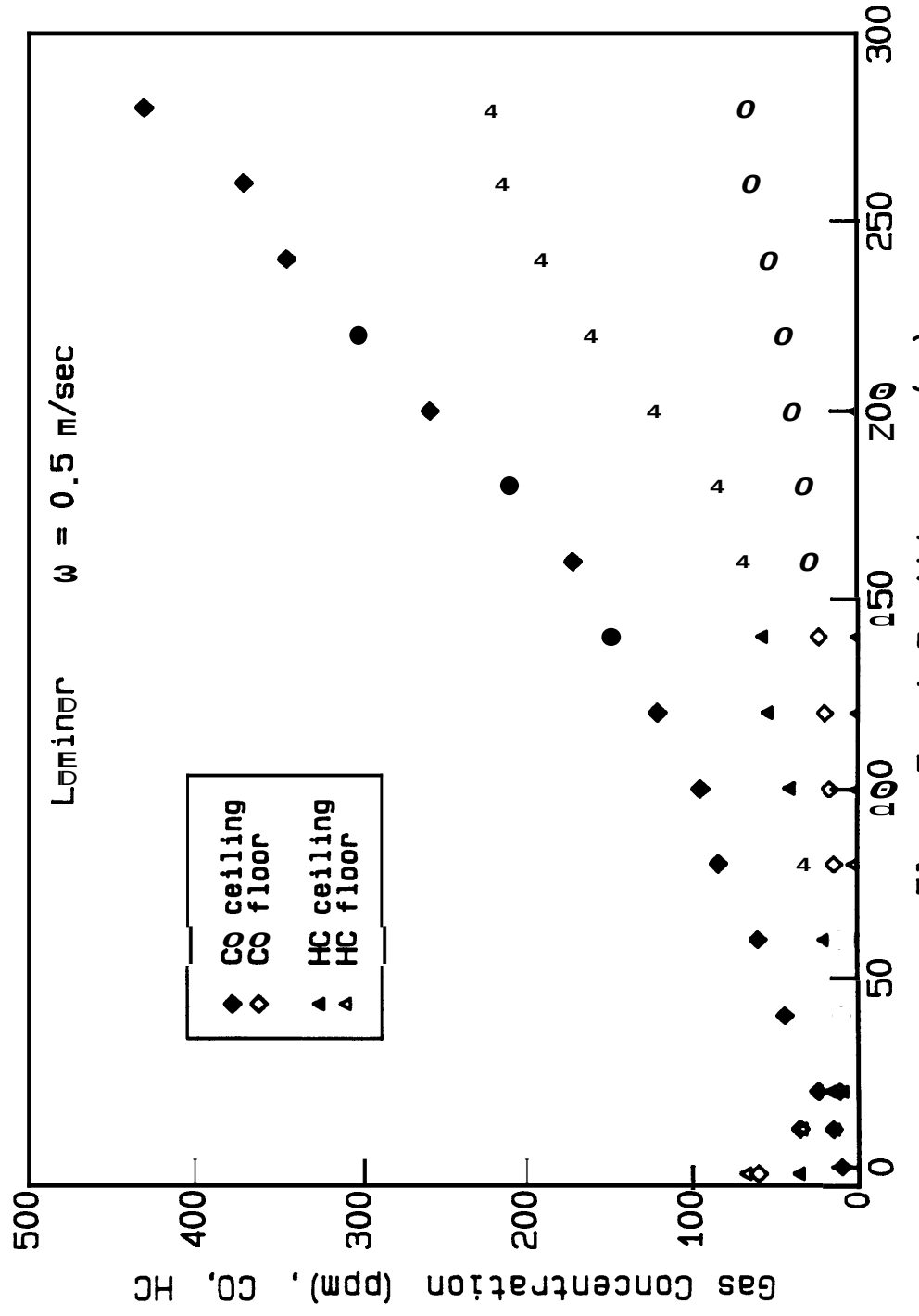

Fig. 6.7 Comparison of the concentrations of CO and unburnt hydrocarbons in the exhaust flows of ceiling and floor tests with laminar flow of 0.5 m/sec.

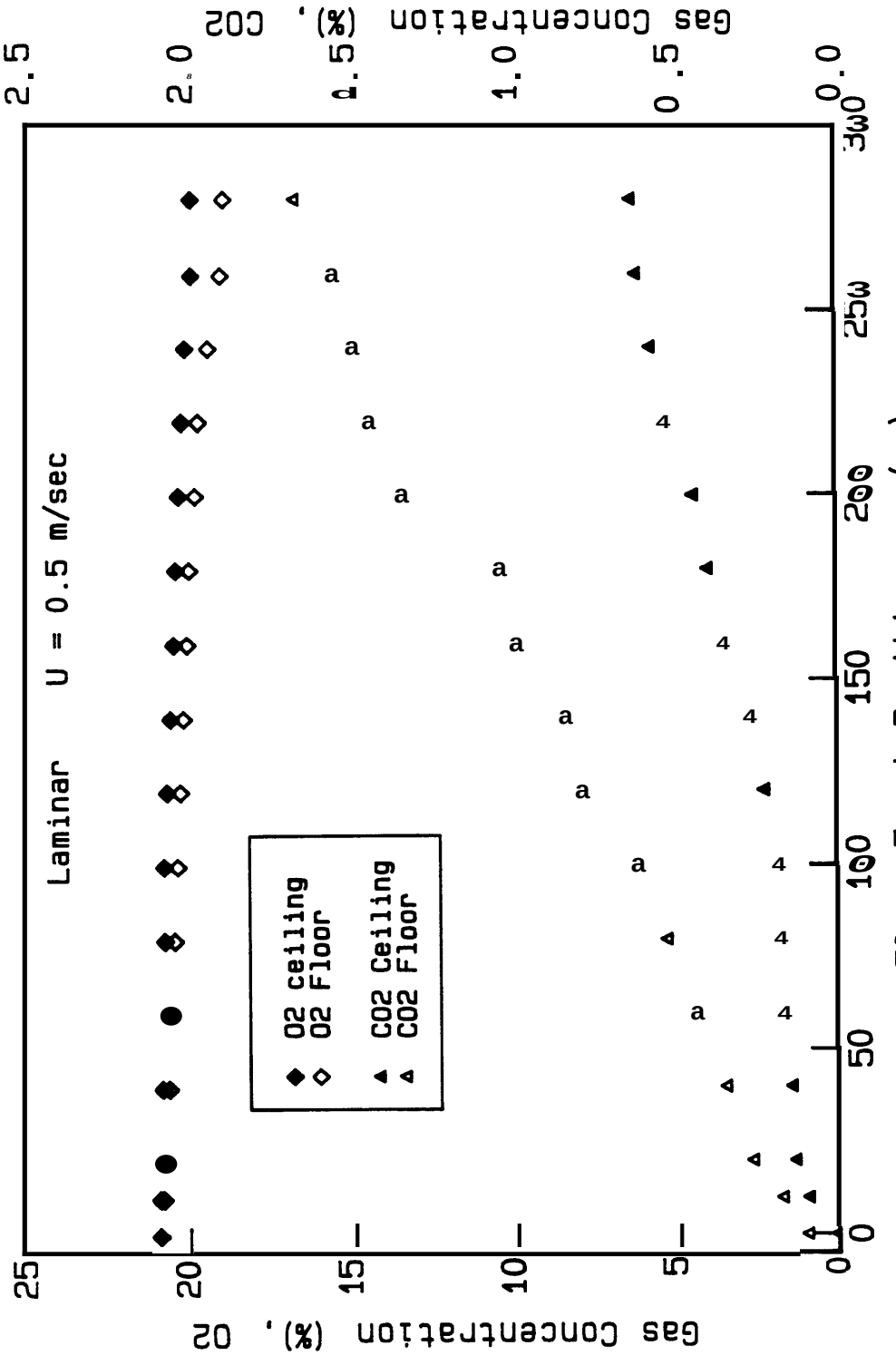

Fig. 6.8 Comparison of the concentrations of O_2 and CO_2 in the exhaust flows of ceiling and floor tests with a laminar flow velocity of 0.5 m/sec.

to 6.14. From these measurements, it can be concluded that at least for the flow conditions tested, the chemical reactions are less complete in the ceiling flame spread than in the floor. A good indication of the completeness of the combustion is the CO and unburnt hydrocarbon concentrations. For the floor case the unburnt hydrocarbon is almost undetectable in all the flows including low flow velocity cases as shown in Fig. 6.7. On the other hand, for flame spread in ceiling configuration, the unburnt hydrocarbons are found in all flow conditions, even at velocities as high as U = 4 m/sec.

One of the main reasons for a weaker chemical reaction in ceiling flame spread is the quenching effect of the wall since the flame is pushed much closer to the fuel surface by buoyancy in the ceiling case, which results in a larger heat loss and a lower flame temperature. Poor mixing is another important mechanism causing weaker combustion in the ceiling configuration. In the ceiling flame spread, the vorticity generated on the wall is damped by the uplifting flow induced by the buoyancy. And the hot fuel vapor tends to stay at the top and cold air stays under the flame and it is possible that insufficient oxygen in the reaction zone inhibits the exothermal reactions to proceed completely. In the floor case, the buoyancy raises the flame from the surface considerably, which favors the gas mixing and subsequently burning of the fuel vapor, and also provides stronger radiation heat transfer from the flame to the solid fuel, facilitating more complete chemical reactions. The buoyancy also introduces additional instability to the gas flow in the floor flame spread which enhances the mixing in the reaction zone. This

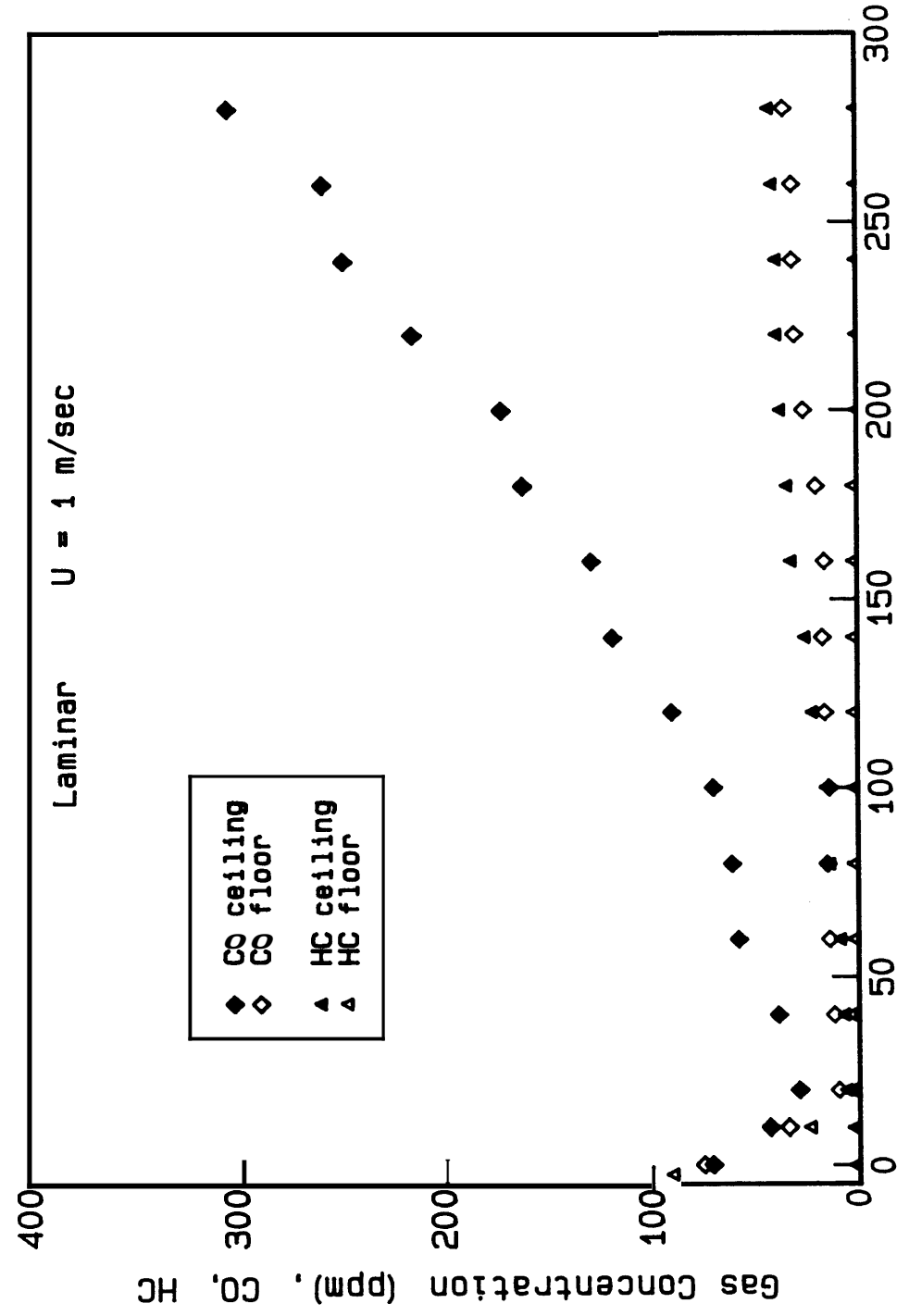

Fig. 6.9 Comparison of the concentrations of CO and unburnt hydrocarbons in the exhaust flows of ceiling and floor tests with laminar flow of 1 m/sec.

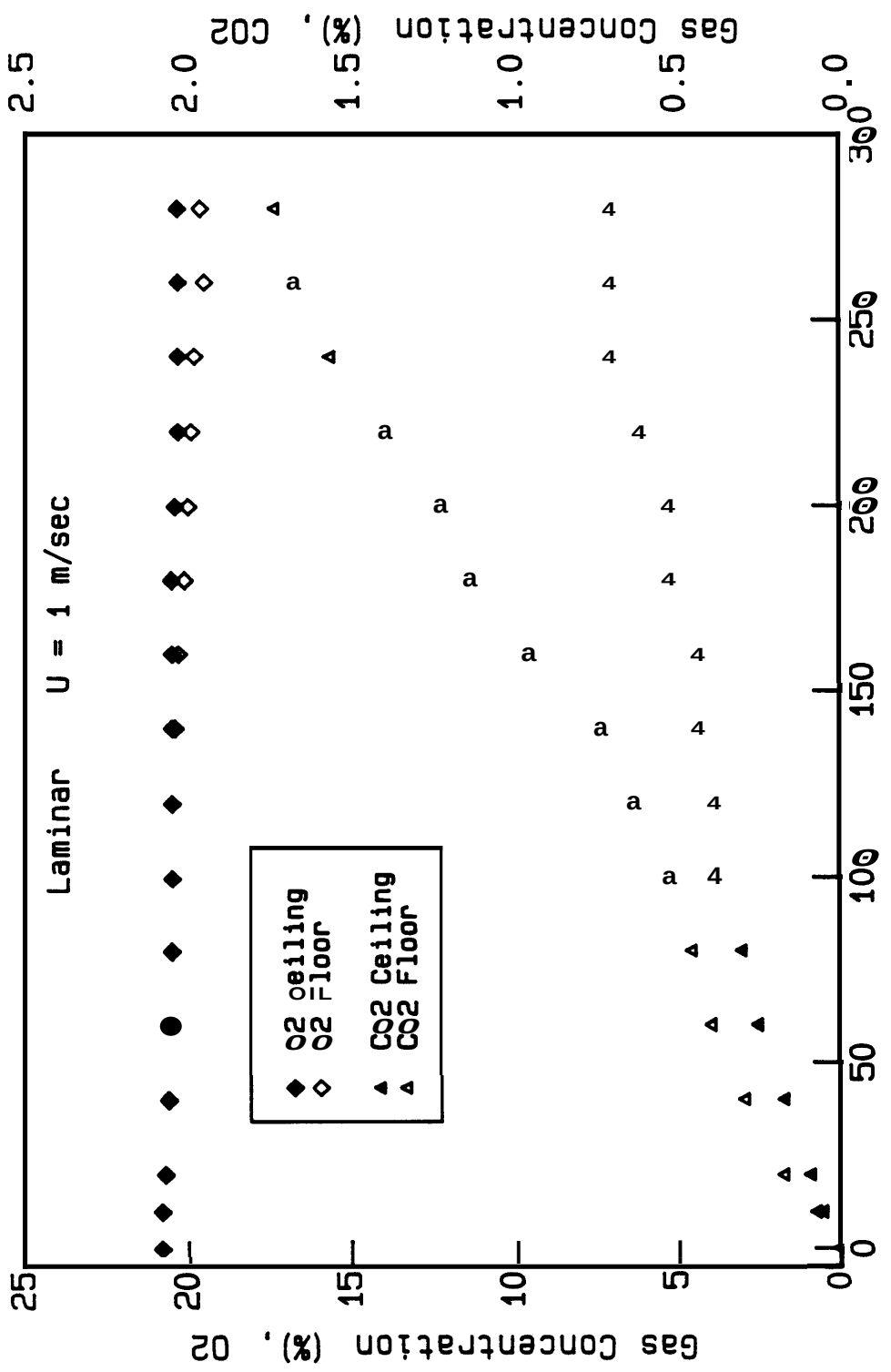

Fig. 6.10 Comparison of the concentrations of O_2 and CO_2 in the exhaust flows of ceiling and floor tests with a laminar flow velocity of 1 m/sec.

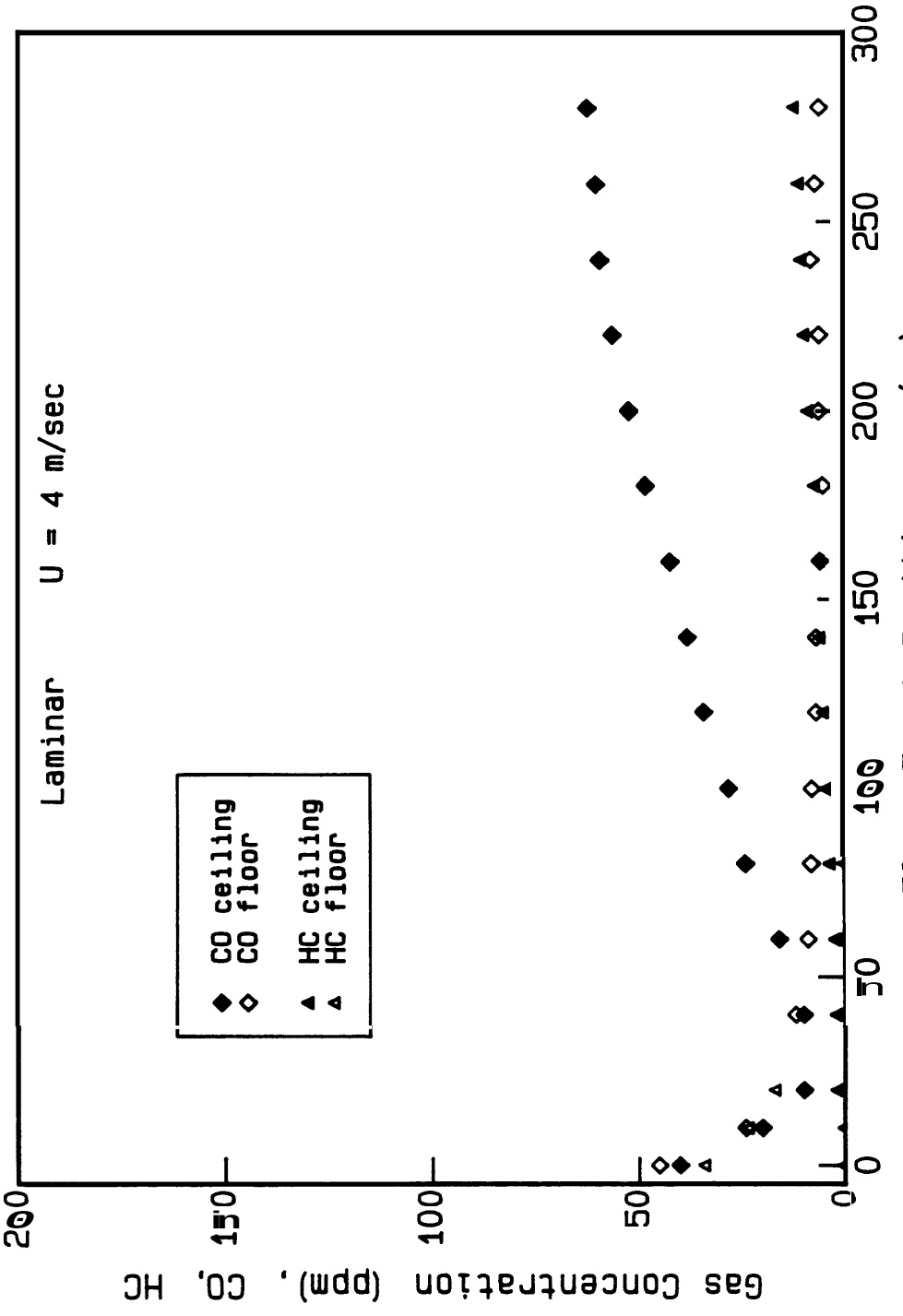

Fig. 6.11 Comparison of the concentrations of CO and unburnt hydrocarbons in the exhaust flows of ceiling and floor tests with laminar flow of 4 m/sec.

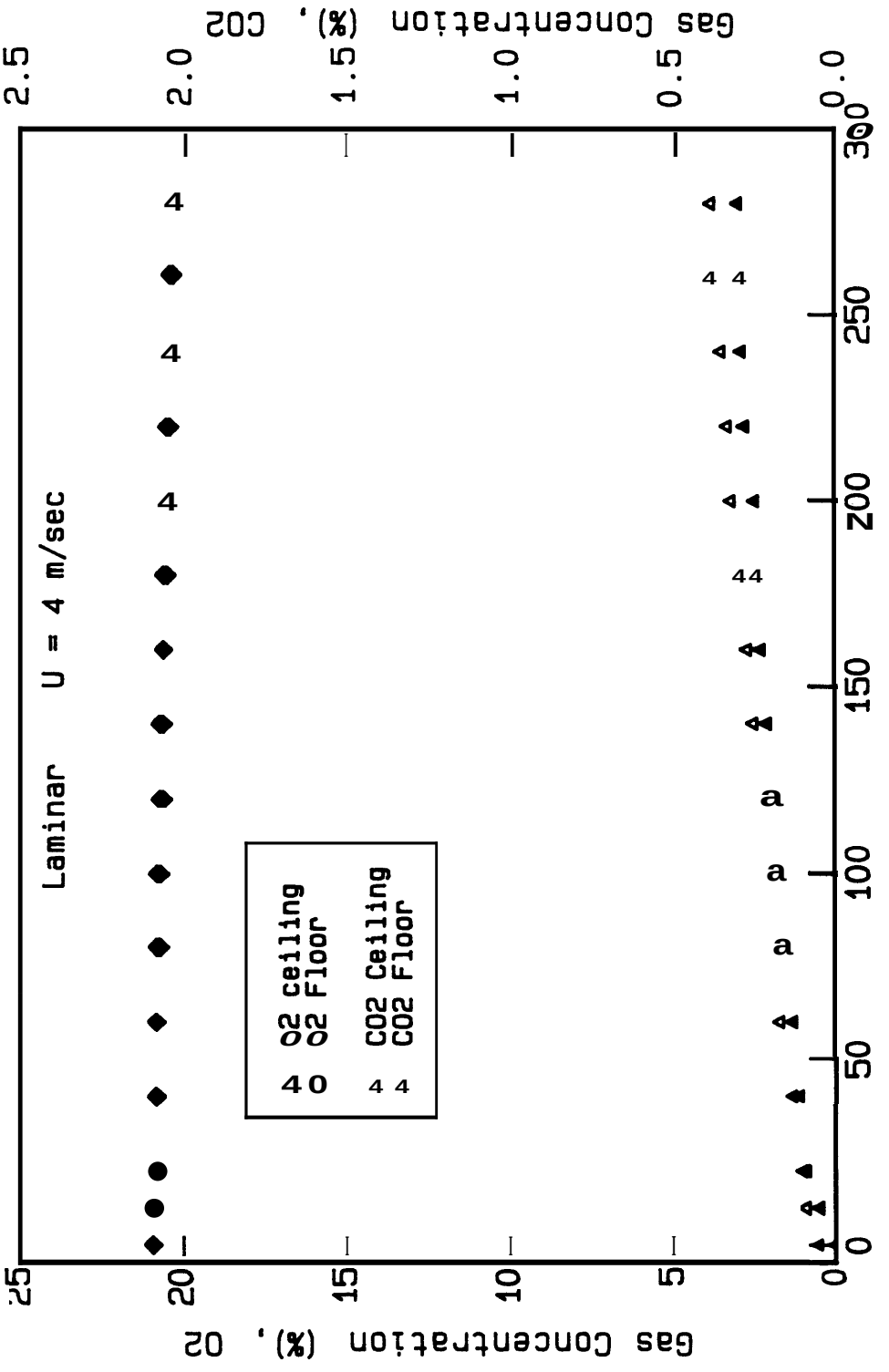

Fig. 6.12 Comparison of the concentrations of O_2 and CO_2 in the exhaust flows of ceiling and floor tests with a laminar flow velocity of 4 m/sec.

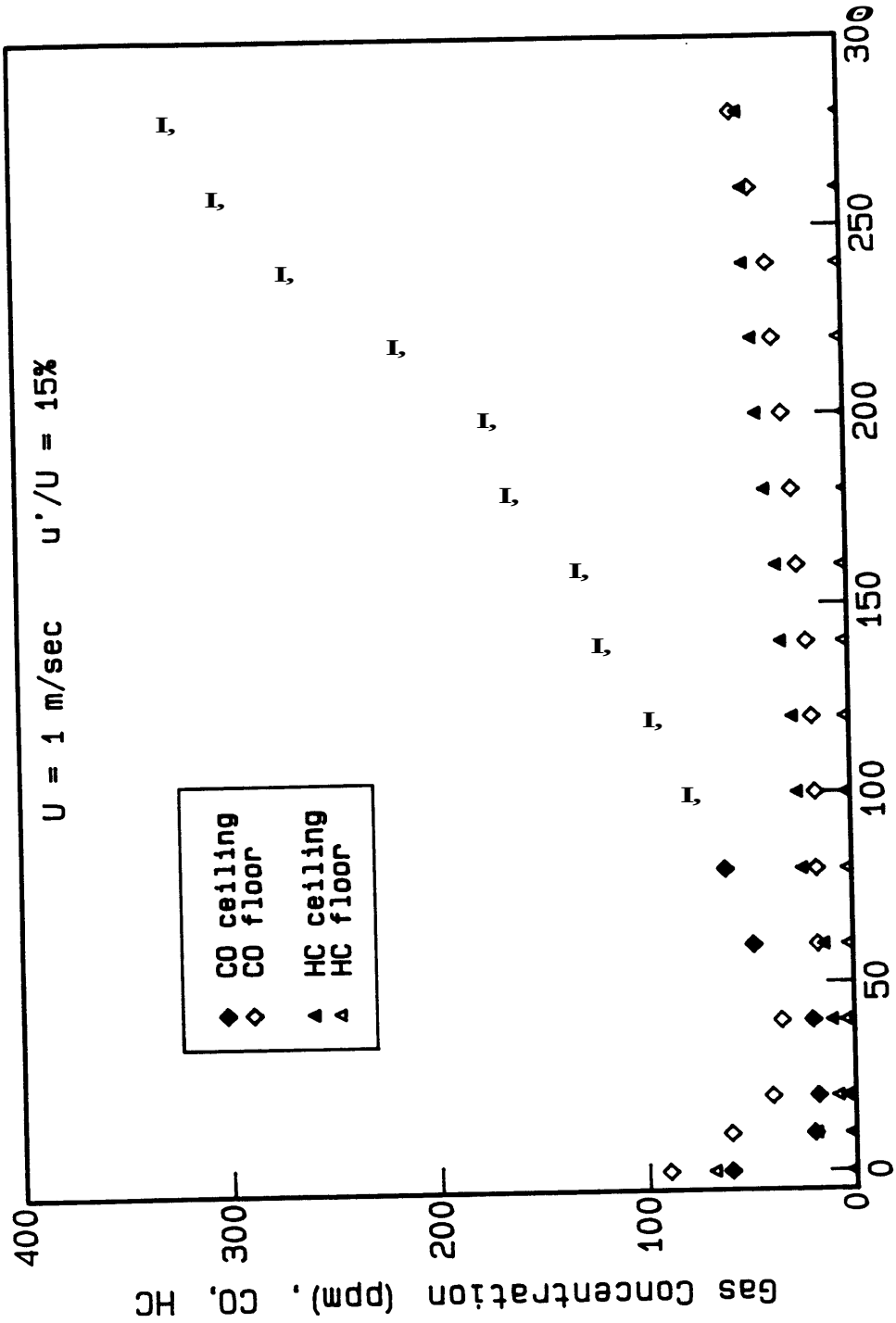

Fig. 6.13 Comparison of the concentrations of CO and unburnt hydrocarbons in the exhaust flows of ceiling and floor tests at U = 4 m/sec and u'/U = 15%.

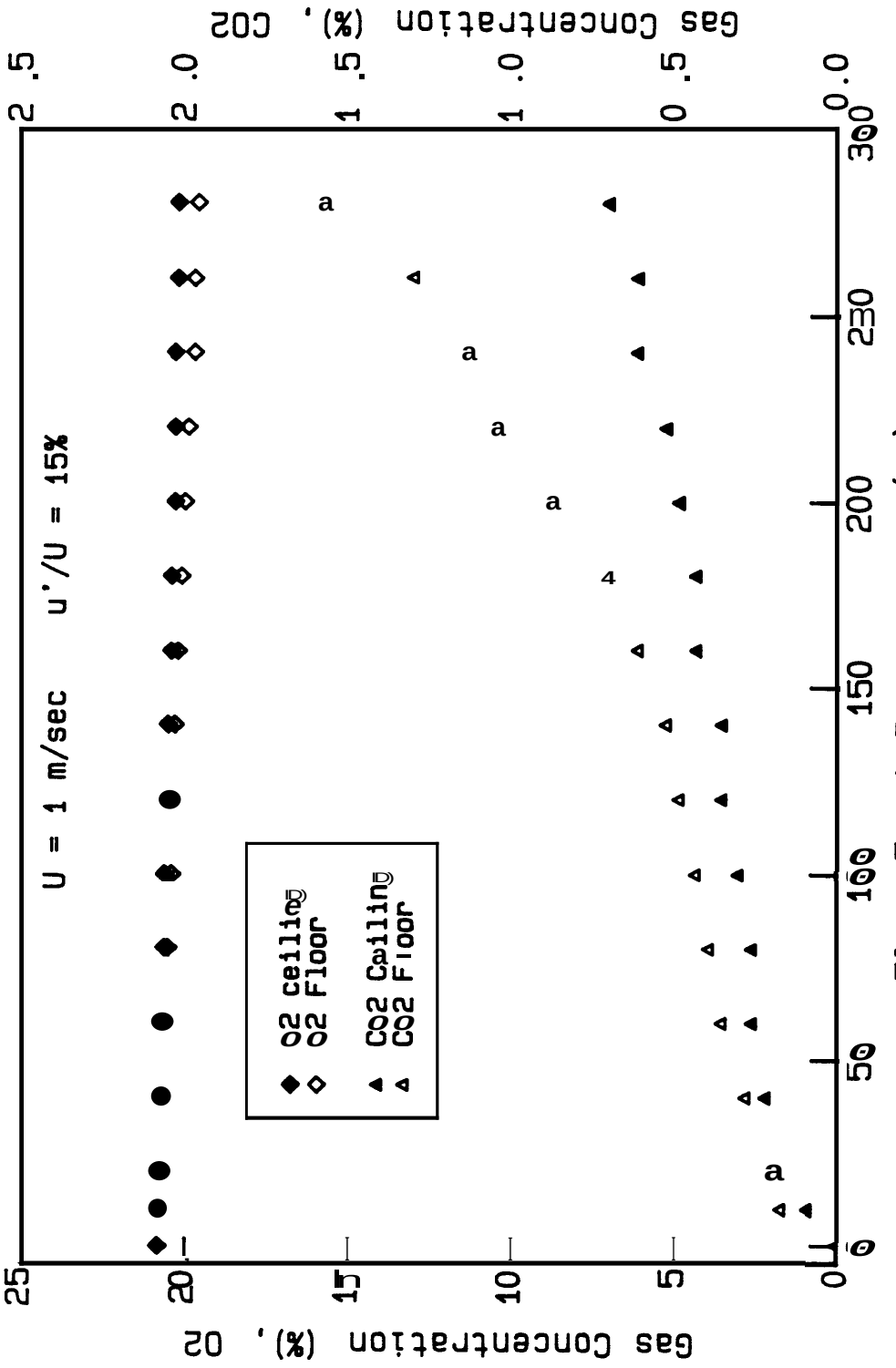

Fig. 6.14 Comparison of the concentrations of O_2 and CO_2 in the exhaust flows of ceiling and floor tests at U = 4 m/sec and u'/U = 15%.

phenomenon is particularly evident at low flow velocities. The result is that the ceiling combustion takes place under local under-ventilated conditions with cold wall quenching effect, which endows a slower flame spread rate. The conclusion obtained above can be used to explain the flame spread rate variation in the ceiling and floor case at low flow velocities. The effect of buoyancy on the chemical reaction seem to become the dominant mechanism and determines the magnitude of the flame spread rate at flows with lower velocities. The combustion is less complete in the ceiling case and less heat is generated, as a result, the flame spreads slower in the ceiling configuration than in the floor one.

From the experimental observations, it is seen that the buoyancy seems to have two opposite and competing effects on the ceiling flame spread process. At relatively high external flow velocity, more oxidizer flows through the combustion area and supplies sufficient oxygen to the reacting zone and also enhances the gaseous mixing, and therefore, the gas phase chemical reactions *can* proceed relatively thoroughly. The main buoyancy effect at high flow velocities is then determined by the enhanced heat transfer to the fuel due to the reduced distance from the flame to the solid surface, which results in a larger ceiling flame spread rate than the floor one. As the flow velocity decreases, the incompleteness of the chemical reaction caused by cold wall quenching and poor mixing becomes the dominant factor to the ceiling flame spread process, resulting in a slower propagation of flame in the ceiling configuration than the floor one. The transition appears to occur at the flow velocity around 0.75 to 1 m/sec for the tests in this study.

6.5 Mass Burning Rate

6.5.1 Velocity and Turbulence Effect

The surface regression rates for four flow velocities U = 1 to 4 m/sec are presented in Fig. 6.15 to 6.18, as functions of the downstream distance from the flame leading edge and the flow turbulence intensity. The regression rates in the ceiling burning display similar characteristics as those in the floor configuration. As seen in these figures, the ceiling surface regression rate decreases with the downstream distance for all the flow conditions as a result of thickening thermal boundary layer and decreasing heat transfer from the flame to the solid surface in the flow direction.

The dependence of the regression rates on the flow velocity can been seen from Fig. 6.19, which compare the surface regression rate results for different velocities with similar flow turbulence intensity. As the flow velocity increases, the growth of the boundary layer along downstream distance is hindered and the flame is pushed closer to the solid fuel surface. Therefore, the convective heat transfer is enhanced and the mass burning rate is increased. Similar result is also observed for other turbulence intensities.

It is also observed that the turbulence intensity has significant effect on the ceiling mass burning process. The experimental results of Fig. 6.15 to 6.18 show that the ceiling surface regression rate increases with the flow turbulence intensity, which is in qualitative agreement with the results of the floor mass burning. Larger turbulence creates stronger eddies which enhance the heat and mass transport

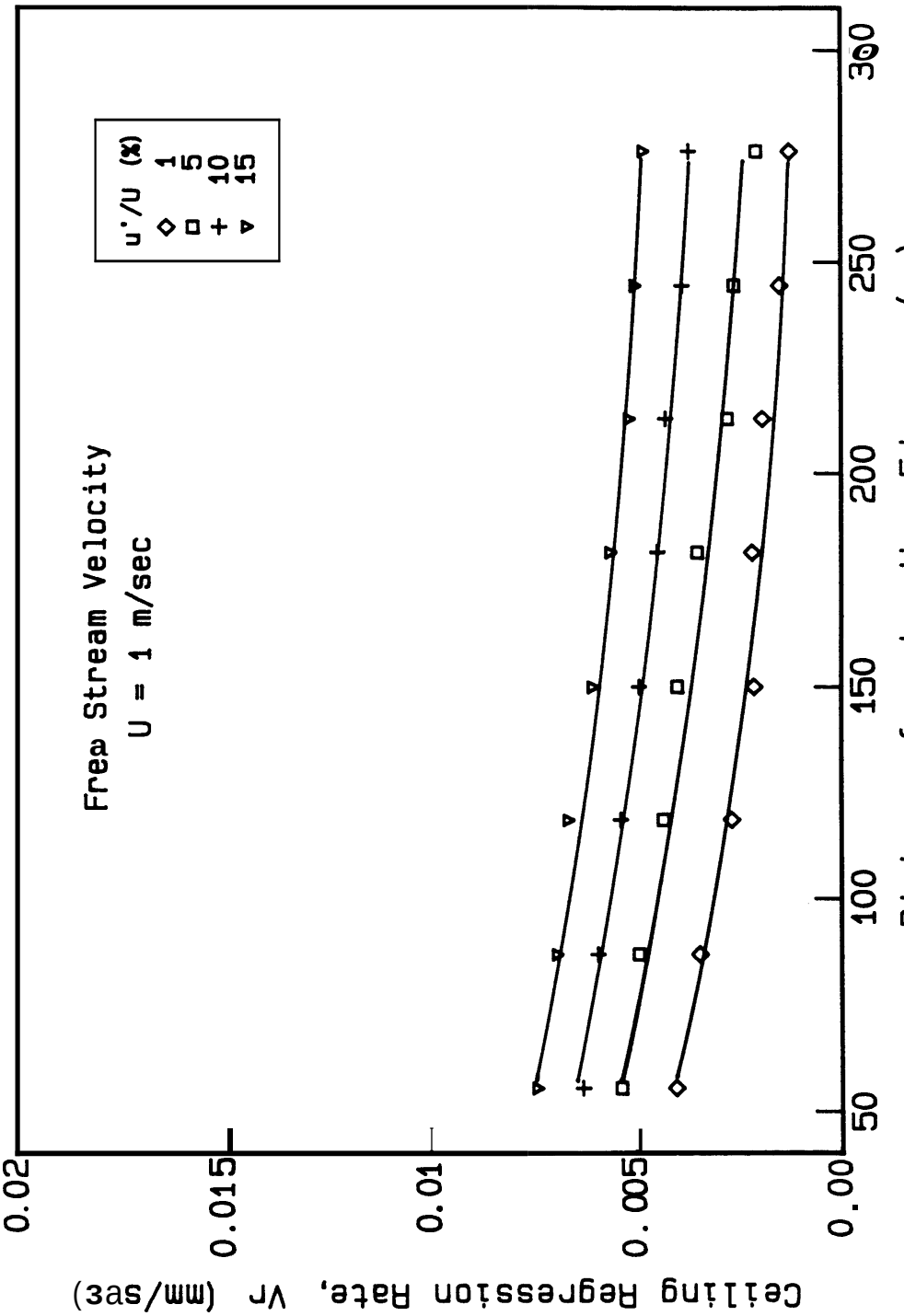

Fig. 6.15 Ceiling regression rate along the PMMA sheet for a flow velocity of 1 m/sec.

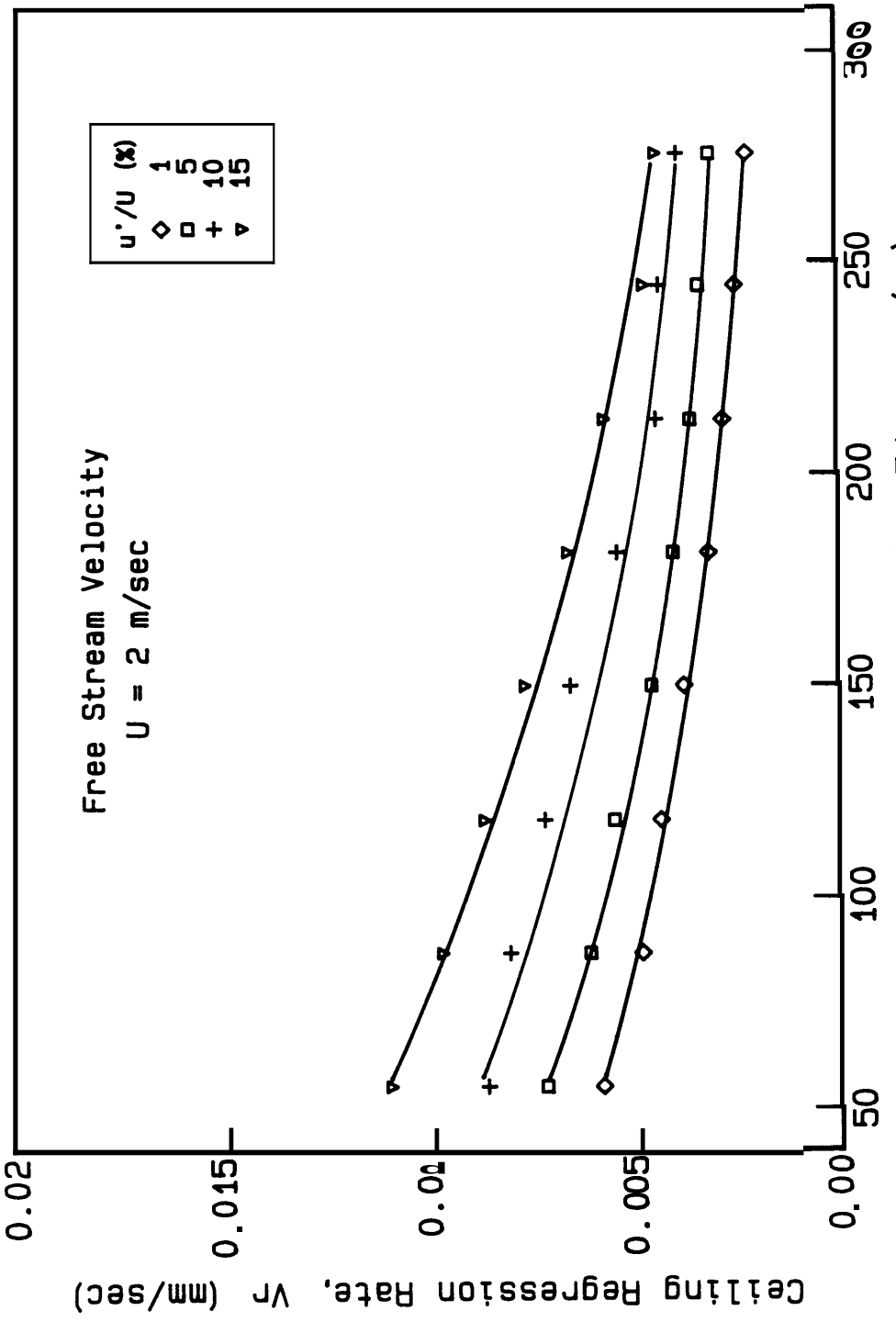

Fig. 6.16 Ceiling regression rate along the PMMA sheet for a flow velocity of 2 m/sec.

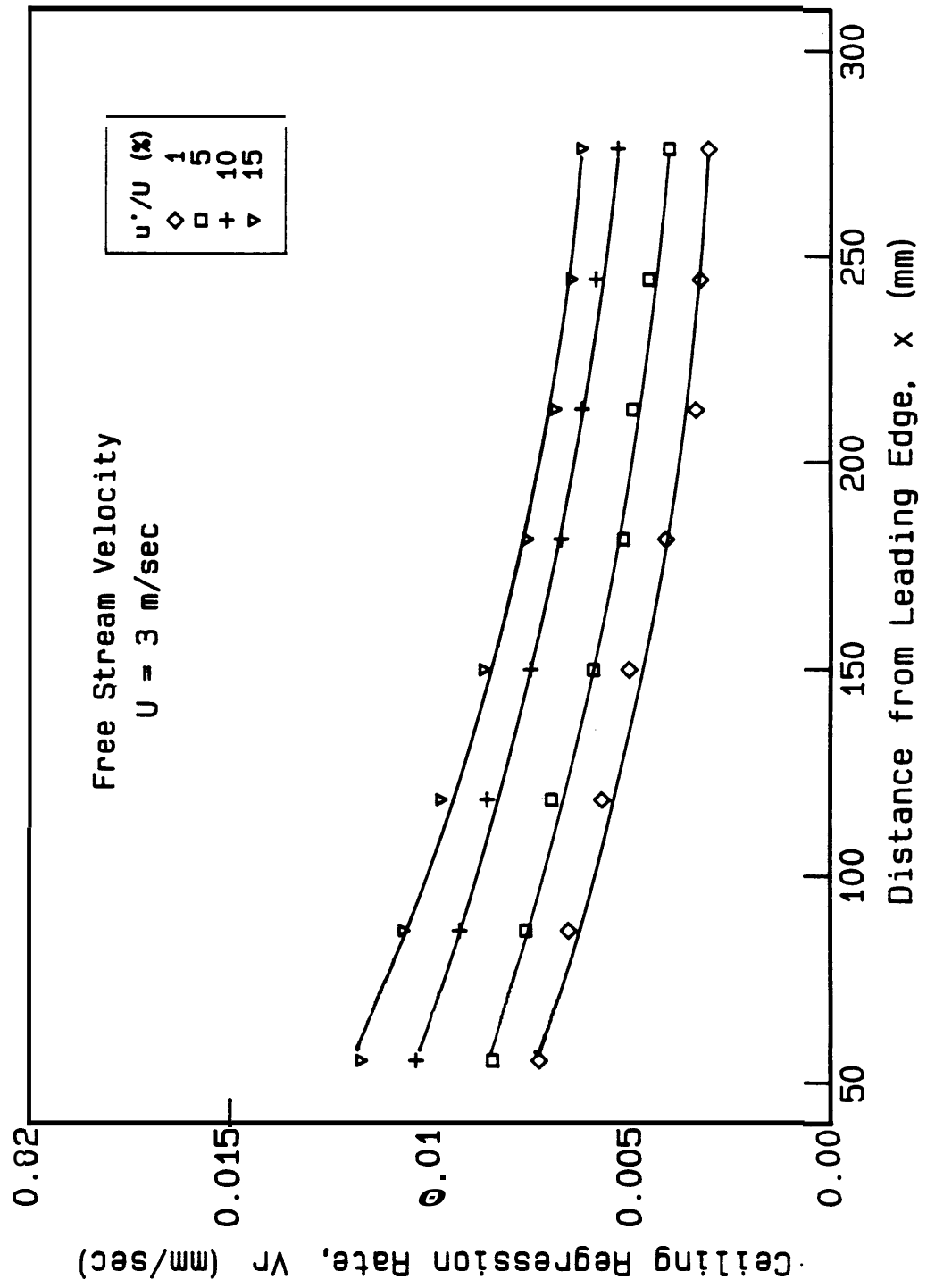

Fig. 6.17 Ceiling regression rate along the PMMA sheet for a velocity of 3 m/sec.

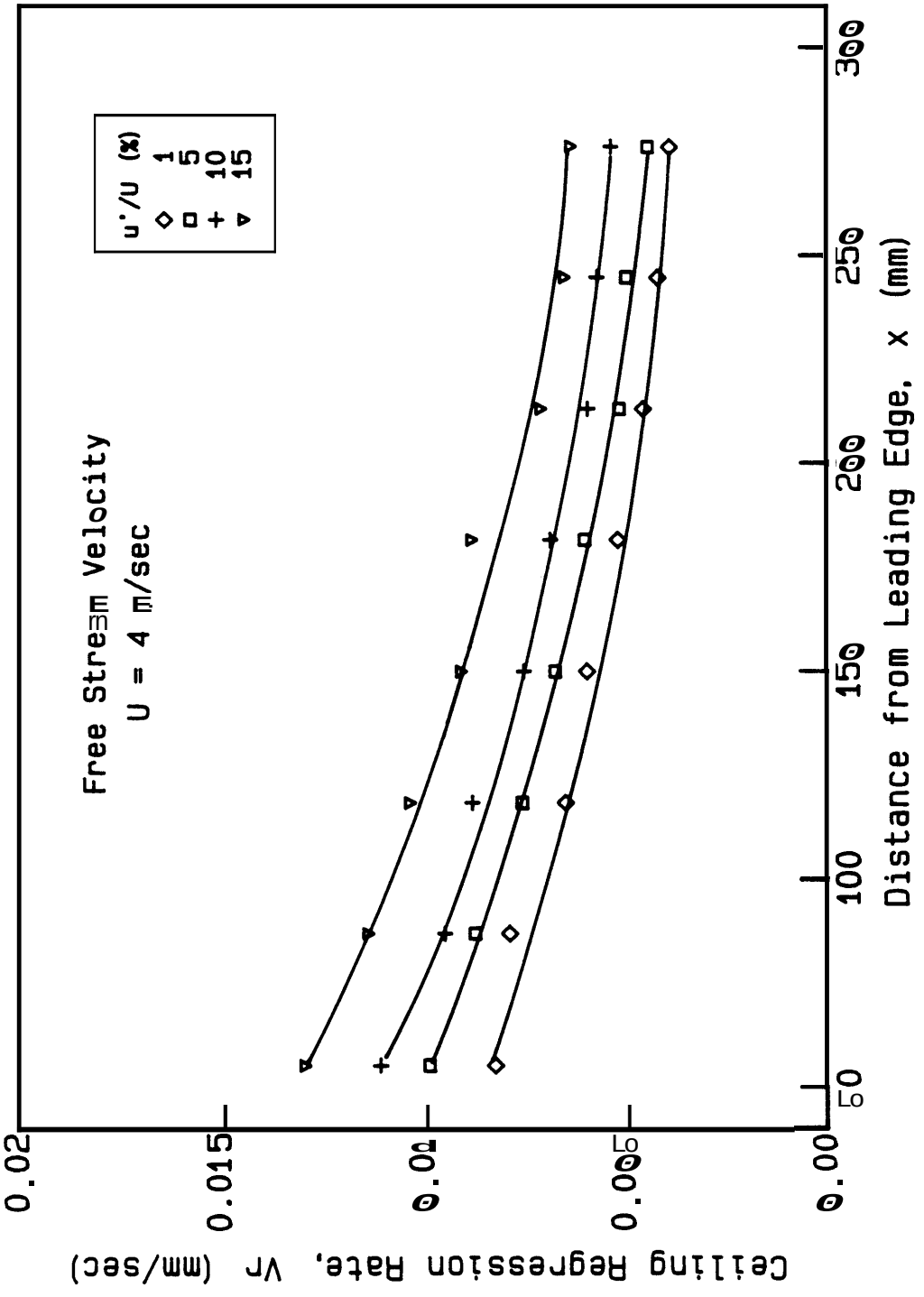

Fig. 6.18 Ceiling regression rate along the PMMA sheet for a velocity of 4 m/sec.

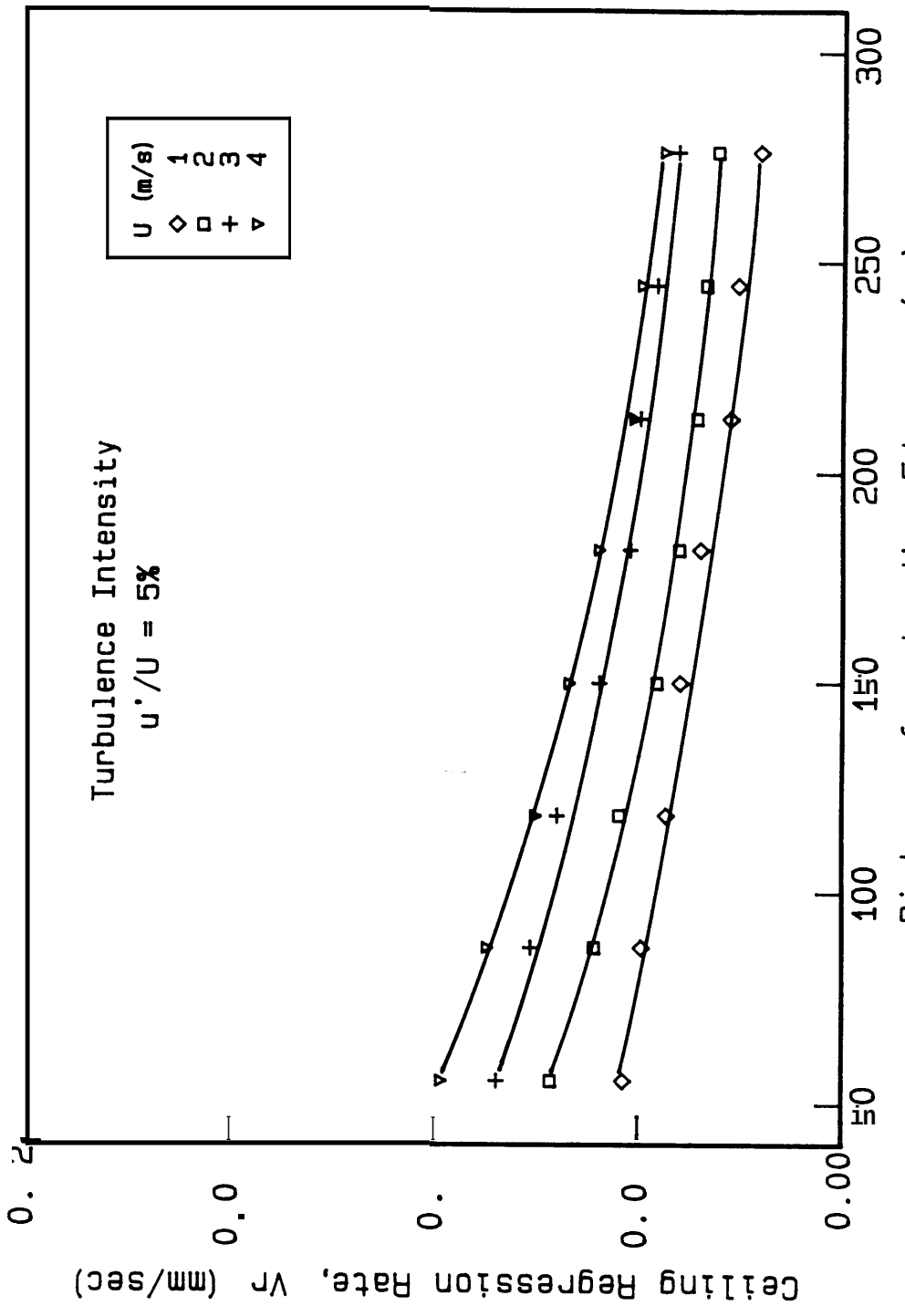

Fig. 6.19 **Ceiling regression rate along the PMMA sheet for a turbulence intensity of 5% with several velocities.**

process, and therefore increases the mass burning rate. However, the enhancing effect of the flow turbulence on the ceiling burning is not as strong as in the floor configuration.

Empirical correlations for non-dimensional mass burning rate and flow parameter are sought for the ceiling case as for the floor problem in Chapter 4. The results are shown in Fig. 6.20 for laminar flow and Fig. 6.21 for turbulent flow. The laminar correlation is

$$\frac{\dot{m}''Lx}{\lambda(T_f - T_p)} = 0.32\ Re_x^{1/2} \tag{6.3}$$

and the turbulent correlation is

$$\frac{\dot{m}''Lx}{\lambda(T_f - T_p)} = 4.1\left[Re_x^{0.8}\left(\frac{u'}{U}\right)\right]^{0.5} \tag{6.4}$$

It is observed that the data points are more scattered in the ceiling than in the floor due to the influence of the buoyancy.

6.5.2 Buoyancy Effect

Comparison has been made between the ceiling and floor regression rates to seek the difference of controlling mechanisms in the two mass burning processes. It is presented in Fig. 6.22 the regression rates of ceiling and floor burning for flow velocity of U = 2 m/sec and turbulence intensities of 1% and 15%. Similar characteristics of the surface regression rate in both cases are also obtained in other flow conditions. It is seen that at low flow turbulence intensity, the ceiling regression

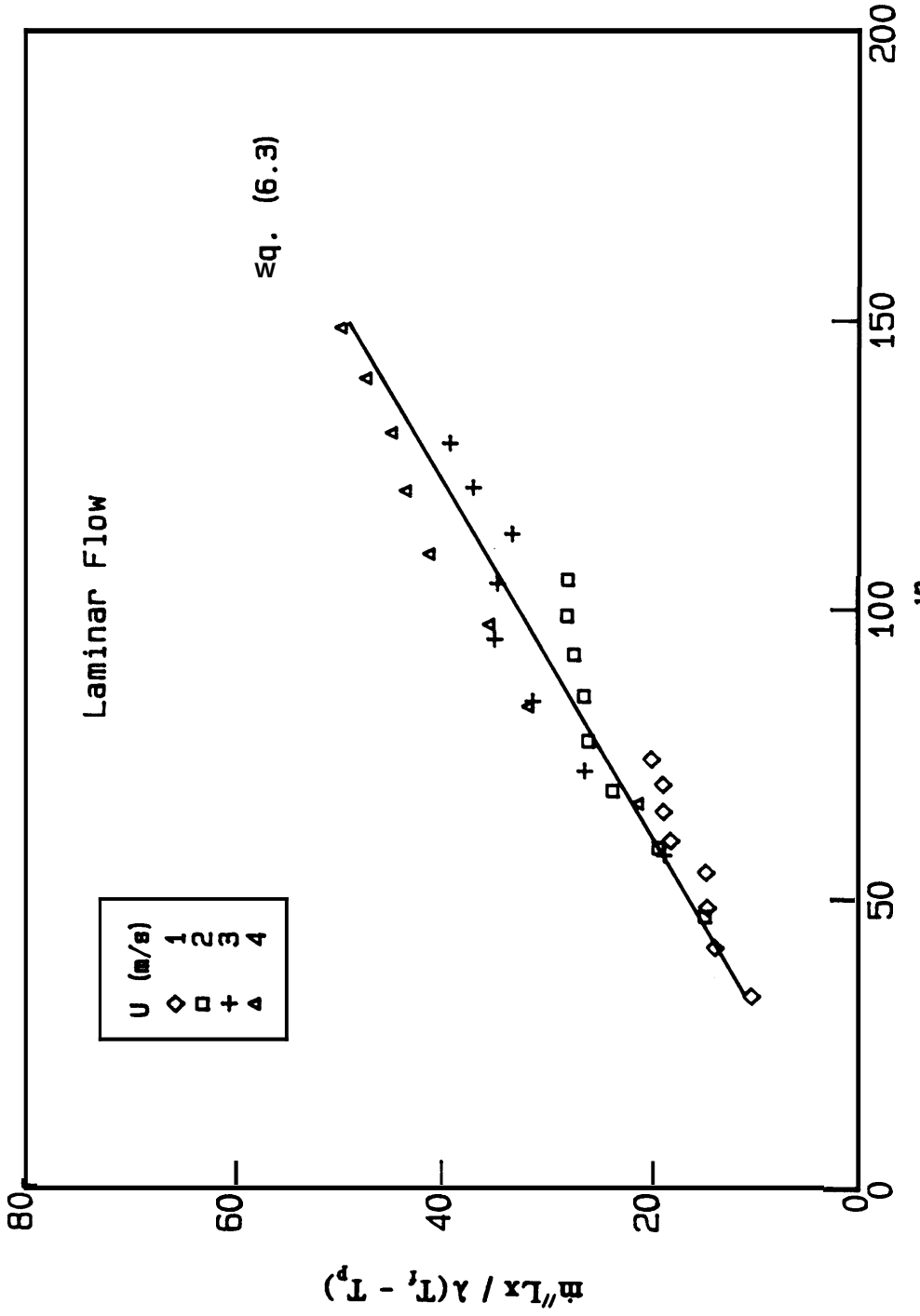

Fig. 6.20 Non-dimensional ceiling mass burning rate for laminar flow versus the square root of the Reynolds number.

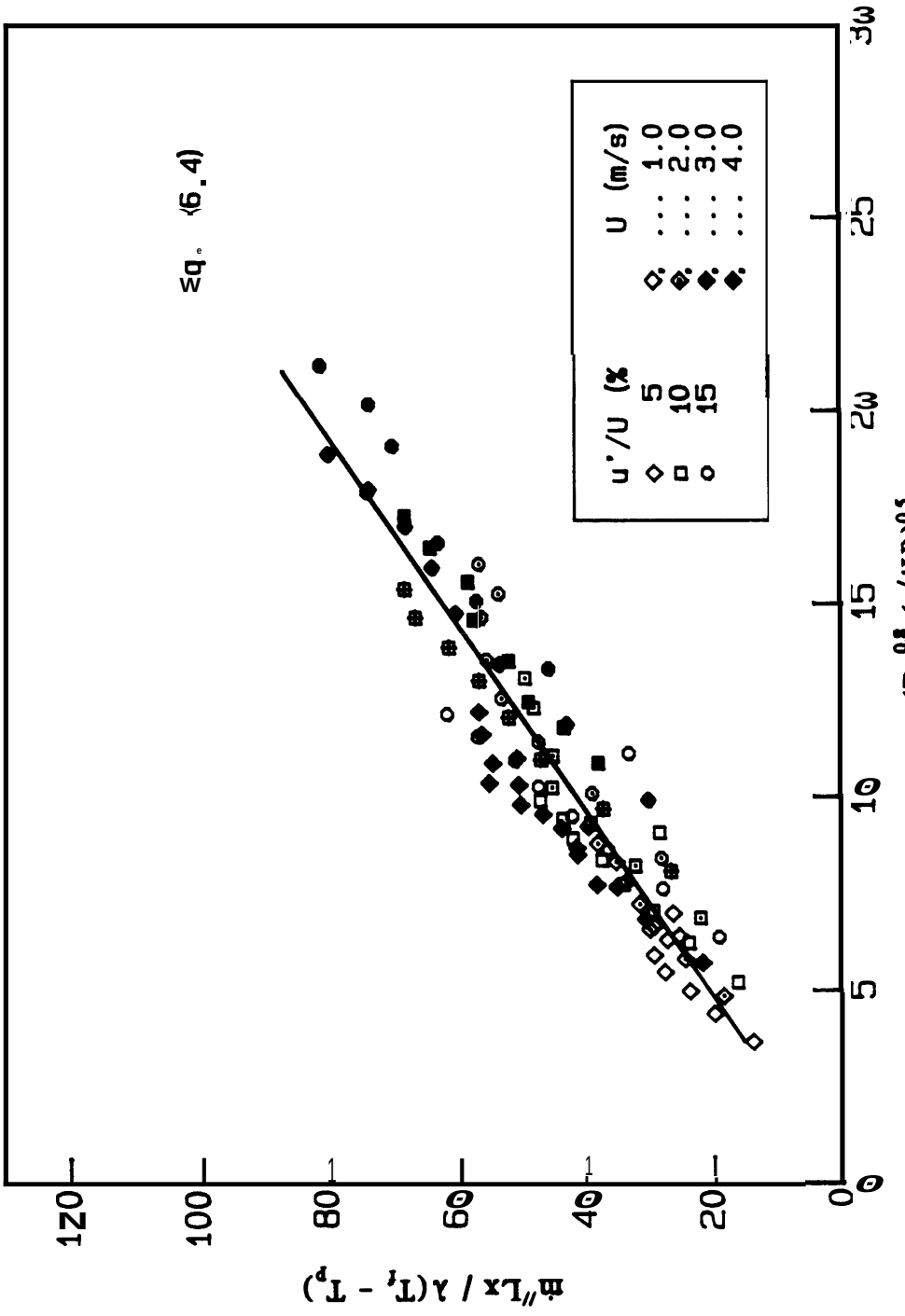

Fig. 6.21 Non-dimensional ceiling mass burning rate for turbulent flow versus the non-dimensional flow parameter.

rate is larger than the floor one. The buoyancy seem to enhance the heat transfer from the flame to the solid by moving the flame closer to the fuel surface in the ceiling burning, resulting in an larger ceiling surface regression rate. As the free stream turbulence intensity increases, the enhancing effect of the buoyancy on the ceiling regression rate gradually diminishes. Eventually the ceiling surface regression rate becomes smaller than the floor one as shown for flow turbulence intensity of 15%. In flows with high turbulence intensities, the strong flow commotion takes the flame closer to the solid surface, reducing the flame stand-off distance in both the ceiling and floor test. The advantage of the buoyancy enhancing heat transfer as for low turbulence intensities becomes less important. The buoyancy effect on chemical kinetics replaces the heat transfer enhancing mechanism and become the more dominant controlling mechanism for high turbulence intensities. From the measurements of the species concentrations in the exhaust flow, it is inferred that the chemical reactions are less complete in the ceiling burning than in the floor, therefore resulting in a smaller heat generation and slower flame spread rate in the ceiling configuration. The exhaust gas concentrations are observed to maintain relatively constant during the mass burning process. The typical results are presented in Table 6.1 for CO and Table 6.2 for unburnt hydrocarbons under different flow conditions. It *can* be seen that more CO and unburnt hydrocarbons are detected in the ceiling than in the floor while less oxygen is consumed and more CO is produced.

The species concentration results support the argument that the ceiling mass burning has less complete chemical reactions than the floor one, which results in a

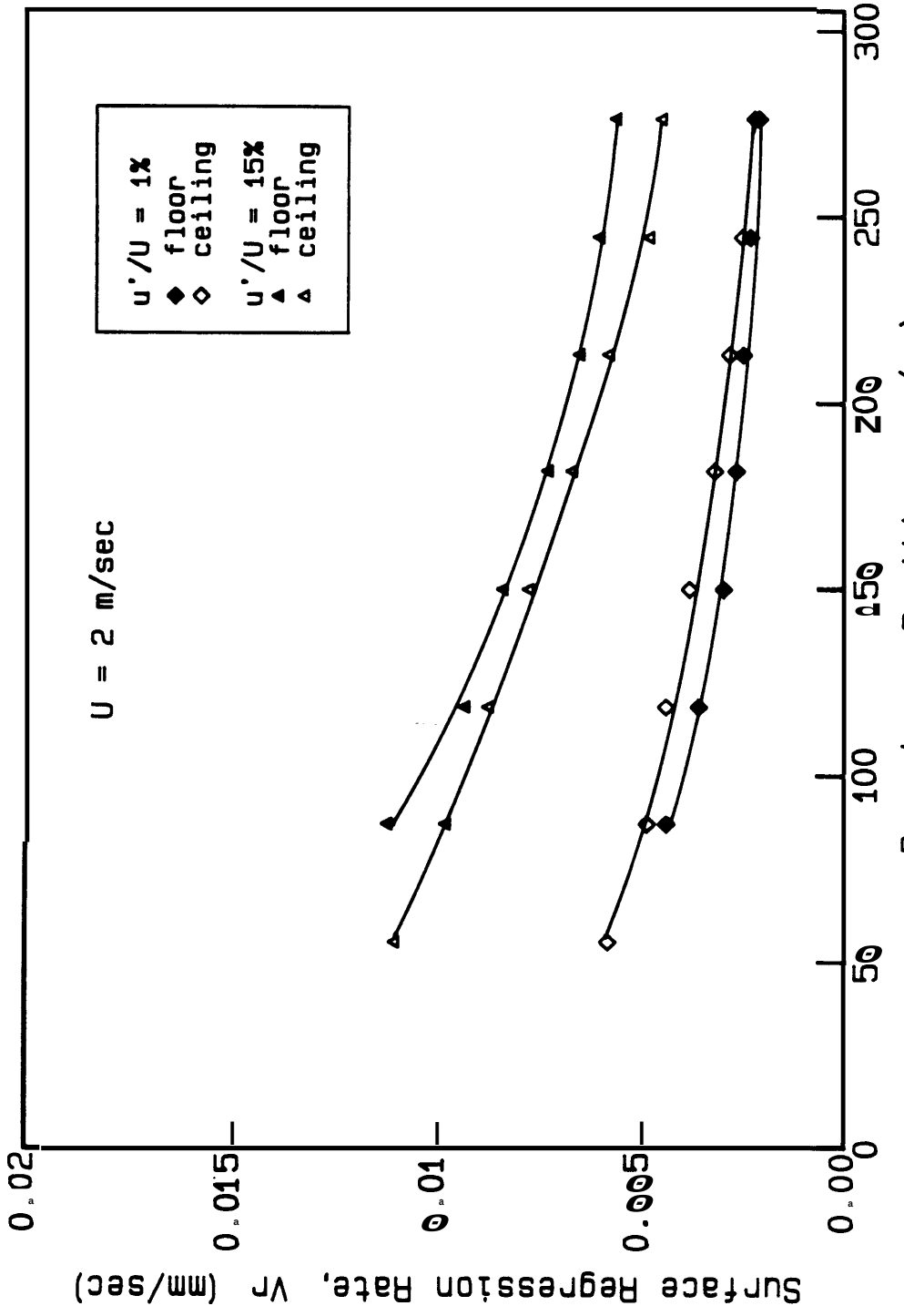

Fig. 6.22 Comparison of surface regression rate of ceiling and floor tests.

Table 6.1 Comparison of CO concentrations in mass burning process for floor and ceiling geometries.

	CO Concentration (ppm)			
	u'/U = 1%		u'/U = 15%	
	ceiling	floor	ceiling	floor
U = 0.5 m/s	435	72	430	69
1.0 m/s	410	44	344	55
4.0 m/s	64	6	40	30

Table 6.2 Comparison of hydrocarbon concentrations in mass burning process for floor and ceiling geometries.

	Unburnt Hydrocarbon Concentration (ppm)			
	u'/U = 1%		u'/U = 15%	
	ceiling	floor	ceiling	floor
U = 0.5 m/s	225	0	177	0
1.0 m/s	40	0	47	0
4.0 m/s	11	0	7	0

smaller ceiling surface regression rate at high turbulent flow. The overall buoyancy effect is determined by the relative magnitude of the enhanced heat transfer from the flame to the solid surface and the less complete chemical reactions in the ceiling case.

6.6 Conclusion

An experimental study is conducted to investigate the controlling mechanisms of solid fuel flame spread and mass burning in ceiling configuration. The results show that the ceiling flame spread and mass burning have many similar characteristics as those observed in the floor case. However, the existence of buoyancy introduces significant difference to the problem, especially in the low flow velocity conditions. The most interesting result is the buoyancy effect on the gas phase chemical kinetics and the flame stand-off distance. It is found that the chemical reactions are less complete in the ceiling than in the floor, mainly by insufficient mixing and wall quenching in the ceiling. It is also observed that the buoyancy pushes the flame closer to the solid surface in the ceiling and lifts the flame away from the surface in the floor burning. These two buoyancy mechanisms have opposite effects on the ceiling flame spread and mass burning process, the former enhancing and the latter hindering. Both mechanisms of buoyancy can be important on the flame spread rate and mass burning rate and the overall effect depends on the flow conditions. The experimental observation suggest that at low flow velocities and high turbulence intensities the hindering effect (slower chemical kinetics) is the

dominant controlling mechanism, while in high flow velocities and low turbulence intensities, the enhancing effect (smaller flame stan-off distance) becomes more important. The difference between the ceiling and floor results diminishes as the flow velocity is increased.

Since the chemical kinetics controlling mechanism seem to be important in the ceiling problem, the frequently used thermal models may need modifications to account for the buoyancy effect, at least in the low flow velocity cases. The experimental results indicate that care should be taken when using data obtained either in the floor or ceiling configuration to model or predict the spread of fire and in the flammability testing of materials.

Chapter 7 Conclusions and Future Work

7.1 Summary of Results

A systematic experimental study has been carried out to investigate the controlling mechanisms of solid fuel flame spread and mass burning in turbulent flows. The primary interest has been focused on the effect of flow velocity, turbulence intensity and buoyancy on the flame spread rate and the surface regression rate. The experiments are conducted in both opposed and concurrent flow conditions with the solid specimen in floor and ceiling configuration. PMMA sheets are used to represent the thermally thick solid fuel for all the experiments and the filter paper sheets are used in the opposed flow flame spread tests as a representative of thermally thin fuels. Flow velocity and turbulence intensity fields are measured with a one-dimensional Laser Doppler Velocimeter operating in duel-beam, forward-scattering mode. An array of thermocouples are placed on the solid fuel sample surface to measure the surface temperature histones from which the flame spread rate can be obtained. Interferometry and Schlieren photography are utilized to acquire qualitative information of the reacting flow. In addition, infrared gas analyzers are employed to study the completeness of gas phase chemical reactions. The flame spread rate and the surface regression rate are measured as functions of the flow velocity and the turbulence intensity. From the experimental data, the following main results are obtained.

Opposed flow flame spread

(1) The flame spread rate of thermally thick PMMA sheet increases initially with the flow velocity, reaches a peak value and then decreases as the flow velocity increases further. The flow turbulence effect is to increase the flame spread rate initially and then decreases it at high turbulence intensity. The transition occurs at about $u'/U = 6\%$.

(2) The flame spread rate of thermally thin paper sheet decreases monotonically, with the flow velocity and turbulence intensity.

(3) The flow turbulence has a significant effect on the flame extinction conditions. The velocity at which the flame extinction occurs decreases with the turbulence intensity.

Concurrent flow flame spread

(1) The flow turbulence has a strong influence on the concurrent flow flame length, surface heat flux, and on the flame spread rate. The most interesting result is that the flow turbulence decreases the flame spread rate, which is mainly caused by the shortening of flame length at high turbulence intensity.

(2) The flame spread rate increases with the flow velocity.

(3) The experimental data of flame spread rate, flame length and surface heat flux agrees well with the formula obtained from a simplified thermal model Eq. (4.3), indicating that the heat transfer from flame to solid surface is the dominant controlling mechanism in the turbulent concurrent flame spread

process and the gas phase chemical reactions is only of secondary importance.

Solid fuel mass burning

(1) The solid fuel surface regression rate decreases with the downstream distance and the flow velocity in both floor and ceiling configuration.

(2) The flow turbulence increases the surface regression by enhancing the mixing and bringing the flame closer to the solid surface.

(3) Empirical correlations between non-dimensional surface regression rate and the non-dimensional flow parameter are obtained as Eqs. (5.9) and (5.10), which show the possibility of incorporating the flow turbulence intensity explicitly in non-dimensional analysis and numerical simulations.

Buoyancy Effect

(1) The buoyancy has two competing effects on the ceiling flame spread and mass burning process. It enhances the beat transfer from the flame to the solid surface by pushing the flame closer to the wall. And at the Same time, it causes the gas phase chemical reactions to proceed less completely in ceiling than in floor through insufficient gas mixing and cold wall quenching.

(2) The overall buoyancy effect is the combined influence of these two mechanisms and is determined by the flow conditions.

7.2 Future Work

Given the potential impact of the results of the present study on the theoretical prediction of the solid flame spread and mass burning, and on the practical applications such as fire controlling and material flammability testing, it is important to extend the work to the other aspects of the problem. For example, it is interesting to know the turbulence length scale effect on the flame spread and mass burning and the radiation characteristics in turbulent flows of large scale problems. The buoyancy effect on the gas phase chemical reactions at low flow velocities needs to be further investigated, which can be accomplished by varying the oxygen concentration in the gas flow, creating different chemical kinetics conditions. Also interesting is the numerical simulation of the problem. The gas phase of the problem may be solved by using random vortex formulation and Navier-Stokes equations with simple chemical kinetics while the solid phase can be treated relatively simply as semi-infinite.

References

1. Magee, R. S., and McAlevy, R. F., III : The mechanism of flame spread, *J. of Fire* and *Flammability,* 2, p.271.

2. Sirignano, W. A. : A critical discussion of theories of flame spread across solid and liquid fuels, *Combustion Science* and *Technology,* 6, p.95, 1972.

3. Williams, F. A. : Mechanisms of fire spread, *Sixteenth Symposium (International) on Combustion,* p.1281, 1976.

4. Emmons, H. W. : Fundamental problems of the free burning fire, *Tenth Symposium (International) on Combustion,* p.95 1, 1964.

5. Williams, F. A. : *Combustion Theory, Second Edition,* The Benjamin & Cummings Publishing Company, Inc., 1985.

6. Fernandez-Pello, A. C., and Hirano, T. : Controlling mechanisms of flame spread, *Combustion Science* and *Technology,* 32, p.1, 1983.

7. Fernandez-Pello, A. C. : Flame spread modelling, *Cornbustion Science* and *Technology,* 39, p.119, 1984.

8. Emmons. H. W. : The film combustion of liquid fuel, *Z. angew. Math. Mech.*, 36, p.60, 1956.

9. Tewarson, A., and Pion, R. F., : Flammability of plastics, *Combustion* and *Flame,* 26, p.85, 1976.

10. Vovelle, C., Delfau, J.-L., Reuillon, M., Bransier, J., and Laraqui, N., : Experimental and numerical study of the thermal degradation of PMMA,

Combustion Science and *Technology, 53,* p.187, 1987.

11. Thompson, H. D. and Stevenson, W. H. : *Laser Velocimetry* and *Particle Siring,* Hemisphere Publishing Co., 1978.

12. Durst, F., Melling, A., and Whitelaw, J. H., : *Principles* and *Practice of Laser-Doppler Anemometry,* Academic Press, 1976.

13. Drain, L E., : *The Laser Doppler Technique,* John Wiley & Sons, 1980.

14. TSI Inc. : *Instruction for Counter Type Signal Processor,* 1985.

15. Meyer-Arendt, J. R., : *Classical* and *Modern Optics,* Prentice-Hall Inc., 1985.

16. Holman, J. P. : *Experimental Methods for Engineers,* McGraw-Hill Book Co., 1978.

17. Comet-Bellot, G. and Corrsin, S. : The use of a contraction to improve the isotropy of grid-generated turbulence, *J. Fluid Mechanics, 25,* p.657, 1966.

18. Corrsin, S. and Karweit, M. : Fluid line growth in grid-generated isotropic turbulence, *J. Fluid Mechanics,* 39, p.87, 1969.

19. Manako, H., Ueda, T. and Mizomoto, M., : Turbulent structure of a diffusion flame in grid turbulence, *Combustion Science* and *Technology,* 59, p.423, 1988.

20. Manako, H., Ueda, T. and Mizomoto, M., : Turbulent structure of a jet diffusion flame in a co-flowing air stream with grid turbulence, *Bull, JSME,* 29, p.3015, 1986.

21. Hinze, J. O. : *Turbulence, Second Edition,* McGraw-Hill Book Co., 1975.

22. Tennekes, H. and Lumley, J. L. : *A first Course in Turbulence,* MIT Press, 1987.

23. Batchelor, G. K. : *An introduction to Fluid Dynamics,* Cambridge University Press, 1987.

24. Omega Co. : *The Temperature Handbook,* 1989.

25. White, F. M. : *Viscous Fluid Flow,* McGraw-Hill Book Co., 1974.

26. Bechman Co. : *Instructions for Oxygen Analyzer OM-11,* 1973.

27. Horiba Inc. : *Instructions* for *Non-dispersive Infrared Gas Analyzer*, 1975.

28. Alterkirch, R. A, Eichorn, R., and Shang, P. C. : Buoyancy effects on flame spreading down thermally thin fuels, *Combustion* and *Flame,* 37, p.71, 1980.

29. Alterkirch, R. A, Eichorn, R., and Rizvi, A. R. : Correlating downward flame spread rates for thermally-thick fuel beds, *Combustion Science and Technology,* 32, p.49, 1983.

30. Fernandez-Pello, A. C., Ray, S. R., and Glassman, I. : Flame spread in an opposed forced flow: the effect of ambient oxygen concentration, *Eighteenth Symposium (International) on Combustion,* p. 579, 1981.

31. Williams, F. A. : A unified view of fire suppression, *Journal of Fire and Flammability,* 5, p.54, 1974.

32. De Ris, J. N. : Spread of a laminar diffusion flame, *Twelfth Symposium (International) on Combustion,* p.241, 1969.

33. Wichman, I. S., Williams, F. A., and Glassman, I. : Theoretical aspects of flame spread in an opposed flow over flat surfaces of solid fuels, *Nineteenth Symposium (International) on Combustion,* p.825, 1982.

34. Ito, A. and Kashiwagi, T. : Temperature measurements in PMMA during downward flame spread in air using holographic interferometry, *Twenty-first Symposium (International) on Combustion,* p.65, 1986.

35. Fernandez-Pello, A. C., Ray, S. R., and Glassman, I. : Downward flame spread in an opposed forced flow, *Combustion Science* and *Technology,* 19, p.19, 1978.

36. Fernandez-Pello, A. C. and Williams, F. A. : Laminar flame spread over PMMA surfaces, *Fifteenth Symposium (Intemational) on Combustion,* p.217, 1975.

37. Fernandez-Pello, A. C. and Williams, F. A. : A theory of laminar flame spread over flat surfaces of solid combustibles, *Combustion* and *Flame,* 28, p.251.

38. Frey, A. E. Jr., and Tien, J. S. : Near-limit flame spread over paper samples, *Combustion* and *Flame,* 26, p.257, 1976.

39. Frey, A. E. Jr., and Tien, J. S. : A theory of flame spread over a solid fuel including finite chemical kinetics, *Combustion* and Flame, 36, p.263, 1979.

40. Ray, S. R., Fernandez-Pello, A. C., and Glassman, I. : An analysis of the heat transfer mechanisms in horizontal flame propagation, *J. of Heat Transfer,* 102, p.357, 1980.

41. Hirano, T. and Sato, K. : Effects of radiation and convection on gas velocity and temperature profiles of flame spreading over paper, *Fifteenth Symposium (International) on Combustion,* p.233, 1975.

42. Sibulkin, M., Hetelhut, W. and Feldman, S. : Effect of orientation and external

flow velocity on flame spreading over thermally thin paper strips, ***Combustion Science*** and ***Technology,*** 9, p.75, 1974.

43. Suzuki, T. and Hirano, T. : Flame propagation across a liquid fuel in an air stream, ***Nineteenth Symposium (International) on Combustion,*** p.877, 1982.

44. Lastrina, F. A., Magee, R. S., and McAlevy, III, R. F. : Flame spread over fuel beds: solid phase energy considerations, ***Thirteenth Symposium (International) on Combustion,*** p.935, 1971.

45. Kayayan, K. M. : ***Flame Spread in Opposed Laminar Flow,*** Master thesis, University of California, Berkeley, 1977.

46. Fernandez-Pello, A. C. : Downward flame spread under the influence of externally applied thermal radiation, ***Combustion Science*** and ***Technology,*** 17, p.1, 1977.

47. Hirano, T. and Tazawa, K. : Effect of thickness on downward flame spread over paper in an air stream, ***Bulletin*** JSME, 26, p.7, 1976.

48. Quintiere, J. G. : A simplified theory for generalizing results from a radiant panel rate of flame spread apparatus, ***J. of Fire and Materials***, 5, p.56, 1981.

49. Perrins, L. E. and Pettett, K. : Measurement of flame spread velocities, *J. of Fire and Materials*, **5**, p.85, 1974.

50. Parker, W. J. : Flame spread model for cellulosic materials, ***J. of Fire*** and ***Materials***, 3, p.254, 1972.

51. Hirano, T., Noreikis, S. E. and Waterman, T. E. : Measured velocity and temperature profiles of flames spreading over a thin combustible solid,

Combustion and ***Flame,*** 23, p.83, 1974.

52. Sibulkin, M., Kim, J. and Creeden, J. V., Jr. : The dependence of flame propagation on surface heat transfer, I: Downward burning, ***Combustion Science and Technology,*** 14, p.43, 1976.

53. Ohki, **Y.** and Tsuge, **S.** : On flame spreading over a polymer surface, ***Combustion Science*** and ***Technology,*** 9, p.1, 1974.

54. Sirignano, W. A. : Theory of flame spread above solids, ***Acta Astronautica,*** 1, p. 1285, 1974.

55. Feng., C. C. and Sirignano, W. A. : Further calculations based upon a theory of flame spread across solid fuels, ***Combustion*** and ***Flame,*** 29, p.247, 1977.

56. Wichman, I. **S.** : Flame spread in an opposed flow over surfaces of solid fuels, ***Combustion*** and ***Flame, 50,*** p.287, 1983.

57. Wichman, I. **S.** and Williams, F. A. : A simplified model of flame spread in an opposed flow along a flat surface of a semi-infinite solid, ***Combustion Science and Technology,*** 32, p.91, 1983.

58. Orloff, L., de Ris, J. and **Markstein,** G. H. : Upward turbulent fire spread and burning of fuel surfaces, ***Fifteenth Symposium (International) on Combustion,*** p.183, 1975.

59. Saito, K., Quintiere, J. G. and Williams, F. A. : Upward turbulent flame spread, First ***Intemational Symposium on Fire Safety Science,*** p.75, 1986.

60. Saito, K., **Willians,** F. A., Wichman, I. **S.** and Quintiere, J. G. : Upward turbulent flame spread on wood under external radiation, ***Twenty-Fourth***

National Heat Transfer Conference, 1987.

61. Di Blasi, C., Crescitelli, S., Russo, G. and Fernandez-Pello, A. C. : Predictions of the dependence on the opposed flow characteristics of the flame spread rate over thick solid fuel, ***Second Intemational Symposium on Fire Safety Science,*** p. 119, 1989.

62. Kim, J. S., De Ris, J. and Kroesser, F. : Laminar free-convective burning of fuel surfaces, ***Thirteenth Symposium (International) on Combustion,*** p.949, 1970.

63. Kosdon, F. J., Williams, F. A. and Buman, C. : Combustion of vertical cellulosic cylinders, ***Twelfth Symposium (Intemational) on Combustion,*** p.253, 1969.

64. Blackshear, P. L. and Murty, K. A. : Some effects of size, Orientation, and fuel molecular weight on the burning of fuel soaked wicks, ***Eleventh Symposium (International) on Combustion,*** p.545, 1967.

65. Kung, H. C. : The burning of vertical wooden slabs, ***Fifteenth Symposium (International) on Combustion,*** 1975.

66. Markstein, G. H. and De Ris, J. : Upward fire spread over textiles, ***Fourteenth Symposium (International) on Combustion,*** p.1085, 1973.

67. Femandez-Pello, A. C. : Upward laminar flame spread under the influence of externally applied thermal radiation, ***combustion Science*** and ***Technology,*** 17, p.87, 1977.

68. Annmalai, K. and Sibulkin, M. : Flame spread over combustible surfaces for

laminar flow systems, Part II: Flame heights and fire spread, ***Combustion Science*** and ***Technology,*** 19, p.185, 1979.

69. Alpert, R. L. : Pressure modeling of fires controlled by radiation, ***Sixteenth Symposium (International) on Combustion,*** p. 1489, 1977.

70. Fernandez-Pello, A. C. : Flame spread in a forward forced flow. ***Combustion*** and ***Flame,*** 36, p.63, 1979.

71. Loh, H. T. and Fernandez-Pello, A. C. : A study of the controlling mechanisms of flow assisted flame spread, ***Twentieth Symposium (International) on Combustion,*** p.1575, 1984.

72. Loh, H. T. and Femandez-Pello, A. C. : Flow assisted flame spread over thermally thin fuels, ***First*** International ***Symposium on Fire Safety Science,*** p.65, 1987.

73. Apte, V. B., Bilger, R. W., Green, A. G. and Quintiere, J. G. : Wind-aided turbulent flame spread and burning over large-scale horizontal PMMA surfaces, private communication, 1989.

74. Mao, C. P. : ***A Study of the Bunting of a Solid Fuel Surface*** *in* ***Partial Enclosures,*** Ph.D thesis, University of California, Berkeley, 1983.

75. Carrier, G., Fendell, F., Butler, G., Cook, S. and Morton, C. : Laminar wind-aided flame spread across a thick horizontal fuel slab, ***Combustion Science*** and ***Technology, 72, p.17,*** 1989.

76. Loh, H. T. : ***Concurrent Flow Flame Spread Study,*** Ph.D thesis, University of California, Berkeley, 1985.

77. Schlichting, H. : ***Boundary-Layer Theory, Seventh Edition,*** McGraw-Hill, Inc., 1979.

78. Arpaci, V. S. : ***Conduction Heat Transfer,*** Addison-Wesley Publishing Co., 1966.

79. Glassman, I. : ***Combustion, Second Edition,*** Academic Press, 1987.

80. Kays, W. M. and Crawford, M. E. : ***Convective Heat*** and ***Mass Transfer,*** McGraw-Hill, Inc., 1980.

81. Burke, S. P. and Schumann, T. E. W. : Diffusion flames, ***Indust. Eng. Chem., 20,*** p.998, 1928.

82. Shvab, V. A. : Relation between the tempearuture and velocity fields of the flame of a gas burner, ***Gos. Energ. izd.,*** Moscow-Leningrad, 1948.

83. Zeldovich, Y. B. : ***Zhur. Tekhn. Fiz.*** 19(10), p. 1199, 1949. (English translation, NACA Tech. Memo. No. 1296, 1960)

84. Spalding, D. B. : The combustion of liquid fuels, ***Fourth Symposium (International)on Combustion,*** p.847, 1953.

85. Spalding, D. B. : ***Some Fundamentals of Combustion,*** Chapter 4, Butterworths, London, 1955.

86. Pagni, P. J. and Shih, T-M. : Excess pyrolyzate, ***Sixteenth Symposium (International) on Combustion,*** p.1329, 1977.

87. Ahmad, T. and Faeth, G. M. : An investigation of the laminar overfire region along upright surfaces, ***J. of*** Heat ***Transfer,*** 100, p.112, 1978.

88. Sibulkin, M., Kulkarni, A. K. and Annamalai, K. : Effects of radiation on the

burning of vertical fuel surfaces, ***Eighteenth Symposium (International) on Combustion,*** p. 611 1978.

89. Sibulkin, M., Kulkarni, A. K. and Annamalai, K. : Burning on a vertical fuel surface with finite chemical reaction rate, ***Combustion*** and ***Flame, 44,*** p.187, 1982.

90. Sibulkin, M. : Free convection diffusion flames from burning solid fuels, *Prog. **Energy Combust. Sci.***, 14, p.195, 1988.

91. Ahmad, T. and Faeth, G. M. : Turbulent wall fires, ***Seventeenth Symposium (Intemational) on Combustion,*** p. 1149, 1976.

92. Morton, B. R. : Modeling fire plumes, ***Tenth Symposium (International) on Combustion,*** p.973, 1965.

93. Delichatsios, M. A. : Turbulent convective flows and burning on vertical walls, ***Nineteenth Symposium (International) on Combustion,*** p.855, 1982.

94. Delichatsios, M. A. : Flame heights in turbulent wall fires with significant flame radiation, ***Combustion Science*** and ***Technology,*** 1986.

95. Delichatsios, M. A. : A simple algebraic model for turbulent wall fires, ***Twenty-first Symposium (International) on Combustion,*** p. 53, 1986.

96. Most, J. M., Harivel, P., Joulain, P., Rutton, B. and Sztal, B. : Influence of a turbulent diffusion flame on transport phenomena to a reacting surface, ***Nineteenth Symposium (International) on Combustion,*** p.375, 1982.

97. Tamanini, F. : A numerical model for the prediction of radiation-controlled turbulent wall fires, ***Seventeenth Symposium (International) on Combustion,***

p. 1075, 1976.

98. Kennedy, L. A. and Plumb, O. A. : Prediction of buoyancy controlled turbulent wall diffusion flames, ***Sixteenth Symposium (International) on Combustion,*** p. 1699, 1974.

99. Shih, T-M. and Pagni, P. J. : Wake Turbulent Flames, ***ASME Paper 77-HT-97***, 1977.

100. Lockwood, F. C. and Ong, P. H. : ***Heat and Mass Transfer in Boundary Layers, Vol. I***, Pergamon, 1972.

101. De Ris, J. and Orloff, L. : The role of buoyancy direction and radiation in turbulent diffusion flames on surfaces, ***Fifteenth Symposium (International)on Combustion,*** p.175, 1975.

102. Orloff, L., Modak, A. T. and Alpert, R. L. : Burning of large scale vertical surfaces, ***Sixteenth Symposium (International) on Combustion,*** p.1345, 1977.

103. Joulain, P., Most, J. M., Fuseau, Y. and Sztal, B. : Influence of coupled convection, conduction and radiation heat transfer on the burning of plastics, ***Seventeenth Symposium (International) on Combustion,*** p.1041, 1976.

104. Joulain, P., Most, J. M., Sztal, B. and Vantelon, J. P. : Theoretical and experimental study of gas-solid combustion in turbulent flow, ***Combustion Science and Technology,*** 15, p.225, 1977.

105. Mao, C.-P., Fernandez-Pello, A. C. and Pagni, P. J. : Mixed convective burning of a fuel surface with arbitrary inclination, ***J. of*** Heat Transfer, 106, p.106, 1984.

106. Van Driest, E. R., On turbulent flow near a wall, ***J.*** of ***Aeronautical Sciences,***

23, p.1007, 1956.

107. Marxman, G. and Gilbert, M. : Turbulent boundary layer combustion in the hybrid rocket, ***Ninth Symposium (International) on Combustion,*** p.371, 1963.

108. Paul, P. J., Mukunda, H. S. and Jain, V. K. : Regression rates in boundary layer combustion, ***Nineteenth Symposium (International) on Combustion,*** p.717, 1982.

109. Marxman, G. : Boundary-layer combustion in propulsion, ***Eleventh Symposium (International) on Combustion,*** p.269, 1967.

110. Marxman, G. : Combustion in the turbulent boundary layer on a vaporizing surface, ***Tenth Symposium (Intemational) on Combustion,*** p.1337, 1965.

111. Ueda, T., Mizomoto, M. and Ikai, S. : Velocity and temperature fluctuations in a flat plate boundary layer diffusion flame, ***Combustion Science*** and ***Technology,*** 27, p.133, 1982.

112. Pagni, P. J. : Diffusion flame analyses, ***Fire Safety Journal,*** p.273, 1980.

113. Smith, M. C. and Kuethe, A. M. : Effects of turbulence on laminar skin friction and heat transfer, ***The Physics*** of ***Fluids,*** 9(10), p.2337, 1966.

114. Blackshear, P. L Jr. and Murty, K. A. : Heat and mass transfer to, from, and within cellulosic solids burning in air, ***Tenth Symposium (Intemational) on Combustion,*** p.911, 1965.

115. Orloff, L. and De Ris, J. : Modeling of ceiling fires, ***Thirteenth Symposium (International) on Combustion,*** p.979, 1971.

116. Orloff, L. and De Ris, J. : Cellular and turbulent fires, ***Combustion*** and ***Flame,***

18, p.389, 1972.

117. Ohtani, H., Hirano, T. and Akita, K. : Experimental study of bottom surface combustion of polymethylmethacrylate, ***Eighteenth Symposium (International) on Combustion,*** p.591, 1981.

118. Ohtani, H., Akita, K. and Hirano, T. : An analysis of bottom stagnation region combustion of polymetric material pieces under natural convection, ***Combustion*** and ***Flame,*** 53, p.33, 1983.

119. Ohtani, H., Akita, K. and Hirano, T. : Scale effects on bottom surface combustion of PMMA pieces with circular and rectangular sections, ***J. of*** Fire and ***Flammability,*** 13, p.203, 1982.

120. Vantelon, J. P., Himdi, A. and Gaboriaud, F. : Bottom surface combustion of polymethylmethacrylate disks, I. Functional dependence of the combustion rate, ***Combustion Science*** and ***Technology,*** **54**, p.145, 1987.

121. Vantelon, J. P., Himdi, A. and Gaboriaud, F. : Bottom surface combustion of polymethylmethacrylate disks, II. Diffusion flame radiative properties, ***Combustion Science*** and ***Technology,*** **54**, p.145, 1987.

122. Mao, C.-P., Fernandez-Pello, A. C. and Humphrey, J. A. C. : An investigation of steady wall-ceiling and partial enclosure fires, ***J. of Heat Transfer,*** 106, p.221, 1984.

123. Wichman, I. S. and Saito, K. : An experimental study of the effects of gravity on flame spread in high oxygen concentration enviroments, ***Combustion*** and Flame, 52, p.291.

124. Mekki, K., Atreya, A., Agrawal, S. and Wichman, I. : Wind-aided flame spread over charring and non-chamng solids: an experimental investigation, *Abstracts of Eighteenth Symposium (Intemationat) on Combustion*, p.103, 1990.

NIST-114A
(REV. 3-90)

U.S. DEPARTMENT OF COMMERCE
NATIONAL INSTITUTE OF STANDARDS AND TECHNOLOGY

BIBLIOGRAPHIC DATA SHEET

1. PUBLICATION OR REPORT NUMBER
NIST-GCR-92-602

2. PERFORMING ORGANIZATION REPORT NUMBER

3. PUBLICATION DATE
March 1992

4. TITLE AND SUBTITLE

6. PERFORMING ORGANIZATION (IF JOINT OR OTHER THAN NIST, SEE INSTRUCTIONS)
University of California
Dept. of Mechanical Engineering
Berkeley, CA 94720

7. CONTRACT/GRANT NUMBER
NIST Grant 60NANB7D737

8. TYPE OF REPORT AND PERIOD COVERED

10. SUPPLEMENTARY NOTES

11. ABSTRACT (A 200-WORD OR LESS FACTUAL SUMMARY OF MOST SIGNIFICANT INFORMATION. IF DOCUMENT INCLUDES A SIGNIFICANT BIBLIOGRAPHY OR LITERATURE SURVM, MENTION IT HERE.)

An experimental study has been carried out to investigate the controlling mechanisms of solid fuel flame spread and mass burning in turbulent flows. The effects of flow velocity, turbulence intensity and buoyancy on concurrent and opposed flame spread rate and surface regression rate have been examined in both floor and ceiling configurations. It is found that for opposed flows, the flame spread rate of thermally thick PMMA sheet increases initially with the flow velocity, reaches a peak value and then decreases as the flow velocity increases further. The flow turbulence effect is to increase the flame spread rate initially and then decreases it at higher turbulence intensity. The flame spread rate of thermally thii paper sheet in an opposed flow decreases monotonically with the flow velocity and turbulence intensity. The flow turbulence also has a significant effect on the flame extinction conditions, resulting in a smaller extinction velocity for larger flow turbulence intensity. For concurrent flow flame spread, it is found that the flow turbulence decreases the flame spread rate for both floor and ceiling geometries, mainly as a result of the flame length shortening at high turbulence intensity. It is also found that flow velocity intensifies the spread of the flame. The experimental data of flame spread rate, flame length and surfac heat flux agree well with the formula obtained from a simplified thermal model, indicating that the heat transfer from flame to solid surface is the dominant controlling mechanism in the turbulent concurrent flame spread and, that the gas phase chemical reaction is of secondary importance. For solid fuel mass burning, it is found that the solid fuel surface regression rate decreases with the downstream distance and the flow velocity in both floor and ceiling configurations.

12. KEYWORDS (6 TO 12 ENTRIES; ALPHABETICAL ORDER; CAPITALIZE ONLY PROPER NAMES; AND SEPARATE KEY WORDS BY SEMICOLONS)

ceilings; flame spread; floors; paper; plastics; polymethylmethacrylate; solid fuels; turbulent flow

13. AVAILABILITY

[X] UNLIMITED

[ ] FOR OFFICIAL DISTRIBUTION. DO NOT RELEASE TO NATIONAL TECHNICAL INFORMATION SERVICE (NTIS).

[ ] ORDER FROM SUPERINTENDENT OF DOCUMENTS, U.S. GOVERNMENT PRINTING OFFICE, WASHINGTON, DC 20402.

[X] ORDER FROM NATIONAL TECHNICAL INFORMATION SERVICE (NTIS), SPRINGFIELD, VA 22161.

14. NUMBER OF PRINTED PAGES
232

15. PRICE
All

ELECTRONIC FORM